UNCLASSIFIED

AD 437 340

DEFENSE DOCUMENTATION CENTER

FOR

SCIENTIFIC AND TECHNICAL INFORMATION

CAMERON STATION. ALEXANDRIA, VIRGINIA

UNCLASSIFIED

DOWNEY PLANT

RESEARCH AND ENGINEERING DIVISION

KINETICS, MECHANISM, AND RESULTANT DROPLET
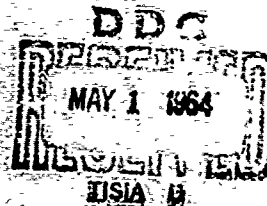SIZES OF THE AERODYNAMIC BREAKUP OF
LIQUID DROPS

by

H. E. Wolfe
W. H. Andersen

AEROJET
GENERAL TIRE
GENERAL

AEROJET-GENERAL CORPORATION
Research and Engineering Division
11711 Woodruff Avenue
Downey California

KINETICS MECHANISM AND RESULTANT
DROPLET SIZES OF THE
AERODYNAMIC BREAKUP OF
LIQUID DROPS

by

H. E. Wolfe
W. H. Andersen

Prepared under U. S. Army Chemical Center

Contract

DA-18 108-405 CML-829

Report

0395-04(18)SP

Reviewed by _____   Date ____ 6 April 1964 _____
           R. B. Mortensen Head
           Terminal Ballistics Dept
           Research Division

                                          No of Pages ____ 275 ____

Approved by _____   Classification UNCLASSIFIED
           H J Fisher   Manager
           Research Division

ACKNOWLEDGMENT

ABSTRACT

A critical review of the breakup of liquids is given, with emphasis on
liquid drops. Evidence is presented that the breakup is a rate process
and hence must be considered from a time-dependent approach rather
than from purely dimensionless parameters, such as Weber or Bond
numbers.

A theoretical model of the aerodynamic breakup of liquid drops is de-
veloped, postulating that the dual breakup mechanisms (bag and stripping)
of liquid drops result from pressure and frictional drag on the drop.
The derivation of a quantitative expression is presented, predicting
aerodynamic breakup times of liquid drops as a function of the gas-flow
properties and the physical properties of the drop. A quantitative ex-
pression is also developed that predicts the mass-mean diameter of
droplets produced by aerodynamic breakup of the drop as a function of
the gas-flow properties and physical properties of the drop.

Using shock-tube techniques, a comprehensive, experimental parametric
study was conducted on the breakup times of drops of water, mercury,
bis, and three silicone fluids with different viscosities. The results
are compared to the available theories; and are shown to be in very good
agreement with the preceding theory.

An experimental study of the size distribution of droplets produced by
the breakup of bis droplets was conducted for various gas-flow velocities
and initial drop sizes. The results are shown to be in good agreement
with the developed theory.

CONTENTS

ILLUSTRATIONS

ILLUSTRATIONS (Cont)

ILLUSTRATIONS (Cont)

1   INTRODUCTION

Knowledge of the dispersion (atomization, dissemination, or breakup) characteristics of liquids is of importance in a wide variety of applications, including

- Liquid-fuel atomization in rockets, internal-combustion engines, and gas turbines

- Insecticidal and agricultural spraying

- Spray drying

- Meteorological studies

- Production of aerosols for therapeutic work and chemical/biological warfare

The mechanism of dissemination of liquids is not well understood   There is no general theory available with which to estimate the particle-size distribution of a liquid as a function of the physical properties of the liquid or to evaluate the atomizing technique employed and its operating conditions Nevertheless, many features of the dissemination process have been elucidated from considerable experimental work and some limited theoretical work performed over the years (References 1 through 5).

The factors that influence the breakup of liquids are, to some extent, a function of the techniques used for performing the breakup, e g , explosive dissemination, nozzle dissemination, and electrical dispersion   Generally, factors that have been found to influence the breakup of liquids include the surface tension, viscosity   and density of the liquid, the density and viscosity of the gas (or other fluid) through which the liquid is moving, the relative velocity between the liquid and gas, the wavelength of any surface disturbances resulting in instability, and the hydrodynamic properties of the gas flow (laminar, turbulent, sub- or supersonic, etc.)

The physical properties of the liquid and of its environment define part of the preceding factors in a given case, whereas the techniques employed for dissemination define the remainder of the factors   For example, it is well known that the efficiency of atomization and dispersion of a liquid through an injection valve depends both on the properties of the liquid (for a given shape of the orifice) and on the shape of the orifice (for a given liquid)

Th..e is evidence that atomization of a liquid occurs in several stages, and that there is little difference whether the breakup of the liquid is brought about by the emergence of liquid into still air at high speed from a nozzle, or by the interaction of a stream of liquid and a fast-flowing gas stream. The various stages occur in the following order·

a. Stretching of the liquid into films, sheets, streams, or jets as a result of accelerating the liquid by some prescribed means.

b. Initiation of small disturbances at the surface of the liquid, in the form of local ripples, protuberances, or waves.

c. Formation of ligaments as a result of air (fluid) pressure and shearing forces.

d. Collapse of ligaments into drops as a result of surface tension

e. Further breakup of these drops in movement through the air or other fluid.

This report is concerned with a theoretical and experimental investigation of the last of these stages, i.e., the aerodynamic breakup of liquid drops. The studies have emphasized the mechanism and rate of the breakup process, with some attention directed to the resulting particle size of the dispersed aerosol. Also considered was the role of the physical properties of a liquid drop on its dispersion characteristics.

2. SUMMARY

A critical review of literature on the aerodynamic breakup of liquids is given, with emphasis on liquid drops. It is shown that the breakup of any geometry liquid may be considered to occur in two main phases: (1) the shearing of sheets, films, or jets from the liquid by the gas-flow forces, and (2) the rapid breakup of these liquid streams by instabilities, which grow exponentially with time. The breakup of liquids is shown to be a rate process and hence must be considered from a time-dependent approach rather than from purely dimensionless parameters, such as Weber or Bond numbers

A theoretical model of the aerodynamic breakup of liquid drops is developed, postulating that the dual breakup mechanisms (bag and stripping) observed for liquid drops result from pressure and frictional drag on the drop. The frictional drag is usually greater than the pressure drag;

however, the original deformation of the drop produced by the aerodynamic flow produces a sharper curvature at the outer edges of the drop than in the middle of the drop. This curvature produces a higher surface-tension pressure at the edges than in the middle of the drop. The surface-tension pressure resists liquid deformation by the gas pressure, and hence drops undergo bag breakup for velocities near the critical velocity required for breakup. For higher velocities, however, the friction stress at the drop edges becomes larger than the surface-tension pressure: the drop then undergoes stripping breakup, since the friction stress is greater than the pressure stress. For certain conditions, the drop exhibits the characteristics of both bag and stripping breakup.

Quantitative expressions are derived to predict the breakup times for both the bag and stripping breakup of liquid drops with given physical properties (size, surface tension, and viscosity) subjected to aerodynamic flow of a given velocity. These expressions are based on how quickly the middle of the drop can be sheared away from the edges of the drop (bag breakup). and how quickly the edges of the drop can be sheared away from the middle of the drop (stripping breakup). For most practical situations. however, one expression is sufficient to describe the breakup times as accurately as they can be measured. The breakup time t is shown to be given by

$$t = \frac{d}{\left[(A^2 + BP)^{1/2} - A\right]}$$

$$A = \frac{16\eta}{d\rho_1} \quad ; \quad B = \frac{2}{\rho_1}$$

$$P = \frac{1}{2} \rho_a u^2 - \frac{2\sigma}{d}$$

where

d	=	the original drop diameter
η	=	viscosity of drop
σ	=	surface tension of drop
ρ_1	=	density of drop
ρ_a	=	density of gas flow
u	=	velocity of gas flow

For low-viscosity liquids and negligible surface-tension forces (either low surface tension or high velocity), the preceding equation simplifies to

$$t = \left(\frac{d}{u}\right) \left(\frac{\rho_1}{\rho_a}\right)^{1/2}$$

For very-high-viscosity liquids and negligible surface-tension forces, the equation becomes

$$t = \frac{32\,\eta}{\rho_a u^2}$$

It is shown that the proposed breakup model can probably be modified to include the erosion of solid particles in gas streams.

A theoretical model is developed for the breakup of the liquid film (or sheet) sheared from the drop by the gas flow; this breakup produces the droplets that are formed by the breakup of the drop. The liquid pieces produced by breakup of the film (and which subsequently form into drops by surface-tension forces) are considered to have a thickness that is determined by the shearing of the film from the drop, a width determined by divergence (expansion) of the sheet as it leaves the drop, and a length determined by the growth of instabilities produced in the lengthwise direction (parallel with the gas stream) of the sheet by the gas stream. The mass-mean diameter, D, of droplets produced by the breakup of the original drop is given by

$$D = \left[\frac{136\,\eta\,\sigma^{3/2}\,d^{1/2}}{\rho_a^2\,\rho_1^{1/2}\,u^4}\right]^{1/3}$$

(The velocity and initial drop-diameter dependence predicted in this equation has previously been found experimentally by Weiss and Worsham.)

A comprehensive, experimental parametric study has been conducted on the breakup times of drops of water, mercury, bis, and three silicone fluids with widely different viscosities, employing various flow velocities and drop sizes. The liquids were chosen to include a wide variation of

physical properties, which were investigated using shock-tube and high-speed photographic techniques   Descriptions of the experimental apparatus and test procedure are presented in detail, and the original experimental data are appended. Experimental breakup times are compared to available theories, and are shown to be in very good agreement with the developed theory. The results are also in agreement with the Gordon theory, if the surface-tension pressure used by Gordon is decreased by a factor of two to four. Experimental photographs of the breakup process demonstrate that the bag and stripping breakup mechanisms are separated by a transition region that includes characteristics of both modes of breakup behavior as predicted   Various characteristics of the breakup process are discussed, including the change of drag coefficient with time

An experimental study was performed to sample and assess droplet-size distributions resulting from the breakup of single drops of bis subjected to various aerodynamic flow velocities and exhibiting both mechanisms of breakup. The mass-mean diameter of the resultant droplets was found to be in good agreement with the derived equation.

It is concluded that the present breakup theory is probably adequate to describe the breakup times of liquid drops of any liquid. the derived mean-drop-size expression is probably adequate, but needs further checking using other liquids. Further studies are also required to elucidate theoretically the entire drop-size distribution function   Associated conclusions and recommendations are also discussed

3.   DISPERSION BACKGROUND

3. :   DISPERSION OF BULK LIQUID

Breakup of a moving jet of liquid was first treated theoretically by Rayleigh (Reference 6) and later extended by Weber (Reference 7.   In these treatments   small perturbations or disturbances acquired in the slip streams at the nozzle for base of the liquid, are shown to be carried forward with the jet   at the same time growing exponentially until violent instability occurs   followed by breakdown of the liquid column. At low jet velocities, the air does not appreciably affect the shape of the jet, and rotationally symmetric (varicose) disturbances are formed on the cylindrical jet   The disturbances are assumed to grow in conformance with the equation

$$S = S_1 \exp(q') \cos(2\pi x/\lambda)$$ (1)

- 5 -

where

S = amplitude of the disturbance at time t and distance x from the nozzle

S_j = average initial amplitude of the disturbance imparted to the jet stream at its base (the nozzle)

q = rate of growth of the disturbance of wavelength λ

Breakup of the jet into droplets occurs where the jet is nicked off by the growth of the varicosity. The wavelength that dominates the breakup is the optimum wavelength, λ_{opt}, for which the rate of growth is a maximum, i.e., q_m. The breakup criteria is: $S_1 \exp(q_m t_b) = d_j/2$, where d_j is the jet diameter. Breakup time, t_b, is then given by

$$t_b = (1/q_m) \ln (d_j/2S_i) \tag{2}$$

The optimum wavelength according to Weber is

$$\lambda_{opt} = 2^{1/2} \pi d_j \left[1 + 3 \left(\frac{\eta^2}{\sigma \rho_1 d_j} \right)^{1/2} \right]^{1/2} \tag{3}$$

where

η = viscosity of liquid jet

σ = surface tension of liquid jet

ρ_1 = density of the liquid jet

Assuming the average jet diameter is equal to the diameter of the jet orifice, the average diameter, d, of the spherical drops initially produced by breakup of the cylindrical jet is

$$d = \left[1.5 d_j^2 \ \lambda_{opt} \right]^{1/3} \tag{4}$$

The growth rate of the optimum disturbance is given by

$$1/q_m = (\rho_1/\sigma)^{0.5} d_j^{1.5} + 3 \eta d_j/\sigma \tag{5}$$

-6-

The breakup distance is $L_b = u_j t_b$ where u_j is the jet velocity Thus, L_b increases with increase in jet velocity while t_b is independent of velocity

As the velocity of the jet is further increased. the breakup to drops becomes partially influenced by interactions of the jet with the air. The air velocity increases over the wave crests and decreases over the troughs; simultaneously, the pressure decreases over the crests and increases over the troughs The net result is that the optimum wavelength for breakup decreases, and the growth rate of the optimum wavelength disturbance increases, leading to a decrease in breakup time breakup distance, and resulting drop size with an increase in jet velocity. As the jet velocity is still further increased, the jet becomes sinuous (wavy) in nature as a result of increased surface interactions with the air. the faster the jet velocity the more the wave motion is intensified. The wave motion leads to rapid breakup of the jet into drops However, the treatment of this case by Weber is semi-emperical in nature, and does not lead to simple equations by which the breakup characteristics of the jet may be readily predicted

The theoretical results of Rayleigh and Weber have been verified by various experimental studies (References 1 through 5) As shown by the study of Haenlein (Reference 8, four characteristic breakup forms were evidenced as the jet velocity was increased viz. drop formation without air influence, drop formation with air influence wave formation leading to drop formation. and immediate complete disintegration of the jet into drops. The latter situation, which was not discussed by Rayleigh and Weber is generally the situation that occurs in practical applications

Castleman (Reference 9) considered the breakup of a high-velocity jet to occur through the formation of ligaments or threads which are drawn from the main jet mass and collapse because of their instability into a number of drops. The ligaments arise through air friction on the jet an effect that causes surface distu.bances to grow according to the Rayleigh-Weber theory At higher airspeeds, finer ligaments are formed and break up to form smaller drops, higher surface tension would cause quicker collapse of the ligaments before they are drawn too finely and would result in larger drops These trends are verified by experiment

Fogler and Kleinschmidt (Reference 10, consider the liquid to be drawn out into thin flat sheets or films rather than ligaments or threads The waves in the film build up rapidly and cause a whipping of the surface so that it curls back on itself to form a hollow tube Such a tube is unstable and breaks off immediately into a series of hollow spheres, which form droplets

Schweitzer (Reference 11) stressed the importance of turbulent flow on the breakup of high-velocity jets. The turbulence gives the liquid a radial component of velocity, helping to overcome the surface-tension forces, and providing surface disturbances for interactions with the air. Schweitzer considered turbulence to be the dominant factor in the breakup of very-high-velocity jets, with air friction enhancing the process, he concluded that viscosity is the most important liquid property that influences the breakup of liquid jets. The turbulent breakup mechanism would help explain the fourth characteristic breakup form observed by Haenlein.

The views of Schweitzer regarding the effects of turbulence on the breakup of high-velocity jets are also supported by the work of various other workers (References 1 through 4), including Merrington and Richardson (Reference 12) who found that the mass-mean droplet diameter, d, depended primarily on the jet velocity and the liquid viscosity; no influence of nozzle size or shape was detected. Their experimental data at high velocities satisfied the emperical equation

$$d \, u_j = 500 \, (\eta/\rho_1)^{0.2} \tag{6}$$

At lower jet velocities, the drop size reached a limiting value, as expected for varicose breakup (refer to Equation 4).

Ohnesorge (References 1 and 3) concluded that the breakup of liquid jets occurs quite generally in three different stages, with the particular stage depending on the value of the Reynolds number, Re, of the jet. These stages consist of varicose breakup, sinuous breakup, and direct atomization from the nozzle; the stages are separated, consecutively, in a plot of the Ohnesorge number, Z, versus Re, using the lines given by

$$Z = 1.025 - 5.08 \, (10^{-4}) \, Re \tag{7a}$$

$$Z = 1.430 - 1.42 \, (10^{-4}) \, Re \tag{7b}$$

$$Z = \eta / \, (\sigma \, \rho_1 \, d_j)^{1/2} \tag{7c}$$

$$Re = \rho_1 \, u_j \, d_j / \eta$$

These relationships show that the jet flow changes from a laminar to a turbulent behavior as the velocity is increased.

Dityakin and Yagodkin (Reference 13) concluded that fluctuations of the jet-flow velocity and the density of the ambient medium lead to a decrease in the average droplet size produced by jet breakup, as well as to a distribution of droplet sizes.

Dunne and Cassen (Reference 14) investigated the instability of a liquid jet with a velocity discontinuity (shock) superimposed on the jet. They found that the perturbation grows in time, and is propagated through the jet as a thin-disc, rotationally symmetric wave whose velocity is the mean of the instantaneous particle velocities immediately in front of and behind the discontinuity. Eisenklam and Hooper (Reference 15) suggested that the breakup of very-high-velocity jets could be partially produced by the internal pressure of the liquid, and could periodically alternate with the turbulent breakup mechanism.

Middleman and Gavis (Reference 16) found that capillary jets of liquids expand or contract upon ejection, depending upon conditions of ejection and fluid properties. Straubel (Reference 17) showed that an electrical potential placed across an injector effected fine atomization of a previously coarse stream. Miesse (Reference 18) found that a transverse ambient-pressure oscillation brought about rapid mixing of a pair of adjacent streams.

Weiss and Worsham (Reference 19) studied the drop sizes obtained on injecting a cylindrical liquid jet of a synthetic wax into a large, hot airstream sustained at high velocity. The relative velocity, u_r, between the liquid jet and the airstream was found to be the variable having the largest effect on particle size. The mass-median diameter of the drop size was found to be approximated by

$$d = u_r^{-1.33} \, v_{inj}^{0.08} \, D_{inj}^{0.16} \, \eta_1^{0.34} \left[1 + \rho_{ao}/\rho_a \right] \tag{8}$$

where

$\quad v_{inj} \quad = \quad$ injection velocity of the liquid

$\quad D_{inj} \quad = \quad$ diameter of the jet

$\quad \rho_{ao} \quad = \quad$ density of the air at $300^\circ F$ and 1-atm pressure

$\quad \rho_a \quad = \quad$ air density

The inv.rse velocity exponent 1.33 compares to a value of 1.0 found earlier by Nukiyama and Tanasawa (Reference 20) for small pneumatic atomizers. and to the value of 1.11 for a metal alloy and 1.68 for a wax found by Marshall (Reference 21) for large venturi atomizers.

Weiss and Worsham concluded that: "The atomization of liquids by large, high-velocity airstreams occurs by direct action of the airstreams on the exposed liquid surface. Therefore, the relative velocity between the liquid and the airstream is of primary importance. Physical properties of the fluids do affect spray fineness, but their net influence is less critical. The exact way in which the liquid is introduced to the air, i. e., the geometry and operation of the injector, is of least importance, particularly at very high air velocities and for customary range of variables."

The preceding conclusions appear to be generally applicable under all c   itions in which high-velocity gases are involved, with the exception of conditions where high-vapor-pressure liquids are concerned (in which case vaporization may also be an important parameter).

The breakup of a tangentially moving liquid sheet, or a conical film such as may be produced by a swirl type of injector, has been considered by various investigators (References 22, 23, and 24) to occur in much the same manner as that of a plain jet. Small disturbances in the sheet develop to form waves, which rapidly grow and break up the sheet; in addition, holes often appear in the sheet. Squire (Reference 23) deduced the optimum wavelength to be given by

$$\lambda_{opt} = 4 \pi \sigma / \rho_a u^2 \qquad (9)$$

where

ρ_a = air density

u = relative tangential velocity of the air

The maximum growth rate is

$$q_m = \left[2 \pi u / \lambda_{opt} \right]\left[2 \sigma / \rho_1 u^2 b \right]^{1/2} \qquad (10)$$

-10-

where b is the film thickness. The average drop size produced by the breakup is

$$d = \left[6b \, \lambda_{opt}^2 / \pi \right]^{1/3} \tag{11}$$

Equation 9 may also be used for estimating drop-size values in the sinuous breakup of liquid jets. It is of significance that Equation 11 predicts the drop size to vary inversely as the 4/3 power of the relative velocity, as found by Weiss and Worsham (Equation 8).

Borodin and Dityakin (Reference 25) showed that the possibility of several predominant wavelengths leading to breakup could lead to a distribution of drop sizes. York et al (Reference 24) assumed that each wave-formed ripple on a liquid sheet behaves as a circular jet of radius $(b\lambda / \pi)^{1/2}$ and obtained for the drop size

$$d = 2(b \lambda_{opt})^{1/2} \tag{12}$$

Equations 11 and 12 have both been shown to be in fair agreement with experimental data.

Taylor (Reference 26) considered the acceleration of two fluids in contact, and showed that the boundary between high- and low-density fluids will be unstable when the acceleration (or force) is directed from the low-density fluid to the high-density fluid. This destabilizing influence is known as Taylor Instability. Acceleration from the denser towards the lighter fluid exerts a stabilizing tendency. The relative tangential velocity on a fluid is always a destabilizing influence (known as Helmholtz Instability). Richtmyer (Reference 27) has considered Taylor instability in the shock-acceleration of compressible fluids.

3.2   DISPERSION OF LIQUID DROPS

Lane (Reference 28) conducted one of the first comprehensive studies of the aerodynamic breakup of liquid drops in an air stream. He subjected a water drop to an essentially steady (gradually increasing) air stream, and found that it becomes increasingly flattened; at a critical velocity of air, the drop was blown out in a concave manner into the form of a hollow bag attached to a roughly circular rim. Bursting of this bag produced a shower of very fine droplets, and the rim, which contained at least 70% of the mass of the original spherical drop broke up later into larger drops. This type of breakup is known as bag breakup.

Lane pointed out that the phenomenon has special interest in connection with the atomization of sprays in that in both cases the mass fraction of very small particles produced is small, and that these small particles result from the breakup of a stretched film. He found that the critical velocity, u_c, required to break the drops was given by: $(u_c - v)^2 d = 612$, where v is the velocity of the drop at breakup and d is the diameter of the orig.nal drop. A relationship of the form

$$C_d \, \rho_a \, (u-v)^2/2 = 4\sigma/d \tag{13}$$

was expected on theoretical grounds, where C_d is the drag coefficient of a sphere. This work led to a value of the constant of about 1200 rather than 612. However, since the drop does not remain spherical but approximates a lens shape before it bursts, the drag coefficient should be closer to that given for a circular disc (about twice the value for a sphere), yielding a value of about 600 for the constant.

Equations of the form of Equation 13 have also been used by other early investigators of droplet breakup (References 1 through 4). The interpretation of this equation is that the relative flow velocity is brought to rest in front of the drop at the stagnation point and is converted to a pressure This pressure pushes the interior of the drop more than the sides of the drop (as a result of pressure distribution), so as to form a bag, which then breaks. Viscosity was found to influence the breakup only when it was very great, and then only tended to retard the breakup.

The breakup of drops subjected to abrupt, fast (transient) air blasts was also studied by Lane. In this case, the drop deformed in the opposite direction to that of bag breakup, and formed a convex surface to the flow of air, the diameter being about twice that of the original spherical drop. The edges of the saucer shape were first drawn out into a thin sheet, then into thin filaments that broke to form drops. This type of breakup is known as shear breakup or stripping breakup.

It was found that the velocities required for breakup in the fast blasts were lower than in the steady stream, the divergence increasing for small drops. This effect was explained by some work of Taylor, who deduced that $(u_c -v)_{steady} = 2^{1/2} (u_c - v)_{transient}$. A measurement of the drop sizes produced by the breakup of a drop showed the resultant mean-mass drop size decreased with an increase in velocity.

-12-

Calculations by Taylor (Reference 28) of the boundary-layer thickness (and hence resultant drop size) of the drop undergoing stripping were roughly in agreement with experimental data obtained at low air velocities, but were too large at the higher velocities.

Hinze (Reference 29) theoretically investigated the breakup of liquid drops in a gas stream by an examination of the slight deformation of the globules, using linearized hydrodynamic equations. He found the critical condition for breakup of a nonviscous liquid suddenly exposed to a constant-velocity gas stream to be

$$\delta/R = 0.17 \; We \tag{14}$$

where

δ = deformation of the drop in the radial direction

R = initial drop radius

In Equation 14, the Weber number, We, is defined by

$$We = \rho_a \, u^2 \, R / \sigma \tag{15}$$

where

ρ = gas (air) density

u = relative velocity between the drop and gas stream

σ = surface tension of the liquid

For liquids with large viscosities, Hinze found

$$\delta/R = 0.095 \; We \tag{16}$$

Hinze thus associated the breakup of liquids with a critical value of the Weber number. For the cases of the breakup of a liquid in a continuously increasingly gas flow (e.g., a falling drop), the constants in Equations 14 and 16 should both be 0.095. The correlation of these equations with limited experimental data of Merrington and Richardson (Reference 12) suggested that the critical value of δ/R, i.e., $(\delta/R)_{cr}$, is generally of the order of unity for breakup; however, highly viscous liquids required larger values (e.g., about 2 in one case).

-13-

The breakup time, t_b, of a nonviscous liquid was computed to be

$$t_b = (1.16 \, R/u) \left[(\rho_1/\rho_a) \, (\delta/R)_{cr} \right]^{1/2} \qquad (17)$$

and that of a highly viscous liquid was found to be

$$t_b = (10 \, \eta_1 / \rho_a u^2) \, (\delta/R)_{cr} \qquad (18)$$

It should be noted that Equations 17 and 18 do not include the case of medium viscosity effects; in addition, the values of $(\delta/R)_{cr}$ required vary with the viscosity.

An experimental study of the aerodynamic breakup of liquid drops was conducted by Hanson et al (References 30 and 31). These investigators found, as opposed to the findings of Lane, that it is possible to produce bag breakup under suddenly applied (transient) flow conditions if the air velocity is only slightly greater than the critical velocity. When the air velocity is considerably above the critical value, shear breakup always occurs. They also found that with some drops undergoing bag breakup, the bag develops a reentrant portion near its middle; this so-called "stamen" increases in length with time, and in some cases completely inverts the bag before breakup occurs.

Also observed was that small dark spots surrounded by concentric rings appeared in the bags (it was not known whether these were the beginnings of rupture). A general conclusion was made that the passage of a normal air shock over a liquid drop does not of itself cause breakup, but rather that it is the relative velocity between the drop and the shocked air which, if sustained for a sufficient time, will cause the drop to break up. The breakup of distilled water, methyl alcohol, and three silicone oils with viscosities of 10, 50, and 100 centistokes, over the 100- to 700-micron range of drop diameters was found to obey the following emperical equations:

$$u_c^2 d = 6.21 \, (10^6) \qquad (19a)$$

$$u_c^2 d = 2.71 \, (10^6) \qquad (19b)$$

$$u_c^{1.8} d = 9.69 \, (10^5) \qquad (19c)$$

$$u_c^{1.62} d = 6.84 \, (10^5) \qquad (19d)$$

$$u_c^{1.36} d = 2.32 \, (10^5) \qquad (19e)$$

-14-

where d is the drop diameter in microns, u is the gas velocity in ft/sec, and the subscript c denotes critical quantity.

The dependence of critical velocity on surface tension for constant drop size was found to go approximately as the surface tension to the ore-third power. This effect contrasted with the one-half power variation found by Lane. The studies showed a negligible effect of viscosity in the critical breakup velocity for viscosities of about 10 centistokes or less, above this value, however, the effects became significant. Increasing viscosity increased the critical velocity required to break up a drop of given diameter. The trend became more pronounced as the drop diameter was decreased.

Priem (Reference 32) studied the breakup of liquid drops by shock waves and concluded that the drops were broken up by the high gas velocity behind the shock front. A similar conclusion was reached by Sato (Reference 33) on the basis of photographic evidence.

Magarvey and Taylor (Reference 34) studied the free-fall breakup of large liquid drops and concluded that the regular breakup is not triggered by internal vibrations. As shown in Reference 35, the time t_n (period) required for a complete oscillation of a liquid drop for the nth spherical function (harmonic) is given by

$$t_n = \left[3 \pi m / \sigma n (n-1) (n+2) \right]^{1/2} \tag{20a}$$

where m is the mass of the drop.

The case of $n = 1$ results in no motion, i.e., the shape of the drop is spherical; the case $n = 2$ is that of the slowest vibration and represents deformation into what is close to an ellipsoidal shape. In this case

$$t_n = \left[3 \pi m / 8\sigma \right]^{1/2} \tag{20b}$$

The cases of $n = 3, 4 \ldots$, correspond to more rapid partial vibrations toward the ellipsoidal shape; these vibrations are anharmonic because their periods do not have a direct relation to the period of the ellipsoidal deformation.

Engel (Reference 36) photographically studied the breakup of water drops behind an air shock. She found the drops, which underwent shear breakup, to first flatten on the leeward side subsequent to the passage of the shock

front. This effect was followed by a radial flow of the drop to give a ring shape, which was then bent in the wind direction by the airflow. The deformation was accompanied by streamers of mist torn off by the moving boundary layer. Flattening of the drop perpendicular to the direction of the airflow is the result of the pressure distribution around the drop.

According to Burgers (Reference 36), the preceding effect is initially described by

$$d_{out} = pt^2 / 3 R \rho \qquad (21)$$

where d_{out} is the outward displacement at the equator of the drop (perpendicular to the direction of the airflow at time t), ρ is the density of the liqu d drop of radius R, and p is the pressure difference between either the windward or the leeward-face stagnation point and points around the equator of the drop.

After the initial rapid flattening, the deformation remained approximately invariant with time, and finally increased again (but at a slower rate than the initial increase). In the final stages in the breakup of the drop, a distinct corrugation appeared in the windward face, an effect which may be caused by surface waves produced by the wind that blows out radially around the stagnation point. The crests of these waves may break or be blown off, and breakup of the remaining portion of the drop into separate sections can then occur.

It is possible that a hole forms in the center of the liquid, forming a ring that breaks into droplets. It was found that large drops lag behind small drops in developing various stages of fragmentation (this behavior decreased as the flow velocity was increased). A change in velocity was found to be more effective on the rate of breakup than a change in drop diameter.

Rabin, Schallenmuller, and Lawhead (References 37 and 38) investigated the aeroaynamic breakup of burning and non-burning liquid drops. They found, as did previous investigators, that the flow field following the relatively weak shock causes the droplet breakup, rather than any impulsive action of the front itself. The critical velocity required to break up a burning drop was found to be slightly lower than for a non-burning drop (an effect attributed to the lower surface tension of a burning drop). It may also be noted, however, that the boundary layer around the burning drop will also differ from that of a non-burning drop. Both bag and shear breakup behaviors were observed.

An analysis of the data revealed that the breakup mechanism (bag vs shear)
could not be explained on the basis of the flow duration as related to the
drop vibrational period (Equation 20b). Data of Lane and of Hanson et al.
(Reference 30 and 31) also were not explainable on this basis. At velo-
cities greatly in excess of the critical value, only shear breakup was ob-
served. at elevated gas pressures, only shear breakup was observed, and
the critical velocity decreased. The critical velocity that ould just cause
breakup for short-duration flow was found to agree with the equation

$$\text{We } / \text{ Re}^{1/2} \doteq 0.45 \tag{22}$$

where the Reynolds number is based on the sphere diameter, and the Weber
number is based on the sphere radius. The drag coefficient for burning
and non-burning drops was found to be approximately unity.

Gordon (Reference 39) has derived an expression from Newton's second
law for the aerodynamic breakup of liquid drops undergoing bag breakup
(it appears, however, that the results are also applicable to shear breakup,
as shown later in this report). An assumption was made that the stagnation
pressure at the front of the drop extrudes a cylindrical plug from the drop.
the extrusion is retarded by surface tension, viscosity,and inertial
forces. The acceleration of the plug is given by

$$\frac{dv}{dt} = \frac{P}{\rho_l d} = \frac{1}{\rho_l d} \left[1/2 \, \rho_a u^2 - (8\sigma/d) - (16\eta \, v/d) \right] \tag{23a}$$

where d is the drop diameter, P is the resultant pressure on the face of
the drop (composed of the stagnation pressure minus the surface tension
pressure minus the viscous pressure), u is the relative velocity between
the drop with surface tension, σ, and viscosity, η, and the air stream with
density, ρ_a, and ρ_l is the liquid density. Integrating Equation 23 gives the
velocity of the plug as a function of time

$$v = (A/B) \left[1 - \exp(-Bt) \right] \tag{23b}$$

where

$$A = \frac{\rho_a u^2}{2\rho_l d} - \frac{8\sigma}{\rho_l d^2} \; ; \; B = \frac{16\eta}{\rho_l d^2} \tag{23c}$$

-17-

Integrating a second time gives the plug displacement as a function of time, and considering breakup to occur when the displacement is equal to the drop diameter gives

$$\frac{2 (16\eta)^2}{\rho_1 d^2 (\rho_a u^2 - 16\sigma/d)} = \frac{16\eta t}{\rho_1 d^2} - 1 + \exp\left[\frac{-16\eta t}{\rho_1 d^2}\right] \qquad (24)$$

where t is the breakup time. This equation simplifies for special cases.

Thus

$$t = (2d/u)(\rho_1/\rho_a)^{1/2} \; ; \; \text{for } \eta < < du(\rho_a\rho_1)^{1/2} \qquad (25a)$$
$$\sigma < < du^2\rho_a$$

$$t = 32\eta /\rho_a u^2 \; ; \; \text{for } \eta > > du(\rho_a\rho_1)^{1/2} \qquad$$
$$\sigma < < du^2\rho_a \qquad (25b)$$

Equations 25a and b may be compared with Equations 17 and 18 as derived by Hinze. Except for a constant factor, the equations are identical. A useful approximation to Equation 24 is

$$t = \frac{2d\rho_1^{1/2}}{(\rho_a u^2 - 16\sigma /d)^{1/2}} + \frac{32\eta}{\rho_a u^2 - 16\sigma/d} \qquad (26)$$

Gordon states that this approximation is never too small, and is at most 37% too large. (Experimental data were not available for a rigorous test of the Gordon theory at the time of its publication.) His theory is compared to results of the present experiments in a later section of this report.

Dodd (Reference 40) considered the bag breakup of liquid drops and argued that the critical velocity required for breakup is the velocity that makes the radius of curvature of the deformed drop a minimum. He concluded that the form of the condition for breakup is the same as that found by Lane, i.e., Equation 13.

Morrell considered the breakup of liquid drops and of jets by transverse shocks in a series of papers (Reference 41, 42, and 43). His results with jets are directly related to drops, since breakup was considered under

-18-

conditions where the breakup was due entirely to the transverse shock and not to the jet instability per se. Originally (Reference 41) he utilized the method of Hinze (Reference 29) for drops and derived an analogous breakup-time expression for a cylindrical jet. He observed experimentally that the breakup occurred by a shear type of mechanism (the breakup time was found to depend on d_j/u). However, large values of δ/R were required to make the data agree with the theory. Morrell pointed out that his data, as well as those of Rabin and Lawhead (Reference 37) and of Lane (Reference 28), showed that the minimum or critical Weber number for breakup should increase as the initial drop (or jet) diameter increases, whereas the data reported by Hanson et al.(References 30 and 31) and by Volynskii (Reference 44) show the opposite. The reasons for this discrepancy are not apparent.

In a later paper (Reference 42), Morrell derived an expression for the breakup of drops as a result of stripping. It was assumed that the liquid issuing from the periphery of the drop forms a sheet, which breaks when the frictional force on the sheet is equal to the tensile force of the liquid. The time-dependence of the breakup was not considered, however. The case in which the dynamic pressure causing breakup of the drop decays exponentially, i e ,

$$\rho_a u^2 = \rho_{ai} u_i^2 \; \exp\left(-t/t_a\right) \tag{27}$$

was also considered for both bag and shear breakup. In this equation. the subscript i indicates initial values, and t_a is the action time (time constant) of the decay. Morrell assumed that when the action time is greater than the natural period t_n of the drop (Equation 20b) or jet, the liquid mass will oscillate and break by a deformation (bag) mechanism. For $t_a < t_n$, the mass will not oscillate and will break by a stripping mechanism. A reasonable correlation of the data was obtained using this assumption. However, Rabin and Lawhead (References 37 and 38) had earlier been unable to correlate either their data or those of Hanson et al. by means of a similar assumption.

It may also be argued that the drop can not initially know either the pressure duration or its decay characteristics, and hence cannot know what frontal shape to assume (convex or concave) to help establish the breakup mechanism

In his later paper (Reference 43), Morrell states that the flow duration (action time) merely affects the extent of breakup. Deformation breakup appeared to become increasingly important as the velocity was increased. The deformation δ was determined (photographically) to be given by

$$\delta/R = 2 + 4 \, We/Re^{1/2} \tag{28}$$

where

$$We = \rho_a u^2 R/\sigma$$

$$Re = \rho_a u R/\eta$$

$$R = \text{the jet or drop radius}$$

Substitution of this expression in the equation originally derived for breakup (Reference 41) gave a complicated expression for the breakup time as a function of the Reynolds and Weber number. This expression always predicted values of the breakup time that were low when compared with the available experimental data. The similarities between Equations 28 and 22 are noteworthy, and the possible use of Equation 28 in Equations 17 and 18 derived by Hinze is also of interest.

Morrell also derived a rate expression for the stripping breakup of jets in his later paper, assuming the liquid to be stripped off in sheets perpendicular to the jet. The volumetric removal rate of liquid from the drop was taken as

$$-\frac{dV}{dt} = 2d_{bl} u_1 \tag{29}$$

where V is the volume of liquid per unit length of jet, d_{bl} is the thickness of the liquid sheet (boundary layer), u_1 is the average velocity in the boundary layer, and the right-hand side of Equation 29 is to be evaluated for the length of the sheet at breakup. This length, δ, was assumed to be given by Equation 28.

Integrating Equation 29 gives for the breakup time

$$t = \pi R^2 / (2d_{bl}u_1) \tag{30}$$

A modified form of the general velocity profile suggested by Sandborn and Kline (Reference 45) was used for the boundary layer, rather than the exponential profile used earlier by Taylor (Reference 28). The boundary layer thickness was found to be given by

$$d_{bl} = (v_1 \, x/ub)^{1/2} \tag{31a}$$

and the average boundary layer velocity by

$$u_1 = 10 \, bu \tag{31b}$$

where

$$b = 0.04 \, (\rho_a/\rho_l)^{2/3} \, (v_a/v_l)^{1/3} \tag{31c}$$

and v is the kinematic viscosity, η/ρ.

Substitution of Equation 31 in Equation 30 gives for the breakup time

$$t = 0.54 \left(\frac{\rho_1}{\rho_a}\right)^{2/3} \left(\frac{\eta_a}{\eta_1}\right)^{1/3} \frac{R}{u} \left[\frac{Re}{1 + 2\frac{We}{\sqrt{Re}}}\right]^{1/2} \tag{32}$$

A comparison of the experimental data with Equation 32 showed satisfactory agreement, except near the threshold (large values of t). It was in this region however, that the breakup was found to occur by the deformation mechanism. Equation 32 may be expected to also hold for liquid drops, except for a small numerical constant (which accounts for the change in geometry). The equation is compared with experimental data in a later section of this report.

A theory of the breakup of liquids in high-velocity gas streams has recently been presented by Mayer (Reference 46), who considered the wind (airstream) to induce disturbances (waves or ripples) in the fluid. Waves of very small wavelengths decay because of viscous dissipation, and very long wavelengths develop slowly because of inertial effects. The other waves grow at an exponential rate, which is determined by the fluid properties.

-21-

It was postulated that when a wave of a certain wavelength has grown to an amplitude comparable to its wavelength, the crest of the wave is shed as a ligament from which droplets (whose diameters are proportional to the wavelength) are also formed.

The derived mean droplet diameter for the primary breakup of the liquid is

$$d = 71.2 \ B \left[(\eta_1 (\sigma/\rho_1)^{1/2} / \rho_a u_a^{\ 2} \right]^{2/3} \tag{33}$$

where $B = F/B^{2/3}$. The parameter F is associated with the crest configuration at the instant of erosion, and the sheltering parameter, B, is associated with the portion of the wave crest exposed to the driving effect of the wind. The value of B is conceptually of the order of unity, and for one specific case it was calculated to be about 0.3. Equation 33 predicts that the average drop size should vary inversely as the 4/3 power of the relative velocity between the liquid and the gas stream (precisely the velocity effect on drop size found experimentally by Weiss and Worsham in Reference 19).

When a liquid drop moves through a fluid (or vice versa), a shearing stress (skin friction) is exerted on the surface of the drop, an effect that may set up an internal circulation within the drop. In addition, the drop will be deformed as discussed previously. These effects significantly influence both the drag and the stability of the drop, and were studied by Bond and Newton (Reference 47). These investigators showed that the relevant parameter is the Bond number, Bo, which may be interpreted as being approximately the ratio of the hydrodynamic head (accelerational or gravitational) pressure to the surface-tension pressure of a liquid.

For a liquid drop accelerated through a gaseous medium, the Bond number may be written as

$$\text{Bo} = \frac{(\rho_1 - \rho_a) \ d^2}{\sigma} \ \frac{dv}{dt} \tag{34}$$

where dv/dt is the acceleration of the droplet relative to its gas environment. Experiments have shown (e.g., Reference 12) that when the Bond number of an accelerated drop exceeds a certain number (about 8 to 12, although the exact value also appears to be a function of the viscosity of the liquid), the drop becomes unstable and will probably break up. The time required for breakup to occur, however, is not specified

It may also be recalled from the previous discussions that a critical
value of the Weber number is also usually required for droplet instability
and breakup. The Weber number (Equation 15) may be interpreted as
being approximately the ratio of the drag pressure to the surface-tension
pressure of a liquid drop.

4.   THEORY OF THE MECHANISM AND RATE OF BREAKUP OF
      LIQUID DROPS

4. 1   INTRODUCTION

A common assumption often made in discussing the breakup of liquids is
that when the maximum force tending to disrupt the liquid exceeds the
surface-tension force that tends to hold it together, the liquid will burst,
i. e., Equation 13 is often assumed to define the breakup criteria.   This
assumption was used in the classical work of Taylor (Reference 48), and
has also been used in many contemporary treatments of the breakup
process (e. g., Reference 49).   The assumption, however, is true only
for small rates of stress loading, and is not valid for high (e. g., shock)
loading rates, since the flow or breakup of a liquid has been shown experi-
mentally to be a rate process   Moreover, in any system in which the
stress tending to break the liquid undergoes a change in a time less than
the breakup time of the liquid, it will be expected that the assumption will
also be erroneous.

The preceding will be true in many situations involving shock-loading of a
liquid.   An examination of the various theoretical treatments of liquid
breakup summarized in the previous section shows that only hydrodynamic
and mechanic approaches have been pursued   Since the available evidence
suggests that the breakup of a liquid is a rate process, the breakup process
should perhaps be amenable to kinetic approaches heretofore not used
This consideration does not indicate that the hydrodynamics and
mechanics of the problem should be ignored   they should be incorporated
in the proper kinetic expression of the problem   The proper kinetic
model should be capable of predicting both the breakup times of the liquid
drop and the initial sizes of the resultant drops (perhaps without recourse
to assumptions previously necessary for solution of the problem).   in
any case, the expressions may allow a deeper elucidation of the roles of
both the physical properties of a liquid and the hydrodynamical properties
of the flow to the breakup characteristics of liquids

4.2   LIQUID FLOW AND BREAKUP AS RATE PROCESSES

Eyring (References 50 and 51) was one of the first to consider flow as a
rate process. He reasoned that for molecular flow to take place in a con-
densed material (solid or liquid), it is necessary that a suitable "hole"
or site be available for a molecule to "jump" or flow into. Production of
the holes was pictured as being brought about by thermal fluctuations of
the molecular energy, i.e., the molecular energy distribution continuously
provides a fraction of the molecules with enough energy to push their
neighboring molecules aside so as to form holes into which other molecules
will immediately jump.

An alternative picture was that in order for a molecule to jump to a
neighboring position, it has to acquire by chance a sufficiently high kinetic
energy (i.e., it must be activated), which enables it to leave the potential
sphere of its immediate neighbor to a new equilibrium position. In
either case, an (activation) energy of sufficient magnitude is required to
both form the holes or site of the new position and move the molecule into
the hole. Eyring argued that the energy required to form a hole of mole-
cular size in a liquid is equal to the energy of vaporization per molecule
of the liquid. He pointed out, however, that a distribution of hole sizes
will always be available as a result of thermal motion, and that it may
not necessarily require a hole of molecular size for molecular flow to
occur.

The absolute specific rate constant, k_r, for any thermal rate process was
derived by Eyring (References 51 and 52) in terms of molecular constants,
and is given by

$$k_r = K \frac{kT}{h} \frac{F^*}{F_i} \exp(-\Delta E^*_o/RT) = K \frac{kT}{h} \exp(-\Delta F^*/RT) \sec^{-1} \qquad (35)$$

where

    K = transmission coefficient

    k = Boltzmann's constant

    h = Planck's constant

    T = temperature (^{o}K)

    F^* = appropriate partition function for the activated molecular
           state

    F_1 = appropriate partition function for the initial molecular state

$\Delta E_o^* =$ difference in the zero-point energies of the initial and the activated state, i.e., the activation energy of the process at the absolute zero of temperature $(0^\circ K)$

$R \quad =$ gas constant

$\Delta F^* =$ Gibbs' free energy of activation when the initial and activated molecules are all in their standard states

Equation 35 gives the specific rate for any molecular thermal rate process. The reciprocal of the specific rate constant, i.e., $1/k_r$, is the time it takes for the specified molecular process to occur.

Eyring showed that to properly consider a flow process in a fluid as a rate process, the specific rate constant (Equation 35) must be interpreted as the frequency (specific rate) with which molecules jump in various directions as a result of thermal motion in the fluid when there is no applied stress. The influence of an applied shear stress on the specific rate was then incorporated by multiplying Equation 35 by an appropriate expression involving the shear stress. The resulting specific rate is

$$k_s = 2k_r \sinh \frac{L_2 L_3 L}{2kT} P_{xy} \sec^{-1} \qquad (36a)$$

also

$$L_2 L_3 L = L/N_a \qquad (36b)$$

where

$k_s \quad =$ absolute specific rate constant unde application of the stress

$P_{xy} =$ applied shear stress

$L_2 L_3 =$ effective area of a molecular "flow unit" on which the force is acting, i.e., the area of the flow unit in the shear plane

$L \quad =$ average jump distance of a molecular flow unit during the flow, i.e., the distance between two equilibrium positions in the direction of motion

$N_a \quad =$ average number of molecular-flow-unit bombs per unit area in the shear plane of the flow unit

$k_r \quad =$ thermal rate constant (Equation 35)

-25-

The influence of the applied stress is to lower the activation energy barrier, and hence the resistance to flow in the direction in which the stress is acting.

Liquid flow is the result of shear strain, and the net velocity of flow in the shear (axial) direction is

$$v = Lk_s \tag{37}$$

The rate of shear of the liquid is given by

$$dv/dr = ds/dt = v/L_1 = Lk_s/L_1 \tag{38}$$

where L_1 is the distance between the shear planes, and r is the radial distance. Thus, Equation 38 indicates that the shear rate is equal to the net number of molecular jumps/sec made by the flow unit in the shear direction, k_s, multiplied by the average distance traversed per jump, L, divided by distance between the fluid planes undergoing the shearing, L_1.

4.3 BREAKUP MECHANISM AND BREAKUP TIME OF LIQUID DROPS

When a liquid drop is subjected to a nonuniform pressure, a shearing of the liquid will occur if the pressure is sufficient to overcome the surface tension of the drop. The geometry of the liquid undergoing the shearing will depend on the (generally time-dependent) pressure distribution on the drop. When the drop is subjected to an aerodynamic fluid (gas) flow, the total drag force exerted on the drop is composed of two components, viz., the pressure drag due to the pressure distribution over the surface of the drop, and the friction drag due to viscous shear at the surface of the drop (Reference 53). It is natural to believe that these two individual stresses are responsible for the two (extreme) breakup behaviors of liquid drops, and in particular that the pressure drag produces bag breakup, while the friction drag is responsible for shear or stripping breakup. The preceding statement appears self-evident; however, the breakup mechanisms of liquid drops have never been explained in this manner before. In the following discussion, this concept is quantitatively developed.

-26-

When a liquid drop is subjected to an aerodynamic gas flow, the stress produced by the gas flow on and around the drop initially deforms the drop. It is known from photographic studies that the drop initially flattens on the leeward side, so that the drop diameter increases with increase in time, and then remains for a short time with an essentially constant diameter while liquid starts to be removed (sheared) from the drop and carried in the gas stream (Reference 36) The drop then starts to expand again this time very slowly with time while breakup is occurring It is known experimentally that the final (essentially stationary) drop diameter prior to breakup is only a weak function of the flow conditions and the properties of the liquid Although a knowledge of the exact shape and size of the flattened drop before shearing is not essential to the present studies, it is of interest to show that the rate and exent of flattening is a function of the Weber number, and includes a mechanism whereby the lateral flattening or spreading of the drop is impeded just prior to the breakup of the drop, thus allowing the gas-flow stress to alter the direction of the liquid flow with subsequent breakup of the liquid This initial deformation of the drop also appears to have an influence on the general mechanism (bag or shear) by which the drop is dispersed

The pressure causing the initial drop deformation is the air stagnation pressure, which is opposed by surface tension and viscous stresses of the deforming drop. The model used by Gordon to describe drop breakup (Reference 39) can be used to describe the drop deformation if the model is modified slightly Stagnation pressure produces the lateral flattening of the drop, and hence this pressure acts through a lateral shear stress The surface-tension pressure retarding the elongation arises from the shape of the drop at any arbitrary time but may be considered to originate mainly from the head of the laterally elongating liquid in the latter phases of elongation. The shear stress causing the deformation will be roughly one-half of the normal stagnation pressure

Velocity of the laterally flowing liquid (drop deformation rate) is hence given by Equation 23b. with a factor of 4 replacing 2 in the A term and a new (unknown) factor K replacing 8/d in the surface-tension expression of the A term For both simplicity and purposes of illustration, a liquid is considered with a low viscosity, so that the exponential term of Equation 23b may be expanded with the retention of only the linear term Integrating Equation 23b (assuming a constant averaged K-K') and considering the drop radius to be that of the original spherical drop R, when time is zero

$$ a - R \quad \frac{f a^{2}}{4 f d} t^{2} \quad \frac{K' \sigma}{2 f d} t^{2} \tag{39} $$

where a is the radius of the flattening drop at time t. Thus, the rate of lateral deformation of the drop is proportional to the difference of two terms that involve the stagnation pressure deforming the drop, and the surface-tension pressure resisting the deformation. For high gas flow or low surface tension, the surface-tension pressure will originally be small as compared with the stagnation pressure, in which case the deformation rate is proportional to the stagnation pressure and the square of the time, and inversely proportional to the liquid density and the drop diameter.

The preceding is, interestingly, the same functional dependence found by Burgers (Reference 36) for the deformation rate of the deforming drop. In fact, the pressure term in Equation 39 is identical to the expression developed by Burger, except that the Burger expression contains a factor of 3 in the denominator, whereas Equation 39 contains a factor of 2 (after the other factor of 2 is included in the stagnation pressure).

While the liquid drop is being flattened by the stagnation pressure, the curvature of the front of the deforming liquid increases. This change in curvature increases the effective surface-tension pressure resisting the drop deformation. When the curvature is sufficiently large, the drop ceases to elongate, and the aerodynamic stress then changes the lateral liquid flow to the horizontal direction, leading to shear and breakup of the liquid.

The value of K in Equation 39 should thus be replaced by a function of the deformation so that the surface-tension pressure increases with an increase in deformation. More accurately, this function should be included in Equation 23b before it is integrated to give Equation 39. The nature of the function depends on the geometry that the drop assumes during its deformation. This geometry is not known in detail, but an inspection of the available photographs on the behavior of liquid drops in gas flows suggests that the drops initially assume approximately the shape of one-half of an oblate spheriod (i. e , a lateral half of an ellipse rotated about its minor axis) before undergoing their final shearing leading to breakup If this sequence is roughly true, then the surface-tension pressure of the outer end of the oblate spheriod must support the aerodynamic flow pressure before the final shearing leading to breakup occurs.

Since the maximum radius of curvature of an oblate spheriod is R^6/a^5, the value of K in Equation 23b can be taken roughly to be a^5/R^6. The (essentially stationary) drop diameter just prior to breakup is then given by the solution of Equation 23b for $v = da/dt = 0$, i.e., for $1/2 \rho_a u^2 = \sigma a^5/R^6$. Therefore

$$a = W^{1/5} R \qquad (40)$$

-28-

where the Weber number is defined by Equation 15. This equation illustrates the insensitive nature of the deformed drop size on the gas-flow conditions and the physical properties of the liquid drop. Although Equation 40 gives only a rough quantitative representation of the experimental data, its overall general agreement with experiment is reasonable in view of the assumptions made, and indicates that a lateral-half oblate spheriod is not a bad approximation to the true shape of the deformed drop. While breakup of the drop is occurring, the drop continues to expand slowly.

For bag breakup, the formation and expansion of the bag aids the drop-deformation process; for stripping breakup, the shearing liquid helps weaken the surface-tension forces that prevent the drop from expanding.

Equation 39, as derived, is for low-viscosity liquids. It is known that the rate of drop deformation also depends on viscosity when the viscosity is large (References 30 and 31). The effect of viscosity is easily included by retaining the exponential term in the integration of Equation 23b.

Subsequent to the initial deforming of the drop, the liquid is either sheared away from the sides of the drop (stripping breakup), or the middle of the drop is sheared away from the sides (bag breakup). This shearing produces a stretching of the liquid to form a film which ultimately breaks to form droplets. The breaking of the film is a very fast process, and it is the rate of formation of this film by shear that thus controls the breakup time of the drop.

The rate of liquid shear is given by Equation 38. High shear stresses cannot be built up in liquids unless the liquid is extremely viscous, and hence the hyperbolic sine quantity in Equation 36a will always be a small number. Since $\sinh x \approx x$ for small x, $\sinh(LP_{xy}/N_akT) \approx LP_{xy}/N_akT$. Therefore

$$\frac{dv}{dr} = \frac{L^2 k_r}{L_1 N_a kT} P_{xy} \tag{41}$$

The rate of shear should be controlled by self-diffusion of the molecules of the liquid, since a molecular flow is involved in the formation of the film from the bulk liquid of the drop. If this assumption is true, then the coefficient of P_{xy} in Equation 41 can be shown to be identically equal to the reciprocal of the coefficient of viscosity of the liquid (References 50 and 51). Hence

$$dv/dr = P_{xy}/\eta \tag{42}$$

-29-

Equation 42 may be applied to the breakup of liquid drops as follows:
Consider a cylindrical tube of liquid of length d and radius R to be
shearing from a drop under the influence of an average pressure head
P_h. At any point whose distance from the axis of the tube is r, the shear
stress is related to the pressure head by $\pi r^2 P_h = 2\pi r d P_{xy}$. Hence

$$P_{xy} = P_h r / 2d \tag{43}$$

Substituting Equation 43 in Equation 42 and integrating under the condition
that $v = 0$ when $r = R$ (assuming dv/dr is negative) gives

$$v = P_h \ (R^2 - r^2)/4d\,\eta \tag{44}$$

The maximum velocity occurs at $r = 0$, and it is related to the pressure
head by

$$P_h = 4d\,\eta\,v/R^2 \tag{45}$$

The pressure head is the difference between the aerodynamic stagnation
pressure and the pressure required to provide the kinetic energy of the
liquid flow. Thus (Reference 54)

$$P_h = P - 1/2\rho_1 v^2 \tag{46}$$

Substituting Equation 46 in Equation 45

$$P = \frac{4d\,\eta\,v}{R^2} + 1/2\rho_1 v^2 \tag{47}$$

where the velocity gives the time rate of displacement of the liquid being
sheared from the drop. To obtain the proper order of magnitude for the
breakup time of the liquid being sheared, it is assumed that R is the
radius of the original liquid drop, and d is the drop diameter. Integrating
Equation 47 and assuming breakup to occur when the length of the tube
being sheared from the drop is 2d gives the breakup time

$$t = \frac{d}{(A^2 + BP)^{1/2} - A}$$ (48a)

where

$$A = 16\eta / d\rho_1 ; \ B = 2/\rho_1$$ (48b)

Equation 48a is a completely general expression for the breakup time; it may be compared to the general breakup-time expression of Gordon (Equation 24). The pressure expression will be of the form

$$P = 1/2 \, \rho_a \, u^2 C_D - k \, \sigma/d$$ (49)

where

u = relative velocity between the air stream and the liquid drop

ρ_a = density of the air stream

C_D = drag coefficient

σ = surface tension of the liquid drop

d = diameter of the original liquid drop before breakup

k = a constant that reflects the drop curvature during breakup (which determines the effective surface-tension pressure retarding the breakup)

Equation 48a may be greatly simplified for certain conditions. Thus, for liquids or flow conditions for which viscous and surface-tension forces are negligible (and for convenience assuming C_D to be unity) Equation 47 becomes

$$t = \frac{d}{u} \, (\rho_1 / \rho_a)^{1/2}$$ (50a)

This expression is very similar to that found by Gordon (Equation 25a), and also by Hinze (Equation 17) for similar conditions, differing essentially only in the value of the numerical constant preceding the function

-31-

(unity in Equation 50a). For extremely viscous liquids and negligible surface tension, Equation 48a becomes

$$t = 32\eta / \rho_a u^2 \qquad\qquad (50b)$$

This expression is identical to that of Gordon (Equation 25b), and differs from that of Hinze (Equation 18) only in the numerical constant.

Equation 48a, as derived, describes the shearing of a plug of liquid from a drop as a result of pressure being exerted on the middle (thus excluding the edges) of the drop. Hence, this equation will apply to the bag break-up of a drop. The same general expression, however, also applies to the shear (stripping) breakup, as may be shown by assuming dv/dr in Equation 42 to be positive and integrating under the condition that the velocity is zero when r is zero. This condition thus provides for the situation that the maximum pressure is exerted on the edges of the drop, as occurs in stripping breakup. Thus, there remains only to identify the pressure distribution and magnitude, using Equation 48a to delineate between the bag and stripping breakup mechanisms. Before considering these individual breakup mechanisms, however, it is necessary to examine certain aspects of Equations 48a and 49.

Equation 48a is a generalized expression for the breakup time of a liquid drop containing given physical properties and subjected to an aerodynamic flow with given properties. This equation is expected to be generally valid except when the liquid is extremely viscous, i.e., when the liquid is a solid. Under the latter condition, it is not permissible to replace the hyperbolic sine function of Equation 36a by the function itself, since very large shear stresses can be built up within the solid. In this case, Equation 36a must be used as written in integrating Equation 41 (final results are given in Reference 55), and the kinetic energy term in Equation 46 will usually be negligible. Thus, the presented theory for the breakup of liquids can also be used, with slight modification, to estimate the mechanical erosion (breakup) of solid particles in aerodynamic flows.

It is possible to use Equation 48a to predict the breakup time of a liquid drop without regard to the general mechanism (bag or stripping) if a suitable value is chosen for k in Equation 49. As will be shown later, Equation 48a is in very good agreement with all of the experimental data if the drag coefficient is considered to be unity, and the value of k is taken as about two. This equation thus affords a rapid calculation of the breakup time of a liquid drop to the accuracy with which it can be measured.

Photographs of the breakup process (provided in a subsequent section
of this report) show that a finite time exists between the time when the
liquid starts to break and the time when breakup is essentially complete
This time during breakup is often comparable to the time required for
the breakup to begin to occur Thus, there is some latitude in defining
an experimental breakup time for comparison with theory

For consistency and general accuracy, the experimental breakup time
has been taken to be the time between the aerodynamic flow hitting the
drop and the time at which breakup of the drop just starts to occur The
total breakup time, however, will usually be slightly larger, and it is
thus natural that the theoretical breakup time may be slightly larger than
the experimental breakup time. The latitude allowed in comparing experi-
ment and theory makes it difficult to check with great accuracy certain
points of the theory, such as the validity of the breakup criteria, as well
as the laminar-flow behavior implied by Equation 42 including the neglect
of end-effects and nonaccelerated flow (Reference 56) This latter
assumption may not be quite true, but photographs of the breakup process
suggest the acceleration to be very small, if any (after the initial liquid-
flow phase) The assumption of an accelerated flow is implicit in the
treatments of Gordon and of Hinze

The equations leading to Equation 48a have used the maximum liquid
velocity, rather than the average velocity, produced by a pressure on the
liquid. This usage is believed to be essentially correct, since employing
an average velocity implies that a parabolic velocity distribution has
been established in the flowing liquid However, the distances required to
establish this distribution are very large as compared to the size of a
liquid drop (Reference 54)

The effects of using the average velocity are easily estimated Average
velocity of liquid ejection is given by $v_a = \int vr\, dr / \int r\, dr$ Hence,
$v_a = R^2 P / 8d\, \eta$ If the average velocity is used, then the total kinetic
energy of flow is twice that used for the maximum velocity flow because
a parabolic velocity distribution is implied (Reference 54) Upon inte-
grating the equations it is found that if an average velocity is involved,
then a factor of $2^{1/2}$ and 2 should respectively be included in Equations
50a and 50b, and the factor of 2 should be removed from the B term in
Equation 48b These factors are generally smaller than the uncertainty
in measuring the breakup time

Another consideration is the value of the drag coefficient to be used in
Equation 49 An inspection of the available literature on the experimental
drag coefficients of various geometry bodies including solid spheres and
deformed liquids, shows that a rather range of values has been

found (References 36, 38, 53, 54, and 57 through 63). Many of the values reported are for steady flow, whereas accelerational drag forces may also be of importance. During the breakup of a liquid droplet, however, the shape of the drop changes continuously throughout the breakup; hence, only some suitable average drag coefficient can properly be used in the breakup-time expression.

In a later section of this report, experimental illustrations are provided showing the change of the drag-coefficient value during the breakup process. The value of the drag coefficient changes from less than unity to greater than unity during the breakup process, and for most practical work it seems sufficient to consider the drag coefficient to be unity. Rabin et al.(Reference 38) actually found the value to be essentially unity over a large range of conditions. The preceding shows that if the value k in Equation 49 is chosen properly, then Equation 48a is an adequate representation of all of the present experimental data if the drag coefficient is taken to be unity. For most practical work, therefore, this representation appears adequate.

As previously discussed, it is known from experiments that the breakup of a liquid drop may occur from either of two (extreme) mechanisms, viz., bag or stripping breakup. An adequate model of liquid-drop breakup should provide an explanation of these two mechanisms; the explanation proposed here is that bag breakup is the result of pressure drag, whereas stripping breakup is the result of friction drag. Thus, two individual expressions of the form of Equation 48a may be written for the breakup time of a liquid drop, with one expression containing the pressure-drag stress in the pressure expression (Equation 48b), and the second expression containing the friction drag stress in the pressure expression. Breakup of a liquid drop with given physical properties by an aerodynamic gas flow with given properties will occur by the mechanism that takes place with the fastest rate, i.e., with the shortest breakup time. When the rates are comparable, the drop should exhibit both bag and stripping breakup behaviors.

A quantitative description of the dual mechanism proposed for liquid-drop breakup requires a knowledge of the average (effective) stress distribution on the drop undergoing breakup. The details of this distribution are not fully understood, but a theoretical study by Tomotika and Aoi (Reference 64) indicated that for a sphere, the frictional drag is twice the pressure drag for all Reynolds numbers. It is assumed that this explanation is also true for liquid drops undergoing breakup, even though the shape deviates from that of a true sphere. The total drag stress on the drop during breakup is given by $1/2 \, \rho_a \, u^2 \, C_D$, and hence for bag and stripping breakup, the pressure expression given by equation 49 may be written.

-34-

$$P_b = (1/3) \left(\frac{1}{2} \rho_a u^2 \right) C_D - k_b \sigma/d \tag{51a}$$

$$P_s = (2/3) \left(\frac{1}{2} \rho_a u^2 \right) C_D - k_s \sigma/d \tag{51b}$$

where k_b and k_s are constants that reflect the surface-tension pressure tending to hold the drop together during bag and stripping breakup

If the frictional drag is always greater than the pressure drag, as indicated by Tomotika and Aoi, then it may be imagined that liquid drops should always undergo stripping breakup. Since the preceding is not true, it is indicated that the surface-tension pressure holding the drop together at its edges is greater than in its middle, i.e., that $k_s > k_b$. In the early part of this section, however, it has already been shown that the initial drop deformation produces a greater curvature at the outer edge of the drop than in its middle, and hence the surface-tension pressure holding the outer edges of the drop is greater than in the middle. It is thus known semiquantitatively that k_s must be greater than k_b.

A calculation of k_b and k_s would require a detailed knowledge (which is unavailable) of the effective shape of the liquid drop during its breakup. However, a theoretical calculation of these constants is presently of little value, since the true stress distribution on the drop undergoing breakup is not known, but rather assumed to be that of a solid sphere. The values of these constants are later determined by a best fit of Equations 48a, 51a, and 51b to the experimental breakup data. In anticipation of these results, respective values of about 4 and 2 were found for k_b and k_s; these values may be employed in using the preceding equations to predict breakup times for drops undergoing either bag or stripping breakup.

A consequence of the dual-breakup mechanism given by Equations 51a and 51b is that at low air-flow velocities, the drop will usually (depending on drop size) undergo bag breakup because the drop-edge surface-tension forces prevent stripping breakup, whereas as the air velocity is further increased, the stripping breakup becomes faster as a result of the overall greater friction stress. The equations also predict the influence of the various other parameters on the breakup mechanism. The predicted behaviors can be observed experimentally.

4.4 INITIAL DROP SIZES PRODUCED BY DISPERSION OF LIQUID DROPS

Two considerations are usually of prime interest in the aerodynamic breakup of liquid drops, viz., the time required to produce the breakup as a function of the air-flow properties and the physical properties of the drop, and the sizes of the resultant droplets produced from the dispersion of the original drop. A quantitative description of the breakup process was developed in the previous section; the following discussion treats the initial mean drop size produced by the (primary) breakup of the original drop.

The drop size produced by primary breakup may differ from the mean drop size, which may be measured at any arbitrary time after the breakup of the drop. Thus, in addition to the drop sizes produced by the primary breakup process, the drop sizes present at any arbitrary time will depend on the following:

a. Secondary breakup of drops produced by the primary breakup (which in turn depends on the properties of the gas flow, e.g., its duration).

b. Vaporization of the primary and secondary drops.

c. Coalescence of the primary and secondary drops.

d. Settling or removal of drops by winds, etc.

The secondary breakup of primary drops can be estimated from considerations involved in the primary breakup process if the gas-flow properties are known, and the remainder of the factors may often be estimated from present knowledge. Therefore, this discussion is confined to the drop sizes produced by the primary breakup.

As discussed in the previous section, the aerodynamic breakup of drops may come about through either the bag or stripping mechanisms. Both mechanisms are believed to be the result of a shearing of the liquid drop by a nonuniform pressure distribution produced by the aerodynamic flow on the drop. This shearing produces a liquid film, which subsequently breaks to give the resultant drops. The breakup time of the drop is controlled by the rate of formation of this liquid film, since the actual breaking of the film is a fast process; however, the geometry of this film, together with the manner in which the film breaks, are the determinants of the resultant droplet sizes.

Although it would appear that the drop sizes produced by the two breakup mechanisms should differ, the present model suggests that they obey essentially some mathematical size-distribution law. Moreover, experimental data obtained in the present studies (to be presented later) suggest that the mean diameter of the resultant droplets produced by the primary breakup of liquid drops from both bag and stripping mechanisms obey (within experimental error) the same mathematical expression for the resultant drop size as a function of gas flow and liquid properties. This suggestion also appears consistent with the observations that a liquid film from which the droplets are produced is formed in both mechanisms, and that the breakup time is essentially monotonically continuous in the transition between the two mechanism's breakup behaviors. For the present study, therefore no distinction is made between the two breakup mechanisms in treating the resulting droplet sizes, and it appears that more experimental drop-size data are required to warrant distinguishing the two mechanisms in the future

Another consideration concerns the manner of describing the droplet sizes produced by the primary breakup process. It is experimentally known that a distribution of droplet sizes is produced, and, ideally, a theory should provide a function that predicts the droplet-size distribution as a function of the gas-flow and liquid drop properties. Although it was not possible to attain this goal during the present studies experimental examples of the distribution are included in a later section

In most theories of liquid breakup, including the treatment to follow, it is assumed that breakup is brought about by instabilities (vibrations) that grow (or decay) with time. The (optimum) wavelength that grows the fastest leads to breakup of the liquid, with the subsequent formation of droplets. This wavelength defines a mean or most probable droplet size, and it is this average that is computed here. However it may be noted that a distribution of instability wavelengths is always present, and these values lead to a distribution of droplet sizes. A knowledge of the mean size allows the remaining size distribution to be estimated (References 1 through 4 and 65).

The following discussion presents the general model considered to describe droplet formation during the primary breakup of liquid drops. This model is based primarily on the stripping breakup of a drop, but essentially the same view may be taken in describing the droplet sizes from bag breakup. The shear stress at the outer surface (or middle) of the drop produces a boundary layer of flowing liquid of average thickness δ. This liquid layer (sheet) upon leaving the drop experiences a small divergence (expansion), which breaks the sheet into individual

strips of average width W. Simultaneous with the ejection of the liquid boundary layer from the drop and its divergence, the parallel gas flow along the surfaces of the layer induces instabilities (vibrations) in the layer in the lengthwise direction. The optimum wavelength instability, λ, grows most rapidly and breaks the layer into pieces of average size $W \delta \lambda$. Surface-tension forces then produce spherical drops with an average diameter, D, from these pieces; thus, $\pi D^3/6 = W \delta \lambda$, or

$$D = \left[6W\delta\lambda / \pi \right]^{1/3} \tag{52}$$

Photographs of the breakup process roughly support the proposed model.

The value of λ has been calculated from the hydrodynamic equations by Squire (Reference 23), who found

$$\lambda = 4\pi \sigma / \rho_a u^2 \tag{53}$$

where

σ = surface tension of the liquid

ρ_a = air density

u = air velocity

The value of δ follows from the breakup model given in the previous section. The shearing of the liquid follows Equation 42. Breakup of the liquid film is assumed to occur when the sheared film traverses a distance equal to the drop diameter, d, producing a triangular-shaped film thickness that varies from zero to δ, or an average thickness of $\delta/2$. Thus, Equation 42 becomes

$$\frac{d}{t(\delta/2)} = \frac{P_{xy}}{\eta} \tag{54}$$

For simplicity, liquids are considered whose viscosity and surface-tension forces are small as compared with the aerodynamic flow forces involved. This consideration includes most practical situations of

-38-

interest. The value of t is then given by Equation 50a, and the shear stress may be considered to be roughly the stagnation pressure, $1/2\rho_a u^2$. Hence

$$\delta = 4\eta / u \, (\rho_a \rho_1)^{1/2} \tag{55}$$

The value of W may be estimated as follows: Consider an arc of length S in the plane of the liquid sheet leaving the liquid drop. From geometry, $S = r\,\theta$, where r is the distance to a point defining the radius of curvature of the arc, and θ is the angle subtended by the arc. Consider the arc to undergo expansion in time t as a result of the divergence of the film; thus, $ds/dt = \theta \, dr/dt$. The derivative dr/dt is the velocity of the liquid sheet, v, whereas dS/dt defines a critical velocity, v_c, for breakup of the sheet into strips. Thus, $v_c = \theta v$.

The distance around the drop comprises 2π radians, and hence the number of strips $N = 2\pi / \theta = 2\pi v / v_c$; the numerical distance around the drop is πd, and hence $W = \pi d / N = dv_c / 2v$. For liquids, as in the preceding, having low viscous and surface-tension forces as compared with the aerodynamic flow forces $\rho_a u^2 = \rho_1 v^2$ (from Equation 47), an expression that defines v in the W expression. The value of v_c may be obtained from this expression and the conventional equation defining the critical aerodynamic velocity required for liquid breakup, i.e.,

$$1/2 \, \rho_a u^2 C_D = 4\sigma/d \tag{56}$$

For simplicity, C_D is considered to be unity. Neglecting the small variation of air density with air velocity

$$W = \frac{d}{2u} \left[8\sigma/d \, \rho_a \right]^{1/2} \tag{57}$$

Combining Equations 52, 53, 55, and 57 gives the average (mass mean) diameter of the droplets produced by the aerodynamic breakup of a liquid drop

$$D = \left[\frac{136\eta \, \sigma^{3/2} \, d^{1/2}}{\rho_a^2 \, \rho_1^{1/2} \, u^4} \right]^{1/3} \tag{58}$$

-39-

Equation 58 was derived for conditions where the aerodynamic flow forces are much larger than the viscous and surface-tension forces (this situation comprises most cases of practical interest, If the liquid viscosity is very great, or if the flow velocity is low and the surface tension is high, then Equation 58 as written may not be valid. In such cases, the various approximations indicated in the derivations should be replaced by the more exact expressions. However, it is possible that Equation 58 may also hold approximately for these cases, since various approximations and errors often have a habit of canceling themselves partially out in a multiparameter expression. In any event, the cube-root dependence of Equation 58 attenuates large changes

It is possible that the factor 136 in Equation 58 should be modified, since various approximations and assumptions are manifested in its value. These considerations include the shear length required for breakup, the value of drag coefficient used, and the relation of shear stress to stagnation pressure. The cube-root dependence, however, again makes such changes secondary.

Equation 58 has two points of special significance. The first is the prediction that the average droplet size produced varies inversely as the 4/3 power of the relative velocity between the gas stream and the liquid. The careful work of Weiss and Worsham (Reference 19) actually disclosed such a relationship, which is further expressed by the theory of Mayer (Reference 46). Evidence is thus accumulating for the support of this velocity-droplet diameter relationship.

The second point of interest in Equation 58 is the prediction that the droplet diameter should vary directly as the 1/6 power of the initial droplet diameter. (This relationship was found experimentally for liquid jets by Weiss and Worsham.) Equation 58 gives good agreement with the data of Weiss and Worsham, as quoted by Mayer It will later be shown that this equation is in good agreement with all of the droplet-size data obtained under the present program.

5   EXPERIMENTAL PROGRAM

5.1   DESCRIPTION OF APPARATUS

5.1.1   Shock-Tube Studies

The rapid development of shock-tube technology in recent years has led
to wide acceptance of the shock tube as a means of inexpensively pro-
ducing accurately controlled, compressible flow conditions of short
duration   Properly designed, the shock tube can be used to generate
flows that may be varied over rather wide ranges without necessitating
the use of complex hardware or sophisticated instrumentation

Data from experimental studies made on the performance of shock tubes
of various sizes and operating ranges have verified that the flow conditions
correspond very closely with values predicted by theory. For all but the
most precise investigations, it is necessary to measure only (1) the
compression and expansion-chamber ambient pressures and temperatures,
and (2) the shock velocity to determine with sufficient accuracy the flow
conditions in the test zone.   The duration of flow can be determined from
the flow parameters and the lengths of the various portions of the shock
tube.

A brief discussion of shock-tube theory is presented in Appendix A of
this report.   Because literature on shock-tube theory is easily available,
the discussion in Appendix A has been limited to a qualitative description
of the flow in the shock tube, a presentation of the equations describing
the flow parameters, and the equations used in determining the duration
of flow

The shock tube used in this study (Figure 1) employs a 29-in -long
compression chamber made of steel pipe (4.5-in   OD x 4-in   ID). The
end of the compression chamber that joins the diaphragm holder con-
tains a transition section to provide a smooth transition in flow from
the circular cross-section of the pipe to the 2-in -sq cross-section of
the diaphragm holder and expansion chamber

The 55-in -long expansion chamber comprises the four following sections

a.   The diaphragm holder (a 2-in -thick piece of micarta)

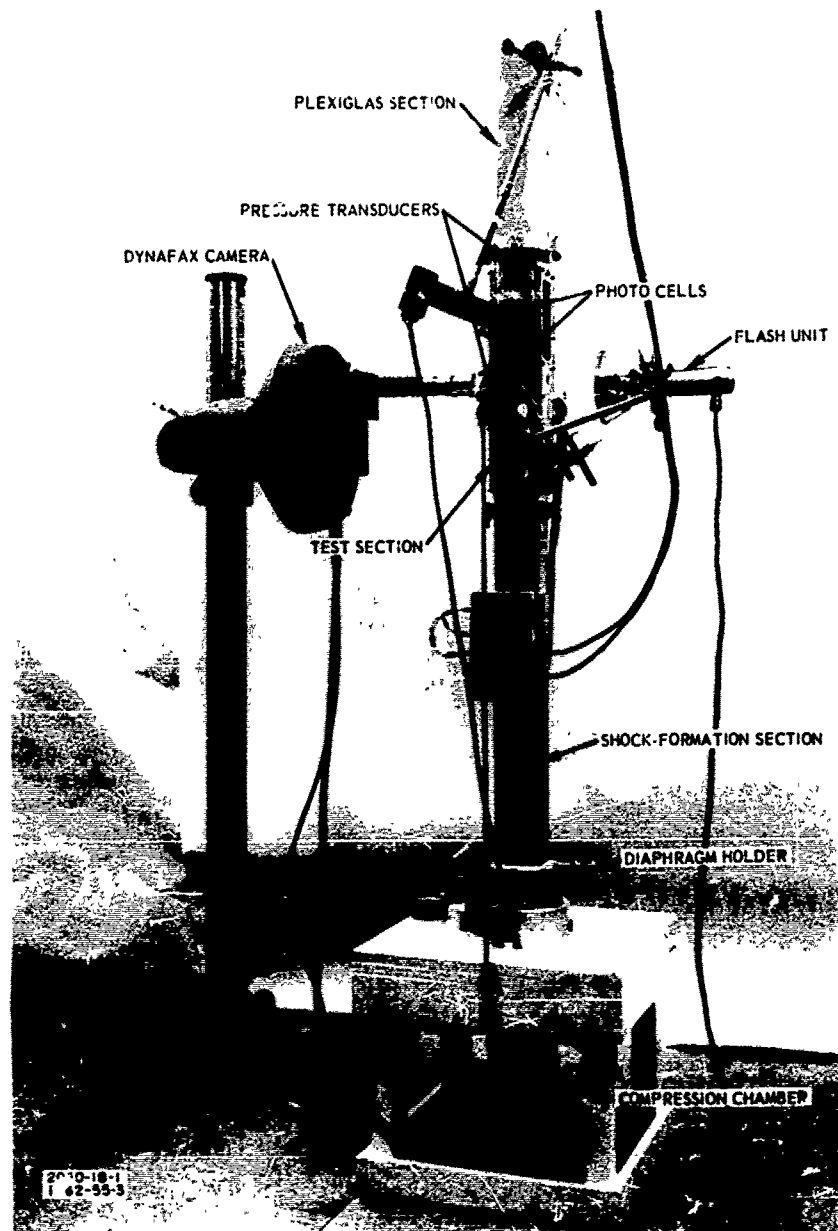b.   A 24-in -long shock formation section with 0 5-in.-thick steel
      walls

-41-

PLEXIGLAS SECTION

PRESSURE TRANSDUCERS

DYNAFAX CAMERA

PHOTO CELLS

FLASH UNIT

TEST SECTION

SHOCK-FORMATION SECTION

DIAPHRAGM HOLDER

COMPRESSION CHAMBER

Figure 1. Shock-Tube and Dynafax Camera.

-42-

c   A 17-in -long test section containing viewing windows

d   A 12-in.-long section made of 0 5-in -thick plexiglass

The expansion chamber is open-ended, permitting the flow behind the shock wave to exhaust to the atmosphere

5.1 2   Diaphragm Holder

Efficient operation of the shock tube requires very rapid removal of the diaphragm separating the compressed gas in the compression chamber from the gas of lower pressure in the expansion chamber   Removal of the diaphragm results in the formation of a plane shock front, which moves into the expansion chamber   Behind the shock is a region of constant flow velocity, pressure, temperature, and density (the region normally used as the test zone)

Bursting or releasing the diaphragm can be accomplished by several methods   (1) static overpressure, causing mechanical failure, (2) puncturing the diaphragm material with a pointed object, initiating mechanical failure, (3) shock overpressure, which exceeds the strength of the material, and (4) electrical discharge or exploding wires   The latter method was chosen for use in this study   Three-mil-diameter Nichrome wire, sandwiched between layers of plastic, was exploded to melt and cut the plastic to initiate opening of the diaphragm

Mylar sheet plastic, of 0 5 and 1 mil thicknesses was selected as the diaphragm material, since it is easily ruptured and does not shatter into fragments that may be carried into the test zone   Pressure tests showed that a 0.5-mil thickness of Mylar stretched over a 2- x 2-in opening is capable of withstanding approximately a 15-psi pressure differential before rupturing, and that the maximum differential is proportional to diaphragm thickness regardless of whether the total thickness is in one layer or several

Figure 2 shows the various components of the diaphragm holder and the wire-positioning jig   which was used to determine the proper length of exploding wire and to ensure its proper position while being fastened to the eyelets on the high-voltage terminals   The eyelets can be seen protruding into the 2-in -sq opening in the micarta base

Figure 3 shows the wire-positioning jig being used to prepare a specimen diaphragm and exploding wire   A single sheet of plastic, placed over the opening in the micarta base, is held in place with small dabs of silicone
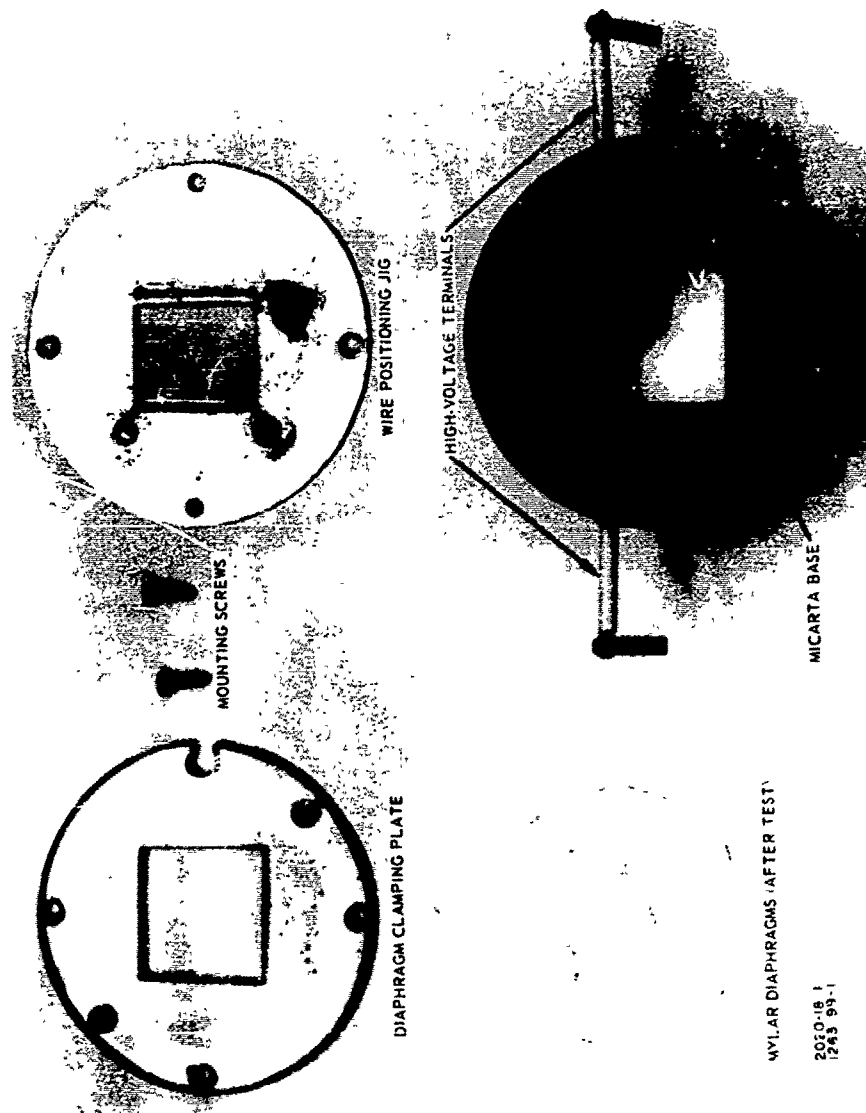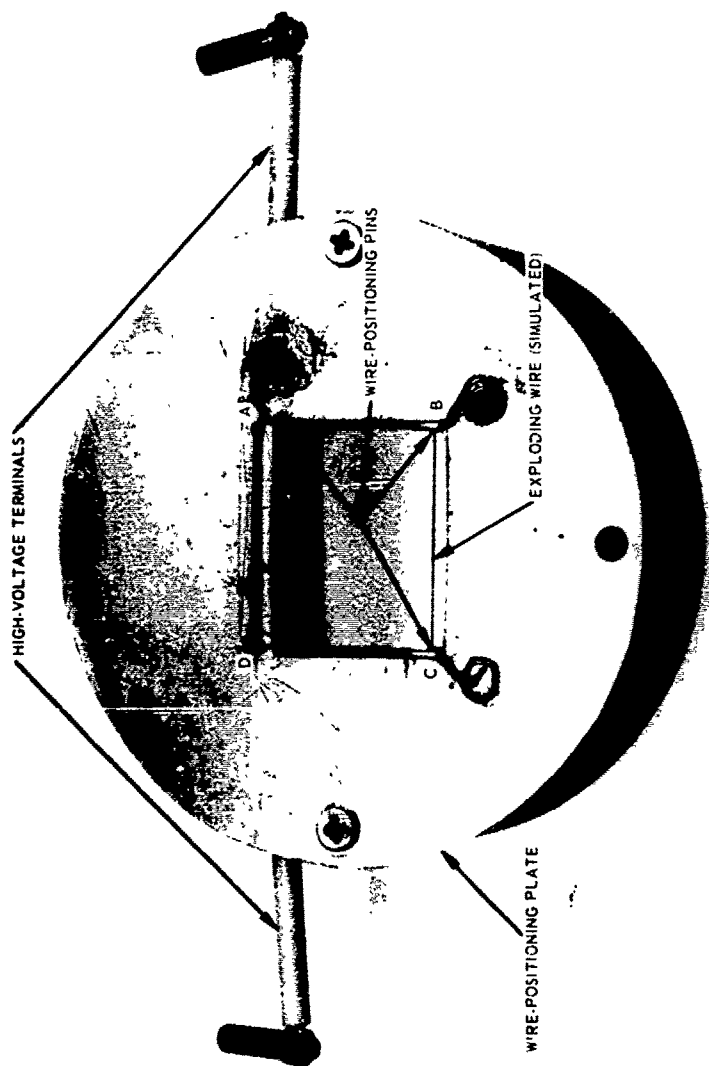
WIRE POSITIONING JIG

MOUNTING SCREWS

DIAPHRAGM CLAMPING PLATE

HIGH-VOLTAGE TERMINALS

MICARTA BASE

MYLAR DIAPHRAGMS (AFTER TEST)

2050-18-1
1243 99-1

Figure 2. Diaphragm Holder Component.

HIGH-VOLTAGE TERMINALS

WIRE-POSITIONING PINS

EXPLODING WIRE (SIMULATED)

WIRE-POSITIONING PLATE

Figure 3. Use of Wire Positioning Jig

grease (or similar agent); the wire-positioning jig is then placed over the plastic and oriented such that the enlarged holes at the ends of Slot AD (shown in Figure 3) are directly over the eyelc. .n the high-voltage terminals.

One end of the exploding wire is threaded through Hole A and a small perforation in the sheet of plastic, and is attached to the eyelet on the high-voltage terminal. The wire is then pulled taut and is passed around the 2-in.-sq opening so that the positioning pins at A, B, and C catch the wire and hold it in position   The loose end of the Nichrome wire is then passed down through Hole D and the plastic sheet, threaded through the terminal eyelet, and tied or wrapped snugly. The wiring steps can be expedited by running the Nichrome wire through a 6-in length of capillary tubing (0 0625-in OD x 0 036-in ID), which can then be used as a needle to puncture the plastic and thread the wire through the eyelets.

After the wire is in position and fastened to the high-voltage terminals, the wire-positioning jig is removed by slipping the Nichrome wire off the positioning pins and lifting the jig away from the micarta base   The loop of exploding wire slips through Slot AD and is left attached in position. A second sheet of plastic is then placed over the first, with th loop of exploding wire sandwiched between the sheets of Mylar. The diaphragm-clamping plate is placed over the plastic and is held in place with two screws. Figure 4 shows the diaphragm holder, complete with a specimen diaphragm and simulated exploding wire

The Nichrome wire is exploded by connecting the voltage terminals across a capacitor, which is charged to a high voltage   A short experimental study was made to determine the optimum energy to use in exploding the wire; too much energy initiated shock waves from the explosion of the wire, while low energy caused the wire to burn slowly, introducing time-delay problems. It was determined that a 9-μf capacitor charged to 1.2 kv provided sufficient energy (6 5 j) to explode the Nichrome wire (35 to 40 ohms dc resistance) without time delay or shock-wave effects

Appearance of the diaphragm after a test run is shown in Figure 5; as illustrated, the explosion of the wire cuts a door, hinged along one side, that opens to release the air from the compression chamber

Behavior of the diaphragm during the opening sequence was investigated by aking high-speed motion pictures of the process   These tests, the results of which are shown in Figures 6 and 7, were made with the expansion section removed and the cam·· placed to view the diaphragm
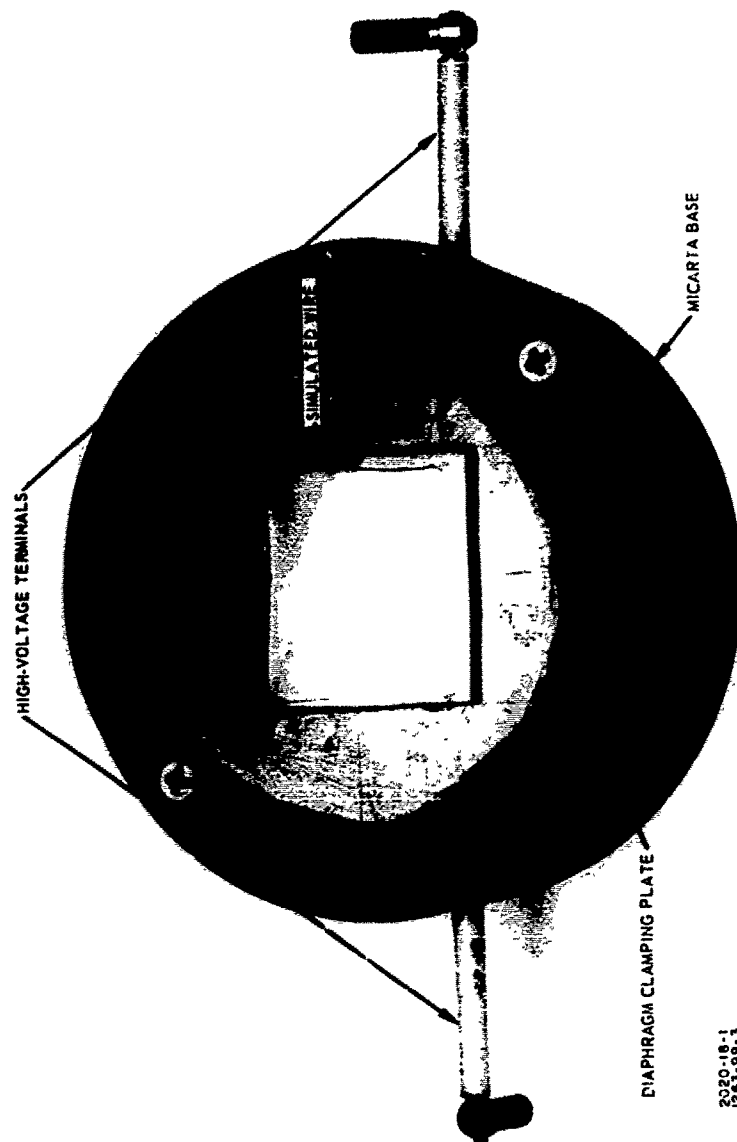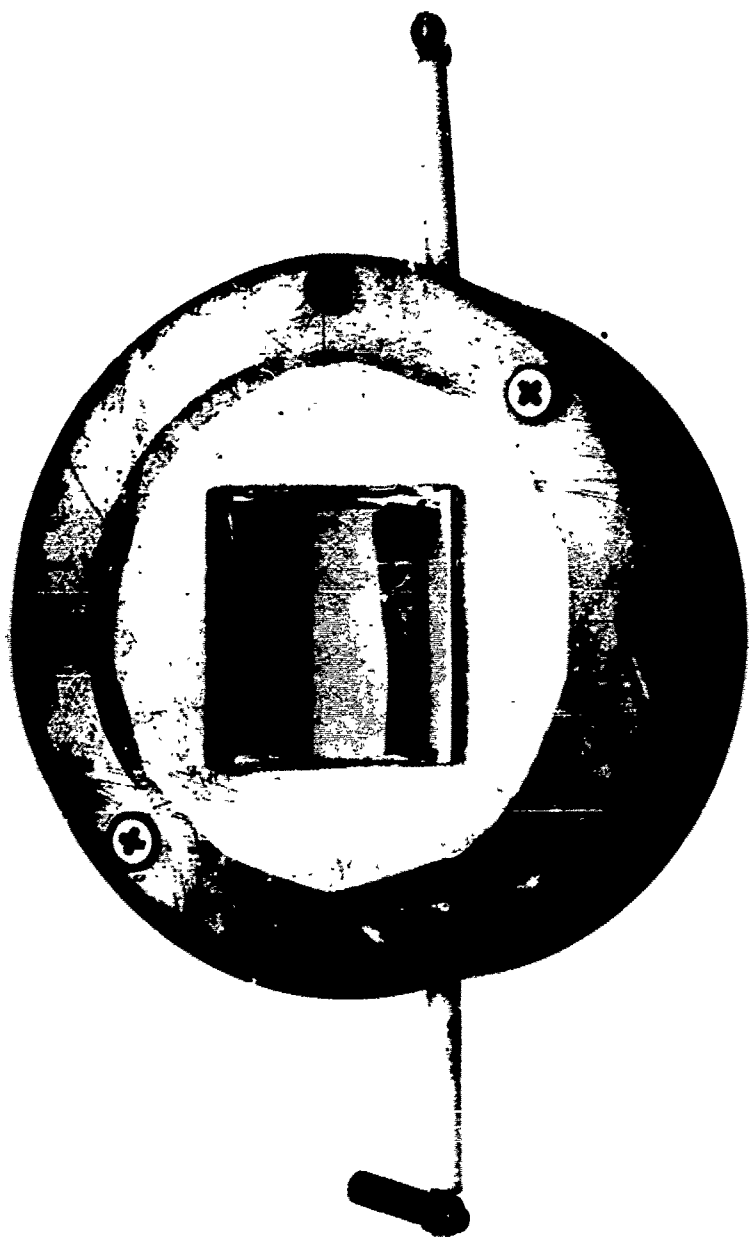
HIGH-VOLTAGE TERMINALS

MICARTA BASE

DIAPHRAGM CLAMPING PLATE

2020-18-1
1263-99-3

Figure 4. Diaphragm Holder.

-47-

Figure 5. Diaphragm After Test.

TEST NO. 219

P=3.1 PSIG
DIAPHRAGM - 2 LAYERS OF 1/2 MIL MYLAR
EXPLODING WIRE - 3 MIL NICHROME (~40 ohms)
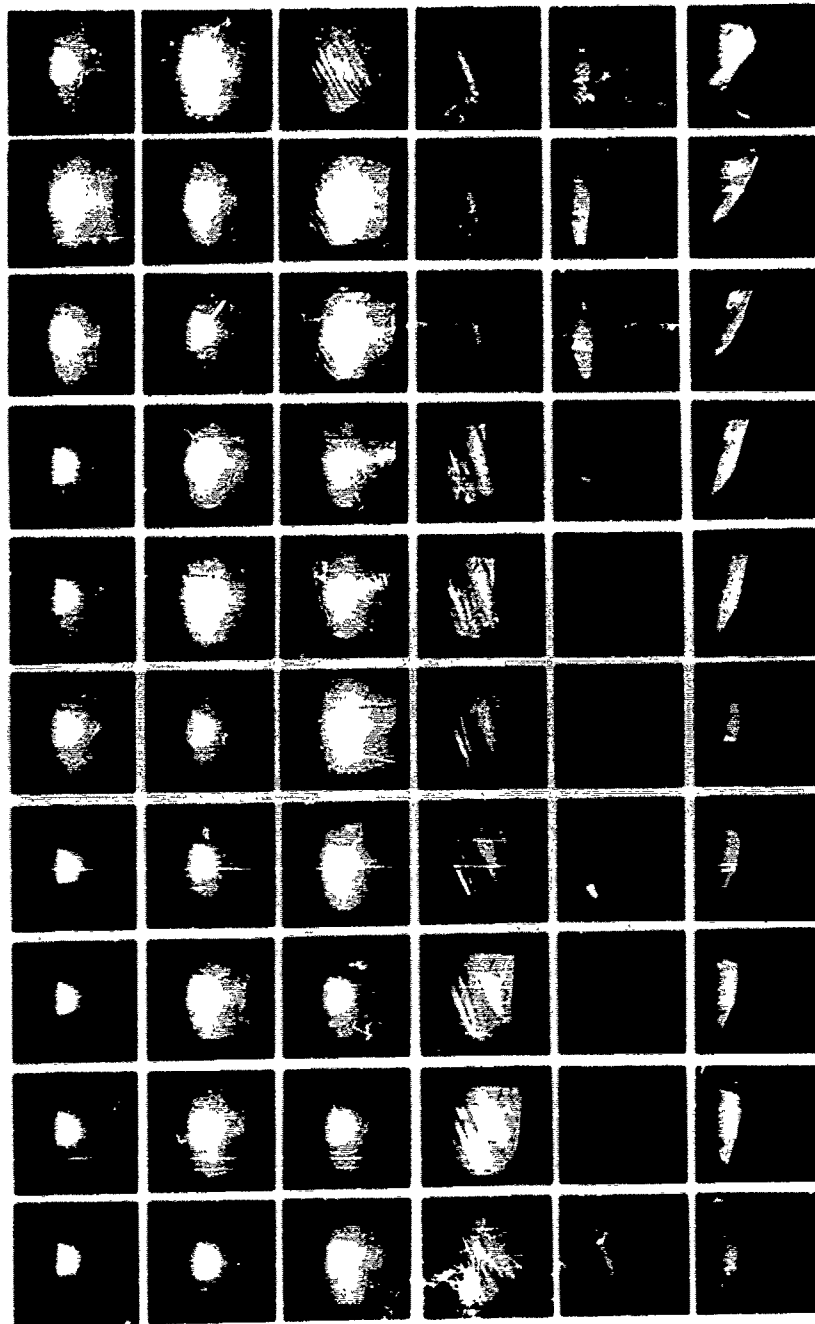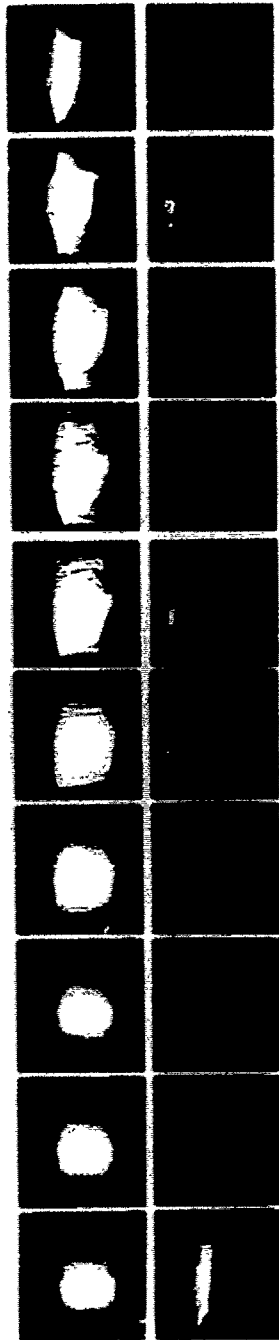ENERGY - 9 μf at 1.2 KV.

0.0781 MSEC/FRAME

Figure ⑴ Diaphragm Opening at Low Pressure

-49-

TEST NO. 221

P=7.5 PSIG   0.0782 MSEC/FRAME
DIAPHRAGM - 2 LAYERS OF 1/2 MIL MYLAR
EXPLODING WIRE - 3 MIL NICHROME (~40 ohms)
ENERGY 9 μf at 1.2 KV.

TEST NO. 222

P=12 PSIG   0.0781 MSEC/FRAME
DIAPHRAGM - 2 LAYERS OF 1/2 MIL MYLAR
EXPLODING WIRE - 3 MIL N CHROME (~40 ohms)
ENERGY 9 μf at 1.2 KV.

TEST NO. 223

P=17.5 PSIG   0.0780 MSEC/FRAME
DIAPHRAGM - 2 LAYERS OF 1/2 MIL MYLAR
EXPLODING WIRE - 3 MIL NICHROME (~40 ohms)
ENERGY 9 μf at 1.2 KV.

Figure 7. Diaphragm Opening at High Pressure.

-50-

from a position on the shock-tube axis looking toward the compression chamber. The 2- x 2-in. diaphragm is shown as it is cut along three sides by the exploding wire and begins to open out of the plane of the picture. The normally transparent Mylar plastic of the diaphragms was made opaque for these tests by spraying the undersurface with flat white and silver paint

Figure 6 shows the opening sequence for a pressure of 3.1 psig in the compression chamber, and Figure 7 contains the sequences for pressures of 7.5, 12, and 17.5 psig. The first frame in each sequence represents the instant at which the electrical energy was applied to the terminals to explode the wire. Electrical arcing at the junction of the exploding wire with the terminals was visible after approximately 0 25 ms or less in all of the tests. With the exception of the test conducted at the lowest pressure, initial rupture and movement of the diaphragm occurred within 0 3 ms, and complete opening occurred in less than 1 ms.

At 3.1 psig, the sequence was considerably delayed, even though noticeable arcing and burning occurred at the same time as evidenced in tests performed at higher pressures Significant rupture and movement of the diaphragm did not occur until after approximately 2 ms elapsed, and the opening was not completed until approximately 3.4 ms elapsed The opening, from initial rupture to completion. required approximately 1 5 ms.

Another noticeable feature in Figure 6 is the apparent reclosing of the diaphragm, an effect that can be seen in the last row of frames in the sequence. This reclosing is apparently due to reverse flow, which was caused by the slight vacuum created by the inertia of the air rushing out of the compression chamber.

It must be remembered that the absence of the expansion chamber creates a different flow history than would be expected with the chamber in place; however, the data in Figures 6 and 7 should be valid for the initial opening phases of the diaphragm.

5.1.3   Instrumentation

The instrumentation used in this investigation does not necessarily represent the combination of components that would normally be selected for use in a shock-tube study of this nature There are various other well-tried methods of acquiring shock-tube operating data that, because of economic, space, or time considerations, might be more desirable These methods are described in detail   in any of the texts and reports on shock tubes (References 66 through 70).

Items of equipment used in this study were all readily available and fulfilled the various requirements for operating voltages, response times, and accuracy. It was, therefore, more expedient to adapt the experimental techniques to fit the available instrumentation rather than to acquire instrumentation to fit the experimental need.

The following equipment was employed during the studies:

a. One Beckman Whitley Model 326-3 Dynafax Camera

b. One Beckman Whitley Model 357 Electronic Flash Unit

c. Two Endevco Model 2501-500 Piezoelectric Pressure Trans-
    ducers

d. Two Photo 1P39 Tubes

e. One Tektronix Model 545 Oscilloscope (with Type 53/54C Dual-
    Trace Preamp and Polaroid Camera)

f   Two Beckman Model 7370 Counters

g. Two Shasta Model 854R Wide-Band Amplifiers

h. One Precision Laboratory Test Gauge (0 to 30 psig; 1/4% full-
    scale accuracy)

i. One High-Voltage Firing Panel (Model 177)

The Beckman Whitley Dynafax Camera is a continuous-writing fram-
ing camera, capable of framing rates of from 200 to 26,000 frames/sec
with shutter speeds of 1.0, 2.5, or 5.0 μsec at maximum framing rate.
This camera has a picture capacity of 224 frames of standard 16mm
frame size on a 33-7/8-in length of 35mm film. The total writing time
available varies from 1.12 sec at 200 frames/sec to 8.62 ms at
26,000 frames/sec.

A Wollensak Raptar f/2.8, 3-in. Telephoto lens (Figure 1) was used for
all of the tests, although various lens-extension lengths were required
at times to obtain the desired magnification and field of view.

Camera speed is controlled by a variac in the camera base, and the
framing rate is indicated directly on a meter on the front of the camera.
More accurate determination of the framing rate can be made by moni-
toring the frequency of an ac-voltage output. from the camera. The
frequency of the ac voltage is equal to the speed of the rotating mirror in
the camera, and is directly related to the framing rate.

-52-

The Beckman Whitley, Model 357, Electronic Flash Unit (Figure 8) is a light source that is designed for use with the Dynafax camera. This unit is capable of supplying single, square pulses of high-intensity, cold light of adjustable duration. Pulse durations available are 8.60, 11.15, 14.85, and 22.35 ms, with rise and decay times of approximately 25 μsec (less than the frame separation at the highest framing rate).

Five methods of triggering the light source are available: (1) making contact between the triggering wires, (2) breaking contact between the triggering wires, (3) using a positive-voltage pulse, (4) increasing the illumination that falls on a photocell (1P39) supplied with the unit, and (5) decreasing the illumination that strikes the photocell. The latter method of triggering was used in this study; the falling drops of liquid were permitted to interrupt a beam of light that was focused on the photocell.

Figure 9 shows the arrangement of the photocell and light beam. Light from an automobile-headlamp type of bulb in the light source is focused into a beam by lenses mounted in the light-source tube, and is directed across the center of the test section through holes in the test-section wall to strike the photocell tube. Interruption of the light beam generates a voltage change, which triggers the flash unit.

Shock-velocity measurements were made during each test by monitoring the shock front time-of-arrival at two pressure transducers, mounted 14.25 in. apart in the test-section wall. These transducers (Figure 10) behave electrically as capacitors whose charge is directly proportional to the pressure applied to the transducer face (as a result, they respond only to pressure changes). With proper impedance matching and control of system RC time constants, the transducers can be calibrated to accurately measure both the magnitude and time history of a rapidly fluctuating pressure. For purposes of this study, it was only necessary to use the transducers to sense the step change in pressure that occurred as the shock front passed over the transducer face.

Because the transducer signals were too small (4 to 200 mvolts) to consistently trigger the oscilloscope and counter, it was necessary to amplify the signals by passing them through Shasta Wide-Band amplifiers (Figure 8) set at a gain of 40 db. Output signals from the Shasta amplifiers were fed into both the Beckman Model 7370 Counter and the Tektronix oscilloscope (also shown in Figure 8). The signal from the lower transducer was used to start the counter, which had been set on the "Time B-A," mode and to trigger the sweep of the oscilloscope; the signal from the upper transducer, used to stop the counter, was fed into the
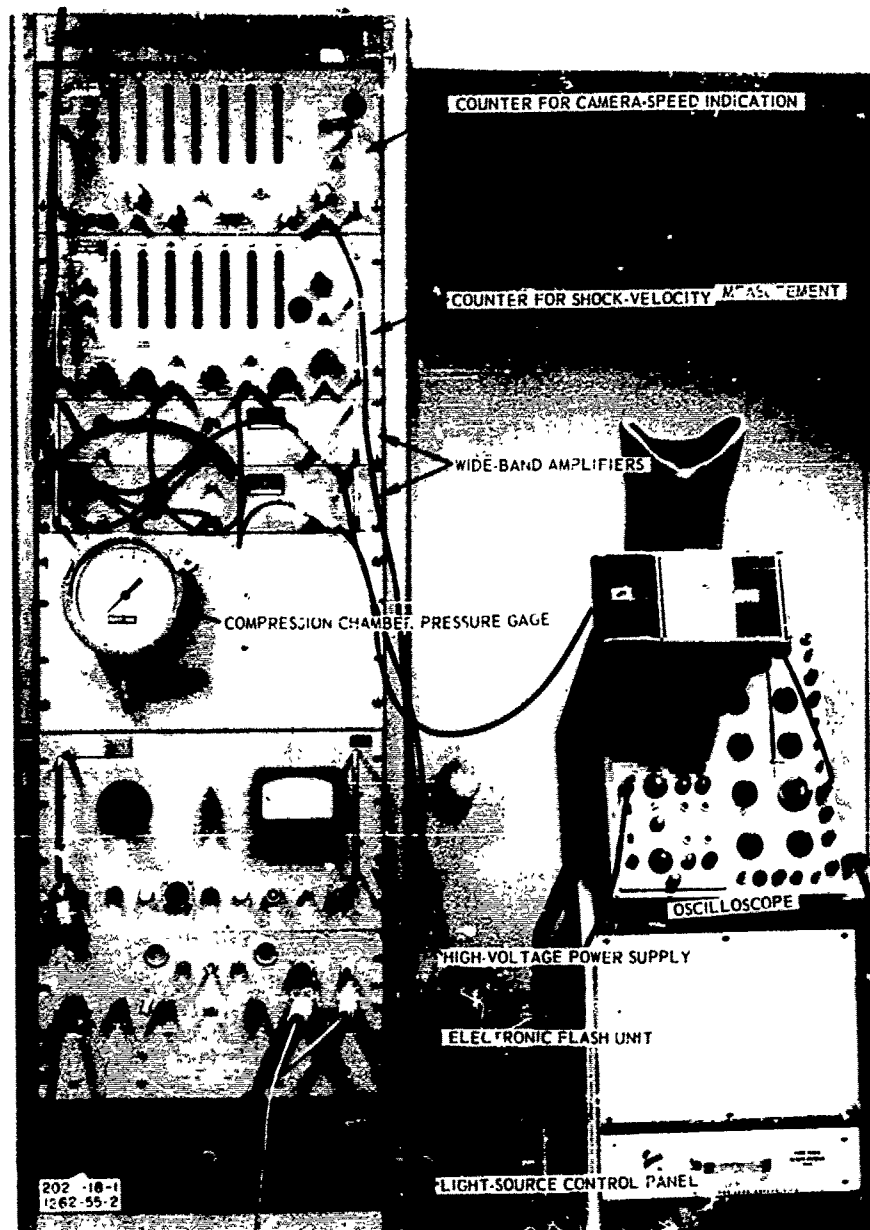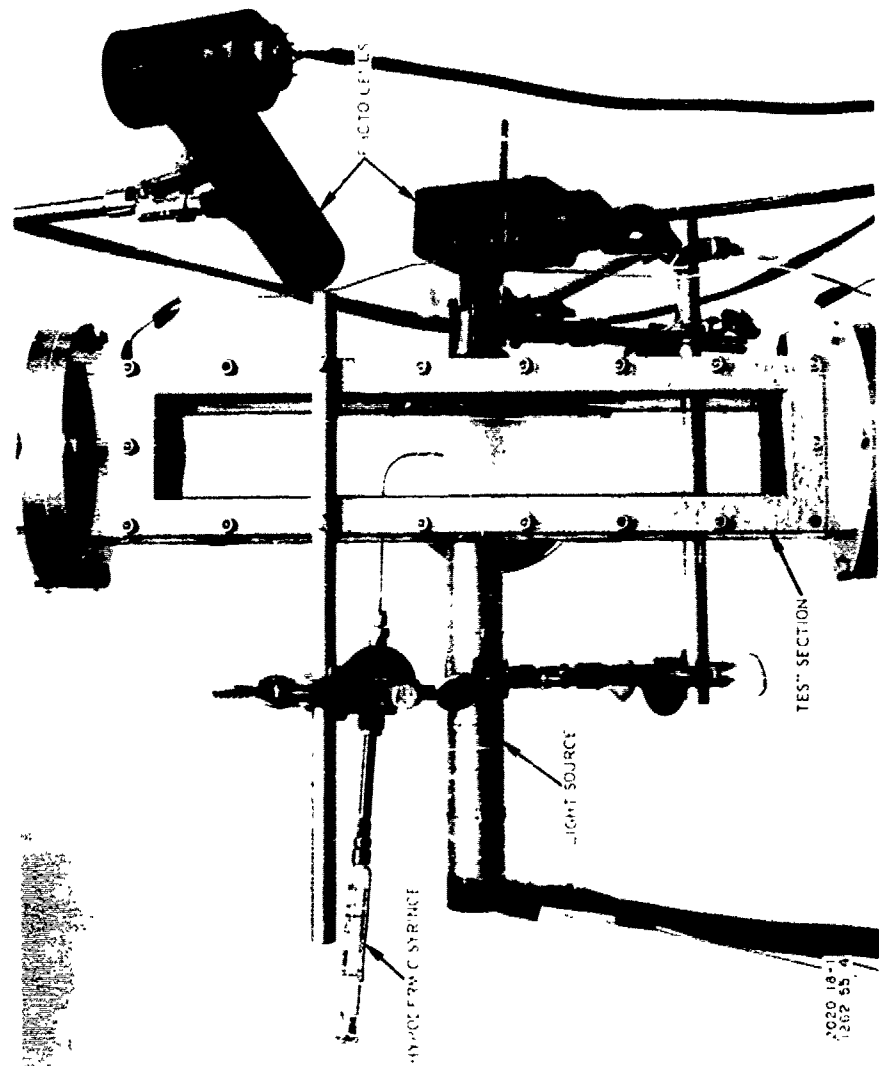
Figure 8. Instrumentation.
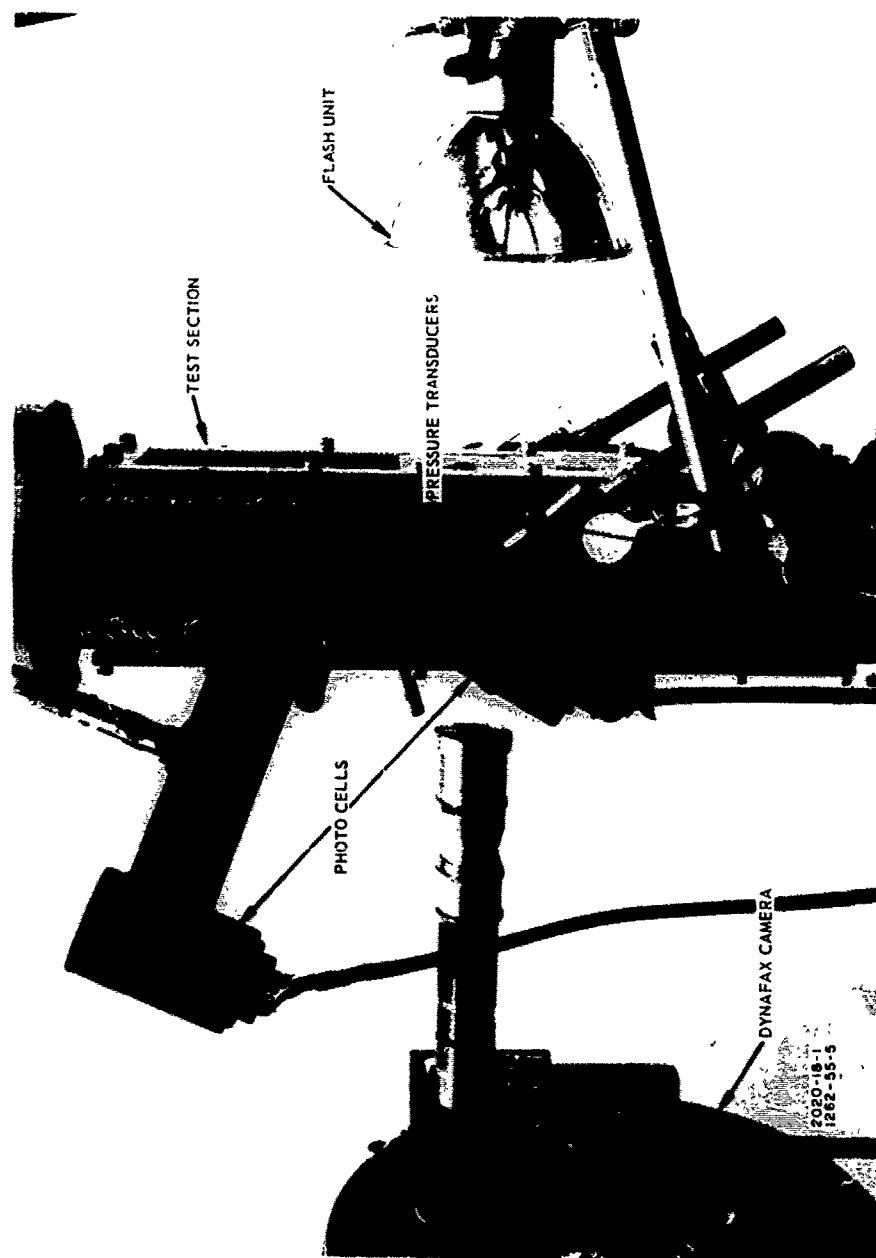
Figure 9. Shock Tube Test Section.

Figure 10. Side View of Shock-Tube Test Section

TEST SECTION

FLASH UNIT

PRESSURE TRANSDUCERS

PHOTO CELLS

DYNAFAX CAMERA

2020-16-1
1262-55-5

vertical-deflection circuit of the oscilloscope   When operated in this
manner, the counter indicated to the nearest 0 1 μsec the time elapsed
between the start and stop signals, and thus represent... the time
required for the shock front to travel the distance between the trans-
ducers

Times between start and stop signals were also obtained from the
oscilloscope pictures by determining the length of the sweep trace before
it was vertically deflected by the stop signal   Accuracy comparable to
that of the counter was obtained from the oscilloscope by delaying the
start of the sweep for an accurately known interval and observing only
the final portion of the trace at a much faster sweep rate   Oscilloscope
data were primarily used for comparisons with the counter data and to
estimate possible errors in time measurement as affected by differences
in wave shape between the start and stop signals and differences in trigger
levels between start and stop circuits of the counter

The counter shown at the top of Figure 8 was used to determine the
camera speed   An ac signal from the camera (with a frequency equal
to the rotating-mirror speed) was fed into this counter, which was set
on the Events Per Unit Time (EPUT) mode and thus counted the number
of ac cycles occurring per second.   Framing rates and frame-separation
times were then calculated from the mirror speed

Prior to the test runs, the pressure gage illustrated in Figure 8 was
observed to determine the pressure level in the compression chamber
(It was necessary to measure this pressure to predict the magnitude of
shock velocity and air velocity for each test)   Shown below the pressure
gage is the high-voltage firing panel, which was used to explode the wires
to burst the diaphragms.   This panel contains triggering circuits, a
high-voltage power supply (to charge the 9-μf capacitance), and firing
circuits (to apply the energy stored in the capacitors to the exploding
wire).   The firing and triggering circuits are designed to have response
times of less than 1 μsec; triggering is accomplished by the voltage
pulse from a 1P39 photocell, receiving light from the flash unit used
with the Dynafax camera

At the bottom of Figure 8 is the control panel for the photocell light
source; this panel contains a battery charger, which was used to re-
charge the automobile battery that supplied the dc voltage to the lamp
in the light source   The lamp, battery, and charger were connected to
a three-way switch with "off, " "operate, " and "recharge" positions

-57-

5.1.4 Microburet

Formation and control of single drops of liquid are most easily accomplished by using a hypodermic syringe and releasing the drops as desired from the tip of a section of capillary tubing. The size of the drops is determined by the liquid density, surface tension, and the outside diameter of the capillary tubing on which they are formed.

If it is assumed that the drop separates from the tubing at the instant when the weight of the liquid in the drop is sufficient to overcome the surface-tension force attaching the drop to the tubing, an expression of the following form can be written (Reference 11)

$$\text{Drop weight} = k \, D_T \, \sigma \qquad (59)$$

where

      k = constant of proportionality (experimentally determined = 3.8)

      D_T = outside diameter of capillary tubing

      σ = liquid surface tension

From Equation 59, the expected drop size can be written as

$$D = k \sqrt{\frac{D_T \sigma}{\rho}} \qquad (60)$$

where

      D = drop size

      ρ = liquid density

Figure 11 shows drop sizes as a function of tubing diameter for the different liquids used during the study. Examination of the curves indicate that it is not practical to attempt to produce drops smaller than about 1.0 mm in this manner because tubing of very small diameter would be required.
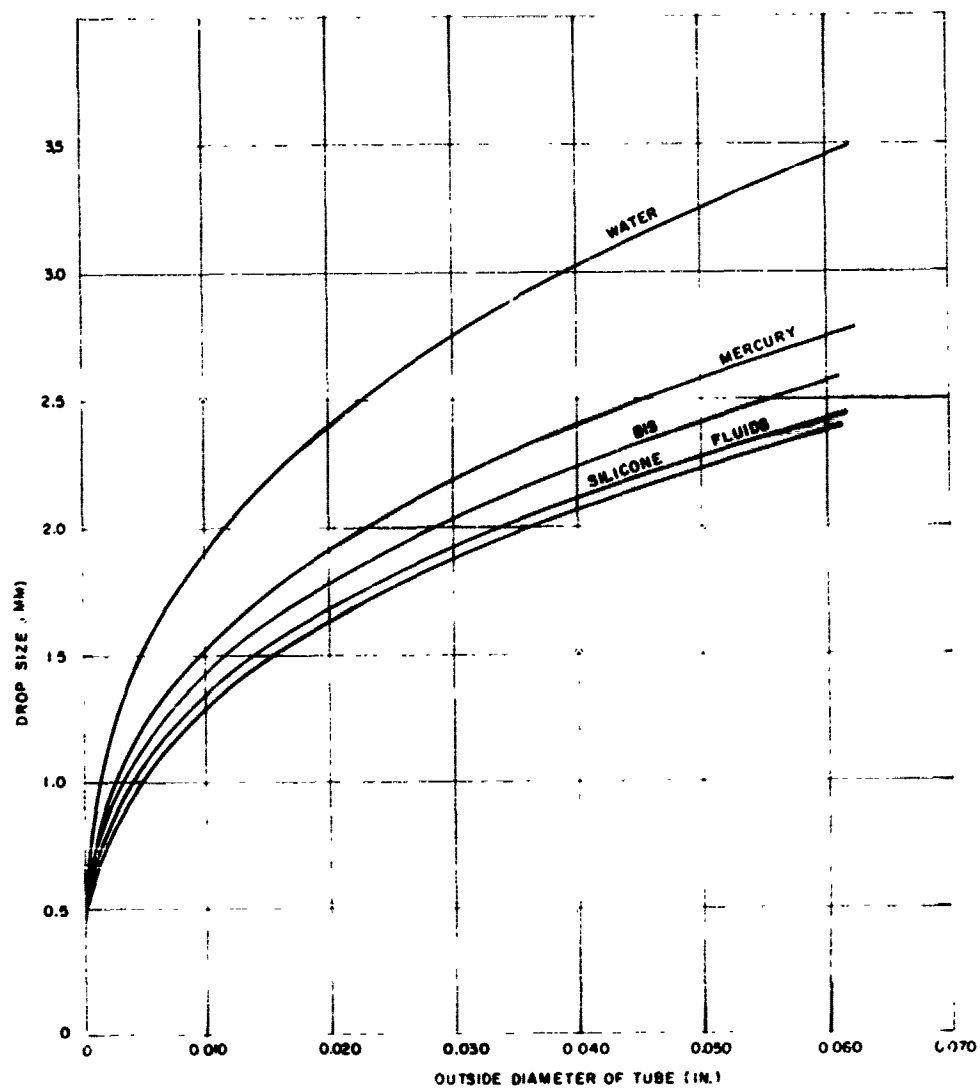
Figure 11.   Drop Sizes versus Tube Diameter for Various Liquids

To produce drops significantly smaller than 1.0 mm, a microburet similar to that used by Asset (Reference 72) was fabricated. A short length (approximately 0.5 in.) of 0.008-in.-OD x 0.00 ,-in. -ID tubing was inserted and sealed in the tip of an 8-in.-long (0.036-i.i. -OD) hypodermic needle. A length of 0.0625-in. -OD x 0.051-in. -ID capillary tubing was slipped over the hypodermic needle and attached to a T fitting near the center of the hypodermic needle; the 0.008-in. - OD tubing protruded approximately 0.125 in. beyond the tip of the 0.0625-in. capillary tubing. Figure 9 shows the 0.008-in. -OD tubing protruding from the capillary of larger diameter (the T fitting is somewhat obscured by the ring-stand clamp holding the microburet in place).

Air, under pressure, is admitted to the T fitting and flows through the annular space between the two pieces of tubing and out around the tip of the 0.008-in. tubing. As the droplets begin to form at the tip of the small capillary, they are blown away by the force of the airflow. By adjusting the rate of air flow, the drop sizes can be varied at will over a considerable range; however, once a fixed airflow is established, the drop sizes are as consistent as those produced with no airflow.

Droplets as small as 500 μ were produced for the study with no difficulty. Droplets smaller than this size, however, showed a tendency to follow erratic trajectories after being blown off the capillary tubing (because of both their small mass and the air turbulence created by the higher air flow rate). Two problems resulted from the preceding behavior: (1) it was difficult to get the drops to consistently enter the light beam and trigger the flash unit, and (2) the drops were frequently outside the field of view of the camera. As a result of these problems, the test data in this report are limited to drop sizes of approximately 500 μ and above.

Figure 12 shows the arrangement of the microburet, the tygon tubing for the air supply, the pressure gage, and the valve used to adjust the airflow through the microburet. Drops larger than 1.0 mm required for the study were all created by selecting various sizes of capillary tubing to attach to the end of the hypodermic syringe.

5.2   TEST PROCEDURE

Prior to each run, each item of equipment and instrumentation was checked to ensure its proper operation, thereby preventing invalidation of the test by failure to obtain all of the desired data   After the preceding steps were taken, the sequence of events described in the following section occurred during the test runs.
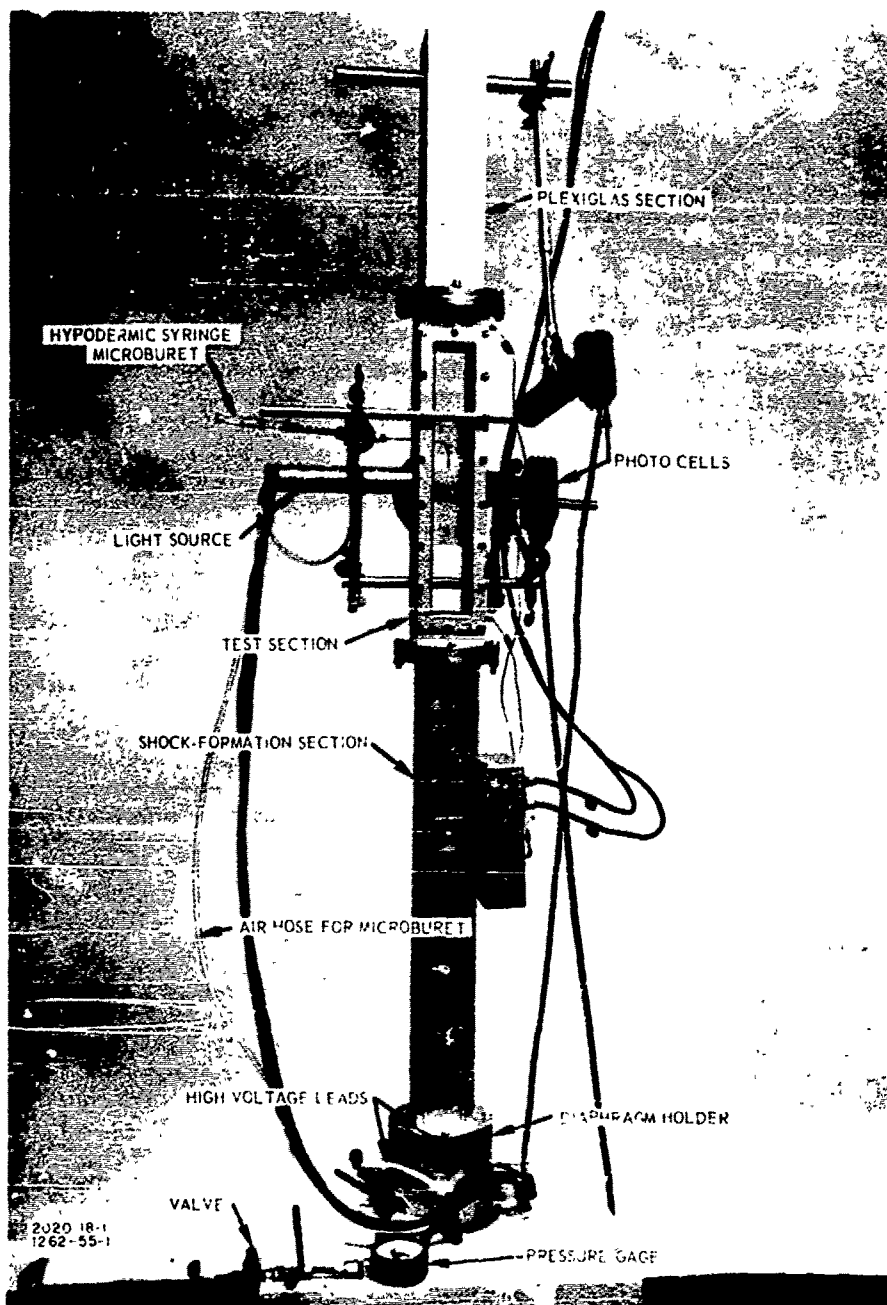
Figure 12. Shock Tube and Related Items.

-61-

5.2.1 Photographic Tests

At the start of the photographic tests, the pressure in the compression chamber was raised to the desired value. Very slow leakage usually occurred around the diaphragm holder, and some adjustment of the air supply was necessary to stabilize the chamber pressure. As the adjustment was being made, the capacitors in the high-voltage panel were charged to 1.2 kv, and the panel was adjusted to maintain the charge. A second operator gradually increased the speed of the camera until the desired number of revolutions per second was displayed on the mirror-speed counter. The camera shutter was then opened, and a drop of liquid was squeezed from the hypodermic needle and was permitted to fall into the light beam to initiate the test sequence.

Because of its high framing rate and short exposure time, the Dynafax camera requires a very intense source of light for adequate exposure; therefore, at high framing rates the camera shutter may be left open (exposing the film to normal room lighting) for as long as 30 sec without film fogging. As the falling drop of liquid entered the light beam, the electronic flash unit was triggered to emit an 8.2-ms pulse of light, which provided the illumination for proper film exposure. The pulse of light from the flash unit also triggered the high-voltage panel, exploding the Nichrome wire and releasing the air in the compression chamber.

The camera continued to take pictures of the falling drop for approximately 2.5 ms, the time required for the shockwave to form and travel the distance from the diaphragm to the test zone. As the shockwave passed through the test section, the falling drop was subjected to the onset of flow behind the shockwave in the time required for the shock to traverse the drop diameter (less than 10 μsec). The flow simultaneously initiated deformation and breakup of the drop, subjecting it to large acceleration forces sufficient to halt its downward fall and carry it out of the top of the camera's field of view in a few milliseconds.

The duration of constant-flow conditions behind the shockwave was approximately 3 ms, a time span that, except for isolated cases, was more than sufficient to cause breakup and carry the shattered droplet out of the field of view. Since the camera had a total writing time of 8 ms, and only 2.5 ms of this time was used before arrival of the shockwave, the remaining 5.5 ms was more than sufficient to record the events of interest. Passage of the shockwave over the pressure trans ducers at the bottom and top of the test section generated voltage signals, which triggered the counter and oscilloscope to record the time required for the shockwave to traverse the distance between the transducers

The test was terminated by essentially following, in reverse, the steps taken to prepare for the test.

5.2.2   Size-Distribution Tests

The procedure followed in conducting the tests to sample the droplet-size distribution resulting from breakup of larger single drops was similar to that discussed in Paragraph 5.2.1. It varied, in that the Dynafax camera was not utilized and it was necessary to place the shock tube in a horizontal position to gain operating space beyond the open end of the expansion chamber.

To remove all unnecessary airflow obstructions from the test section, the droplets were introduced into the test zone by mounting the hypodermic syringe and needle outside the shock tube and permitting the drops to fall from the needle tip through a hole in the test-section wall. The light source and photocell were relocated and adapted so that when the falling drop approached the shock-tube centerline, the light beam was interrupted to both trigger the high-voltage firing panel and explode the Nichrome wire to release the air in the compression chamber.

Test preparations consisted of arranging 12 standard microscope slides in a plywood holder, creating a 4- x 6-in. plane-sampling surface. The plywood holder was then mounted on a moveable stand, with the center of the sampling surface concentric with the shock-tube axis and the plane of the surface normal to the tube axis; the stand was positioned to place the sampling surface a predetermined distance from the open end of the expansion chamber.

The test was conducted following the same procedure used in the photographic tests. After the test was completed, the microscope slides were removed, and photomicrographs of the sampled material were taken at three locations along the centerline of the slide. To provide data from which the radial distribution of sampled material could be determined, recordings were made of the coordinates of each of the photomicrographs on the slide surface. The sampled material was also washed from the slides and put into a solution, permitting assays to be made of the amount of material collected for material-balance calculations.

5.3   PARAMETRIC STUDIES

5.3.1   Measurement of Breakup Time

Correlation of the experimental results with the theoretical model of breakup mechanism developed in Section 1 of this report requires the following data:

a. Time required for breakup to occur

b. Physical properties of the liquid being shattered

c. Airflow conditions to which the liquid is subjected

To prove useful, the correlation requires that the data represent a wide range of values of the various significant parameters.

Although considerable experimental data on single-drop breakup are available in the literature, this information proved to be of limited use in the present study for two reasons: (1) it does not cover the range of variation in liquid physical properties needed for correlation with theory, and (2) much of the work reported did not include the use of high-speed motion picture equipment to record the breakup. As a result, data on the breakup time are not readily available.

A complete parametric study was therefore undertaken to record, with high-speed motion picture equipment, the breakup of liquid drops of different sizes and different physical properties while subjected to a wide range of flow conditions.

The following listing shows the parameters employed for the test and the range of values over which they were varied.

Parameter	Approximate Range of Variation
Relative velocity	50 to 450 ft/sec
Surface tension	18 to 487 dynes/cm
Liquid density	0.75 to 14 gm/cm^3
Liquid viscosity	0.5 to 170 centipoise
Drop size	500 to 3000 μ

To cover the preceding range of variation, several liquids were chosen to be used in the study. These liquids and their physical properties are shown in Table 1.

Experimental results obtained during the study are presented in Table 2; plates made from motion-picture films showing the qualitative behavior of the drops during breakup are provided in Appendix B. The breakup-time values listed in Table 2 represent the elapsed time from the first signs of deformation until the drop begins to break up.

-64-

Table 1. Physical Properties of Liquids.

Liquid	Temperature (°C)	Surface Tension (dynes/cm)	Viscosity (centipoise)	Density (gm/cm³)
Water	25	72.00	0 890	0.998
Mercury	20	487 00	1.550	13.600
Silicone fluids				
GE SF (9t) 0.65	25	17.50	0.470	0.758
GE SF (96) 10	25	22.30	9.520	0.938
GE SF (96) 200	25	23.30	1'ᵃ ⁵	0.966
Bis	25	27.60	5.970	0.915

Table 2. Experimental Breakup Time Results.

Test	Drop Size (mm)	Air Velocity (ft/sec)	Relative Velocity (ft/sec)	Breakup Time (msec)
WATER				
117	3.0	128	134	1 29 to 1.45
119	3.0	214	221	0.69 to 0 73
121	3 0	357	362	0.24 to C.27
122	3.0	448	455	0 14 to 0 18
123	3 0	63	71	3.24 to 3.32
158	2.0	63	69	2 63 to 2.83
186	1.4	101	107	1.37 to 1 49
187	1.9	78	84	1.64 to 1 80
188	1.9	47	53	2.35 to 2.58
189	1 8	189	195	0.43 to 0.51
191	1.9	347	350	0 20 to 0.31
192	1 7	436	441	0 12 to 0 23
214	1 0	57	63	2.08 to 2.24
217	1.2	76	81	1.45 to 1.61
236	0 76	79	85	1.16 to 1 27
237	0.78	68	75	1.07 to 1 15
238	0.78	90	95	0.89 to 0 97
239	0.78	103	108	0 77 to 0.84
240	0 81	117	120	0 69 to 0 77
241	0.67	55	61	1 89 to 2 00
261T	0.53	122	127	0.66 to 0 77
261B	0.57	122	127	0 62 to 0.66
262	0 53	197	203	0 50 to 0 54
263	0 62	333	339	0.12 to 0.19
264	0 44	425	432	0 04 to 0.12
267	1 9	79	?	1.15 to 1 27

Table 2. Continued

Test	Drop Size (mm)	Air Velocity (ft/sec)	Relative Velocity (ft/sec)	Breakup Time (msec)
MERCURY				
132	2 1	457	460	0 63 to 0 75
135	0 82	351	358	0 77 to 0.85
138	0 69	224	230	1 62 to 1 66
164	1 2	168	173	2 95 to 3 14
GE SF(96)0 65				
151	2 3	68	75	1 11 to 1 23
152	1. 0	131	137	0 61 to 0. 69
153	2 1	120	126	0 43 to 0 63
154	2. 2	228	235	0 16 to 0 27
155	1 9	375	381	0. 10 to 0 14
156	2 1	467	472	0 08 to 0 12
160	1 4	43	49	1 49 to 1. 61
193	1 3	436	441	0 08 to 0 12
194	1 5	345	350	0 12 to 0 20
195	1 4	195	260	0 20 to 0 27
197	1. 4	41	48	1 45 to 1 52
GE SF(96)10				
140	2 0	442	450	0 06 to 0 14
142	2 2	220	228	0 29 to 0. 41
143	2. 2	123	130	0 94 to 1 00
148	2 0	360	366	0 10 to 0 22
150	2 0	83	90	1 43 to 1 51
161	1 4	45	51	1 43 to 1 55
198	1 1	98	103	0 78 to 0 86
199	1 4	188	193	0 35 to 0 43
200	1 4	338	343	0 12 to 0. 20
201	1 4	430	436	0. 08 to 0 16

Table 2. Continued.

Test	Drop Size (mm)	Air Velocity (ft/sec)	Relative Velocity (ft/sec)	Breakup Time (msec)
GE SF(96)200				
125	2 1	67	75	4 00 to 4 35
127	2. 2	117	123	
128	2 2	121	127	1 85 to 2 01
129	2. 2	208	215	0 92 to 1 00
130	2 1	357	363	0 51 to 0 59
131	2 1	450	456	0. 55 to 0. 57
162	1. 4	32	38	
203	1. 5	75	81	
204	1 5	192	197	0 74 to 0 82
205	1 5	340	345	0 39 to 0 43
206	1 5	398	403	0 32 to 0 35
208	1 4	63	68	
232	1 2	161	164	
243	0 9	60	63	
244	0 9	74	77	
248	1 0	109	105	1 62 to 1 77
249	0. 9	102	107	2 05 to 2 13
251	1 0	114	118	1 54 to 1 65
255	1. 0	160	165	1 34 to 1 46
257	0. 9	173	179	0 96 to 1 04
258	0 9	181	184	0. 89 to 1 00

-68-

5.3.2   Size-Distribution Tests

Because of time limitations and the large amount of work involved in determining size-distributions, these tests were not as comprehensive as the breakup-time tests.   This investigation was limited to the use of one liquid, three drop sizes, and five relative velocities. Sampling distance was also varied, but only for purposes of determining the optimum distance at which valid samples could be taken.

Bis was used as the test liquid because it has a very low vapor pressure, which reduces evaporation of the sampled material to a minimum. Another advantage of this material is that considerable previous experience had been gained on its behavior in aerosol form, typical spread factors for bis droplets on glass had been determined, and chemical-assay techniques to determine the quantity of bis sampled had been worked out and tested.

Drops of bis (1.6 and 2.7 mm in diameter) were subjected to relative velocities of approximately 100, 200, 300, and 400 ft/sec, and the aerosol from the shattered drops was sampled at distances of from 12 to 48 in. from the open end of the shock-tube expansion chamber. The results of these tests yielded size distributions for the shear or stripping type of breakup.

Bis drops approximately 0.6 mm in diameter were subjected to air velocities of approximately 70 ft/sec to determine size distributions resulting from bag breakup, which requires a combination of small drop size and low relative velocity.   Samples of this material were obtained only after the 1-ft plexiglass section had been removed from the expansion chamber, thereby reducing to 8 in. the distance from the point at which breakup started to the end of the expansion chamber. In these tests, the sampling surface was placed approximately 4-3/8 in. from the open end of the expansion chamber.

Results of the size-distribution tests are presented in Appendix C in three forms: (1) tabulations of assessment data taken from photomicrographs of the sampled aerosols, (2) plates made from photomicrographs of a portion of the sampling tests, and (3) plots of cumulative percent mass vs drop size for all of the sampling tests.

6.   CORRELATION OF RESULTS WITH THEORY

6 1   QUALITATIVE DESCRIPTION OF BREAKUP

The following sections discuss the qualitative behavior of liquid drops
undergoing breakup in a fast-moving gas stream.   The results were
obtained by photographing free-falling drops of liquid as they were
struck from below by the flow behind a plane shockwave moving upward

As noted earlier in this report, substantial evidence by various authors,
e. g., Hanson (Reference 30), Priem (Reference 32), Sato (Reference
33), and Rabin (Reference 37), indicates that breakup is brought about
by the onset of the flow behind the shockwave rather than from the
shockwave itself.   The time required for the shockwave to travel over
the drop (of the order of 10 μsec) is small as compared with the elapsed
time between shock arrival and the instant the drop begins to shatter
(approximately 500 μsec or greater).   Therefore, it is highly unlikely
that during such a short interval of time the shockwave could initiate the
events observed during breakup.

The first observable stage of breakup after the drop is subjected to the
gas flow is a characteristic flattening of the downwind side of the drop.
Such behavior was also noted by Engel (Reference 36)   As the flattening
of the leeward side continues, a noticeable growth in the lateral diameter
of the drop takes place at a point approximately 1/3 of the drop diameter
from the leading face of the drop, or at the point approximately coinciding
with the zero pressure point on a sphere in steady flow.

Flattening of both the windward and leeward faces continues until the
drop assumes a shape similar to an oblate spheroid; if the flow velocity
is low enough, the drop may be flattened into a disc shape with a
diameter roughly twice that of the original drop.   At this point, if the
relative velocity is sufficiently great, the flow of gas over the front face
and sides of the drop begins to initiate surface disturbances, which
appear to be small wavelets   The greater the relative velocity, the
greater the number of the disturbances.   As these disturbances move
away from the stagnation point and approach the edge of the distorted drop,
they are stripped off and carried away by the gas flow as sheets and liga-
ments of liquid, which subsequently collapse into numerous small droplets.

Erosion of the periphery of the deformed drop continues until all of the
mass of the drop has undergone breakup through the stages of sheet and
ligament formation and collapse into droplets that are carried away by
the gas flow   Measurements made from the various films taken during

the parametric study showed that although the drop undergoes tre-
mendous acceleration, the breakup process is so rapid that the bulk
of the material in the drop acquires no more than approximately 10 to
20% of the gas velocity before it is reduced to aerosol form, the shower
of smaller droplets is then rapidly accelerated up to some velocity
near the gas velocity.

Figure 13 depicts the breakup characteristics described in the preced-
ing sections. The sequences shown are for 3-mm drops of water sub-
jected to various relative velocities ranging from a low of 71 ft/sec to
a maximum of 455 ft/sec. The relative velocity for each drop is
noted above the first frame in each sequence, and the figures below
each frame denote the elapsed time (in milliseconds) from the instant
the drop was subjected to the flow.

The solid diagonal lines between the sequences are "iso-time" lines,
denoting times of roughly 1/2 and 1 ms after time zero   By following
a particular diagonal, it is possible to determine the effect of varying
the relative velocity on the rate of deformation and breakup of the drop
and the formation of surface disturbances. Also of interest is that the
liquid being stripped from the periphery of the drop does not follow a
path parallel to the general flow (it appears to diverge to form a cone-
like cloud of droplets with the remaining bulk of the drop located at the
apex)   This behavior was found to be particularly useful in establishing
a model from which to derive the expression describing the expected
droplet sizes resulting from breakup (see Section 4 4).

The effect of liquid viscosity on breakup is shown in Figure 14, where
2.1-mm drops of silicone oils with viscosities of 0 47, 9.52, and
169.5 centipoise were subjected to a relative velocity of 127 ft/sec
Iso-time lines denoting times of 0.5, 1 0, and 1.5 ms after time zero
are shown for reference.

As shown in Figure 14, a change in viscosity of more than two orders of
magnitude does not appreciably alter the mode of breakup   Increasing
the viscosity retards the deformation process, however, an effect that
permits the drop to acquire a larger velocity (and thus reduce the relative
velocity) before the actual stripping process sets in   As a result, an
increase in the size of the droplets stripped off would be expected with
increasing viscosity.

In addition, at higher viscosities, the material being stripped from the
periphery of the drop leaves in the form of large sheets and ligaments,
rather than as small sheets or ligaments or even droplets (as occurs at
low viscosities)   This effect is shown in a comparison of the sequence
for the 0.47-centipoise viscosity in Fig re 14 with that for a viscosity of
169 5 centipoise.

EFFECT OF RELATIVE VELOCITY ON THE
BREAKUP OF WATER DROP SIZE = 3.0 MM

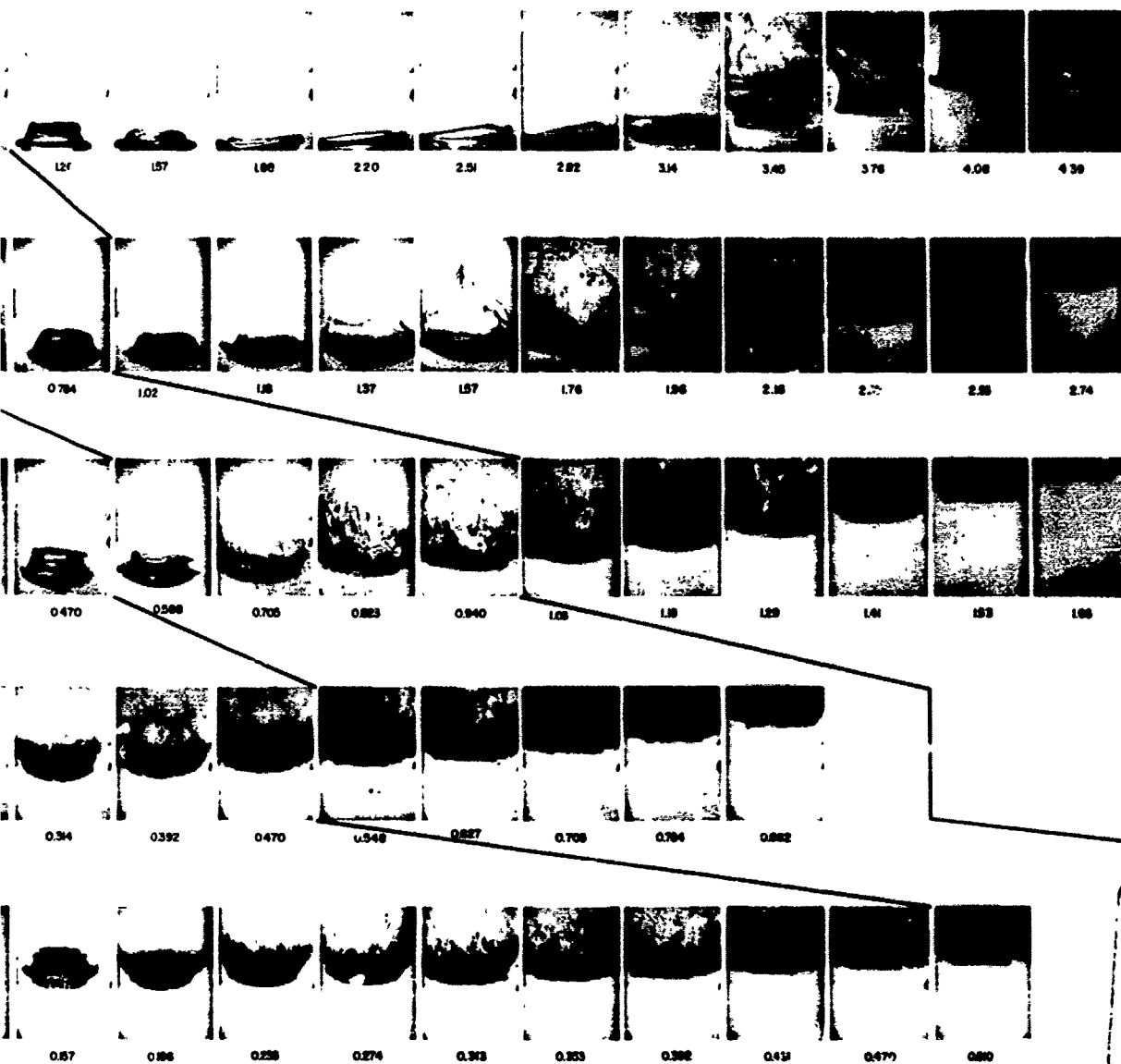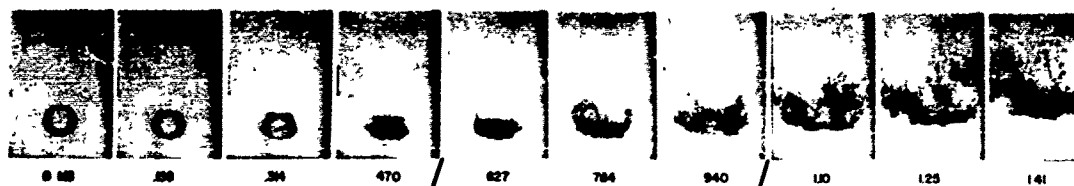Figure 13. Effect of Relative Velocity on
the Breakup of 3.0-mm Water Drops.

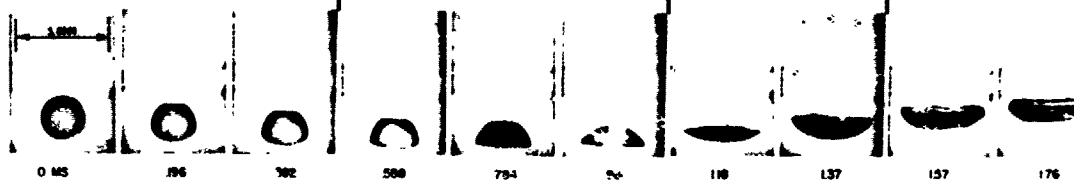EFFECT OF VISCOSITY ON BREAKUP

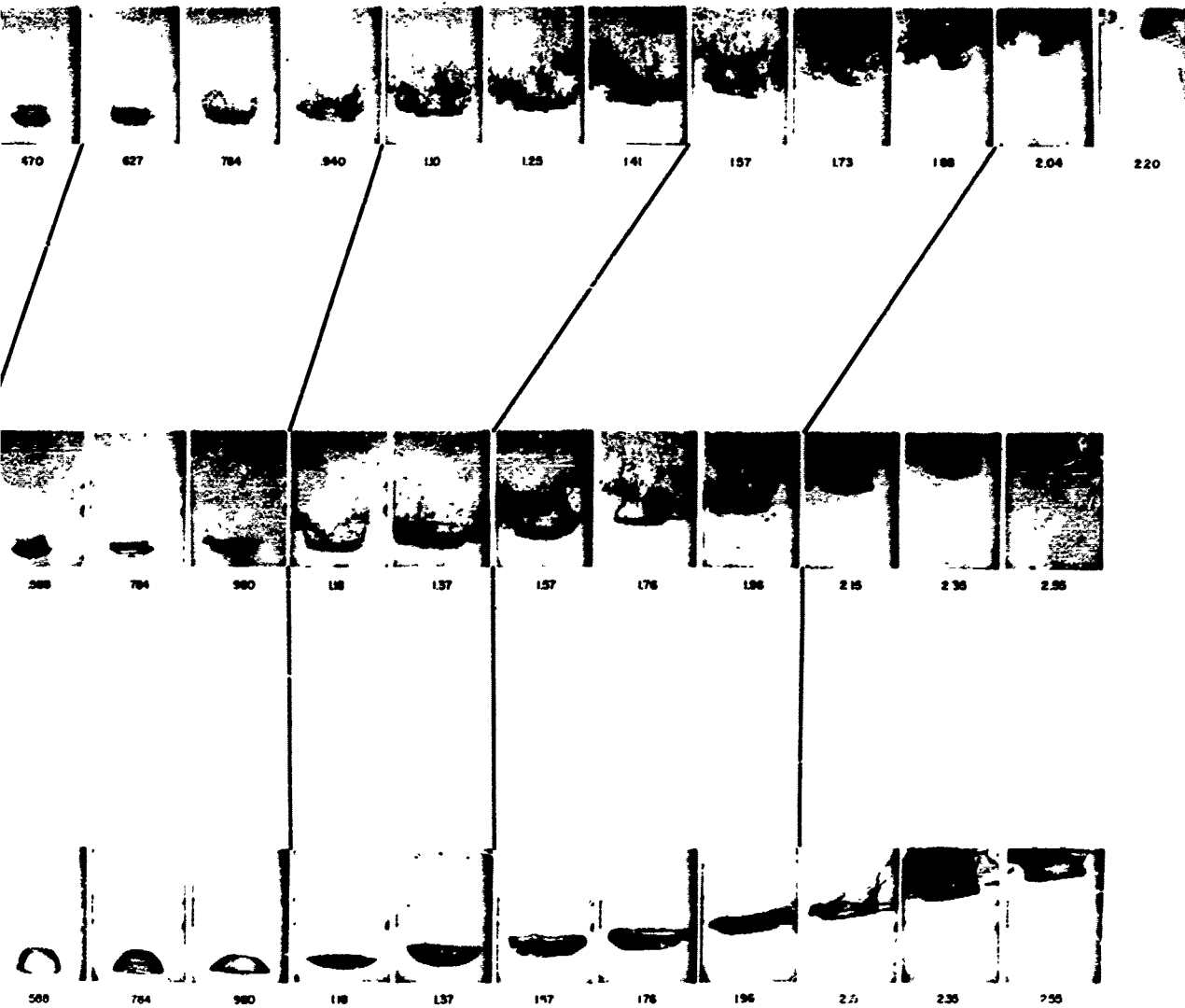DROP SIZE 2.1 MM RELATIVE VELOCITY 127 FPS

Figure 14. Effect of Viscosity on Breakup.

-75-

The large sheets and ligaments must undergo secondary breakup to produce droplets, and they appear to accelerate more rapidly than the bulk of the drop; therefore, a further decay in relative velocity is likely before breakup is completed. Again, larger droplets should be expected from the liquids of higher viscosity

Unfortunately, time limitations prevented undertaking the work necessary to experimentally investigate the effect of viscosity change on the droplet sizes produced during breakup.

Lane (Reference 28), in conducting one of the first comprehensive studies of breakup in a steady air stream, encountered a mode of breakup quite different from the stripping behavior. He noted that the drop flattened to a disc configuration, and instead of stripping occurring at the edges, the center of the disc was blown out in the direction of flow to form a large hollow bag attached to a roughly circular rim (the open mouth of the bag faced the oncoming flow). Measurements indicated roughly 70% of the original drop mass was contained in the rim. Lane also studied droplet breakup using fast transient blasts of air and obtained the stripping behavior. He thus concluded that the two different breakup modes were due to the differences between steady and transient flow

Hanson et al. (References 30 and 31) showed that both modes of breakup could be produced in transient blasts. They noted that bag breakup occurred when drop sizes and relative velocities were close to the critical values.

As a part of this study, specific efforts were undertaken to investigate both modes of breakup and to attempt to expand the knowledge of the characteristics of the two types of behavior. The results of these efforts are summarized in Figure 15, which shows the effect of increasing relative velocity on the mode of breakup Water was used as the test liquid, and the drop sizes were held nearly constant The first sequence for a relative velocity of 61 ft/sec. clearly demonstrates the bag breakup mode, i. e., typical flattening, bag formation, bag rupture and collapse of the rim into a ring of large drops. Hanson et al (References 30 and 31) discovered that after the formation of the bag has taken place, circular ripples (similar to the surface waves resulting from a stone thrown into a quiet pond) form on the thin surface of the bag and apparently initiate bag rupture.

The breakup behavior shown in the second sequence of Figure 15 was produced by holding the drop size nearly constant and increasing the relative velocity to 85 ft/sec. In this case, the usual flattening and
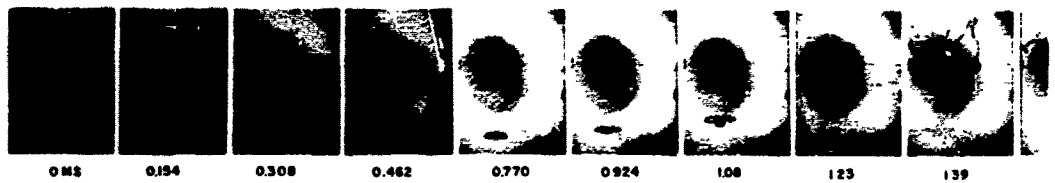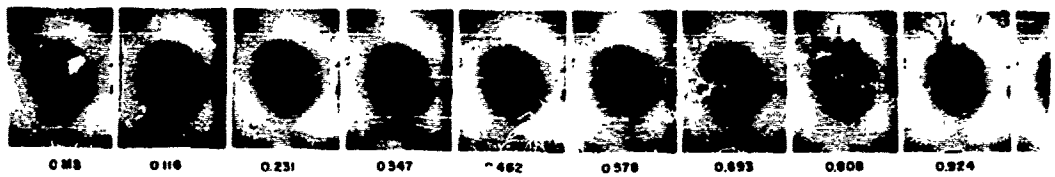
EFFECT OF RELATIVE VELOCITY ON THE
MODE OF BREAKUP OF WATER DROPS

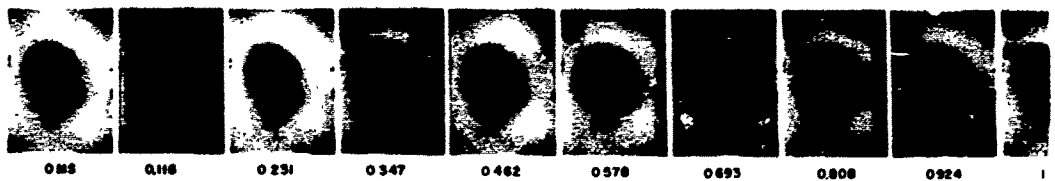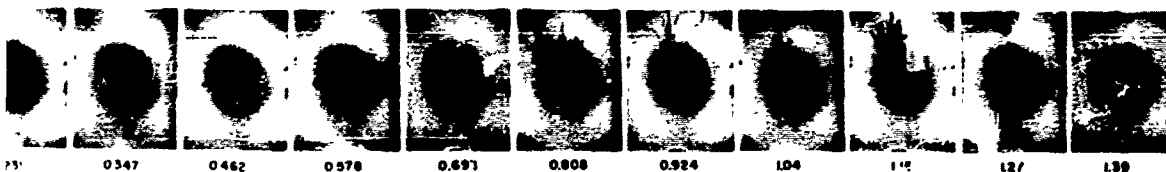## EFFECT OF RELATIVE VELOCITY ON THE MODE OF BREAKUP OF WATER DROPS

Figure 1. Effect of Relative Velocity on the Mode of Breakup of Water Drops.

beginning of bag formation occurred; however, a re-entrant or stamen portion of liquid formed at the center of the flattened drop As the bag continued to form, the stamen remained attached to '.. bag and elongated to form a ligament of liquid, centered within the bag rim The usual rupture of the bag and rim occurred, and the stamen appeared to collapse into a series of larger drops

The remaining sequences of Figure 15 indicate that as the relative velocity is gradually increased, more of the mass of the drop becomes concentrated in the stamen portion, with less mass available to form the bag portion. This effect continues with increasing velocity until a majority of the drop mass is contained in the center stamen portion   At this point, the bag no longer forms, instead a thin rim or lip of liquid forms around the periphery of the center potion of the flattened drop Rather than being blown out into a bag, the lip is merely stripped off the edge of the drop as a sheet, which subsequently shatters into small droplets.

A good example of the behavior that might be expected to follow after the effect shown in the last sequence in Figure 15 is illustrated in the first sequence in Figure 13.

Based on the results summarized in Figure 15 and other test evidence included in Appendix B of this report, it appears that there is a smooth transition in behavior in going from the bag to stripping breakup modes In addition, the evidence indicates no reason why a different transition would occur in going from stripping to bag breakup

A more detailed study of the qualitative aspects of breakup can be made by referring to series of plates in Appendix B   These plates were made from the test films used to obtain the data presented in Table 2. All pertinent information, including drop sizes, relative velocity type of liquid, and time between frames, is presented on each plate for reference purposes. A scale factor has also been included to facilitate recording length measurements directly from the plates.

6 2   AERODYNAMIC BREAKUP TIMES

For convenience and consistency, the experimentally derived breakup values in Table 2 were taken as the interval of time between the first signs of deformation and the time at which the drop just began to break It is evident, however. from the breakup photographs (Appendix B) that the entire breakup of the drop requires a finite time thereafter, and that this time is usually comparable to the time required to initiate the breakup. Thus, it is to be expected that there should be a small factor

-81-

(of the order of 1. 5 to 3) between the experimental breakup times as measured and those predicted by the theory, with the theoretical times being the greater. A theory for the aerodynamic breakup time of liquid drops was developed in Section 4. 3, and the final expression without regard to breakup mechanism (i. e , bag or stripping) was given in Equation 48a. Figure 16 compares Equation 48a to all of the experimental breakup times; the agreement is seen to be very good (except perhaps for a small constant factor, which may be expected on the basis that the experimental times represent the time for initiation of the breakup rather than for all of the breakup to occur).

The value used for the surface-tension pressure in the theory was $2\sigma/d$. A factor of 2 was used because it allowed a good fit of the data, and also because if a larger value was used the surface-tension pressure was in some cases greater than the aerodynamic flow pressure. The preceding would imply that breakup should not occur, whereas experimental breakup did occur. It may be noted, however, that if a drag coefficient greater than unity is operative, then a value greater than 2 could be used (Equation 49). There is some evidence that this assumption may be true, as will be shown later when the values of the drag coefficient throughout the breakup of the drop are computed. However, there is great convenience in not attempting to use a drag coefficient in the breakup-time equations. Hence, Equation 48a may be considered to be a reliable expression in predicting the aerodynamic breakup times of liquid drops if a value of about $^{\gamma}$ is used for k in Equation 49 and the drag coefficient is considered to be unity.

Euqation 48a was derived using the maximum liquid-flow velocity, but it was discussed that an average velocity may be involved if a hyperbolic velocity distribution was established. Because short distances were employed, it was not believed that this involvement could occur. Figure 17 shows a comparison of the experimental data to theory if an average velocity is used. The agreement with theory is still good, except that the constant-factor difference is slightly larger than using Equation 48a as written. From the photographs of the times involved for complete breakup to occur once breakup is initiated, it appears that use of the maximum velocity expression, i. e., Equation 48a, is to be preferred.

In Section 4. 3, an explanation was presented for the dual-mechanism breakup behavior of liquid drops, and the results were summarized in Equations 51a and 51b. A comparison of the experimental data to these equations is shown in Figures 18 and 19; the drag coefficients were taken as unity and best theoretical fits of the data were obtained using respective surface-tension pressures of $4\sigma/d$ and σ/d for the stripping and bag breakup modes. The agreement between experiment and theory for stripping breakup is very good, except for the expected constant factor.
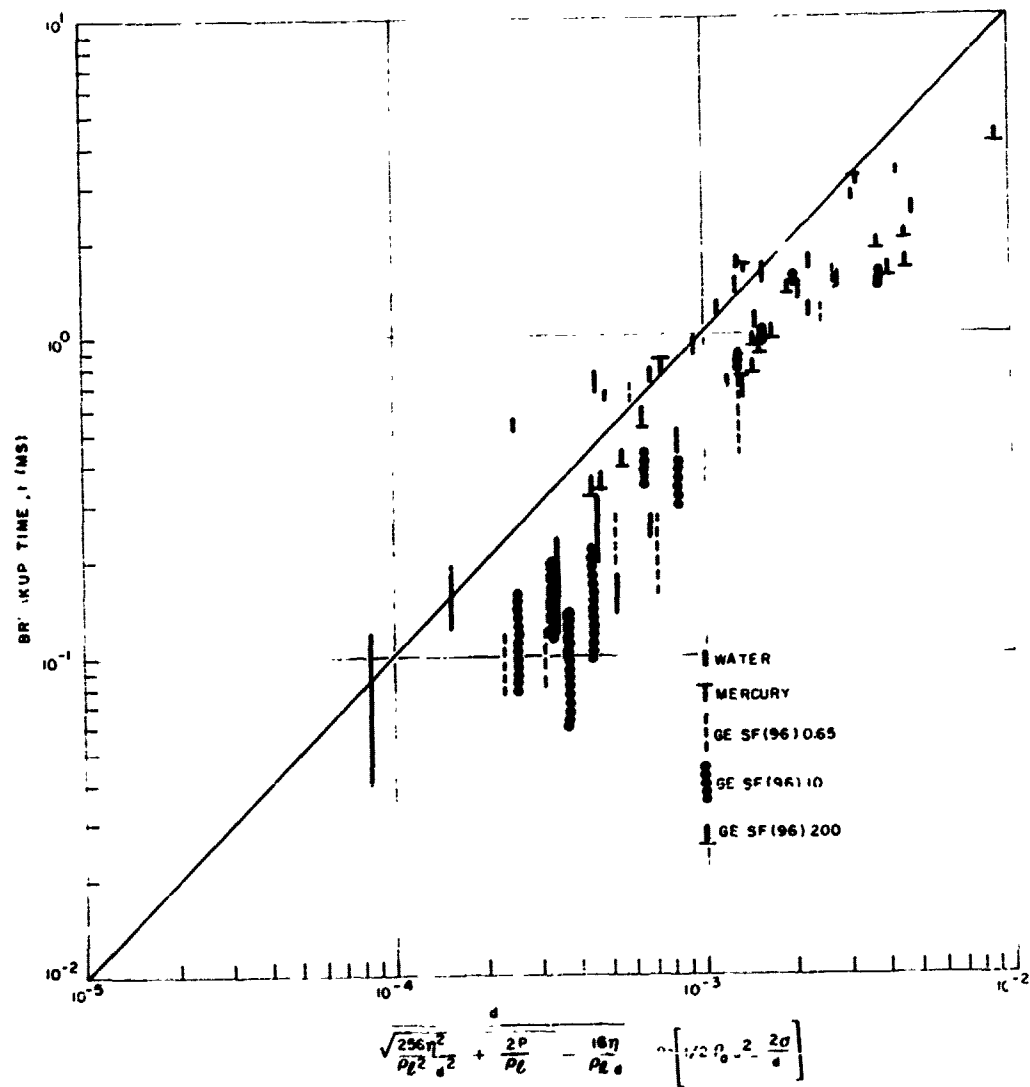
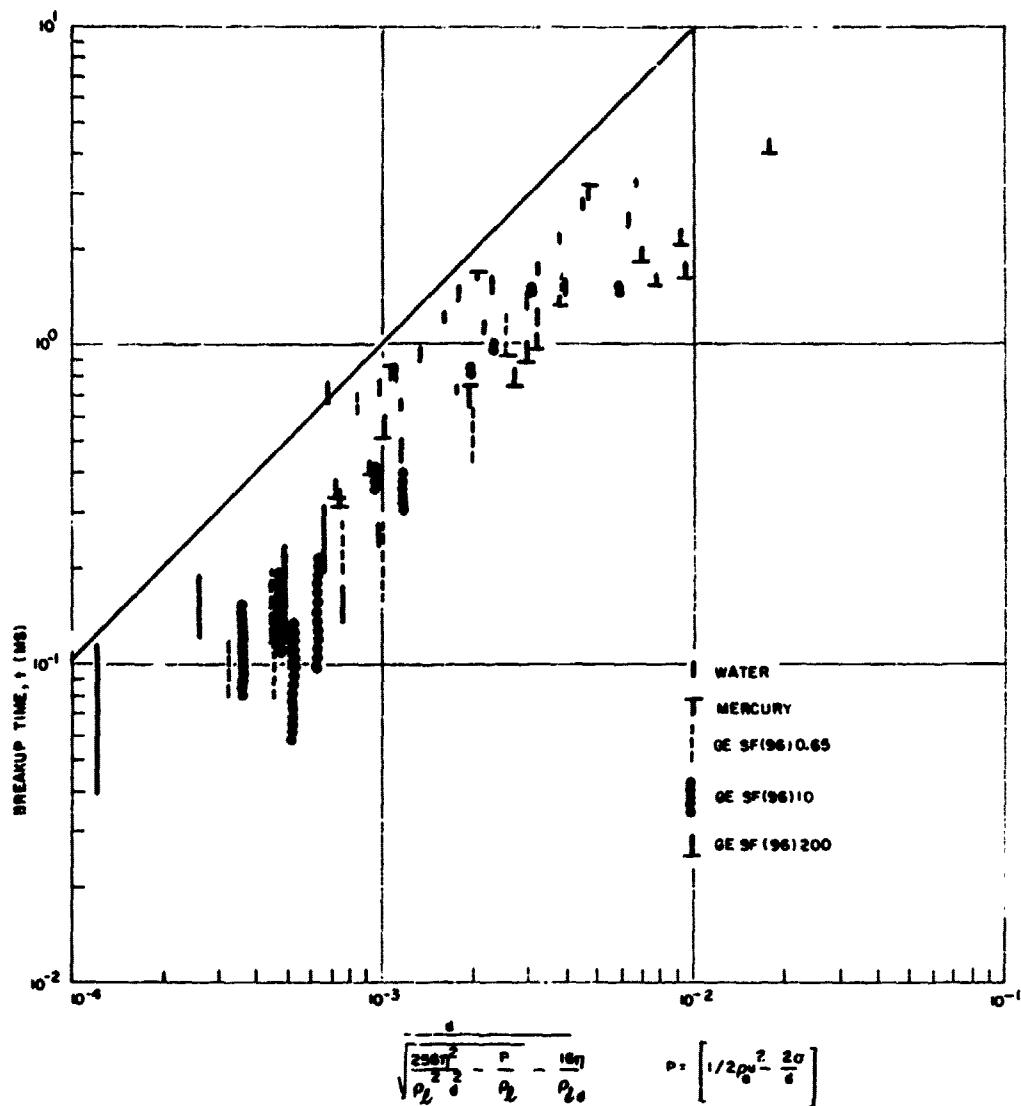Figure 16. Comparison of Experimental Drop Breakup Times with Equation (4c)

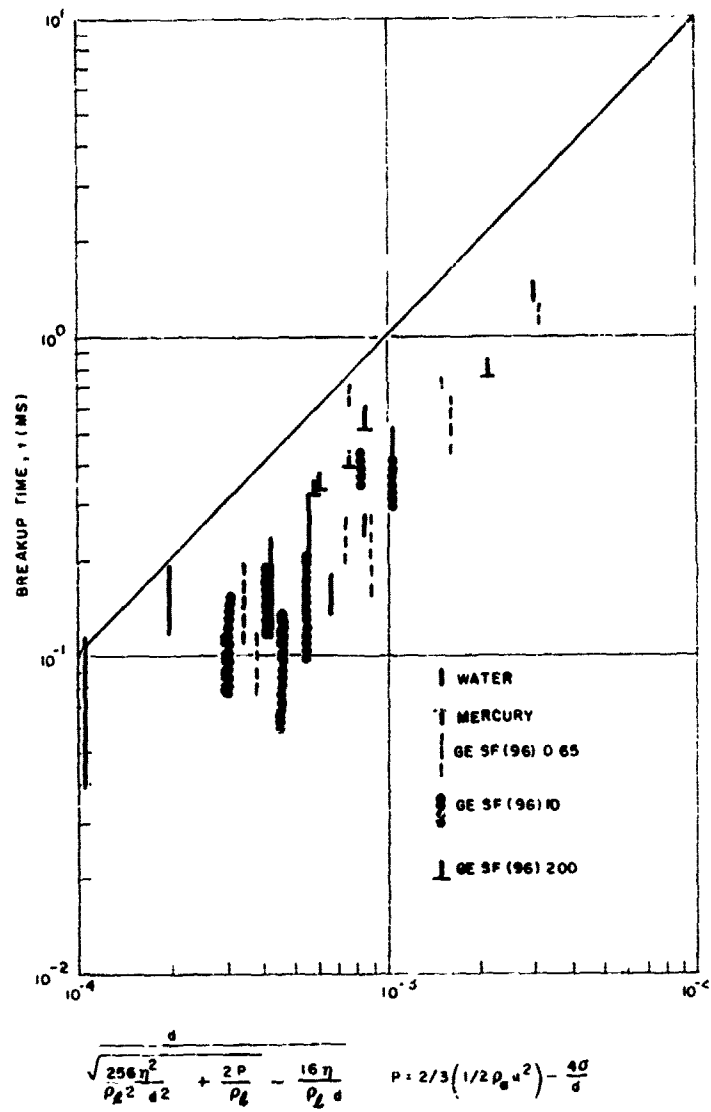Figure 17. Comparison of Experimental Drop Breakup Times with Equation (48a) Modified to Use Average Flow Velocity.

-84-

$$\frac{d}{\sqrt{\frac{256\,\eta^2}{\rho_\ell^2\,d^2} + \frac{2P}{\rho_\ell}} - \frac{16\,\eta}{\rho_\ell\,d}} \qquad P = 2/3\left(1/2\,\rho_g u^2\right) - \frac{4\sigma}{d}$$

Figure 18   Comparison of Experimental Stripping Breakup
Times with Equation (51b).

-85-

$$\frac{d}{\sqrt{\frac{256\eta^2}{\rho_1^2 d^2} + \frac{2P}{\rho_2}} - \frac{16\eta}{\rho_2 d}} \qquad P = 1/3\left(1/2\,\rho_a\,u^2\right) - \frac{\sigma}{d}$$
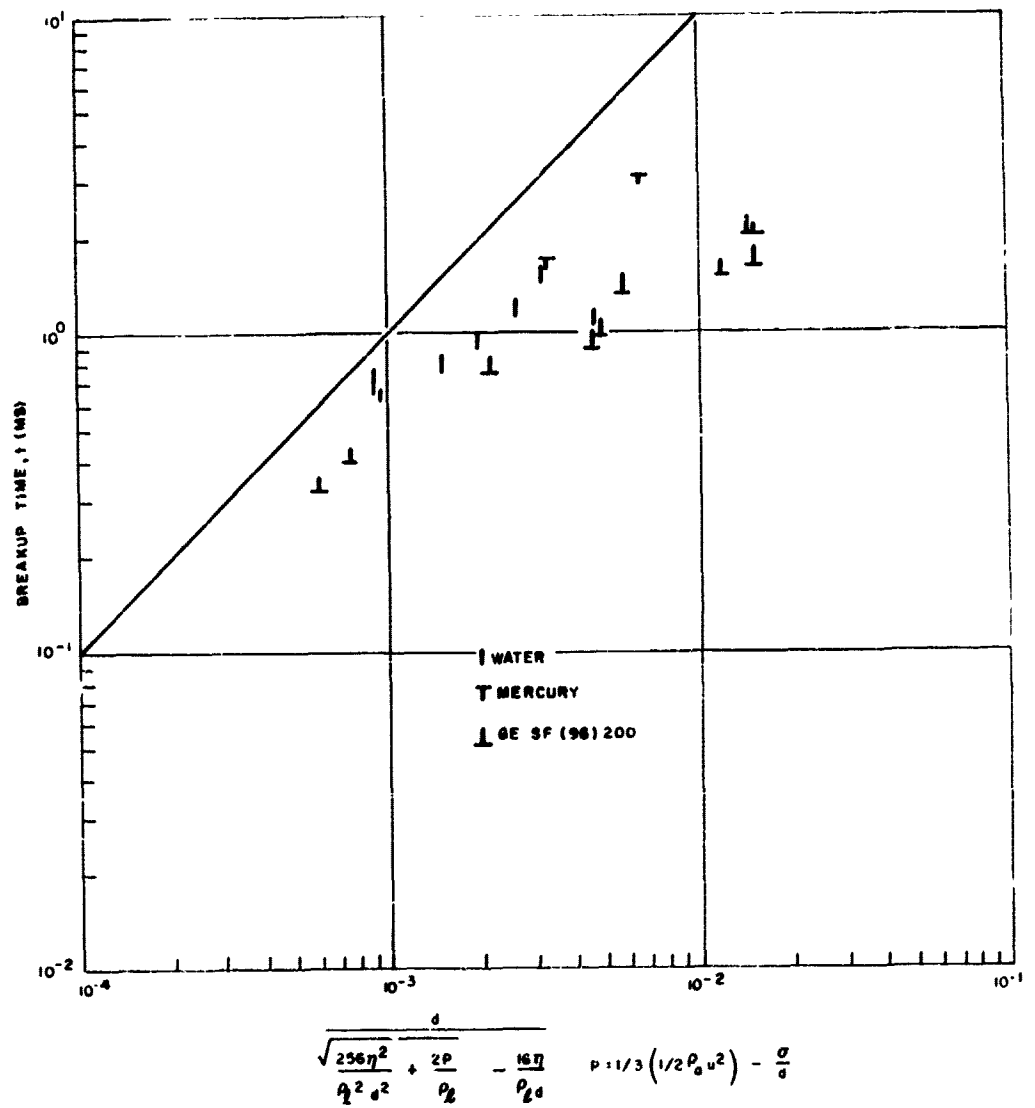
Figure 1ᵒ. Comparison of Experimental Bag Breakup
Times with Equation (5.3)

-8ᵒ-

The agreement for bag breakup is not quite so good; however, the agreement can be made very good if a drag coefficient greater than unity is used. Since the factors 1/3 and 2/3 in Equations 51a and b are not exact but merely representative, it can be said that the experimental data support the hypothesis presented in Section 4.3 to explain the dual-mechanism breakup behavior of liquid drops.

A theory of the bag breakup times of liquid drops was given by Gordon and was summarized in Equations 24 and 26. A comparison of Equation 26 with the experimental data is given in Figure 20; the agreement is seen to be fairly good (except for a constant factor), although several points deviate rather considerably from the data. It is found, however, that the Gordon pressure expression as written in Equation 23 predicts that breakup should not occur for a number of the drops where breakup was experimentally found to occur (as a result of the large surface-tension pressure, $8\sigma/d$, which he used)

The preceding data were replotted, replacing the factor 8 by 4, 2, and 1. A value of 4 was found to give the best agreement with experiment, and this value is used in Figure 21 (a value of 2 is also not too bad, although not as good as 4, the latter value allowed most, but not all, of the data to be used). It is apparent from Figure 21 that the Gordon theory with a modified surface-tension pressure is in good agreement with experiment, except for an expected constant factor (This factor is generally larger than that found by Equation 48a.) The Gordon theory reduces to a simplified breakup time expression, Equation 25a, for cases where viscosity and surface tension are negligible. This expression is of interest because of its computational ease.

Figure 22 compares the theory to experimental data for water and the low-viscosity silicone fluid. Although the agreement is generally good, it appears that the effects of surface tension may be entering in slightly and should be included. The breakup theory derived in Section 4.3 also reduces to the Gordon expression, except it is a factor of 2 smaller (see Equation 50a); thus, it also is in satisfactory agreement with the experimental data. The limiting expression of Gordon for large viscosity and negligible surface tension (Equation 25b) is identical to that derived in Section 4.3 (Equation 50b).

The theory is compared with experimental data for the high-viscosity silicone fluid in Figure 23. A comparison of the results with Figures 16 and 21 indicates that this fluid is not sufficiently viscous for reliable use of the simplified equation.

Hinze developed a theory of the breakup of liquid drops for the (1) limiting cases of negligible viscosity and surface tension, and (2) large viscosity
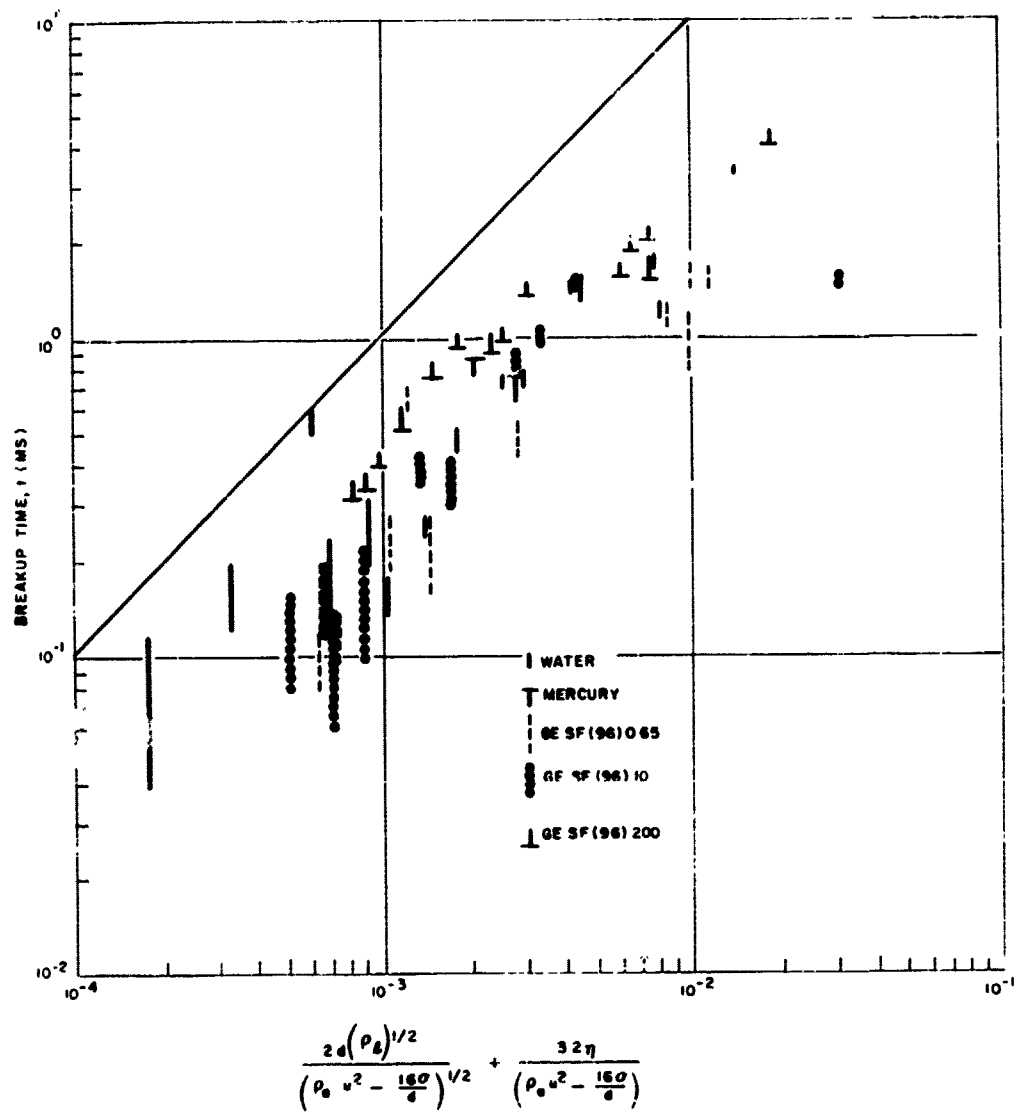
Figure 20   Comparison of Experimental Drop Breakup Times with
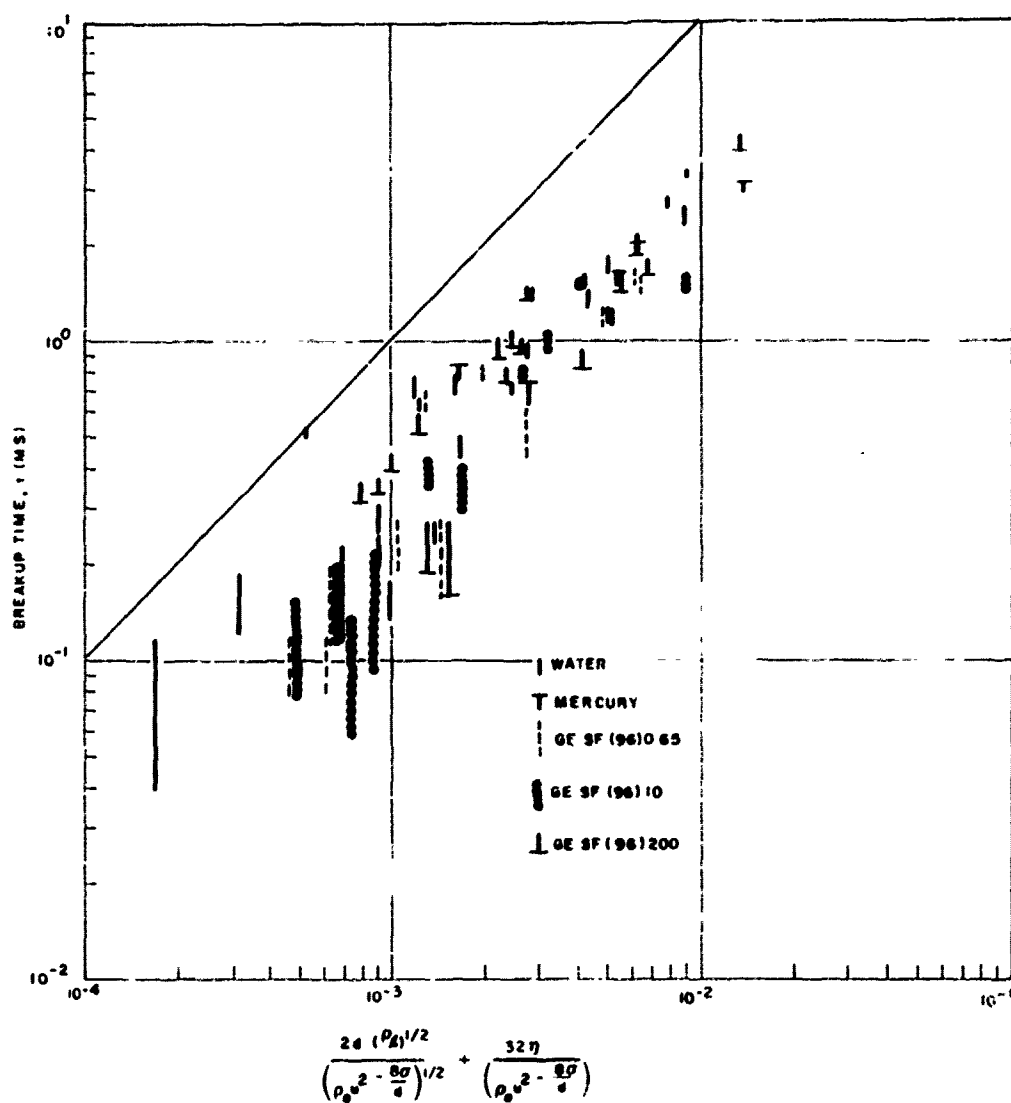Gordon Theory, Equation 26).

Figure 21. Comparison of Experimental Drop Breakup Times with
Gordon Theory, Equation (26), with
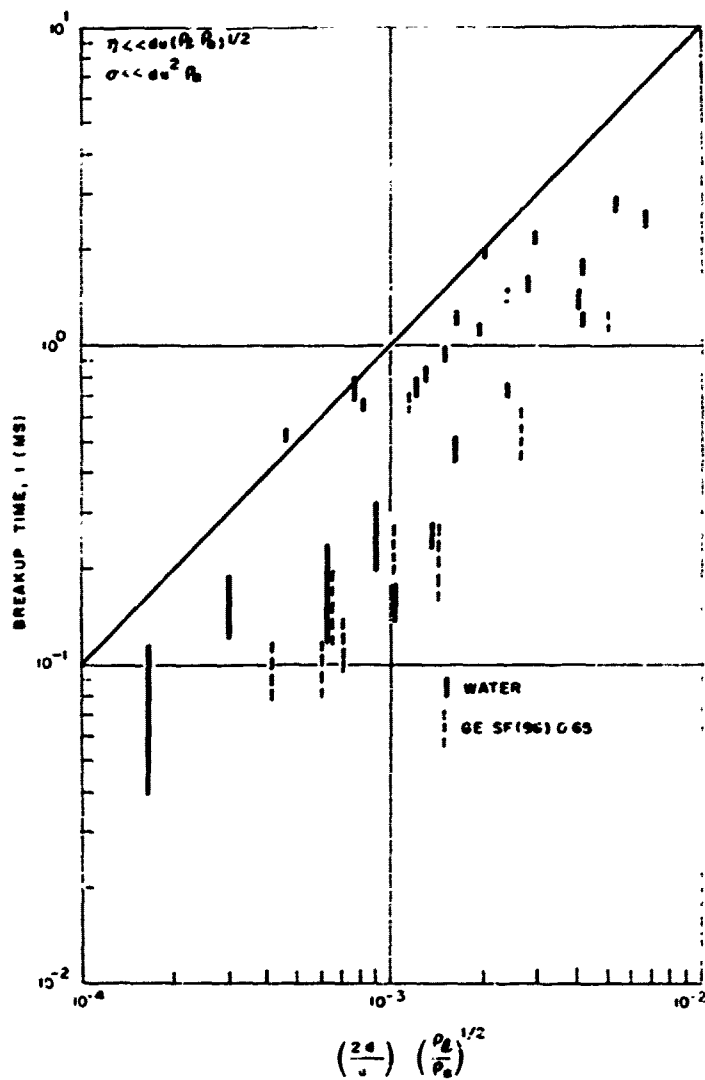Reduced Surface Tension Pressure.

Figure 22.   Comparison of Special Case of Gordon Theory with
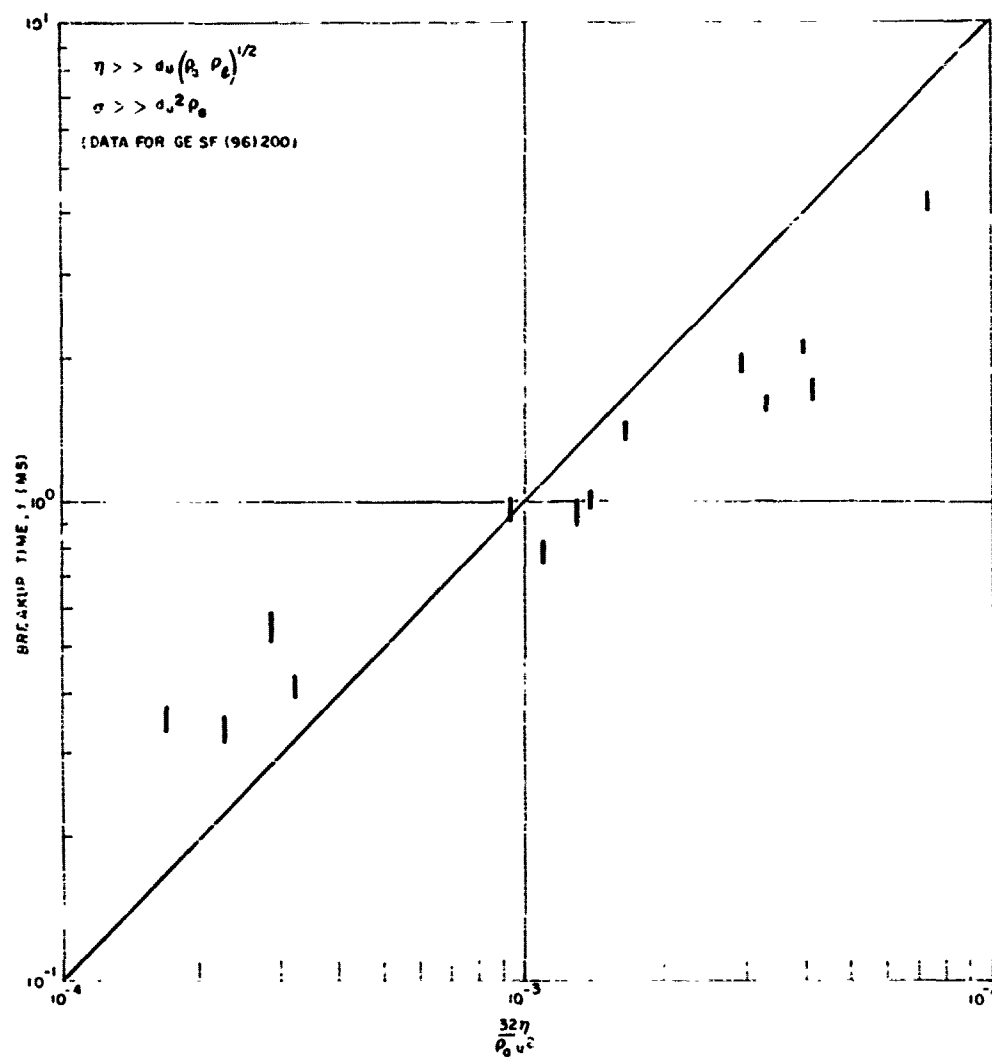Experimental Breakup Times.

Figure 23   Comparison of Limiting Case of Gordon Theory with
Experimental Breakup Times.

and negligible surface tension. His expressions for the breakup times are given in Equations 17 and 18. These expressions are compared with the experimental breakup times of water and the high-viscosity silicone fluid in Figures 24 and 25; the agreement appears to be generally less satisfactory than for the Gordon theory and that developed in this report.

As summarized in Equation 32, Morrell developed a theory for the transverse stripping breakup of liquid jets. A comparison of this theory with the experimental data is given in Figures 26 and 27 Figure 26 shows that there is a drop-size effect not apparently accounted for in the theory, and both illustrations show that there is considerable deviation between the experimental data and the theory.

The early experimental data of Lane (Equation 13) as well as that of Hanson and Domich (Equation 19a) showed that there is a relationship between the critical flow velocity required to break the drop and the diameter of the drop. These relationships are plotted in Figure 28 together with all of the experimental breakup data tabulated as to breakup mechanism. As expected, bag breakup occurred near the critical velocity for a given drop diameter, whereas as the velocity was further increased, the breakup behavior exhibited both breakup-mechanism characteristics. At higher velocities, only the shear breakup behavior was observed.

6.3   DROPLET-SIZE DISTRIBUTIONS

Experimental droplet-size distributions produced by the aerodynamic breakup of bis drops are given in Appendix C. Figure 29 shows the mass-mean diameters of the droplets produced by various velocity gas flows, for various initial drop sizes, and for both bag and stripping breakup behaviors.

A theory for the average droplet size produced by the aerodynamic breakup of liquid drops was developed in Section 4.4. The average droplet size is given by Equation 58, and a comparison between experiment and theory is given in Figure 29. Agreement between experimental data and theory is very good, considering the relative scatter in the experimental data. In view of this scatter, it is difficult to draw further definite conclusions regarding the validity of Equation 58. Experimental data suggest that the effect of the initial drop diameter may be slightly greater than the 1/6 power dependence predicted. However, Weiss and Worsham (Reference 19) found the 1/6 power for the stripping of liquid jets.
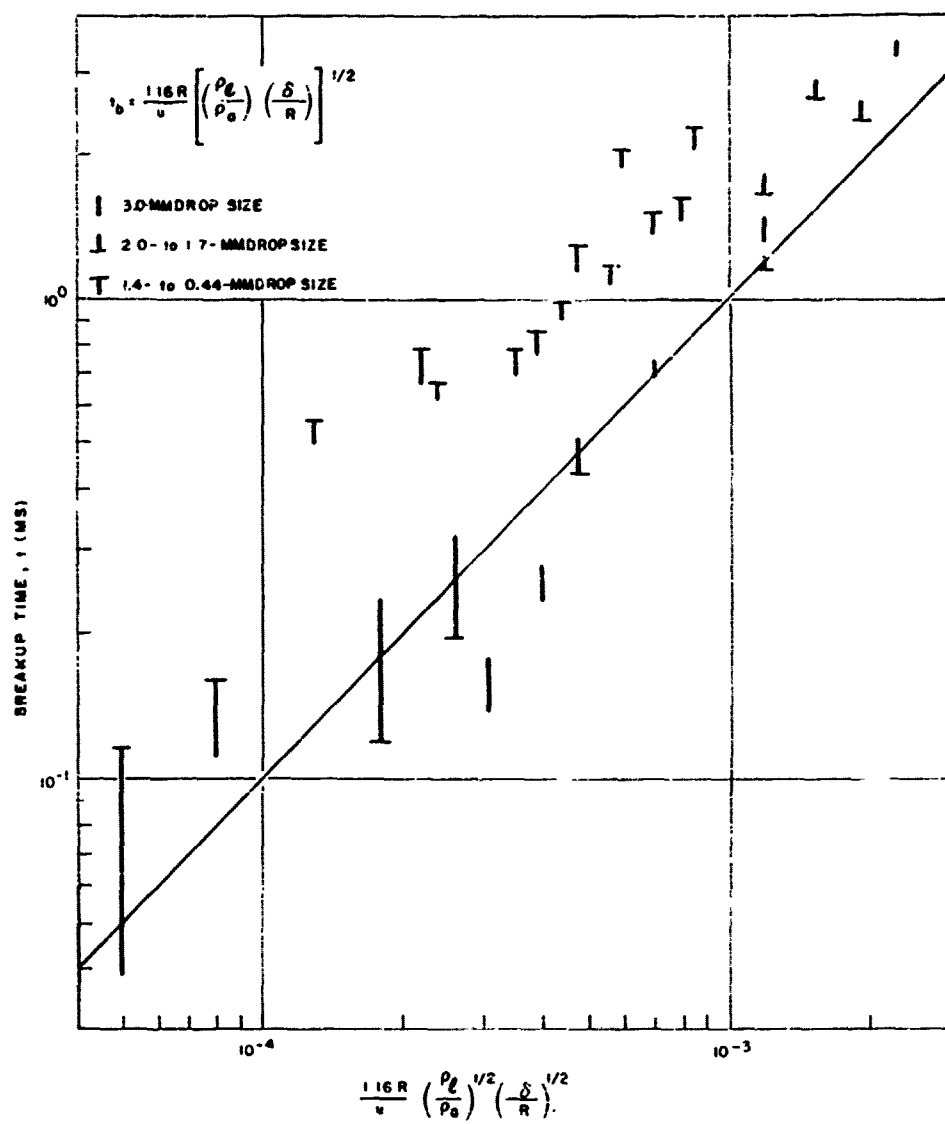
Figure 24. Comparison of Experimental Breakup Times with Hinze
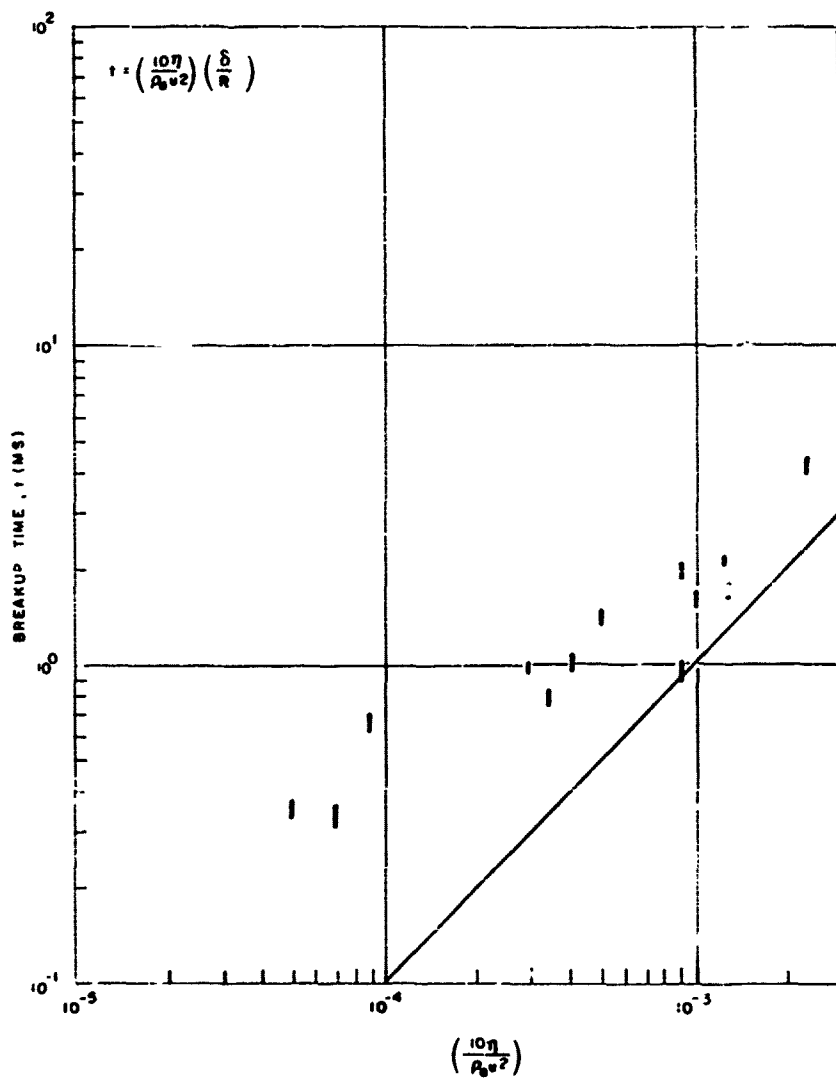Theory - Low Viscosity ⌐.⌐ (Water).

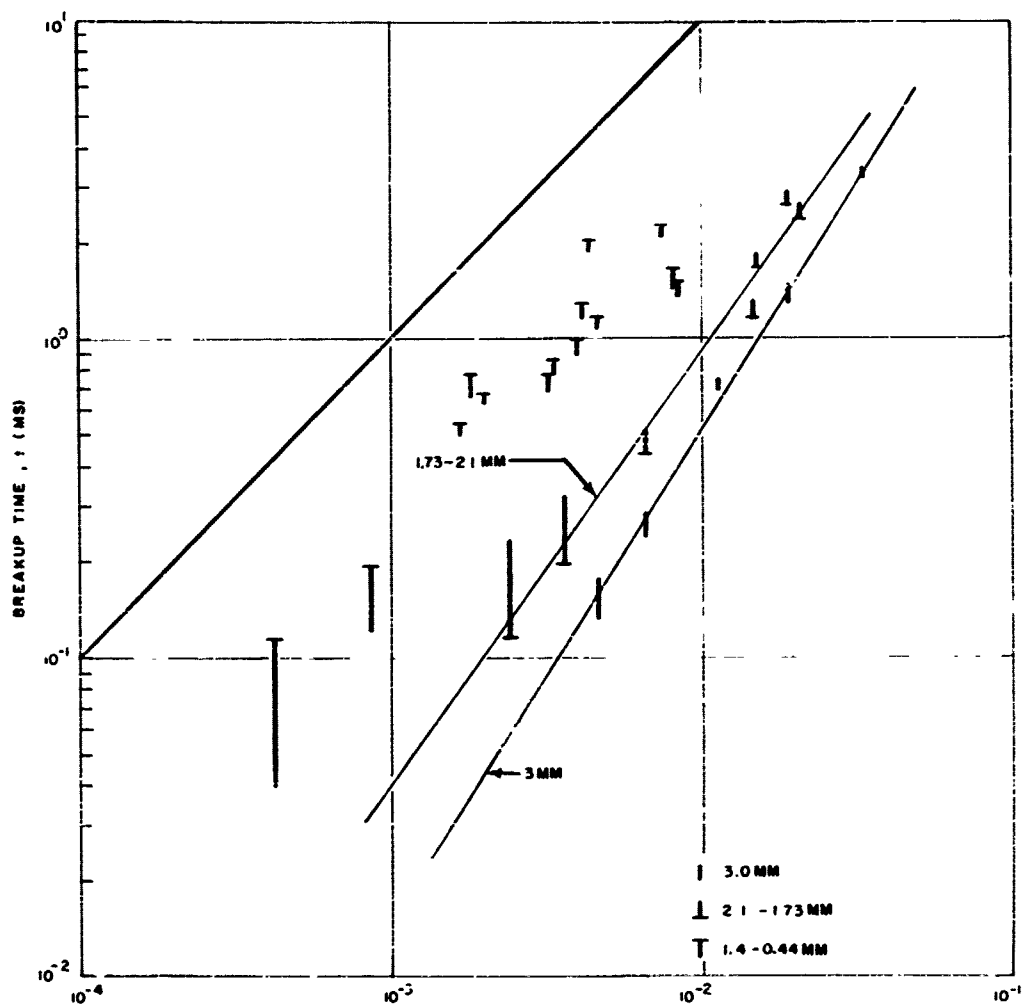Figure 25. Comparison of Experimental Breakup Times with Hinze Theory - High Viscosity Case (GE 5F(96(200).

$$0.536 \left(\frac{\rho_{\ell}}{\rho_a}\right)^{2/3} \left(\frac{\eta_a}{\eta_{\ell}}\right)^{1/3} \frac{R}{u} \sqrt{\frac{Re_o}{\left(1 + \frac{2\,We_J}{\sqrt{Re_o}}\right)}}$$

Figure 2o.   Comparison of Exp rimenta! ": ɔ Breakup Times with Morrell Theory for Stripping Breakup of Liquid Jets (Water).

-95-

WATER

T MERCURY

GE SF (96) 0 65

GE SF (96) 10

GE SF (96) 200

BREAKUP TIME, t (MS)

10^1

10^0

10^{-1}

10^{-2}

10^{-4}　　10^{-3}　　10^{-2}　　10^{-1}

$$0.536 \left(\frac{\rho_\ell}{\rho_g}\right)^{2/3} \left(\frac{\eta_g}{\eta_\ell}\right)^{1/3} \frac{R}{u} \sqrt{\frac{Re_0}{\left(1 + \frac{2 We_0}{\sqrt{Re_0}}\right)}}$$
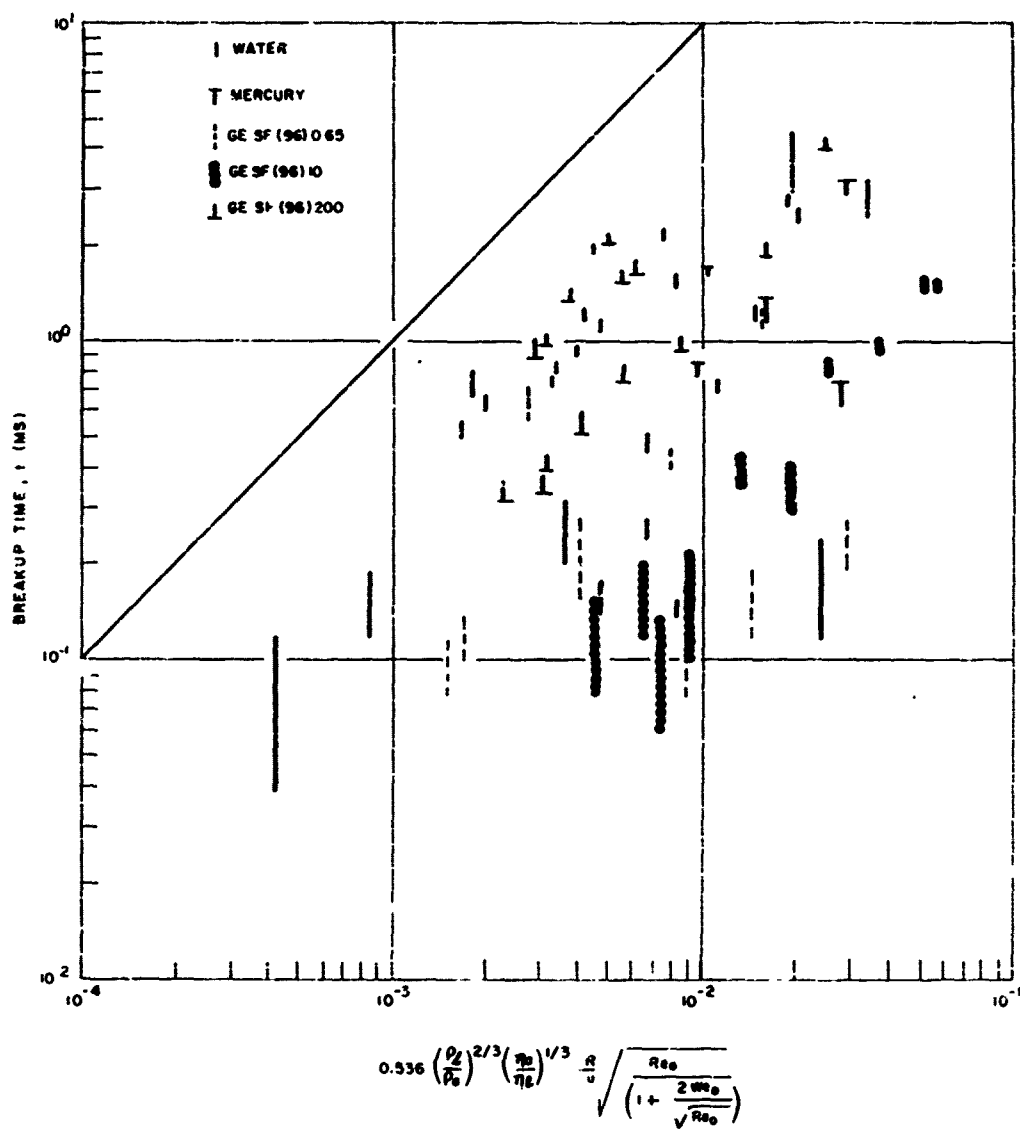
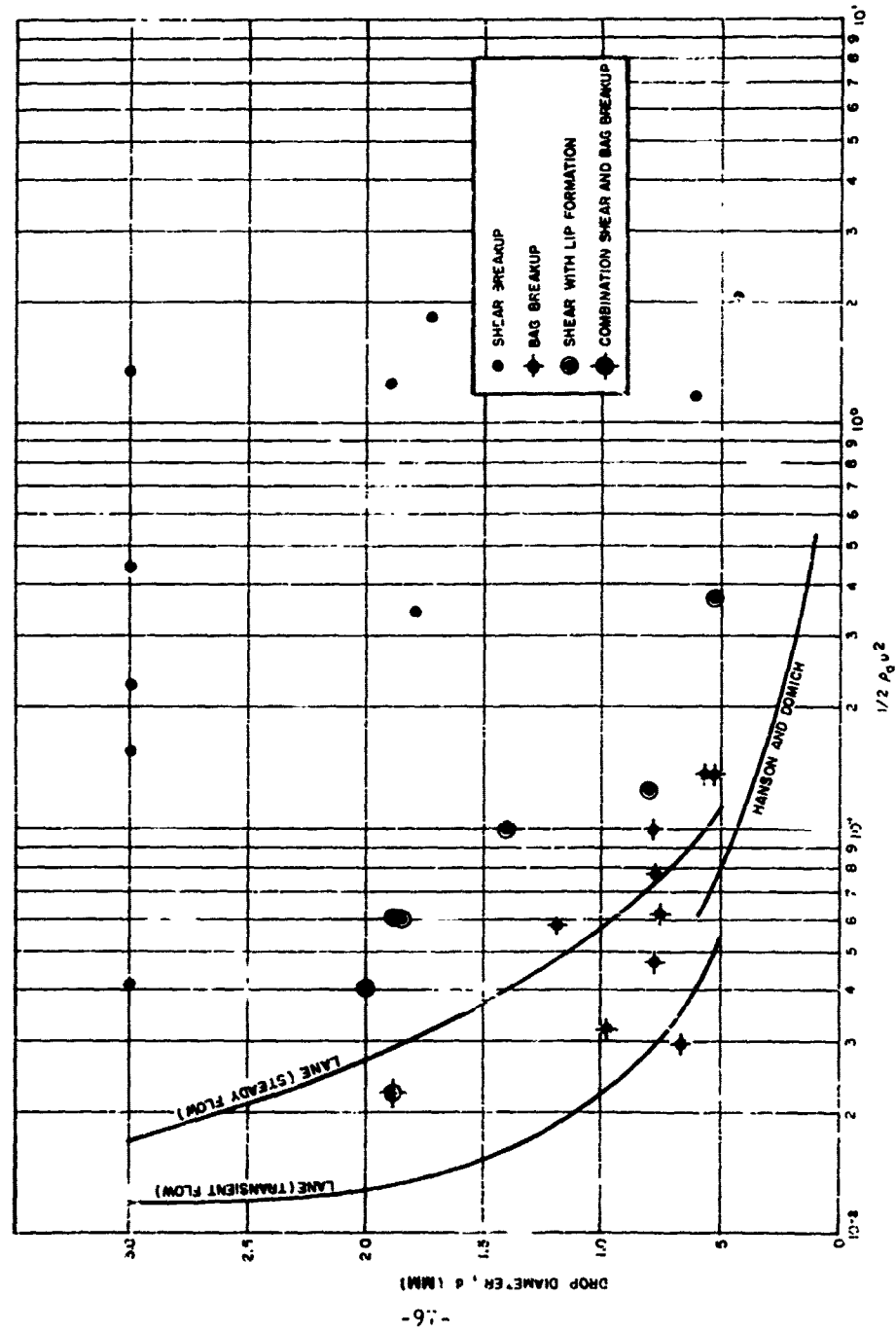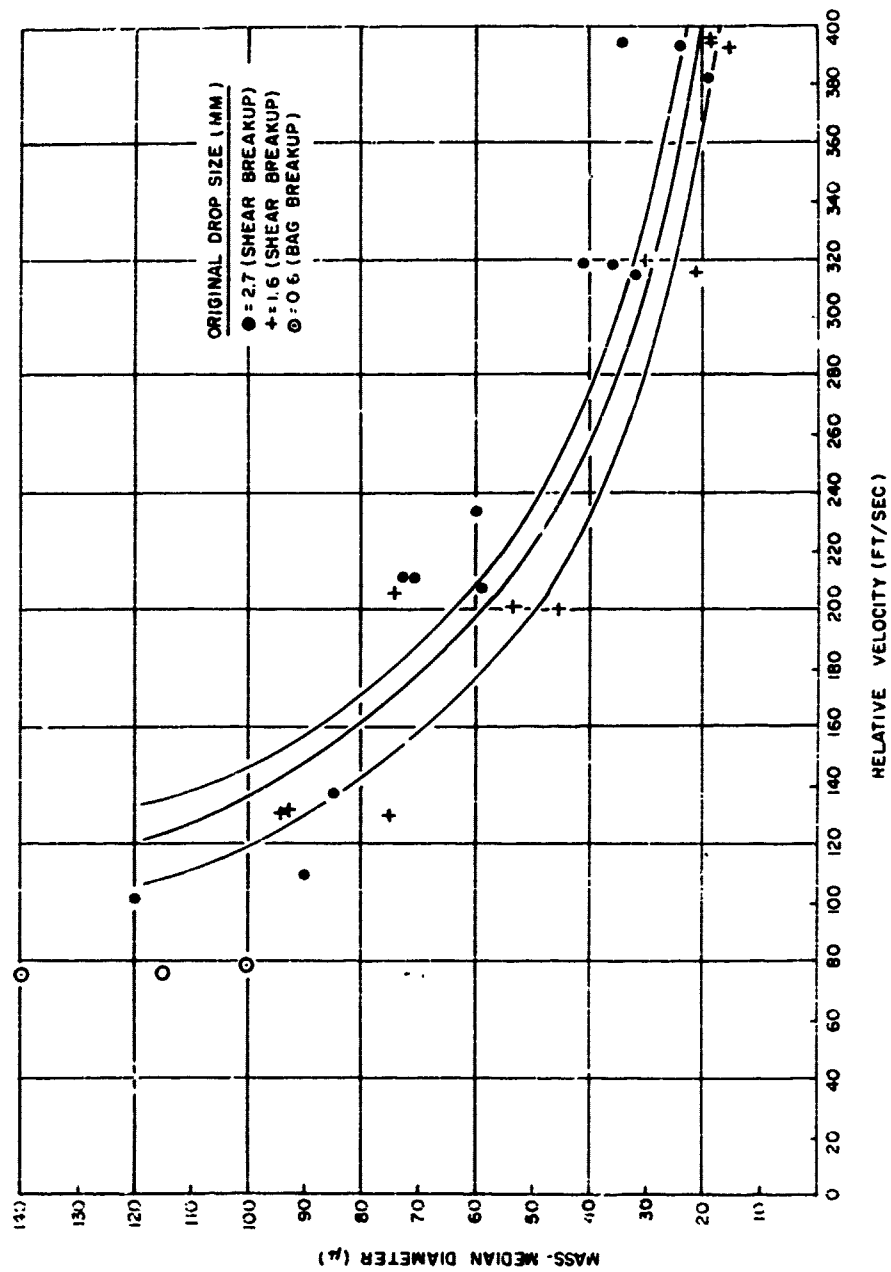Figure 17. Comparison of Experimental Drop Breakup Times with Morrell
Theory for Stripping Breakup of Liquid Jets.

-95-

2020-28 'Figure 28. Comparison of Experimental Results from Breakup of Water with Critical Size Curves Obtained by Hanson and Domich (References 30, 31) and Lane (Reference 28).

Figure 29. Comparison of Experimental Average Mass Droplet Sizes with Equation (58)(Bis).

OCC-29-1

-98-

The experimental data also suggest that the average drop size produced by bag breakup may not quite lie on the curves for shear breakup Again, however, it is difficult to draw definite conclusions but the comparison between experiment and theory is generally very encouraging (further experimental data, however, are required for a final evaluation)

As summarized in Equation 33. Mayer developed a theory for the average droplet size produced by the aerodynamic breakup of liquid drops A comparison of the theory with the experimental data is given in Figure 30 A value of B of about 0 1 is required to bring the theory to the same magnitude as the experimental data, but the functional varia tion still does not appear to agree with the experimental results The value of B is somewhat arbitrary, but was stated to be conceptually of the order of unity It would appear that the Mayer theory is less ade- quate than the theory developed in this report (which contains no arbitrary constants)

6 4 DRAG-COEFFICIENT MEASUREMENTS

As indicated in Section 4 3, experimentally determined drag coefficients for spheres and deformed liquids being accelerated in a gas stream show a wide range of values

The results of drag-coefficient measurements made on 3/32-in -diameter nylon spheres and some of the liquids used in this study are shown in Figures 31 through 40 In these illustrations the position, velocity, acceleration, lateral diameter (except for the nylon spheres) and drag co-fficient of the sphere or drop is shown as a function of time after being subjected to the flow In each case, the sphere or drop was in free-fall prior to onset of flow, and is thus depicted as having a slight negative velocity (assuming the air-flow direction to be positive) before being accelerated in the flow direction

Inspection of the data indicates that there is no characteristic shape of the drag-coefficient-vs-time curve and that the peak values of the curve may vary from $C_D = 0$ 90 to 4 4 for different tests

The value of the drag coefficient for the drop or sphere undergoing acceleration is written as shown in Equation 61
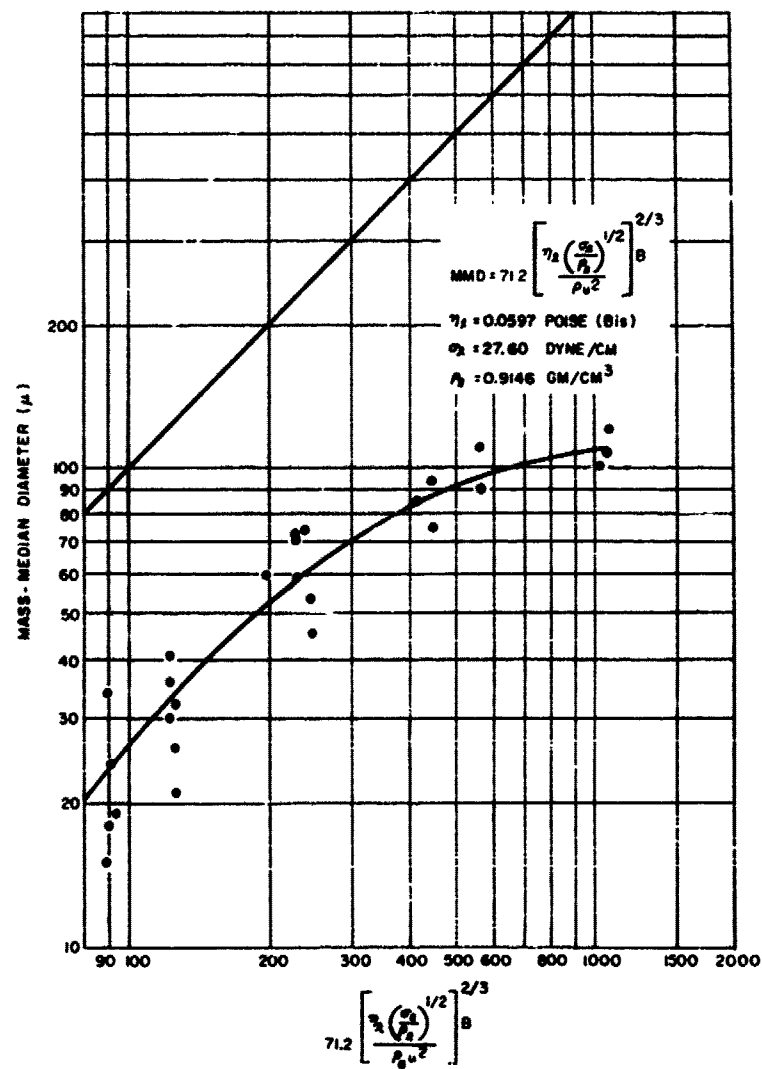
Figure 30. Comparison of Experimental Average Mass Droplet
Size with the Mayer Theory.
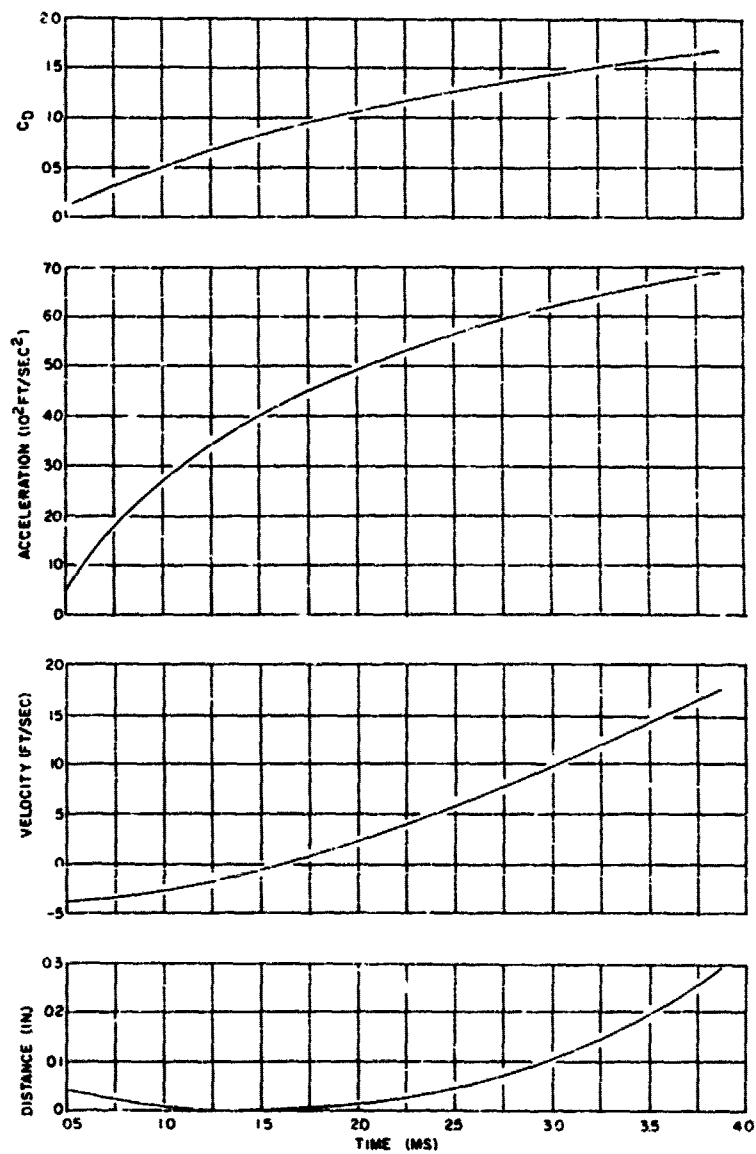
Figure 31. Motion of a 3/32-in.-Diameter Nylon Sphere Subjected to an Airflow of 208 ft/sec.

-10.-
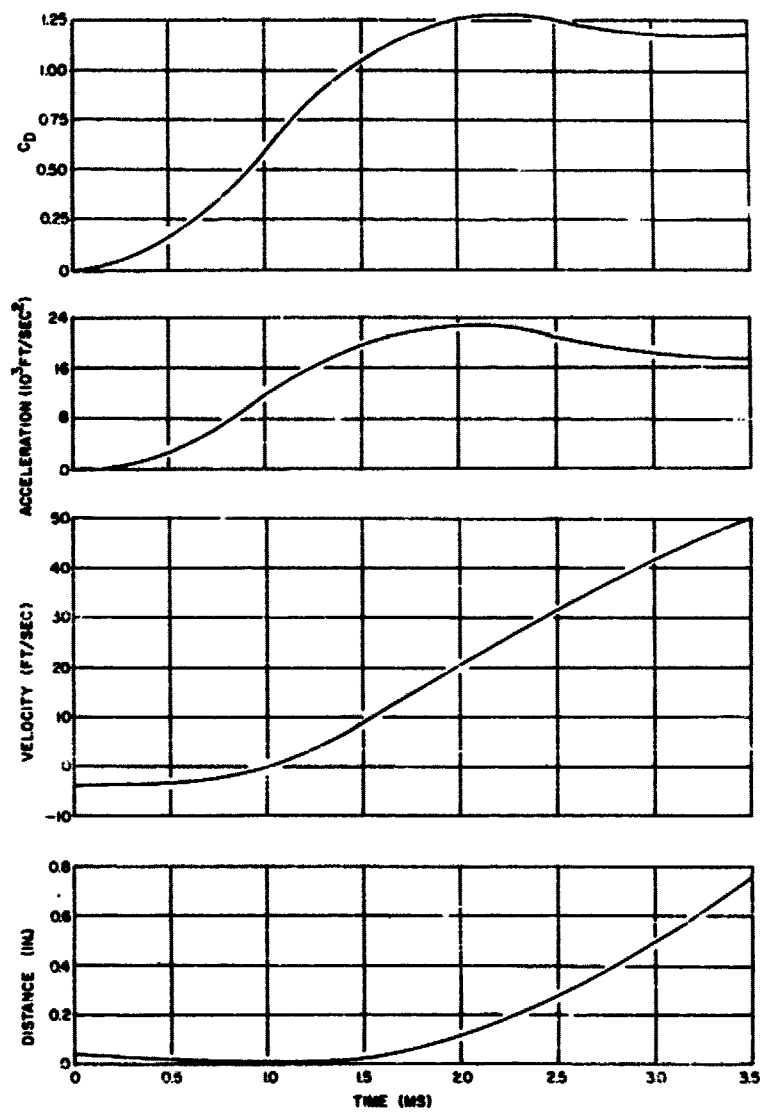
Figure 32. Motion of a 3/32-in.-Diameter Nylon Sphere Subjected to an Airflow of 386 ft/sec.
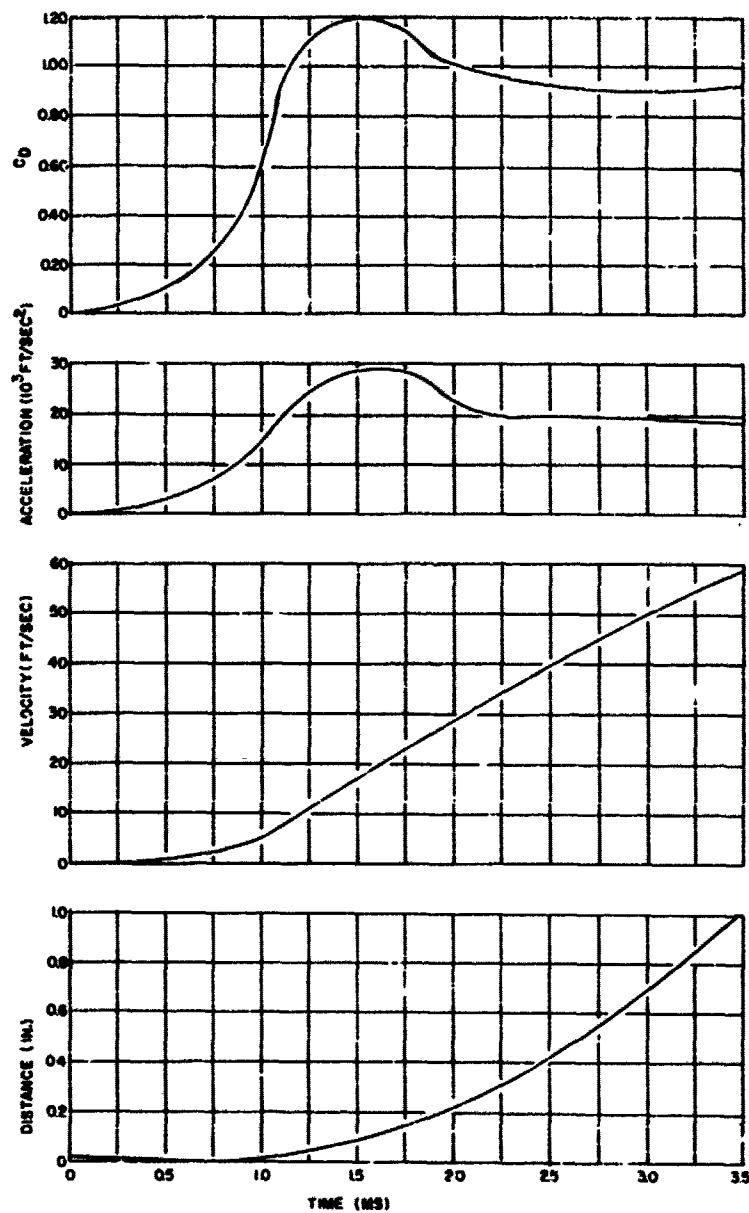
Figure 33. Motion of a 3/32-in.-Diameter Nylon Sphere Subjected to an Airflow of 434 ft/sec.

-103-

Figure 34. Motion of a 1.36-min.-Diamete. Drop of G. E. SF(96) 0.65
Silicone Fluid Subjected to an Airflow of 43 ft/sec.

Figure 35. Motion of a 1.25-min.-Diameter Drop of G.E. SF(96) 200 Silicone Fluid Subjected to an Air Flow of 161 ft/sec.

Figure 36. Motion of a 2.2mm-Diameter D. p of G. E. SF(96)200
Silicone Fluid Subjected to an Airflow of 208 ft/sec.

-10 -

Figure 37. Motion of a 1.45mm-Diameter Drop of G. E. SF(96)200
Silicone Fluid Subjected to an Airflow of 340 ft/sec.

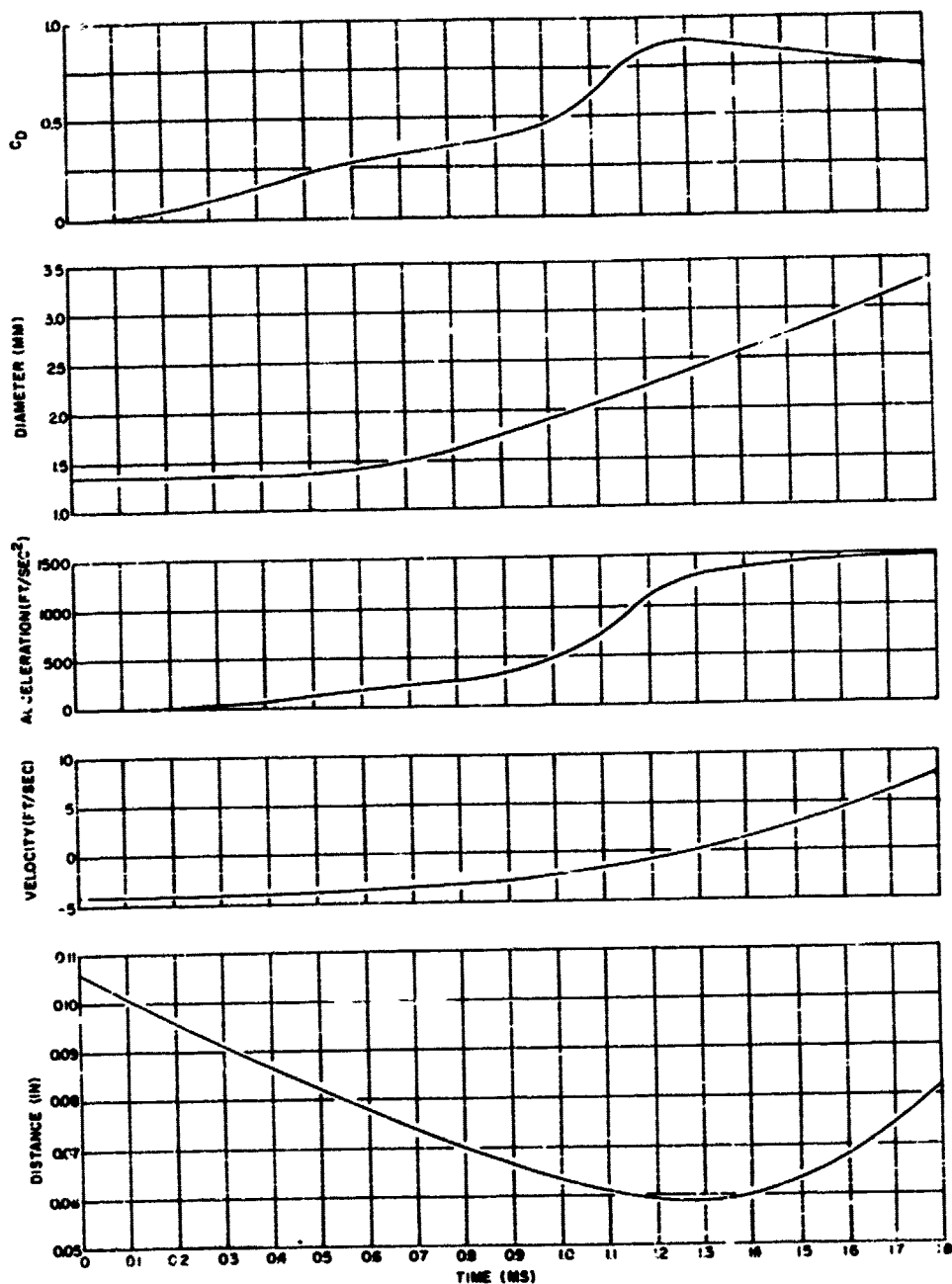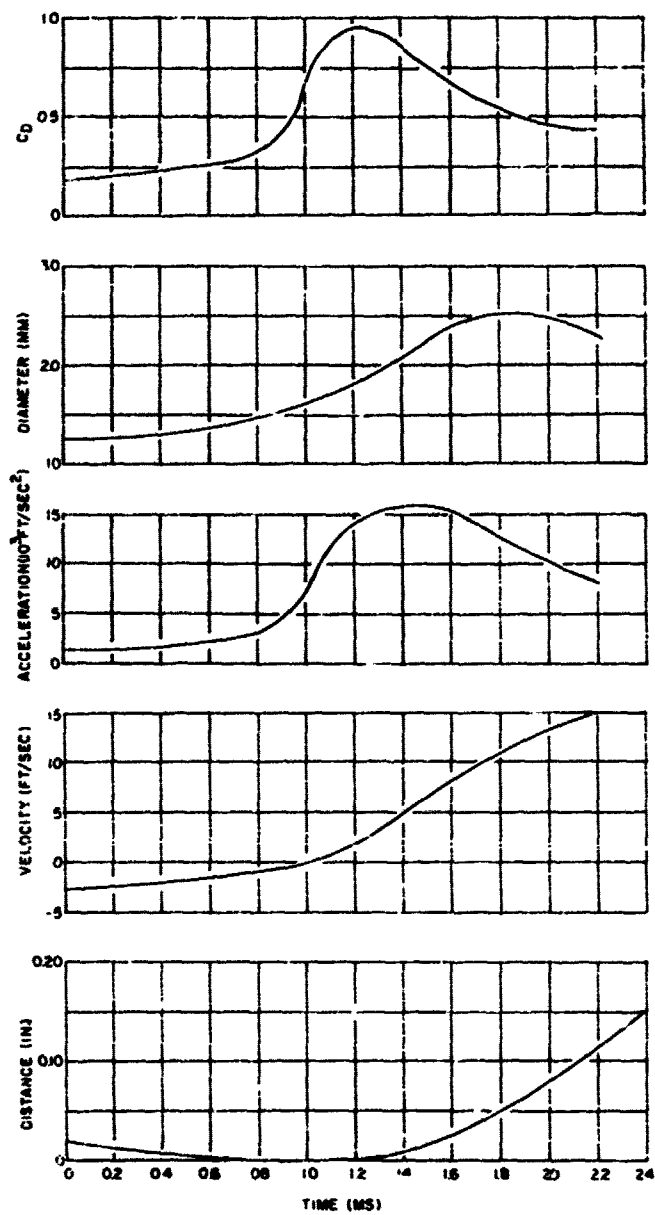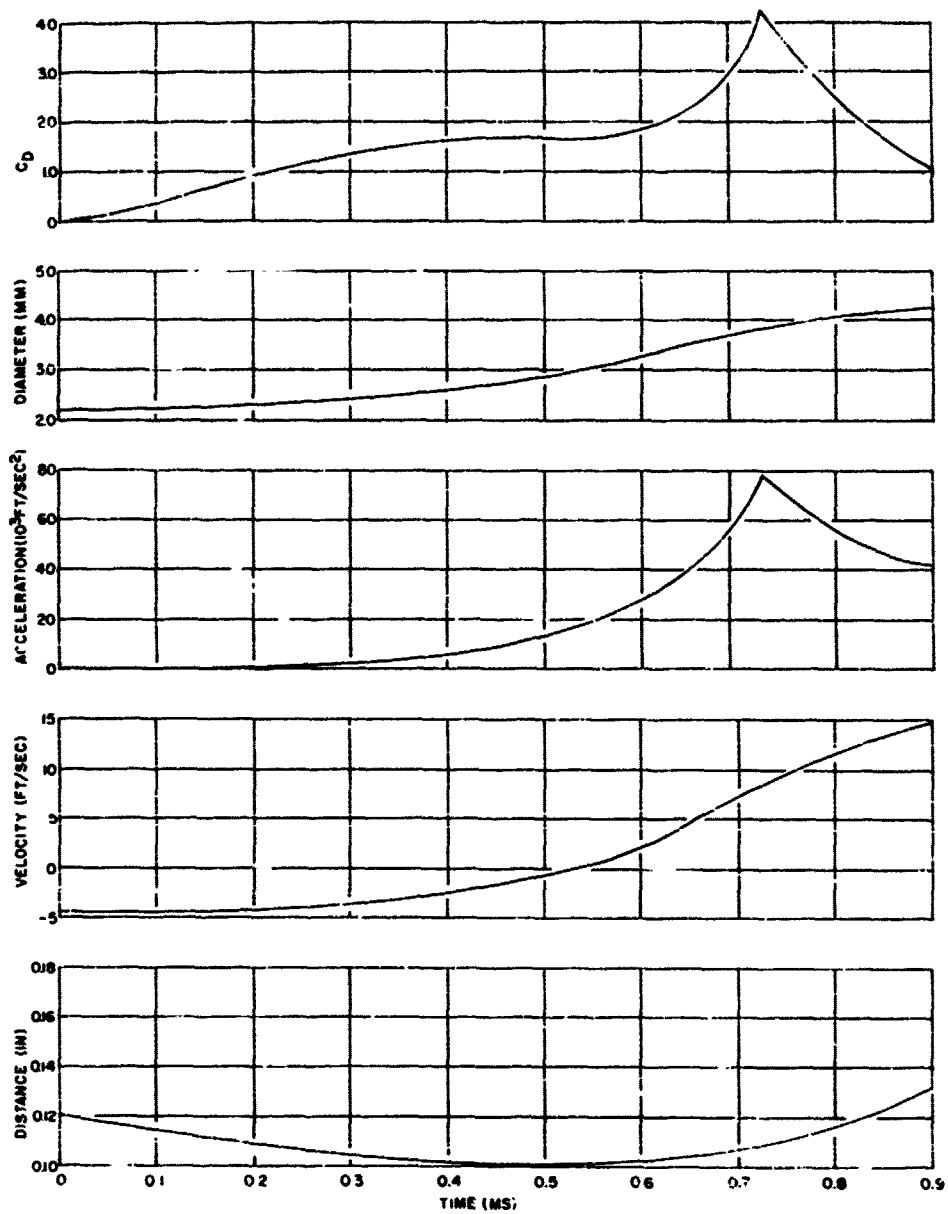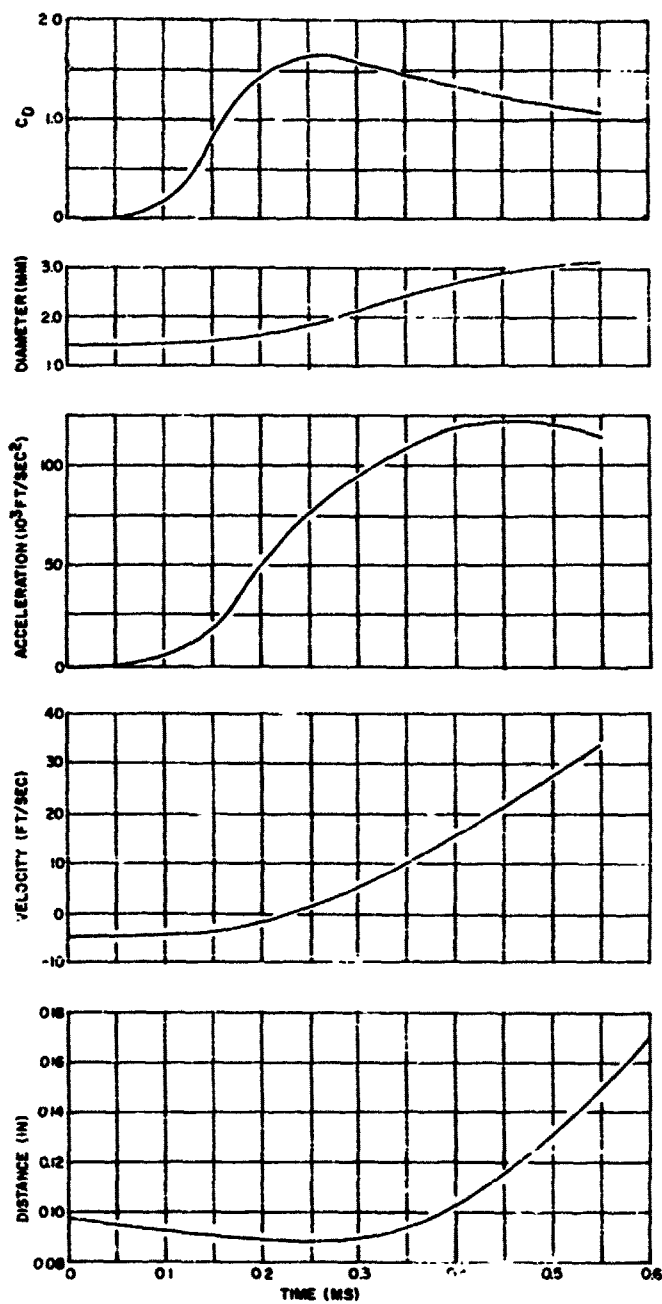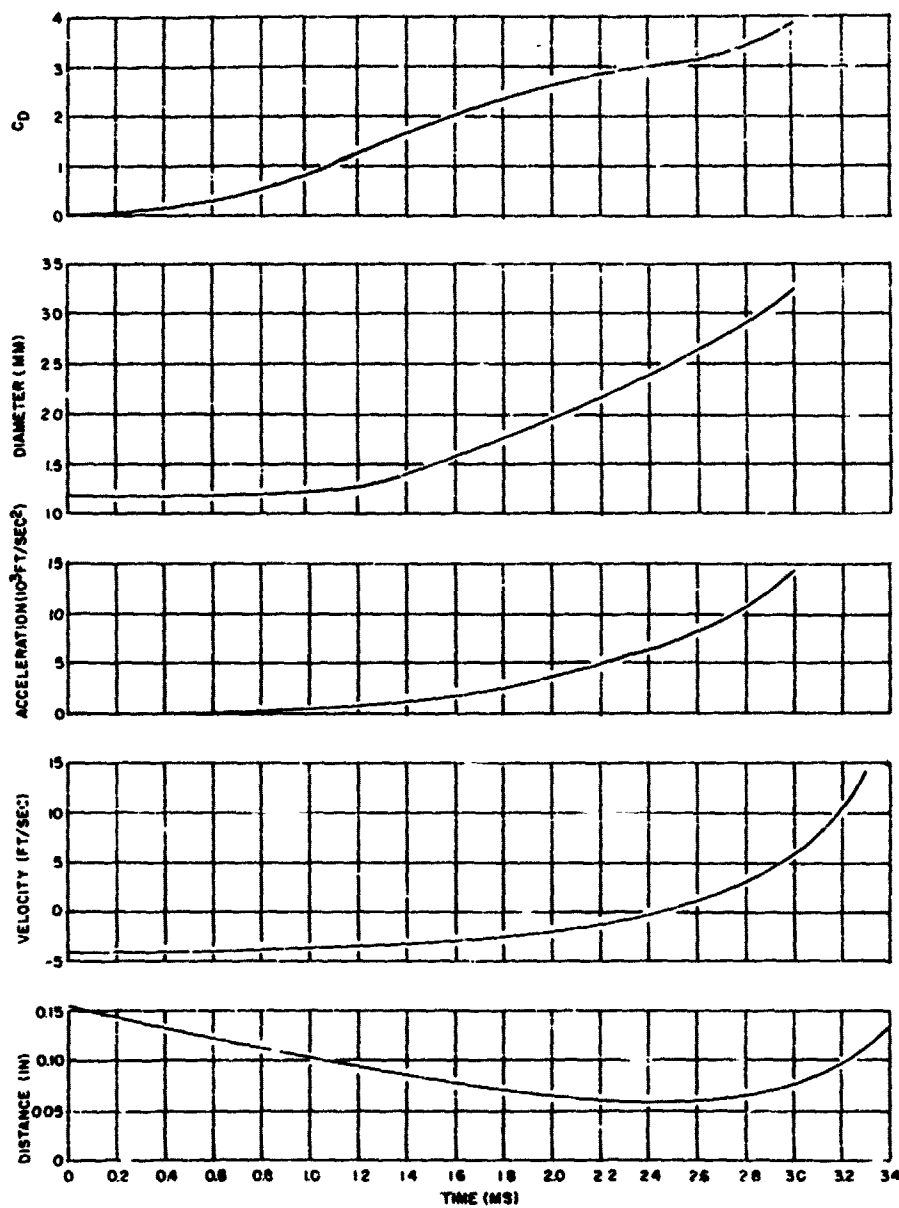Figure 3f. Motion of a 1.2mm-Diameter Drop of Mercury
Subjected to an Airflow of 168 ft/sec.
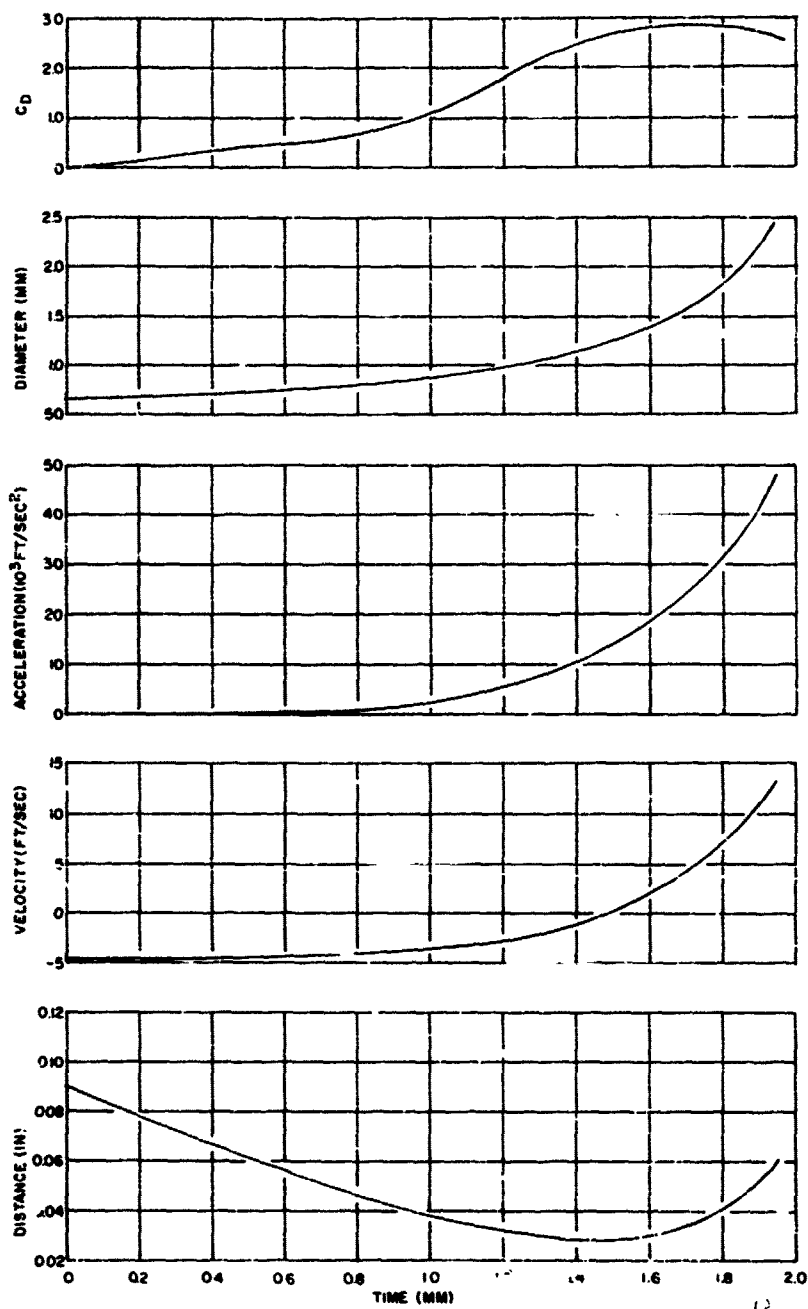
Figure 39. Motion of a 0.69mm-Diameter Drop of Mercury
Subjected to an Airflow of 221 ft/sec.
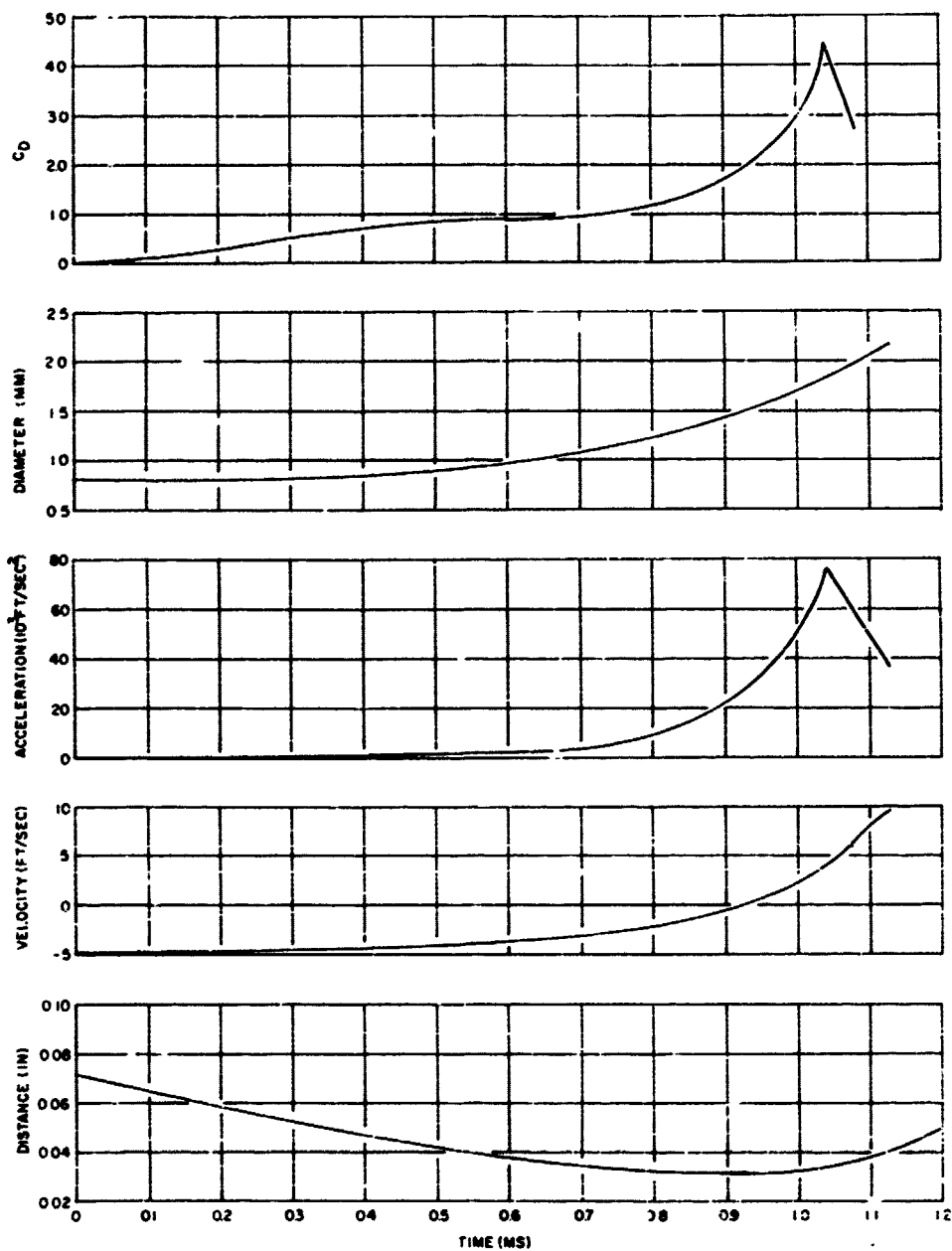
Figure 40. Motion of a 0. 82mm-Diam + Drop of Mercury
Subjected to an Airflow of 351 ft/sec.

$$C_D = \frac{4 \rho_l D_o^3}{3 \rho_a (V-v)^2 D_i^2} \frac{dv}{dt} \tag{61}$$

where

ρ_l	=	liquid or solid density
ρ_a	=	air density
V	=	air velocity
v	=	velocity of sphere or drop
D_o	=	original drop or sphere diameter
D_i	=	lateral diameter or deformed drop
$\dfrac{dv}{dt}$	=	acceleration of sphere or drop

Equation 61 indicates that the drag coefficient is directly proportional to the acceleration and inversely proportional to the square of the relative velocity and the square of the diameter of the drop normal to the airflow direction.

A comparison of the drag-coefficient curves to the corresponding acceleration curves indicates that the drag coefficient is influenced more by acceleration changes (which are very great) than by changes in relative velocity and lateral diameter. This effect leads to the possibility of rather large uncertainties in the calculated values of the drag coefficient, since the acceleration is determined by a numerical differentiation of the velocity curve (and the velocity curve is obtained in a like manner from the distance or position curve). The errors arise from the process of taking the difference between two values that are close together (close spacing of the readings is necessary to retain reasonably accurate representation of the curves).

Attempts to eliminate these errors by utilizing digital computer techniques to generate best-fit curves to the raw data and compute drag coefficients were unsuccessful because complex expressions were necessary to yield a satisfactory fit over the range of data. Hand-calculation techniques were then resorted to.

-111-

Although uncertainties in the drag-coefficient values are present, it is not felt that they are of sufficient magnitude to account for the wide range of peak values, nor to account for the widely differing shapes of the drag-coefficient curves.

It thus appears that no simple expression can be found to predict drag-coefficient values for small spheres or liquid drops being accelerated in a moving gas stream.

7.   CONCLUSIONS AND RECOMMENDATIONS

The studies described in this report have encompassed a considerable amount of literature work, original theoretical studies, and unique experimental studies. The following discussion summarizes major points of these studies and provides recommendations for future work.

The studies have shown that the breakup of a liquid is a rate process and should be considered from a time-dependent point of view. This consideration is particularly important when high-speed gas flows of transient nature are involved (e. g., shock loading), since the gas-flow acting on the liquid may be a rapidly changing function. It is also suggested that the aerodynamic breakup of bulk liquid with any geometry may be considered to occur in two main phases. The first phase comprises the shearing of layers, sheets, films, or jets from the liquid by the gas-flow forces; the second comprises the rapid breakup of these liquid streams by instabilities that grow exponentially with time. An estimate of the aerodynamic breakup time of the liquid may be made by quantitatively treating the first phase, whereas the resultant droplet sizes may be estimated by quantitatively treating the second.

The preceding concept was applied to liquid drops, and theoretical expressions were derived for both the breakup times of the original drop and the resultant droplet sizes produced by breakup. Experimental breakup times of drops of a variety of liquids with a wide range of physical properties were determined for several drop sizes over a wide range of gas-flow velocities. These studies were conducted using shock-tube and high-speed photographic techniques; agreement between experimental data and theory was very good, and it may be concluded that the breakup-time theory developed in this report is valid and adequate for general use. It would be of interest, however, to extend the experimental studies to much higher gas-flow velocities and much smaller initial drop sizes.

The experimental breakup times were also compared to the available theories in the literature. It was found that there is good agreement between the Gordon theory and experiment if the surface-tension pressure used in the Gordon theory is decreased by a factor of 2 to 4. The breakup theories of Hinze and Morrell were found to be generally unsatisfactory for use.

Liquid drops are observed to break by either a bag or stripping mechanism, and it was postulated that bag breakup is due to pressure drag, whereas stripping breakup is due to friction drag (friction drag was considered to be always greater than the pressure drag. A theory was presented showing that the original drop deformation produced by the gas flow increases the curvature and hence the surface-tension pressure at the outer edges of the drop. This effect explains why bag breakup occurs near the critical velocity required for breakup, whereas stripping breakup occurs at higher velocities. The experimental results are generally in agreement with the theory. It would be of interest to extend the theoretical studies so that a more rigorous treatment may be developed.

In the development of the model for the aerodynamic breakup of liquid drops, it was pointed out that with certain modifications, the treatment should also be suitable to describe the breakup (erosion) of solid particles in high-velocity gas flows. It would be desirable to conduct both experimental and theoretical studies along these lines (these studies may have direct applicability to the problem of the breakup of particle agglomerates).

Preliminary experimental studies were conducted to obtain the droplet-size distributions produced by the aerodynamic breakup of liquid drops, and the experimentally determined mass-mean diameters of the resultant drops were compared with the theory that was developed in this report. Agreement was very good, considering the relative scatter in the experimental data and the fact that the theory contains no arbitrary constants. The experimental data were also compared to the theory of Mayer; agreement was less satisfactory than with the theory developed in this report, and moreover contains a constant that must be evaluated from the experimental data. It is concluded that the developed theory is at present, most reliable for use. As a final recommendation, it is suggested that further studies, both experimental and theoretical, be conducted with regard to obtaining the droplet-size distributions produced by the aerodynamic breakup of liquid drops.

REFERENCES

1. E. Giffen and A. Muraszew, The Atomization of Liquid Fuels, John Wiley & Sons, Inc., New York, 1953.

2. J. P. Longwell, "Combustion of Liquid Fuels, " Combustion Processes, Princeton University Press, 1956, pp. 407-443.

3. C. C. Miesse, "From Liquid Stream to Vapor Trail, " Proc. Gas Dynamics Symp., Northwestern Univ., Evanston, Ill., 1956, pp. 7-26.

4. A. A. Putnam et al., Injection and Combustion of Liquid Fuels, WADC Tech. Rept. 56-344, 1957.

5. J. D. Lewis, "Studies of Atomization and Injection Processes in the Liquid Propellant Rocket Engine, " Fifth AGARD Combn. and Propulsion Coll., Pergamon Press, 1963.

6. Lord Rayleigh, Proc. Lond. Math. Soc. 104, (1878), Phil. Mag. 34, 153 (1892); Theory of Sound, Dover Pub., New York, Vol. II, p. 360, 376 (1945).

7. C. Weber and Z. F. Angew, Math. U. Mech. Vol. II, 136 (1931), English Translation, "On the Breakdown of a Fluid Jet, " Ninth Progress Rept., Project MX-833, Sect. II, Univ. of Colorado, Boulder, Colorado.

8. A. Haenlein, "Disintegration of a Liquid Jet, " NACA TM 659, 1931.

9. R. A. Castleman, J. Res. Nat. Bur. Standards 6, 369 (1931).

10. B. B. Fogler and R. V. Kleinschmidt, Ind. Eng. Chem. 30, 1372 (1938).

11. P. H Schweitzer, J. App. Phys. 8, 513 (1937).

12. A. C. Merrington and E. G. Richardson, Proc. Phys. Soc. 59, 1 (1947).

13. I. F. Dityakin and V. I. Yagodkin, "Effect of Periodic Oscillations of Velocity and Density of a Medium on Disintegration of Liquid Jets, " NASA TT F-63, April 1961.

14. B. Dunne and B. Cassen, J. App. Phys. 25, 569 (1954), 27, 577 (1956).

15. P. Eisenklam and P. C. Hooper, "The Flow Characteristics of Laminar and Turbulent Jets of Liquid, " Imperial College Rept. JRL 42, 1958.

16. S. Middleman and J. Gavis, Phys. Fluids 4, 355 (1961).

17. H. Straubel, Naturwissenschaften 40 337 (1953).

REFERENCES (Cont)

18.   C. C Miesse, Jet Propulsion 25, 525 (1955)

19   M. A. Weiss and C. H. Worsham, ARS J. 29, 252 (1959)

20.   S Nukiyama and Y. Tanazawa, Trans. Soc Mech. Eng (Japan) 4, 86,
      138 (1938), 5, 62, 68 (1939):6, 11-7, 11-15 (1939); 6, 11-18 (1940)

21.   W. R. Marshall, Chem. Eng. Prog , Monograph Series 2, 5, 1954

22.   H. Lamb, Hydrodynamics, 6th Ed. , Dover Pub , 1932

23   H B. Squire, Brit. J. App. Phys. 4, 167 (1953)

24   J .. York, H. E. Stubbs, and M. R. Tek, Trans ASME, 75, 1279 (1953)

25.   V. A. Borodin and Y. F. Dityakin, "Unstable Capillary Waves on Surface
      of Separation of Two Viscous Fluids, " NACA Tech. Memo 1281, 1951

26   G. I. Taylor, Proc. Roy. Soc. A201, 192 (1950).

27.   R. D. Richtmyer, Comm Pure App. Math, 13, 297 (1960;

28.   W. R. Lane, Ind. Eng. Chem. 43, 1312 (1951).

29.   J. O. Hinze, App. Sci. Res Al, 253, 273 (1949).

30   A. R. Hanson, F G. Domich, and H S. Adams, "An Experimental
      Investigation of Impact and Shock Wave Breakup of Liquid Drops, " Rept
      125, Univ. of Minnesota, Nov. 1955: also Phys. Fluids 6, 1070 (1963)

31.   A. R. Hanson and F G Domich, "The Effect of Liquid Viscosity on the
      Breakup of Droplets by Air Blasts - A Shock Tube Study, " Rept. 130,
      Univ. of Minnesota, June 1956, also Phys. Fluids 6, 1070 (1963)

32.   R J. Priem, Jet Propulsion 27, 1084 (1957).

33.   K. Sato, "Interaction of Burning Liquid Droplets and Shock Waves, " Rept
      1487, Aerojet-General Corp. , Azusa, Calif. , Aug. 1958

34   R. H Magervey and B. W. Taylor, J App. Phys. 27, 1129 (1956)

35.   Lord Rayleigh. Theory of Sound, Vol. II, Dover, 1945, p 373.

36   O. G. Engle, J Res NBS 60, 245 (1958).

37   E. Rabin and R. Lawhead, "The Motion an Shattering of Burning and Non-
      burning Propellant Droplets " AFOSR TN-59-129, Rocketdyne, March 1959

REFERENCES (Cont)

38. E. Rabin, A. R. Schallenmuller, and R. B. Lawhead, "Displacement and Shattering of Propellant Droplets, " AFOSR TR60-75, Rocketdyne, March 1960

39. G. D. Gordon, J. App. Phys. 30, 1759 (1959).

40. K. N. Dodd, J. Fluid Mech. 9, 175 (1960).

41. G. Morrell, "Breakup of Liquid Jets by Transverse Shocks, " Eighth Symp. (Int.) on Combustion, Williams & Wilkins Co. , Baltimore, pp. 1059-1068, 1962 (presented Aug. 1960).

42. G. Morrell, "Critical Conditions for Drop and Jet Shattering, " NASA TN-D-677, Nov. 1960.

43. G. Morrell, "Rate of Liquid Jet Breakup by a Transverse Shock Wave, " NASA TN-D-1728, Feb. 1963.

44. M. S. Volynskii, Doklody Akad. Nauk, U.S.S R. 62, 301 (1948).

45. V. A. Sandborn and S. J. Kline, Trans. ASME, 83, 3.7 (1961).

46. E. Mayer, ARS J. 31, 1783 (1961).

47. W. N. Bond and D. A. Newton, Phil. Mag. 5, 794 (1928).

48. G. I. Taylor, Proc. Roy. Soc. (London) A138, 41 (1932).

49. F. D. Rumscheidt and S. G. Mason, J. Colloid Sci. 16, 238 (1961).

50. H. Eyring, J. Chem. Phys. 4, 283 (1936).

51. S. Glasstone, K. J. Laidler and H. Eyring, The Theory of Rate Processes, McGraw-Hill Book Co. , Inc. , New York, 1941, Chapter IX.

52. H. Eyring, J. Chem. Phys. 3, 107 (1935).

53. A. A. Putnam et al , Injection and Combustion of Liquid Fuels, WADC Tech. Rept. 56-344, 1957, Chapter 5

54. L. Prandtl and O. G. Tietjens, Applied Hydro and Aeromechanics, Dover Publications, Inc. , New York, 1937, Chapter III.

55. A. Tobolsky, R. E. Powell, and H. Eyring, "Elastic-Viscous Properties of Matter, " The Chemistry of Large Molecules. Interscience, New York, 1943, pp. 125-190.

56. J R. Partington, An Advanced Treatise on Physical Chemistry, Vol. 2, The Properties of Liquids, Longmans. Green & Co. , New York, 1951.

REFERENCES (Cont)

57. A. C. Charters and R. N. Thomas, J. Aeronautical Sci. 12, 4 (1945).

58   R. R. Hughes and E. R. Gilliland, Chem. Eng. Progress 48, 497 (1952).

59   R. D. Ingebo, "Drag Coefficients for Droplets and Solid Spheres in Clouds Accelerating in Airstreams," NACA TN 3762, Sept. 1956.

60. A. Putnam, ARS J. 31, 1467 (1961).

61. P. P. Wegener and H. Ashkenas, J. Fluids Mech. 10, 550 (1961)

62. E. R. Benton and D. A. Knapton, ARS J. 32, 1608 (1962)

63. C. T Crowe, J. A. Nicholls, and R. B. Morrison, Ninth Symp. (International) on Combustion, Academic Press, New York, 1963, pp. 395-406.

64. S. Tomotika and T. Aoi, Quart. J. Mech. App. Math, 3, 140 (1950).

65. R. A. Mugele and H. D. Evans, Ind. Eng. Chem 43, 1317 (1951).

66. W. Bleakney, D. K. Weimer, and C. H. Fletcher, Rev. Sci Inst. 6, 807 Nov. (1949).

67   F. W. Geiger, C. W. Mautz, and R. N Hollyer, Jr , "The Shock Tube as an Instrument for the Investigation of Transonic and Supersonic Flow Patterns," Eng. Res. Inst., Univ. of Mich., Project M720-4, ATI 63892, 1949

68   I. I. Glass, W. Martin, and G. N. Patterson, "A Theoretical and Experimental Study of the Shock Tube." UTIA Report 2, Nov 1953, Inst of Aerophysics, Univ of Toronto.

69   J. N. Bradley, Shock Waves in Chemistry and Physics, John Wiley & Sons, New York, 1962.

70. A. G. Gaydon and I. R. Hurle, The Shock Tube in High-Temperature Chemical Physics, Reinhold Pub. Corp., New York, 1963.

71. C. E. Mendenhall et al , College Physics, D. C. Heath & Co , Boston, 1944, p. 152

72   G. Asset, Am. Ind. Hygiene Assoc J 20, 56 (1959)

73   "Resume of the Theory of Plane Shock and Adiabatic Waves with Applications to the Theory of the Shock Tube. " N.L. TN 139, Mar 1950.

APPENDIX A

SHOCK-TUBE THEORY

A-1 INTRODUCTION

The following discussion begins with a qualitative description of shock-tube behavior. For simplicity, the description is limited to the particular case where air is used in both the compression and expansion chambers and the expansion chamber is open-ended.

As shown in Figure A-1a, the gases in the compression and expansion chambers are at the same temperature but at different pressures, with P_3 being greater than P_0. Since the expansion chamber is open-ended, the pressure and temperature therein are assumed to be at local ambient values. Pressure P_3 is maintained at a value greater than P_0 by an airtight diaphragm separating the two chambers.

If the diaphragm separating the two regions is suddenly removed, a compression wave progresses into the expansion chamber, while a rarefaction wave simultaneously moves toward the closed end of the compression chamber. After some distance, the compression wave steepens into a plane shock wave, which moves through the expansion chamber at a velocity, w, determined by the pressure ratio, $P_3/P_0 = P_{30}$. Passage of the shock wave imparts a uniform velocity, u, to the expansion-chamber gas and raises its pressure, density, and temperature to P_1, ρ_1, and T_1, so that $P_0 < P_1 < P_3$, $\rho_0 < \rho_1 < \rho_3$, and $T_1 > T_0$. The pressure-distance conditions are depicted in Figure A-1b, where the shock wave has reached the test location and the rarefaction wave is progressing toward the closed end of the compression chamber.

The contact surface (sometimes called the "cold front") represents the boundary between the compression and expansion-chamber gases. It also moves through the expansion chamber with the velocity u, as does the compression chamber gas at P_1 behind the contact surface.

The region behind the contact surface is compression-chamber gas that is expanded down to pressure, temperature, and density P_1, T_2, ρ_2 by the rarefaction wave so that $P_0 < P_1 < P_3$, $T_2 < T_0$, and $\rho_1 < \rho_2 < \rho_3$.

In Figure A-1c, the shock wave is shown as having arrived at the open end of the expansion chamber; the contact surface has continued to move through the expansion chamber at the velocity u, and the rarefaction wave has collided with, and rebounded from, the closed end of the compression chamber.

Figure A1. Shock Tube Pressure Diagrams.

-A3-

The exit of the shock wave from the open end of the expansion chamber creates a rarefaction wave, which moves back onto the expansion chamber as shown in Figure A-1d, where it has reached the test location.

The region between the shock wave and the contact surface, being a zone of constant pressure, temperature, density, and particle velocity, is ideally suited as an aerodynamic test region of short duration. Testing time available is the elapsed time from the passage of the shock wave to the arrival of one of the following:

- The contact surface

- The reflected rarefaction from the compression chamber

- The rarefaction wave from the open end of the expansion chamber

In Figure A-1, the testing time would be represented by the time for the events from (b) to (d) to occur. For this particular case, the testing time is terminated by the arrival of the rarefaction from the open end of the expansion chamber.

A-2   SHOCK-TUBE THEORY

The equations describing the conditions in the shock tube are derived by making use of the equations of continuity, momentum, motion, and energy, plus the equation of state for ideal gases. Assumptions are made that the flow is inviscid, that shock compression occurs adiabatically, and expansion is isentropic.

One of the most important expressions in shock-tube behavior is that showing the relationship between the pressures in the various regions. Adopting the subscript notation of Figure A-1 and writing the pressure ratio P_3/P_0 as P_{30}, the relationship between the compression-chamber pressure and the shock pressure can be written as

$$P_{30} = \cfrac{P_{10}}{\left[1 - \cfrac{(P_{10} - 1)}{(\alpha + 1)(\alpha P_{10} + 1)}\right]^{1/\beta}} \qquad (A-1)$$

-A4-

where

F_{30} = ratio of compression-chamber pressure to expansion-chamber pressure

P_{10} = ratio of pressure behind shock wave to expansion-chamber pressure ahead of shock wave

α = $\dfrac{\gamma + 1}{\gamma - 1}$

β = $\dfrac{\gamma - 1}{2\gamma}$

γ = C_P/C_V = specific heat ratio for the gas

In Equation A-1 and the following expressions, it has been assumed that γ remains constant and has the same value in all of the flow regions. Work reported in Reference 68 substantiates this assumption for the normal operational range of shock tubes similar to those used in the present study.

The speed of the shock wave is given by

$$w = a_o \sqrt{\beta (\alpha\, P_{10} + 1)} \qquad (A-2)$$

where

a_o = speed of sound in the gas ahead of the shock

The flow velocity behind the shock wave is given by

$$u = a_o \frac{(P_{10} - 1)}{\gamma \sqrt{\beta (\alpha\, P_{10} + 1)}} \qquad (A-3)$$

The density ratio across the shock wave is written as

$$\rho_{10} = \frac{1 + \alpha\, P_{10}}{P_{10} + \alpha} \qquad (A-4)$$

-A5-

Using the ideal gas law, the temperature ratio across the shock wave becomes

$$T_{10} = P_{10} \left[\frac{P_{10} + \alpha}{\alpha P_{10} + 1} \right] \qquad (A-5)$$

A complete derivation of Equations A-1 through -5 can be found in numerous sources available in the open literature (References 66 through 70 and 73).

To illustrate the variation of the parameters given in Equations A-1 through -5 with change in compression-chamber pressures, values were calculated for various pressures used in this study. The results of the calculations are shown in Figure A-2, where the initial conditions in the expansion chamber were assumed as follows:

$$P_o = 14.25 \text{ psia}$$

$$T_o = 535 \text{ }^o R$$

$$\rho_o = 0.0719 \text{ lb/ft}^3$$

$$a_o = 1135 \text{ ft/sec}$$

The shock tube used in this study was located at an elevation of approximately 1000 ft above sea level in an air-conditioned room, with the temperature maintained at an average value of 75°F. Thus, the conditions used for the calculations are typical of values encountered during the tests

Figure A-3 shows the variation of pressure, temperature, and density behind the shock wave with flow velocity for the range covered in this study.

Duration of the testing time was calculated from the various expressions describing flow conditions in the shock tube (Equations A-1 through -5) and the lengths of the various portions of the tube. To compute the testing time available, the following nomenclature was employed:

L_t = distance from diaphragm to test location

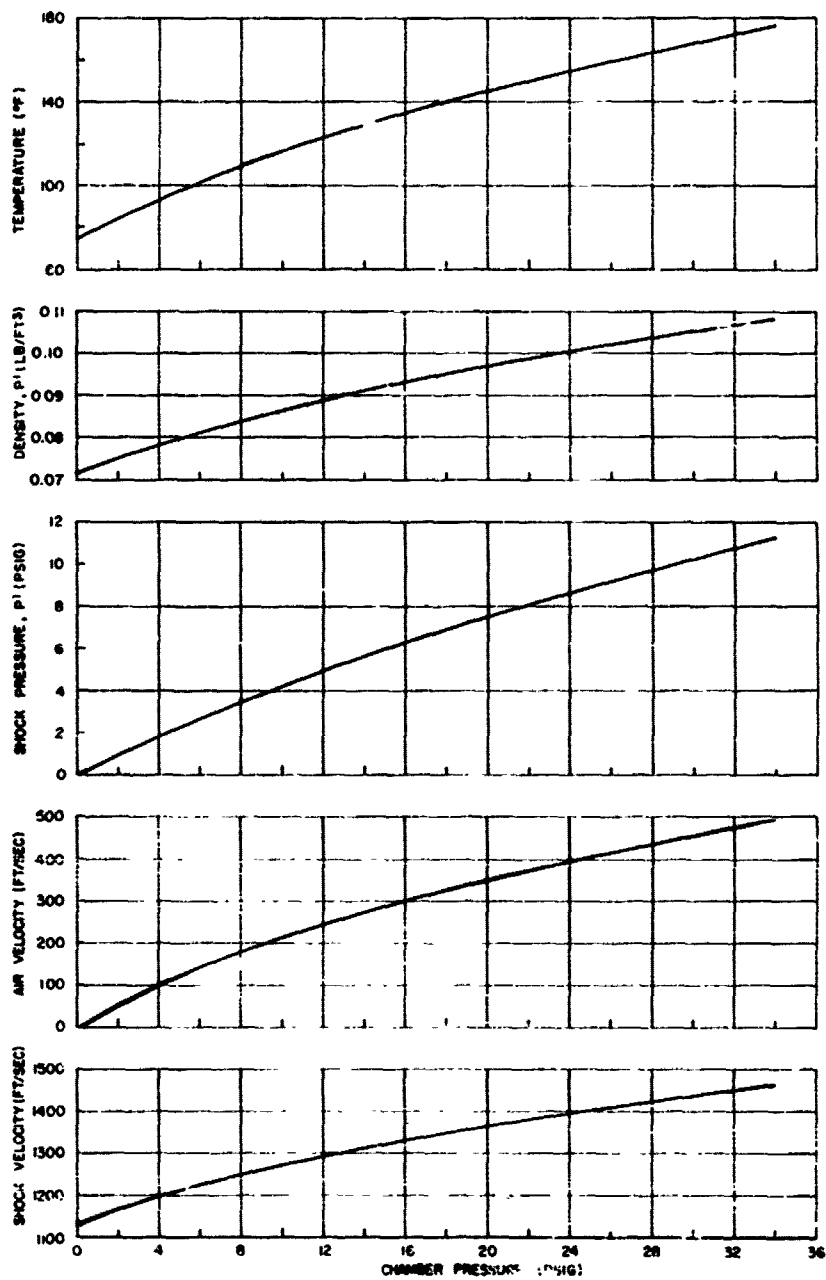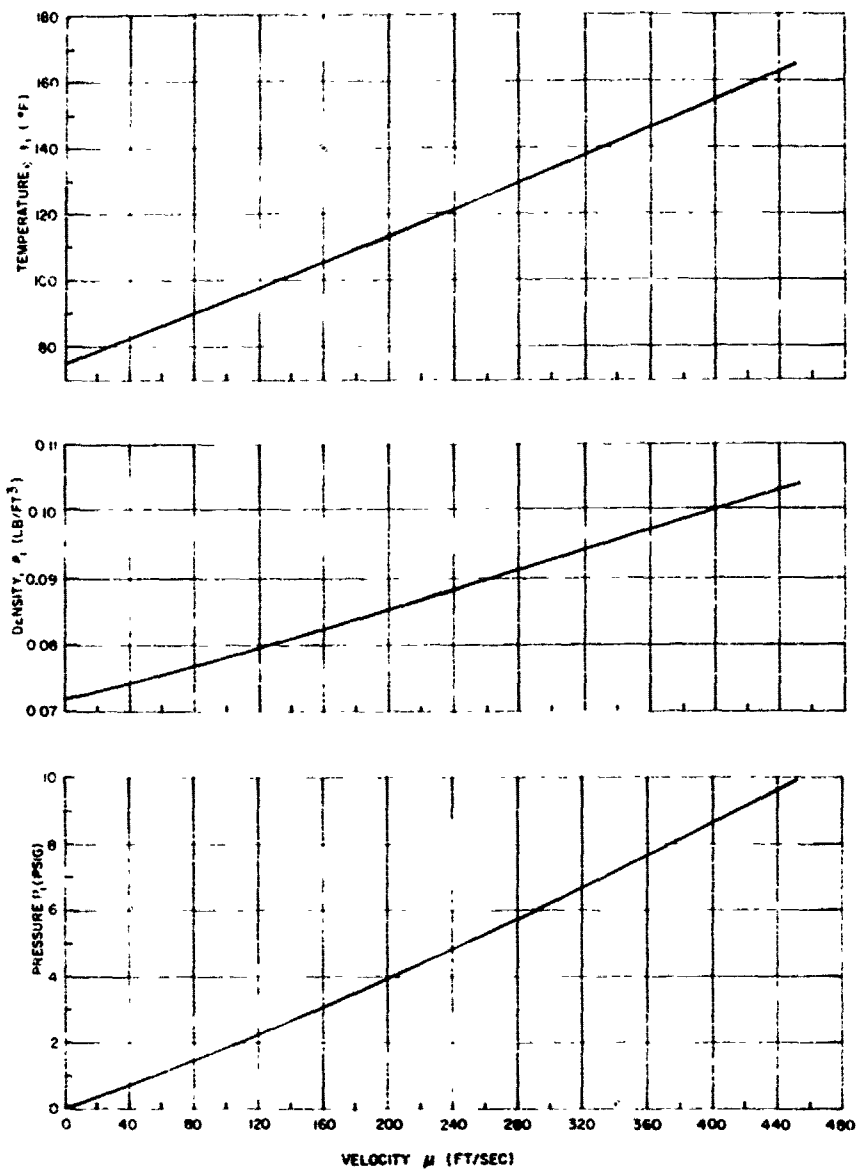L_e = distance from diaphragm to end of expansion chamber

Figure A2. Shock Tub‧ Flow Conditions as a Function of
Compression Chamber Pressure

-A7-

Figure A3. Conditions Behind Shock Wave as a Function of Flow
Velocity Behind Shock Wave.

-A8-

L_c = length of compression chamber

t_{sw} = time for shock wave to arrive at test location

t_{cw} = time for cold front to arrive at test location

t_{fw} = time for foot of rarefaction to arrive at test location

t_{rf} = time for head of rarefaction to catch its foot

t_{rc} = time for head of rarefaction to overtake cold front

t_{rw} = time for head of rarefaction to arrive at test location

X_{rf} = distance for head of rarefaction to catch its foot

X_{rc} = distance for head of rarefaction to overtake cold front

t_{re} = time for rarefaction head from open end of expansion chamber to arrive at test location

All other nomenclature is identical to that used in Equations A-1 through -5 and Figure A-1.

The time required for the shock to arrive at the test location is given by

$$t_{sw} = \frac{L_w}{a_o} \sqrt{\frac{(\alpha + 1)}{\alpha P_{10} + 1}}$$ (A-6)

The time required for the contact surface (cold front) to arrive at the test location is

$$t_{cw} = \frac{L_w}{a_o} \frac{\sqrt[\gamma]{\beta(\alpha P_{10} + 1)}}{(P_{10} - 1)}$$ (A-7)

-A9-

The time required for the foot of the rarefaction to arrive at the test location is

$$t_{fw} = L_w \left[\frac{a_o (P_{10} - 1)}{\gamma \sqrt{\beta (\alpha P_{10} + 1)}} - a_3 \left(P_{13}\right)^{\frac{1}{\alpha + 1}} \right]^{-1} \qquad (A-8)$$

where $a_3 = a_o$ if $T_3 = T_o$ as assumed for this study.

The time required for the head of the rarefaction to overtake its foot is

$$t_{rf} = \frac{L_c}{a_?} \left(P_{13}\right)^{\frac{-\alpha}{2(\alpha + 1)}} \qquad (A-9)$$

Also, it can be shown that

$$t_{rc} = 2 t_{rf} \qquad (A-10)$$

The time required for the rarefaction head to arrive at the test location (if the cold front arrives first) is given by

$$t_{rw} = t_{rf} + \frac{(L_w - X_{ri})}{u + a_2} \qquad (A-11)$$

where $a_2 = a_3 (P_{13})^{\frac{1}{\alpha + 1}}$.

-A10-

The time required for the rarefaction head to arrive at the test location (if the head has overtaken the cold front and arrives first) can be expressed as

$$t_{rw} = t_{rc} + \frac{L_w - X_{rc}}{u + a_1} \qquad (A-12$$

where $a_1 = a_o \sqrt{T_{10}}$

The distance required for the head of the rarefaction wave to overtake its foot is given by

$$X_{rf} = (a - 1) a_3 t_{rf} - a L_c \left[\frac{t_{rf} a_3}{L_c} \right]^{\frac{a-2}{a}}{}_3 \qquad (A-13$$

The distance required for the head of the rarefaction wave to overtake the contact surface is

$$X_{rc} = X_{rf} + (u + a_2) t_{rf} \qquad (A-14$$

The time required for the head of the rarefaction from the open end of the expansion chamber to arrive at the test location is given by

$$t_{re} = \frac{L_e}{w} + \frac{(L_e - L_w)}{(a_1 - u)} \qquad (A-1\mathsf{5}$$

-A11-

The time-of-arrival of the various phenomena described in Equations A-6 through -14 is shown in Figure A-4 for the range of chamber pressures used in this study Figure A-5, obtained from Figure A-4, shows directly the testing time available for the same range of compression-chamber pressures

A-2 SHOCK-TUBE PERFORMANCE

In all but the most precise shock-tube investigations, it is customary to determine the flow conditions behind the shock wave either from the state of the expansion and compression-chamber gases before rupturing the diaphragm, or from the state of the expansion-chamber gas ahead of the shock wave and a direct measurement of shock velocity. The latter method, which yields a more accurate prediction of flow conditions than the former, is the procedure used in this study.

The sources of disagreement between theory and actual behavior in the shock tube are primarily the result of departure from the assumptions of adiabatic compression, isentropic expansion, and constant specific-heat ratio, and to losses due to boundary-layer effects.

Variation of the specific-heat ratio has been investigated (Reference 68); the results indicate that for shock velocities below about Mach 3, the differences between using constant and variable specific-heat ratios are not noticeable   The assumptions of adiabatic compression and isentropic expansion are also considered quite good over this range of shock velocities.

Since this study was conducted at shock velocities below Mach 2, it would be expected that the results should agree quite well with theory This assumption is verified in Figure A-6, where experimental shock velocities in the shock tube used in this study are compared with theory. Assuming no error in shock-velocity measurement, the experimental values show a maximum departure of 1.6% from the theoretical values.

Errors in shock-velocity determinations are caused by errors in the measurement of the time required for the shock wave to traverse a known distance and in the measurement of this distance. The distance between the transducers used in the shock tube was 14 25 in. (accurate to within $\pm$ 1/64 in), and the counter used to record the time required for the shock wave to traverse the distance between the transducers was calibrated to the nearest 0.1 μsec

-A12-
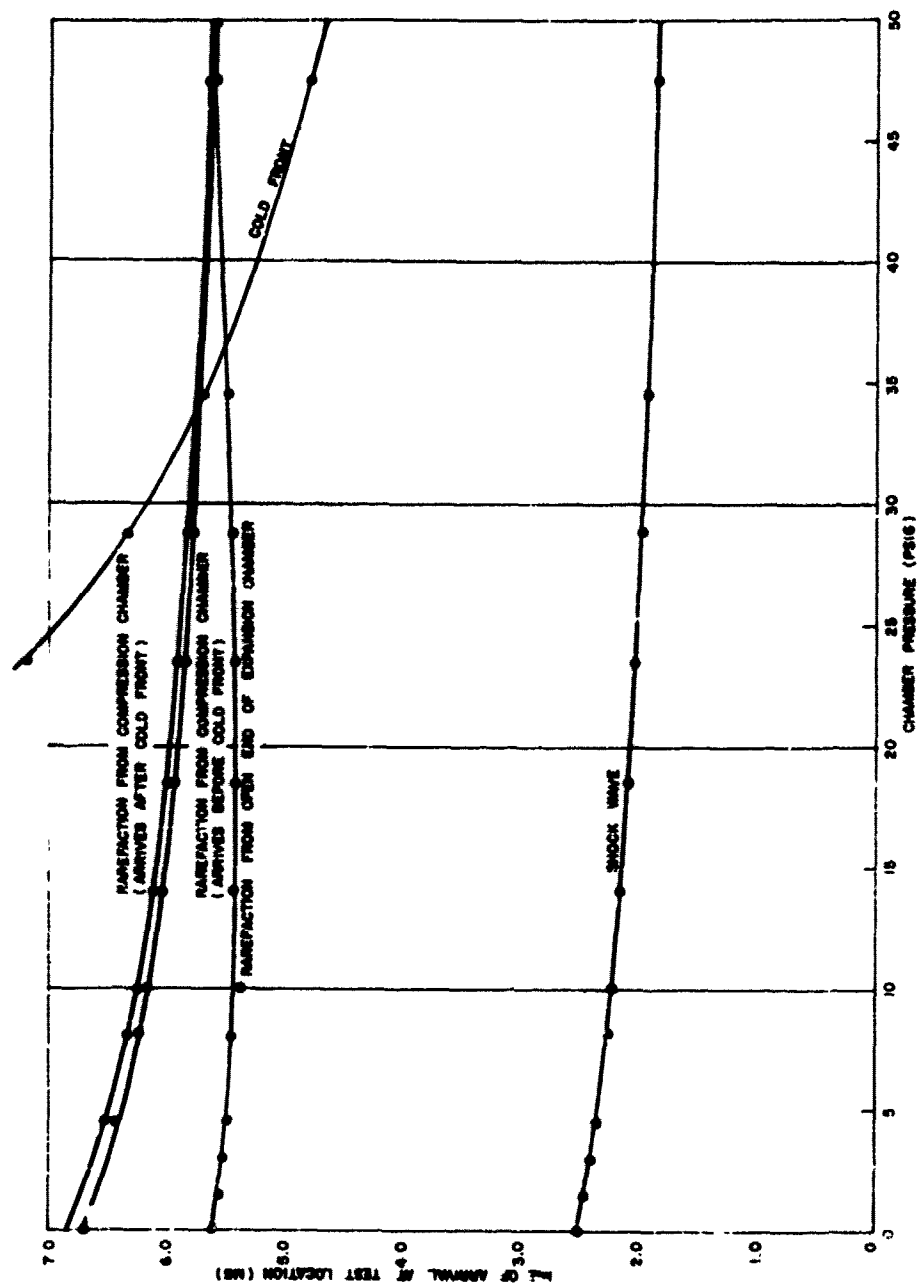
Figure A4. Time of Arrival of Disturbances as a Function of Compression Chamber Pressure.
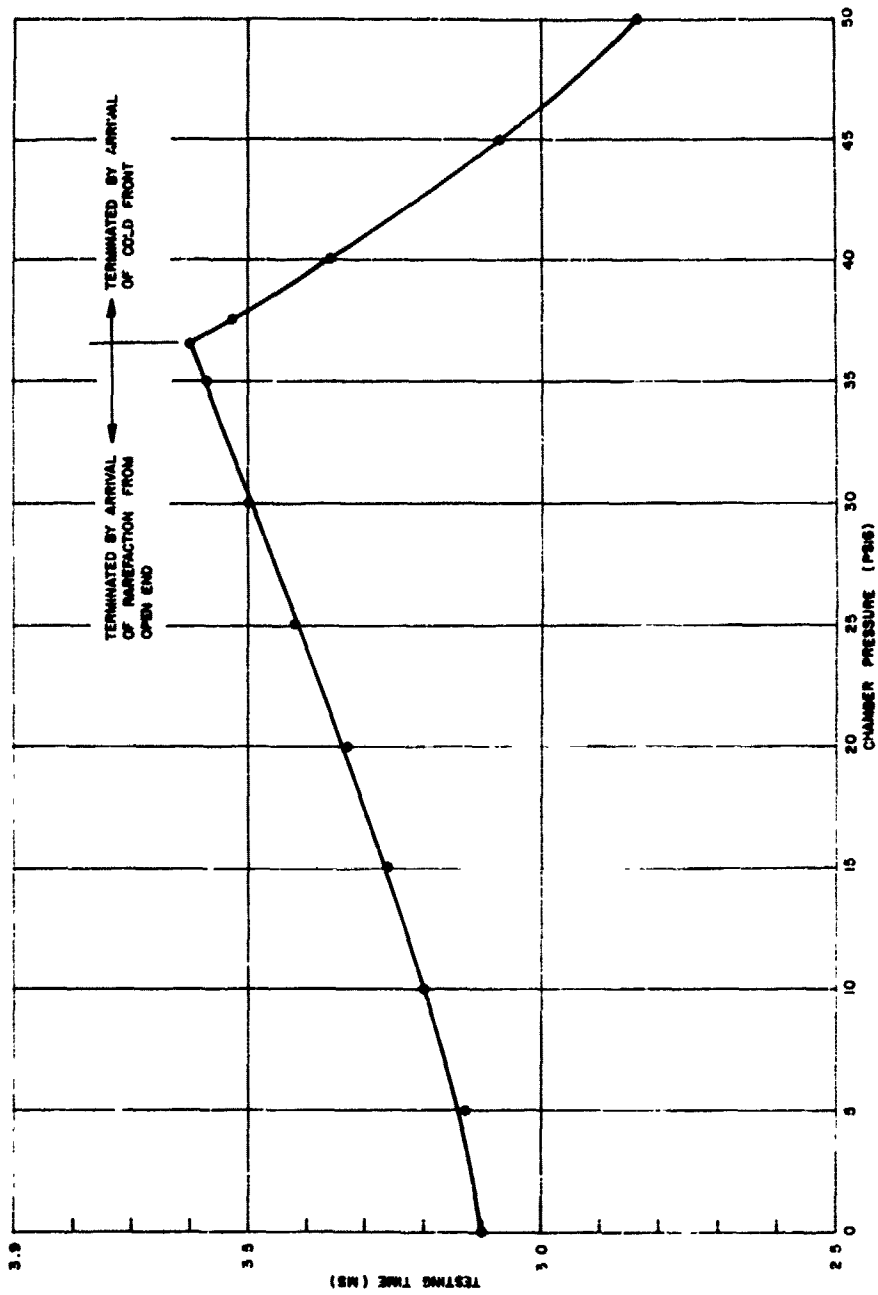
Figure A5. Shock Tube Testing Time as a Function of Compression Chamber Pressure.
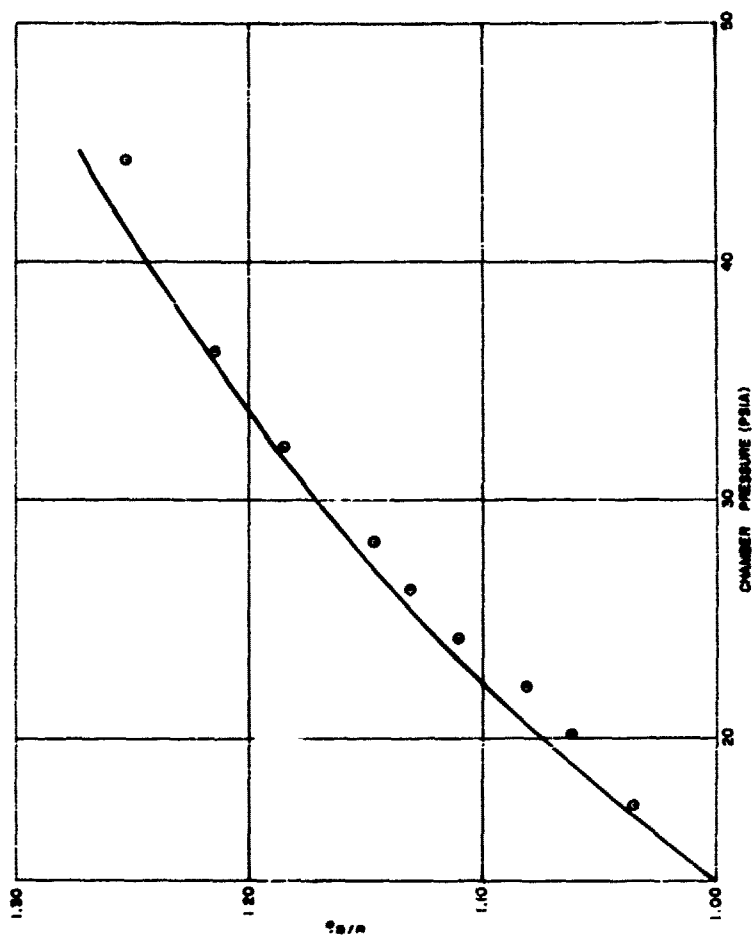
Figure A6. Comparison of Experimental Results with Theoretical Shock Velocities.

-A15-

The primary source of error in shock-velocity measurements is associated with the signal output from the transducers: this output does not rise instantaneously to its peak value with the arrival of the shock wave, and it is difficult to adjust both the start and stop circuits of the counter to trigger at exactly the same voltage level.

At the start of the study, measurements were made of the wave shape of the output signals from the two transducers. The results showed the waves to be nearly identical in shape over the range of interest. Typical output signals from the transducer used to stop the counter are shown in Figure A-7; superimposed on the curves are the voltages used to adjust the start and stop circuits of the counter. Voltages equal to or less than the lower "NO GO" trigger level failed to trigger the circuit, while signals equal to or greater than the upper "GO" trigger level resulted in triggering. The difference between these levels then represents the maximum uncertainty in trigger voltage between the start and stop circuits, and a corresponding uncertainty in the recorded time is thus determined.

The total uncertainty in shock-velocity measurements is represented by the combination of errors in distance and time measurements. Assuming the worst combination of these effects to occur simultaneously, a maximum error of $\pm$ 0.85% in shock velocity could be expected for the range of velocities covered in this study

Using shock-tube theory to obtain a relation between shock velocity and air velocity behind the shock wave, a curve similar to that shown in Figure A-8 is obtained. Applying the possible errors in shock-velocity measurements to the illustrated curve results in a possible error of approximately $\pm$ 28% for an air velocity of 60 ft/sec, while the same technique yields an error of only $\pm$ 3% for an air velocity of 450 ft/sec. Inspection of the curve in Figure A-8 shows that while the accuracy of shock-velocity measurement is practically constant, large errors in air velocity can be expected at shock velocities near the speed of sound, since the air velocity approaches zero as the shock velocity approaches the speed of sound ahead of the shock wave

It should be mentioned that while the preceding discussion implies the possibility of rather large errors in the air velocities, it is not likely that errors of this magnitude are present in the data With careful attention given to the adjustment of the trigger levels on the counter, the operator could soon develop a technique of reaching settings extremely close to the lower trigger-level voltage. As a result, it is improbable that errors in air-velocity measurements as large as those derived from Figure A-8 actually . . red.

-A16-

TEST 241   P = 3.0 PSIG

10 μ SEC/cm
0.5 V/cm
TRIGGER LEVEL: 0.204 -0.385 V
w = 1168 FT/SEC
COUNTER = 1016.3 μ SEC

"GO" VOLTAGE

"NO-GO" VOLTAGE

TIME (μSEC)

TEST 204   P = 10 PSIG

10 μ SEC/cm
2V/cm
TRIGGER LEVEL : 0.865 - 1.505 V
COUNTER 940.3 μ SEC
w = 1264 FT/SEC

"GO" VOLTAGE

"NO-GO" VOLTAGE

TIME (μSEC)
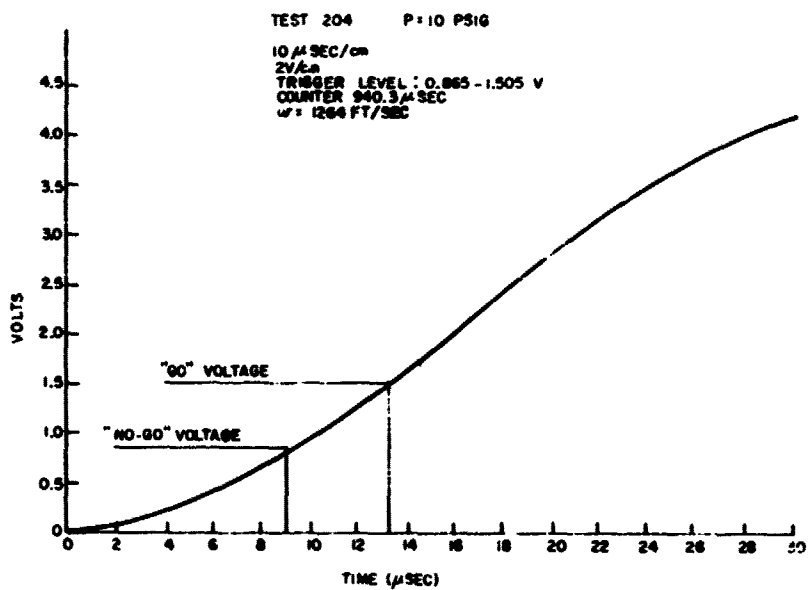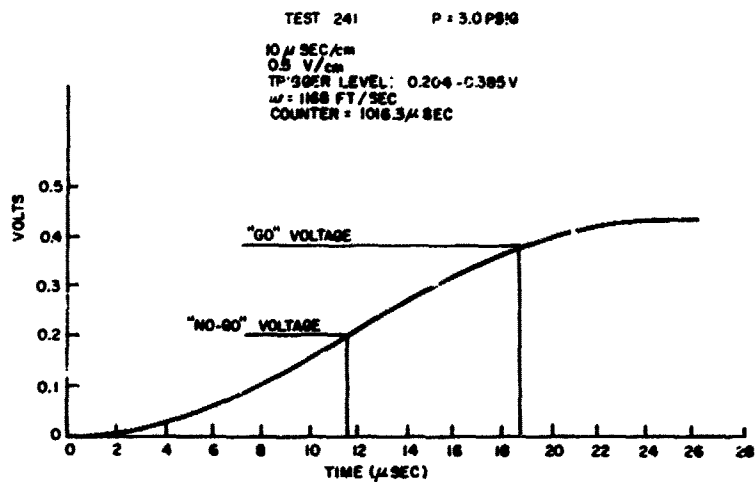
Figure A7.   Transducer Output Signals.

-A17-
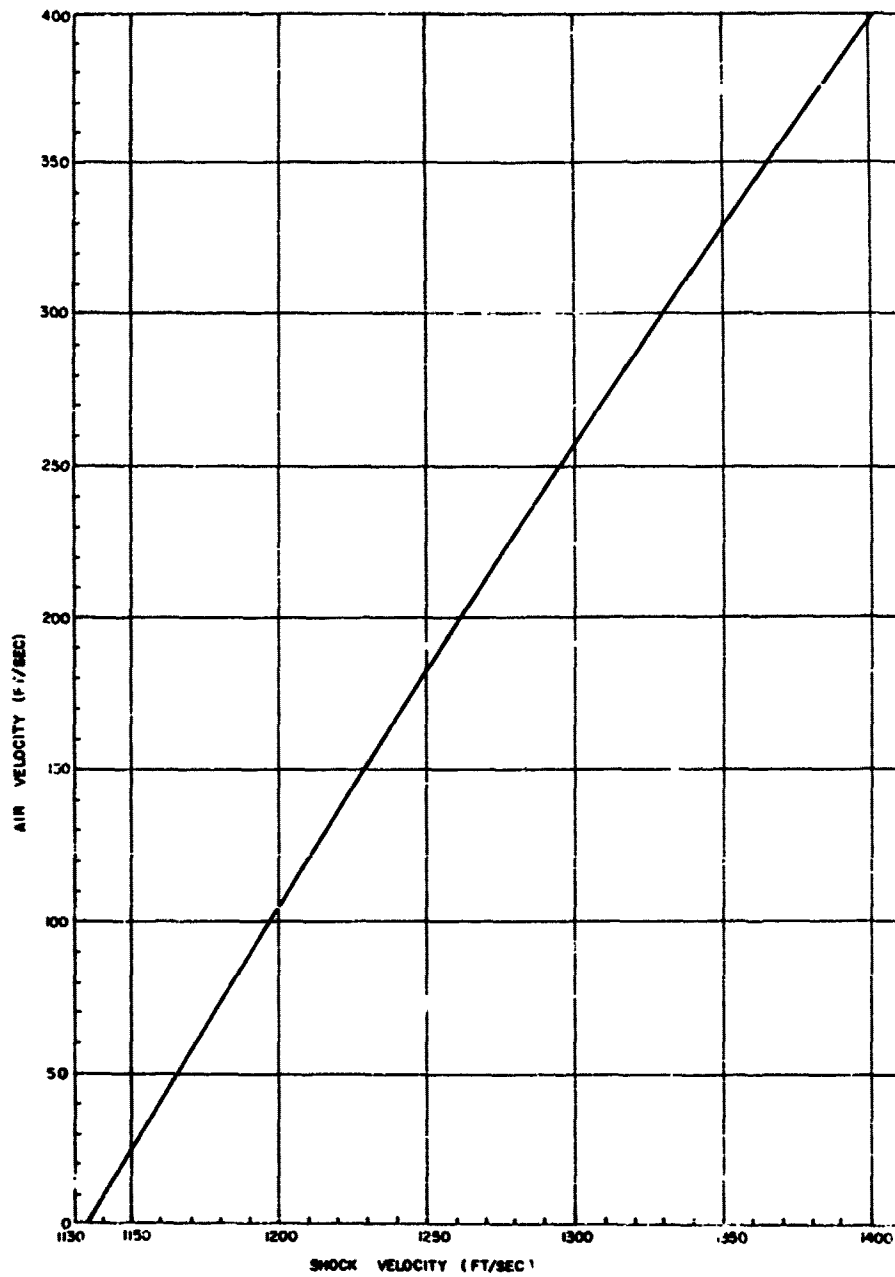
Figure A9. Flow Velocity Behind Shock Wave as a
Function of Shock Velocity.

-A18-

APPENDIX B

This appendix contains plates made from the high speed motion picture films taken during the study. The series of plates contained herein represent each of the test conditions listed in Table 2 in Section 5 3 of this report. They have been included to provide a source of comprehensive information on the qualitative aspects of droplet breakup as well as detailed quantitative data on the behavior of drops during deformation acceleration and subsequent breakup in a fast moving air stream

Test 117
Liquid Water Relative Velocity 134 ft/sec
Drop Size 3.0 MM Time per Frame 0 1171 msec

10 MM
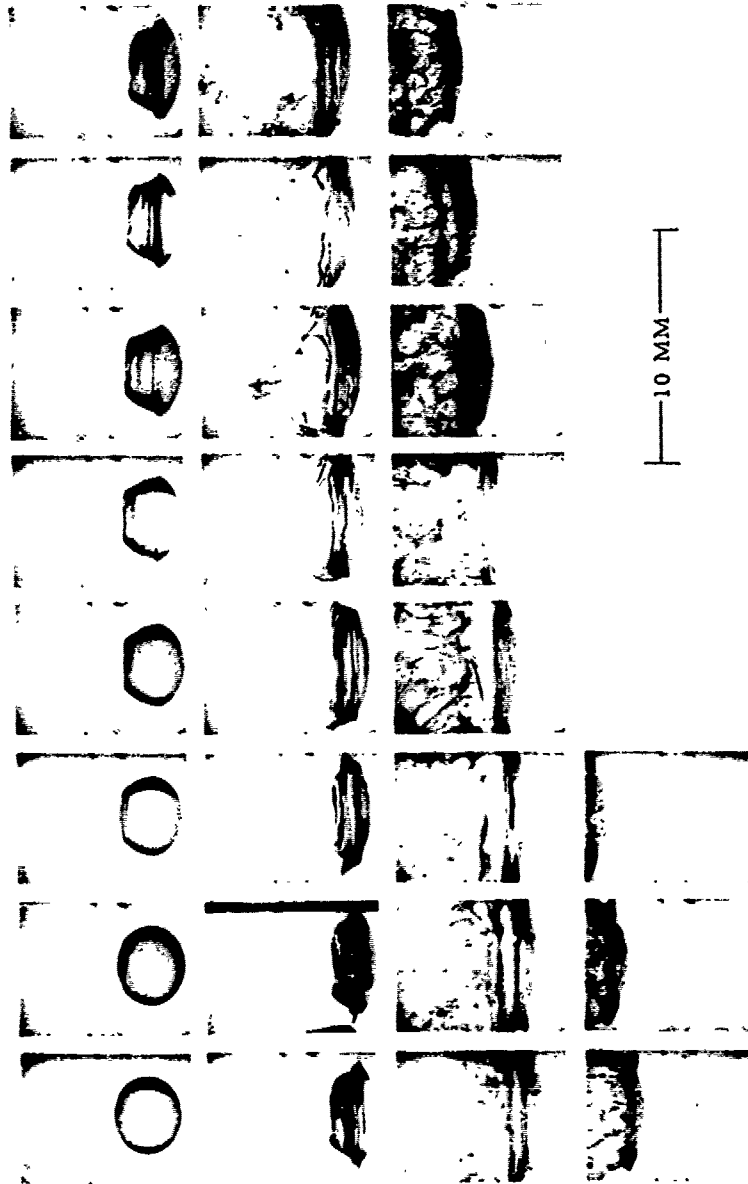
Test 119

Liquid Water   Relative Velocity 220 ft/sec
Drop Size 3 0 MM   Time per Frame 0 0786 msec

10 MM
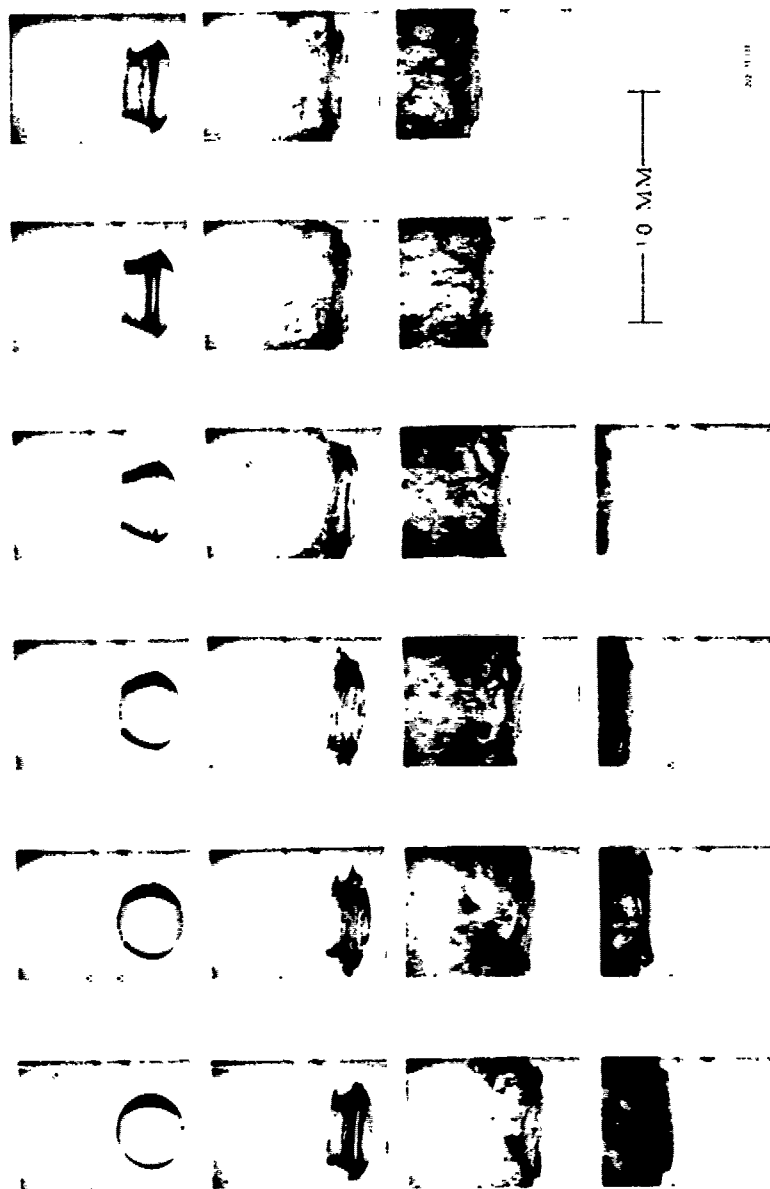
Test 121
Liquid-Water   Relative Velocity 362 ft/sec
Drop Size 3 0 MM   Time per Frame 0.03910 msec

10 MM

Test 122

Liquic Water   Relative Velocity 455 ft/sec
Drop Size 3 0 MM   Time per Frame 0 0392 msec

10 MM

Test 123

Liquid-Water   Relative Velocity 70 ft/sec

Drop Size 3.0 MM   Time per Frame 0.1171 msec

10 MM

Test 158

Liquid-Water   Relative Velocity 69 ft/sec
Drop Size 2 0 MM   Time per Frame 0 1178 msec

10 MM

Test 186

Liquid-Water   Relative Velocity 107 ft/sec

Drop Size 1 8 MM   Time per Frame 0.0785 msec

10 MM

Test 187

Liquid Water Relative Velocity 84 ft/sec

Drop Size 1 9 MM Time per Frame 0 1170 msec

10 MM

Test 188

Liquid - Water   Relative Velocity 53 ft/sec

Drop Size 1 9 MM   Time per Frame 0 1174 msec

10 MM

Test 189

Liquid Water   Relative Velocity 195 ft/sec

Drop Size 1.8 MM   Time per Frame 0.0391 msec

10 MM

Test 191
Liquid-Water   Relative Velocity 350 ft/sec
Drop Size 1 9 MM   Time per Frame 0 0391 msec
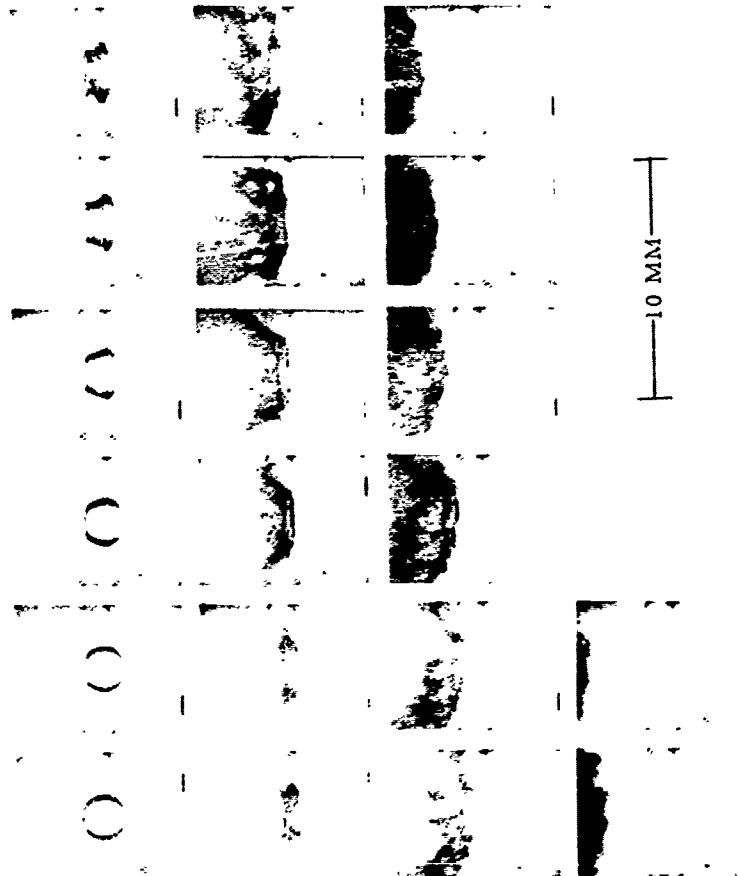
10 MM

Test 192

Liquid Water   Relative Velocity 441 ft/sec
Drop Size 1 7 MM   Time per Frame 0 0391 msec
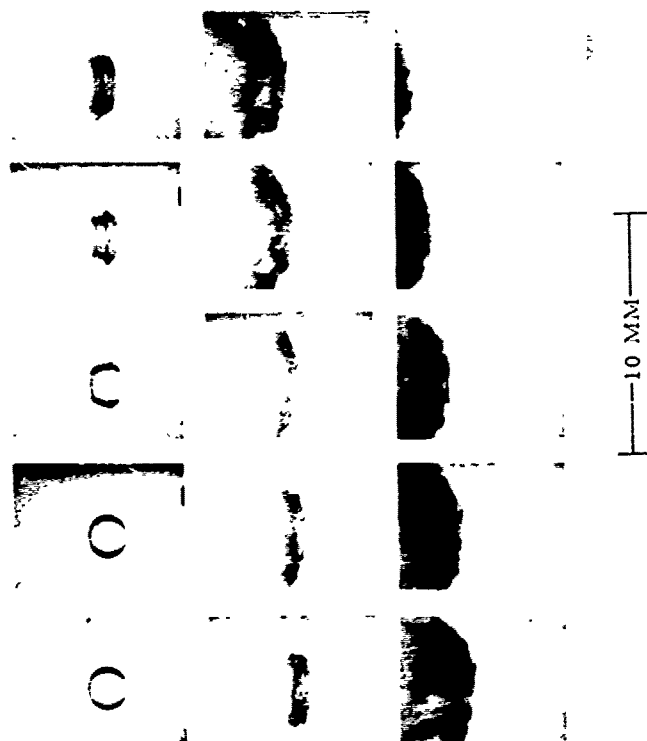
—10 MM—

Test 214

Liquid-Water   Relative Velocity 63 ft/sec
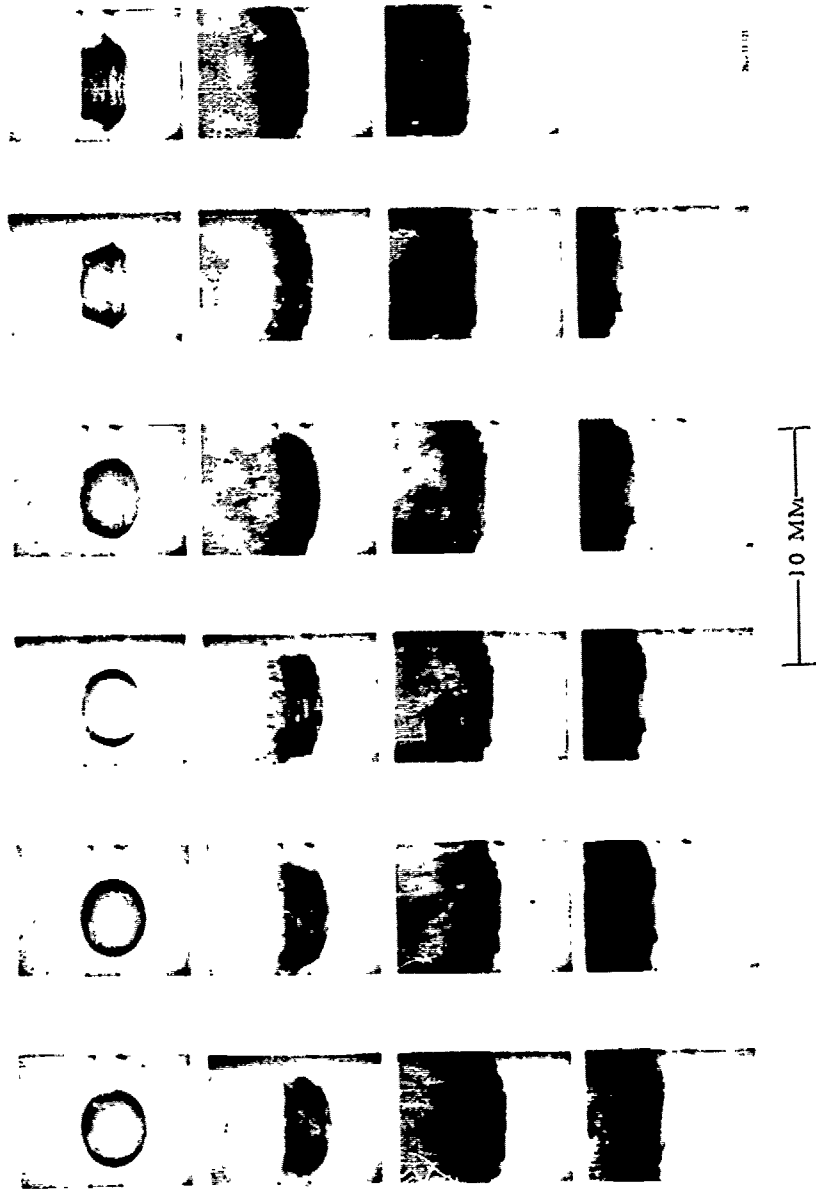Drop Size 1.0 MM   Time per Frame 0.0791 msec
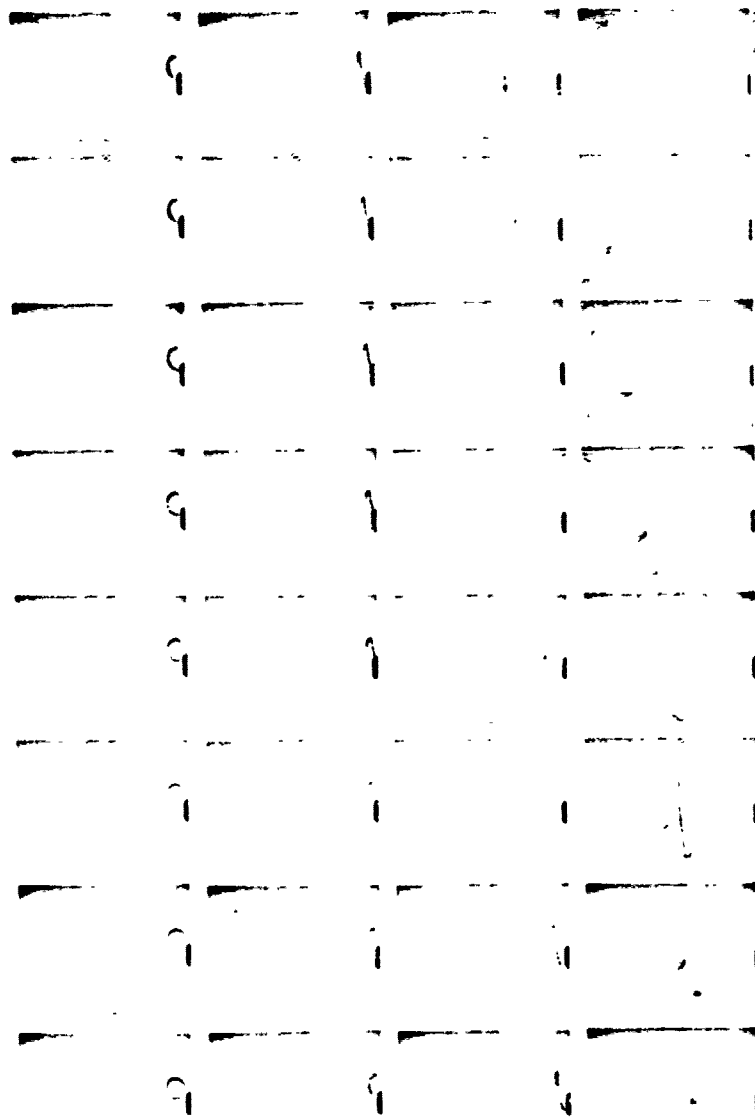
├─ 10 MM ─┤

Test 217

Liquid Water   Relative Velocity 81 ft/sec
Drop Size 1 2 MM   Time per Frame 0.0766 msec
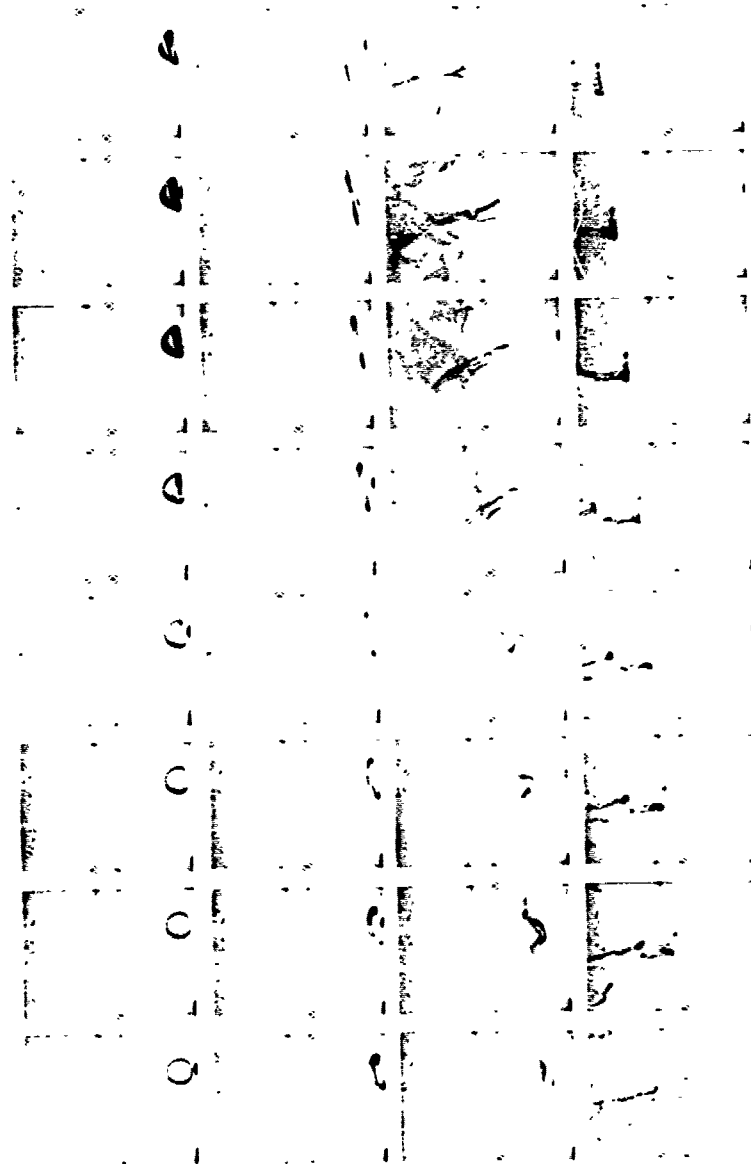
10 MM

Test 234
Liquid-Water   Relative Velocity 65 ft/sec
Drop S.ze 0 7 MM   Time per Frame 0 0766 msec
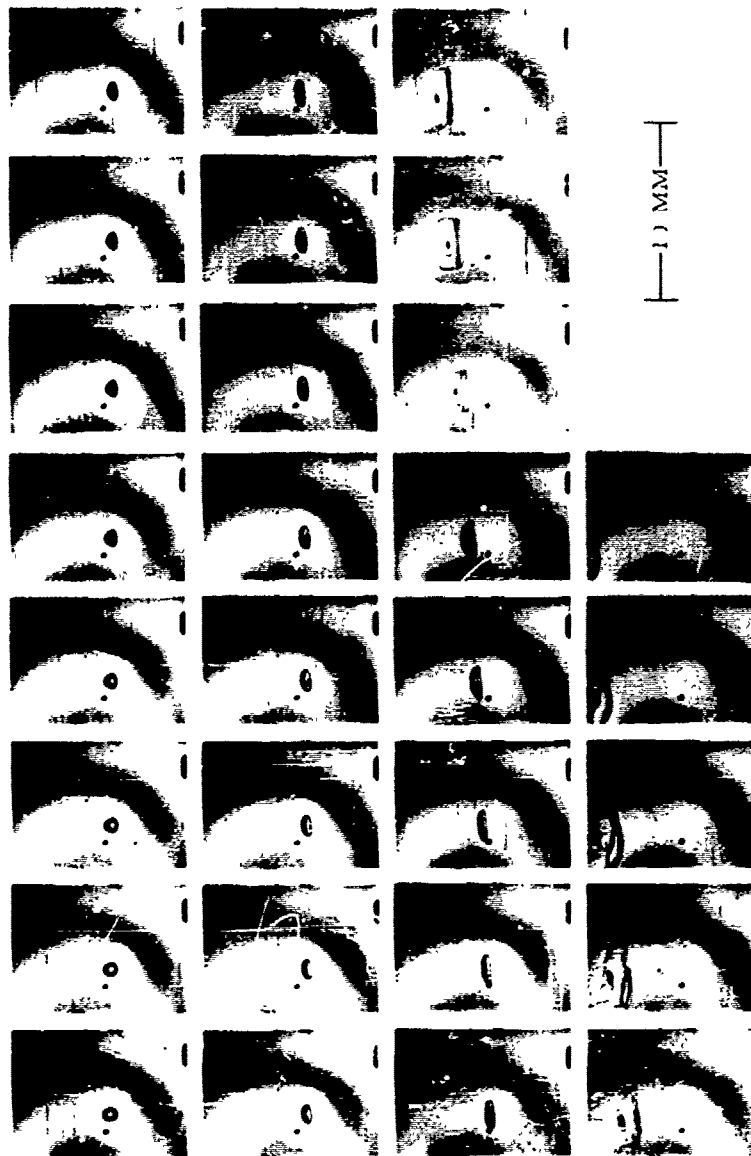
10 MM

Test 236

Liquid-Water   Relative Velocity 85 ft/sec
Drop Size 0. 8 MM   Time per Frame 0. 0770 msec
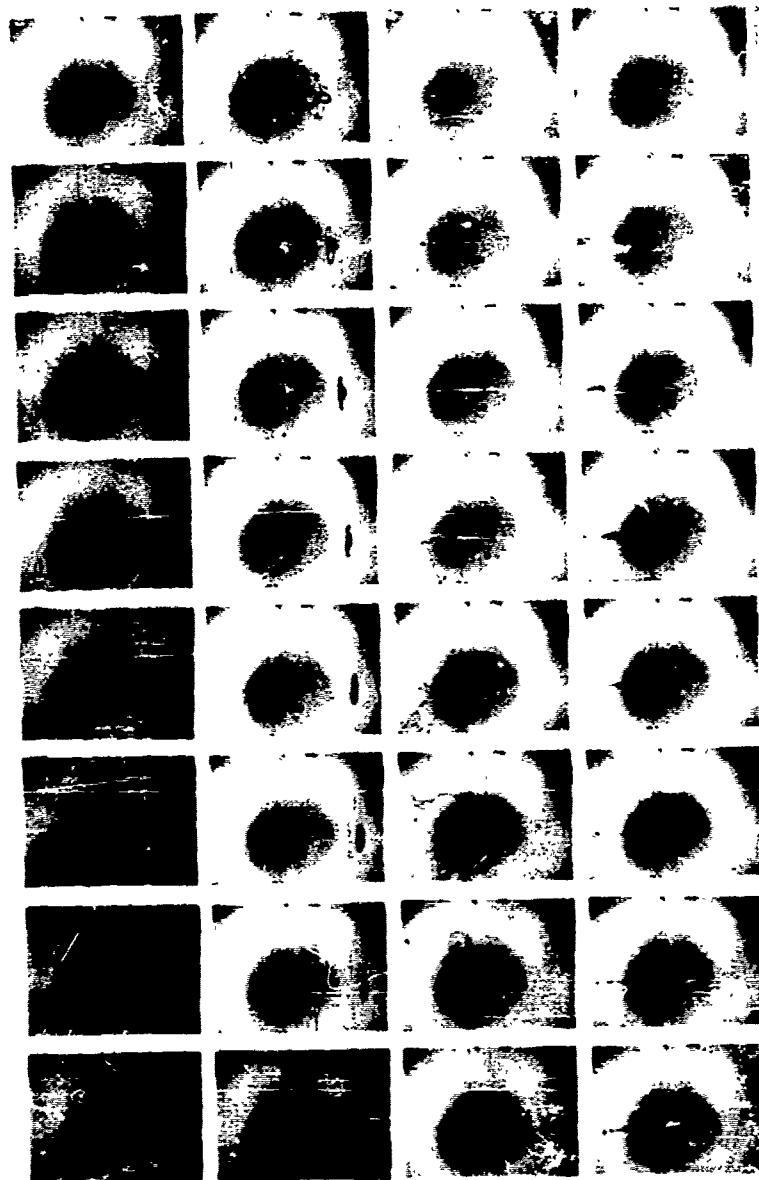
|—10 MM—|

Test 237

Liquid Water   Relative Velocity 75 ft/sec
Drop Size 0 8 MM   Time per Frame 0 0766 msec
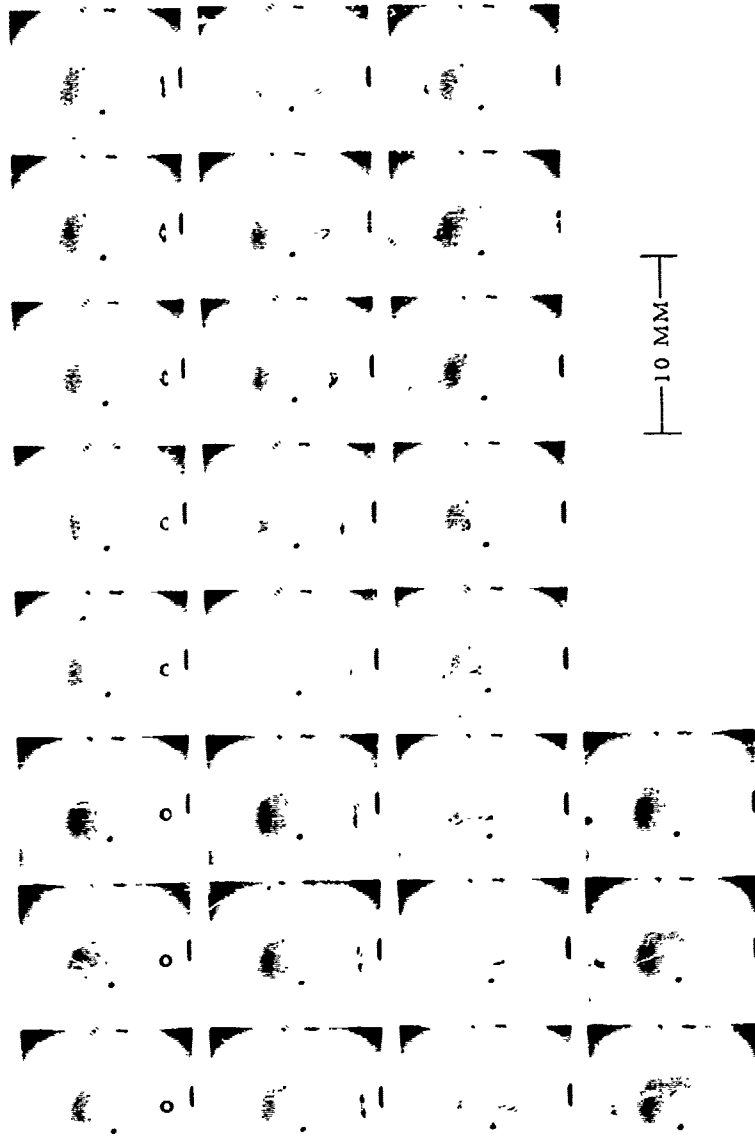
10 MM

Test 238
Liquid Water   Relative Velocity 95 ft. sec
Drop Size 0 8 MM   Time per Frame 0 0775 msec
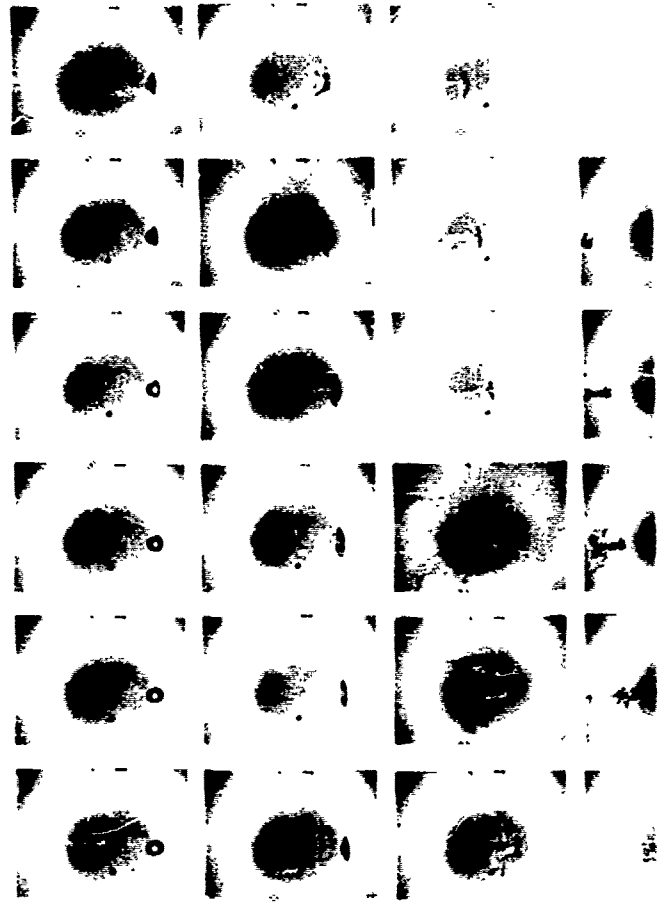
Test 239
Liquid Water   Relative Velocity 108 ft/sec
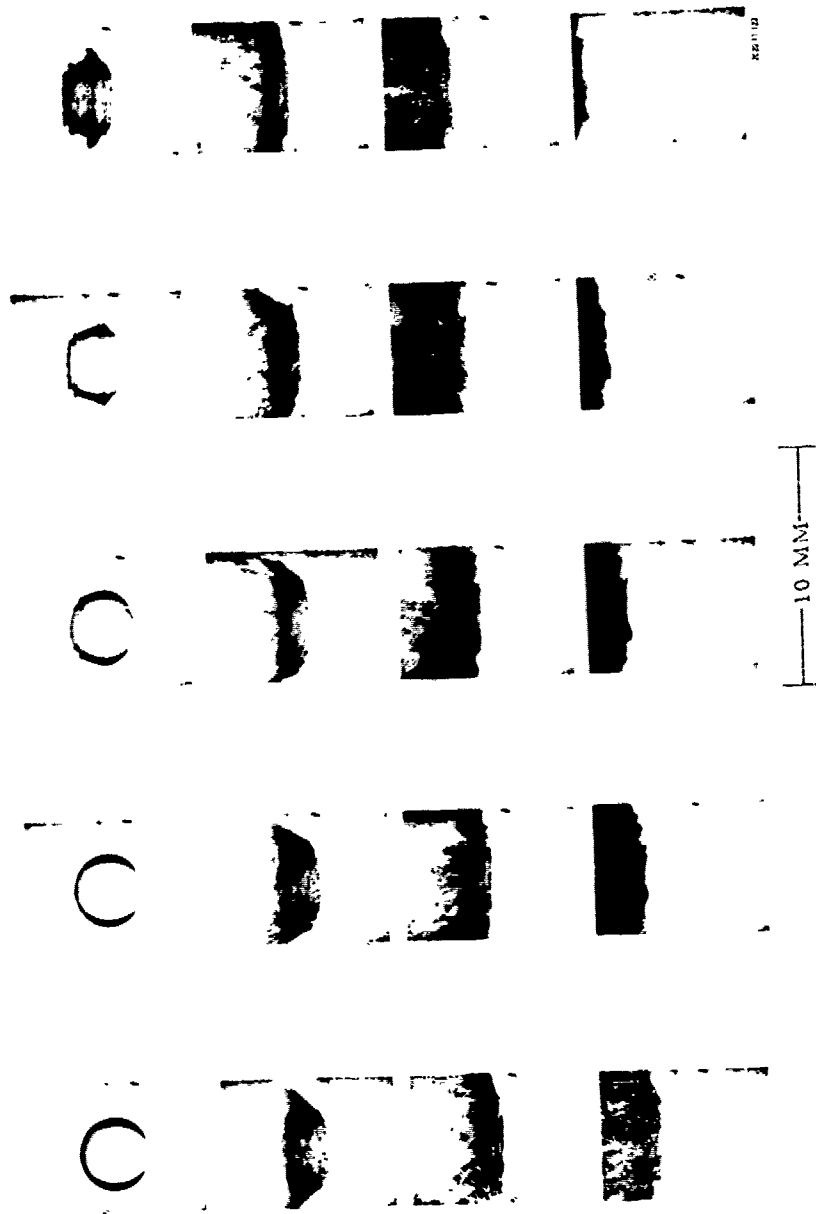Drop Size 0 78 MM   Time per Frame 0.0766 msec
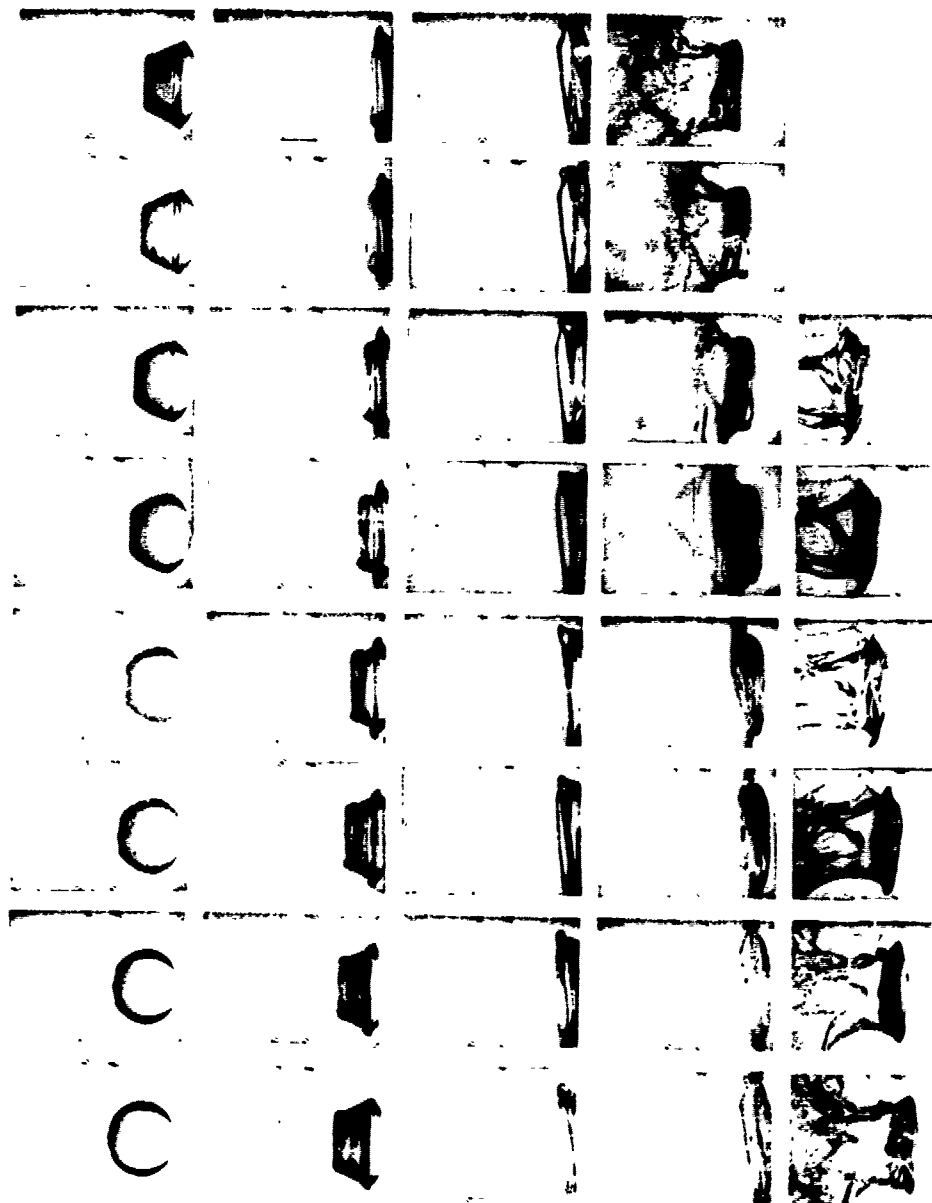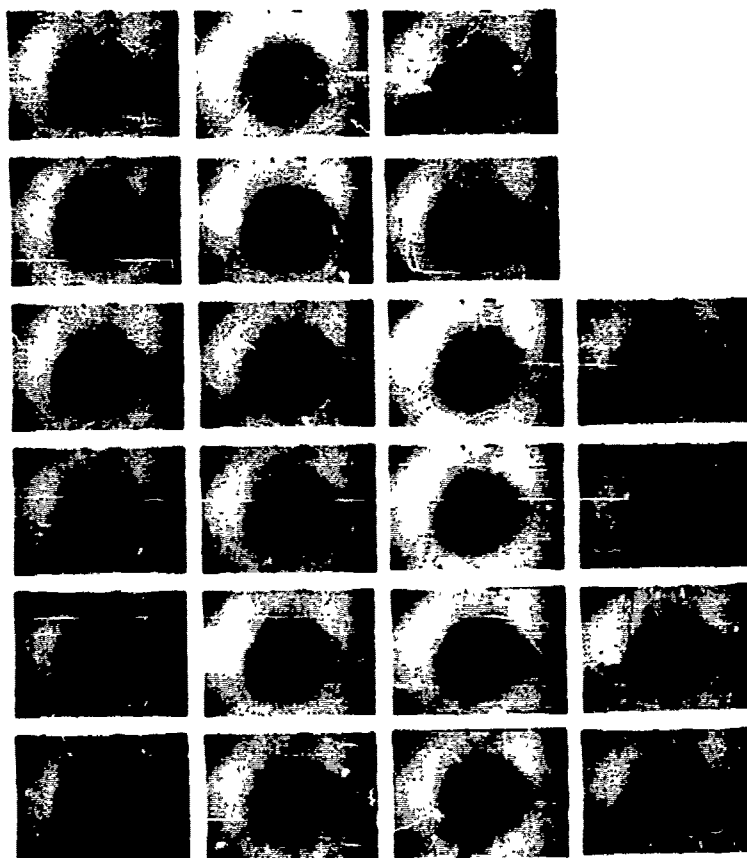
10 MM

Test 240
Liquid Water   Relative Velocity 120 ft/sec
Drop Size 0 81 MM   Time per Frame 0 0384 msec
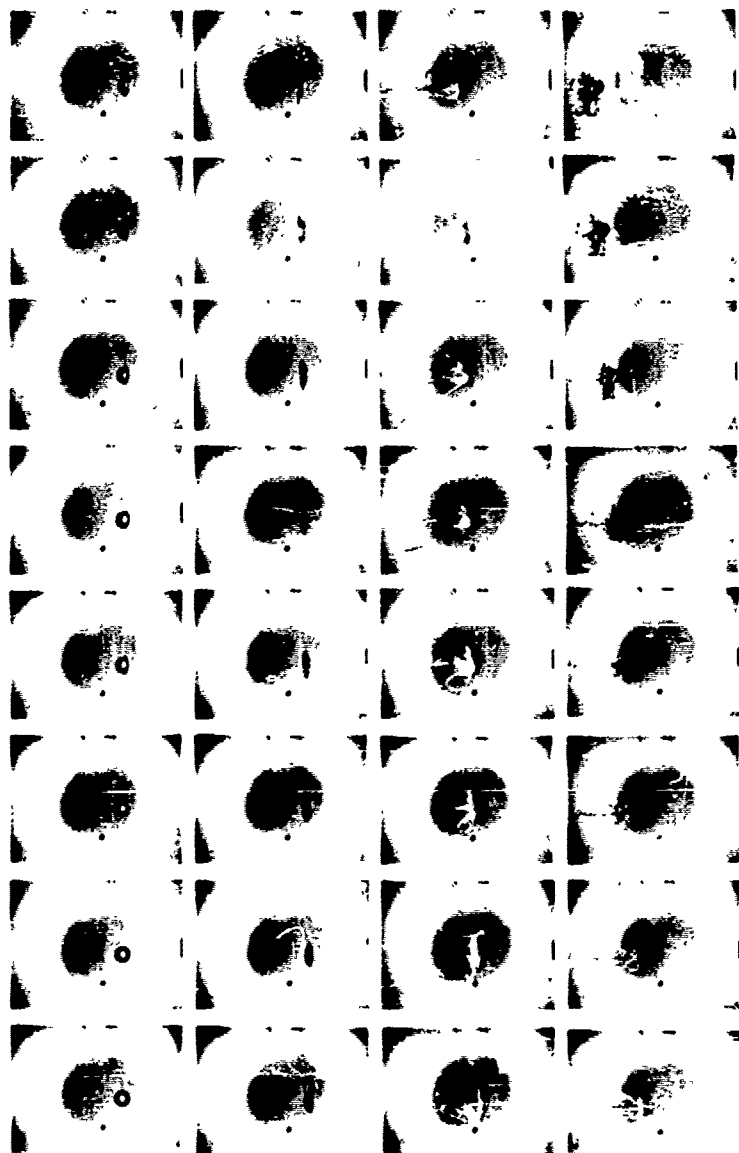
10 MM

Test 241

Liquid-Water Relative Velocity 61 ft/sec

Drop Size 0 67 MM Time per Frame 0 0770 msec
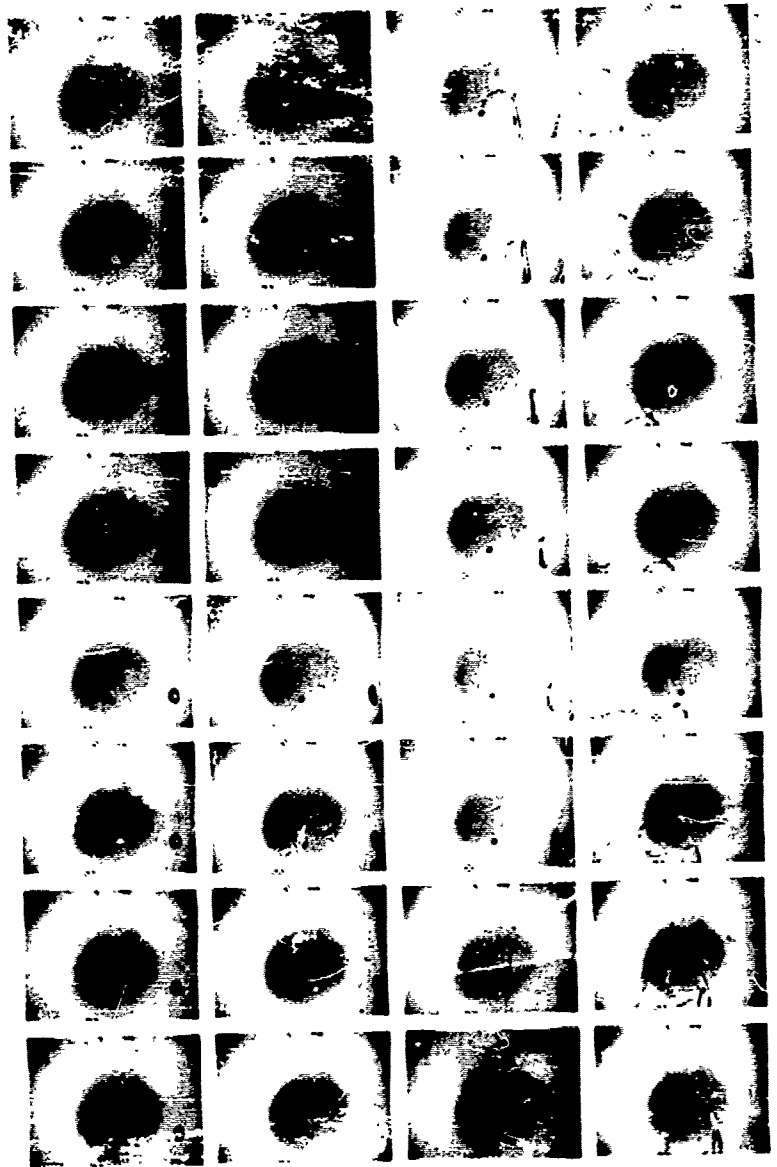
├─ 10 MM ─┤

Test 261

Liquid Water   Relative Velocity 127 ft/sec

Drop Size Upper 0.53 MM   Time per Frame 0.0772 msec
           Lower 0.57 MM

B23

Test 262
Liquid-Water Relative Velocity 203 ft/sec
Drop Size 0 53 MM Time per Frame 0 0388 m sec
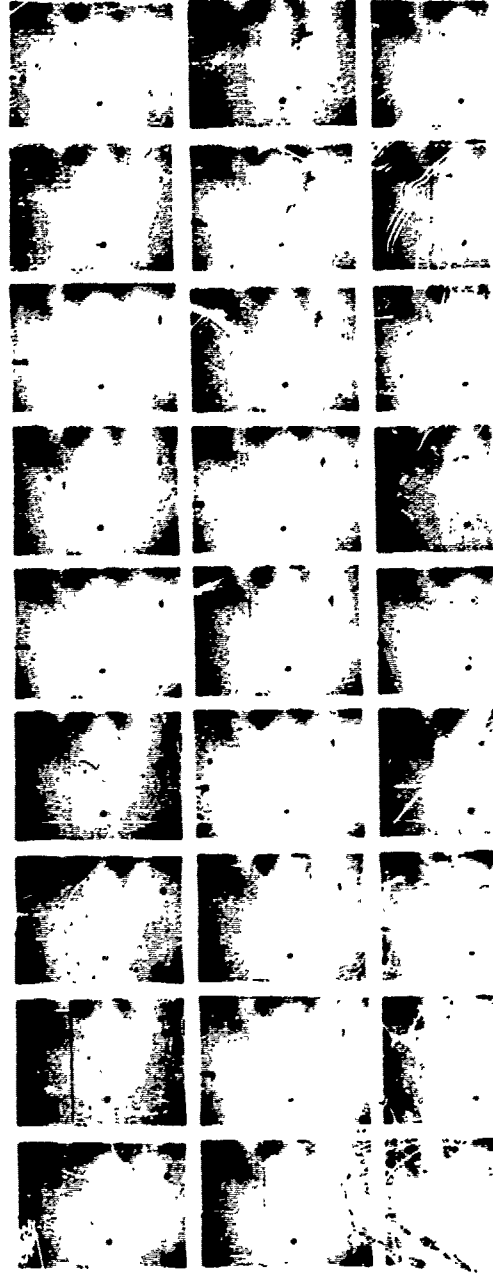
Test 263

Liquid Water   Relative Velocity, 339 ft/sec
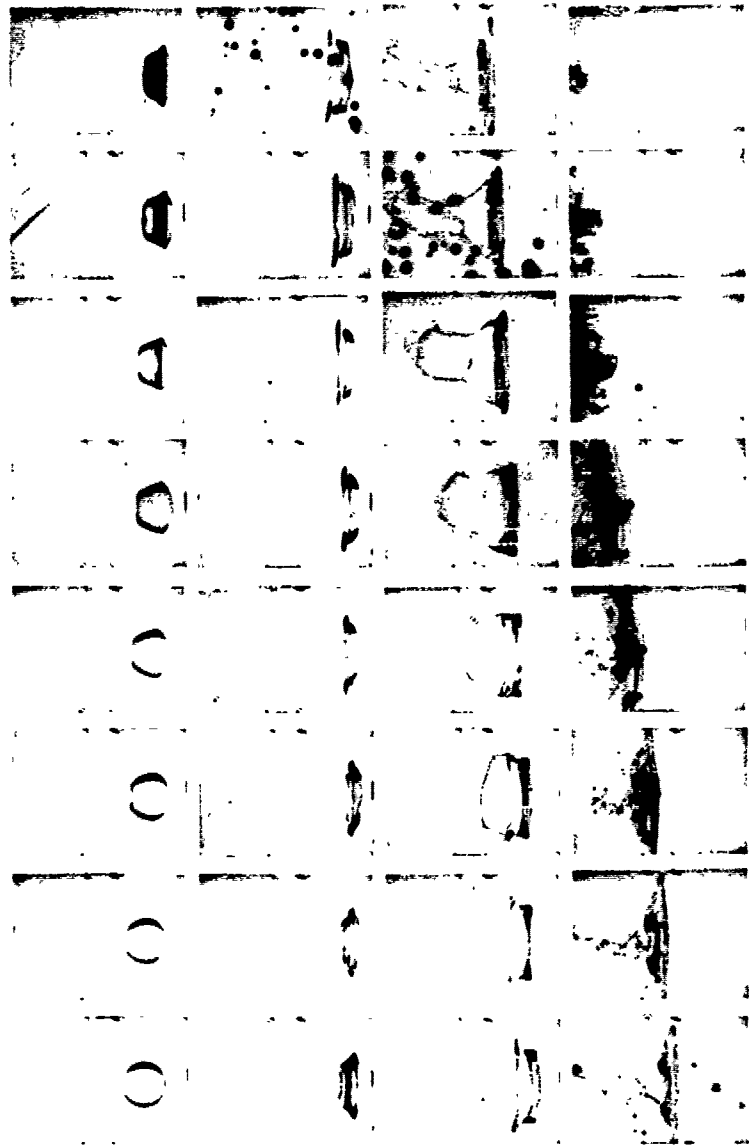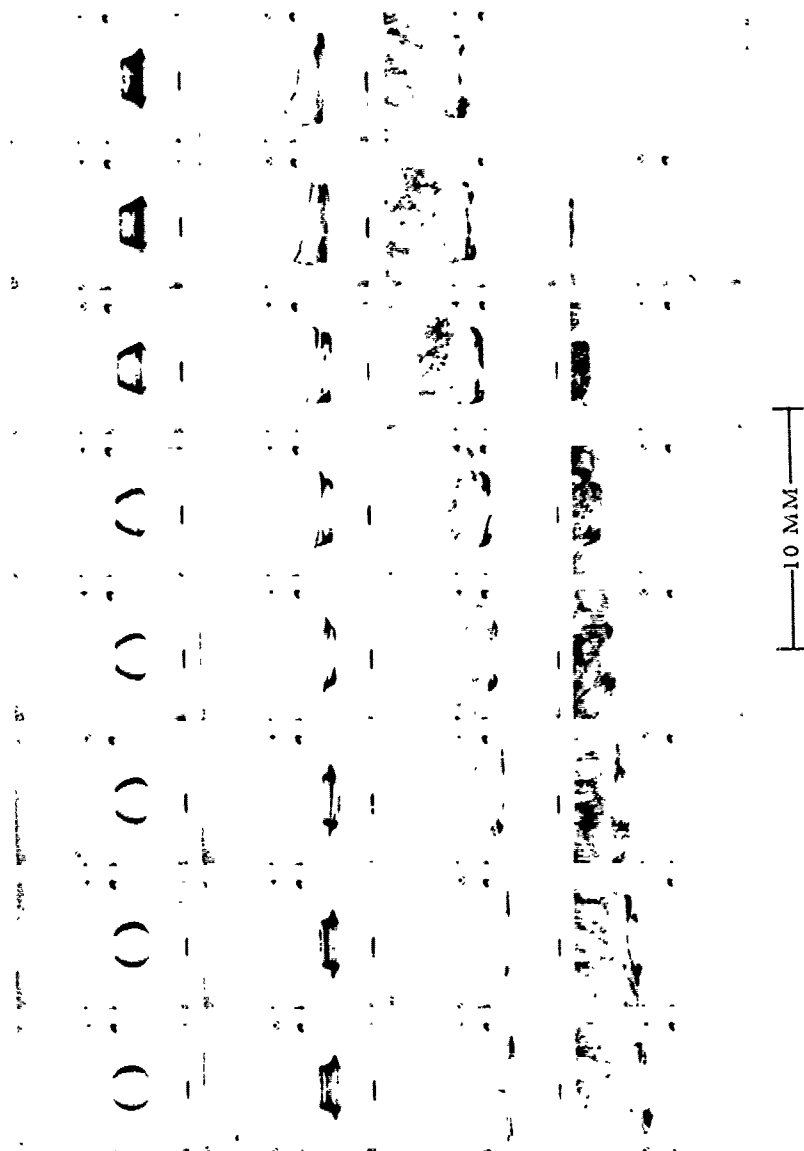
Drop Size 0. 6 MM   Time per Frame 0. 0388 msec
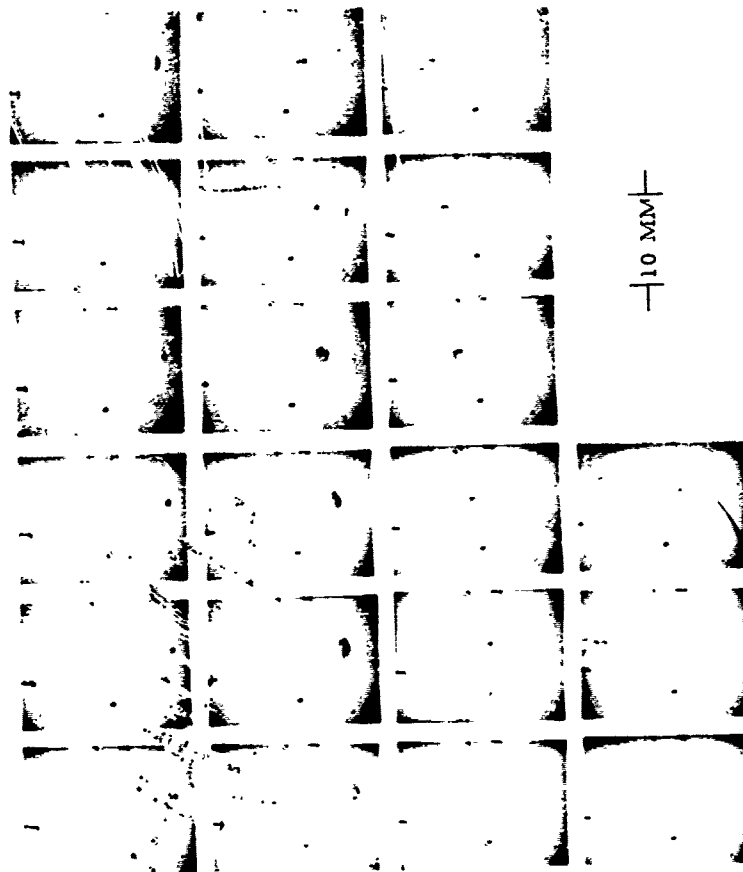
10 MM

Test 264

Liquid Water   Relative Velocity 432 ft/sec

Drop Size 0.44 MM   Time per Frame 0.0386 msec
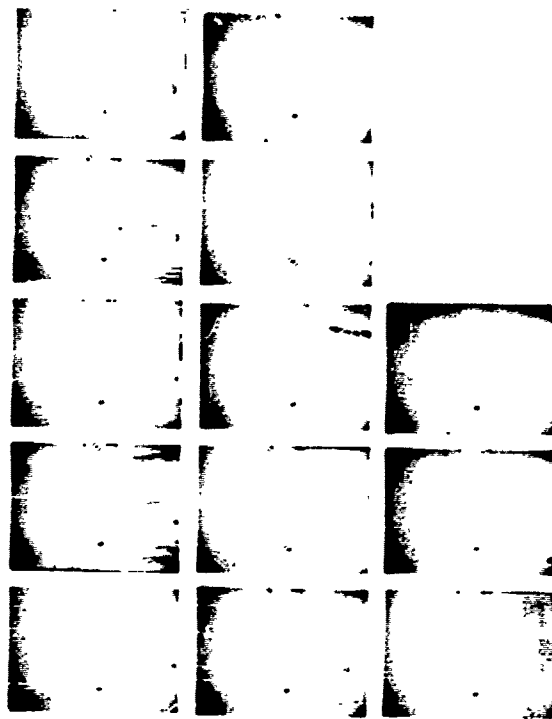
—|10 MM|—

Test 266
Liquid Water   Relative Velocity 60 ft/sec
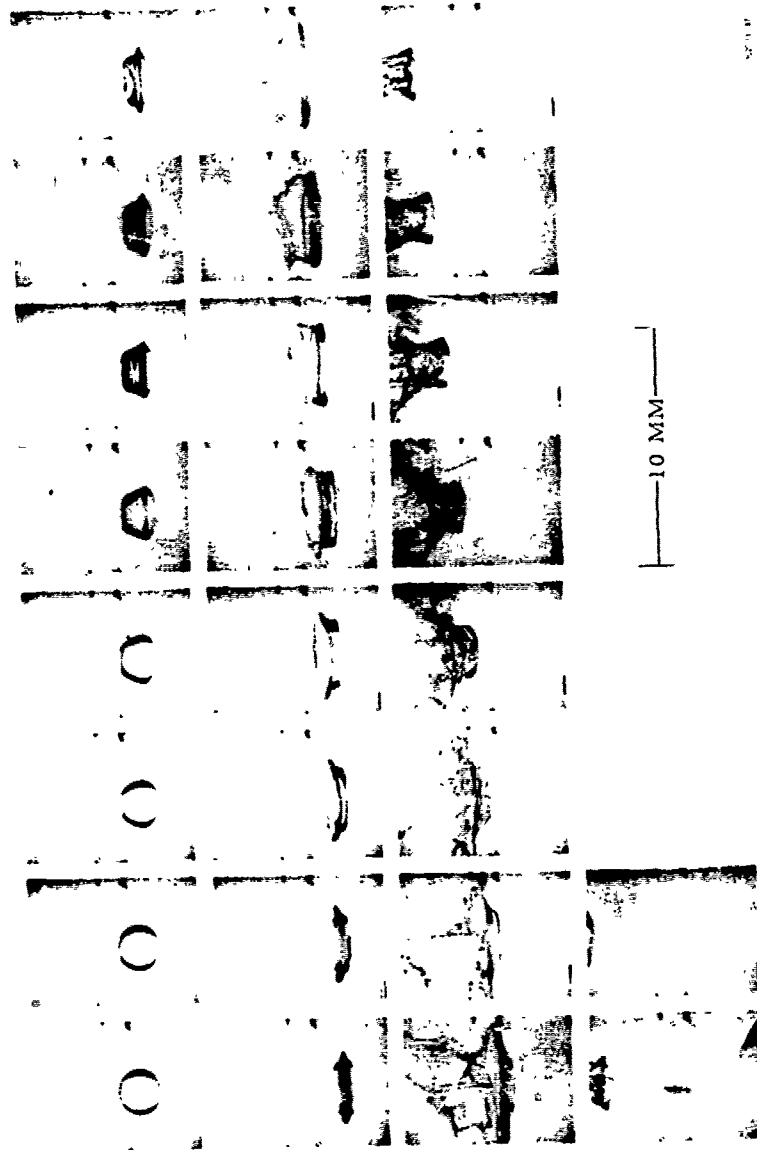Drop Size 1.8 MM   Time per Frame 0.1158 msec

10 MM

B27
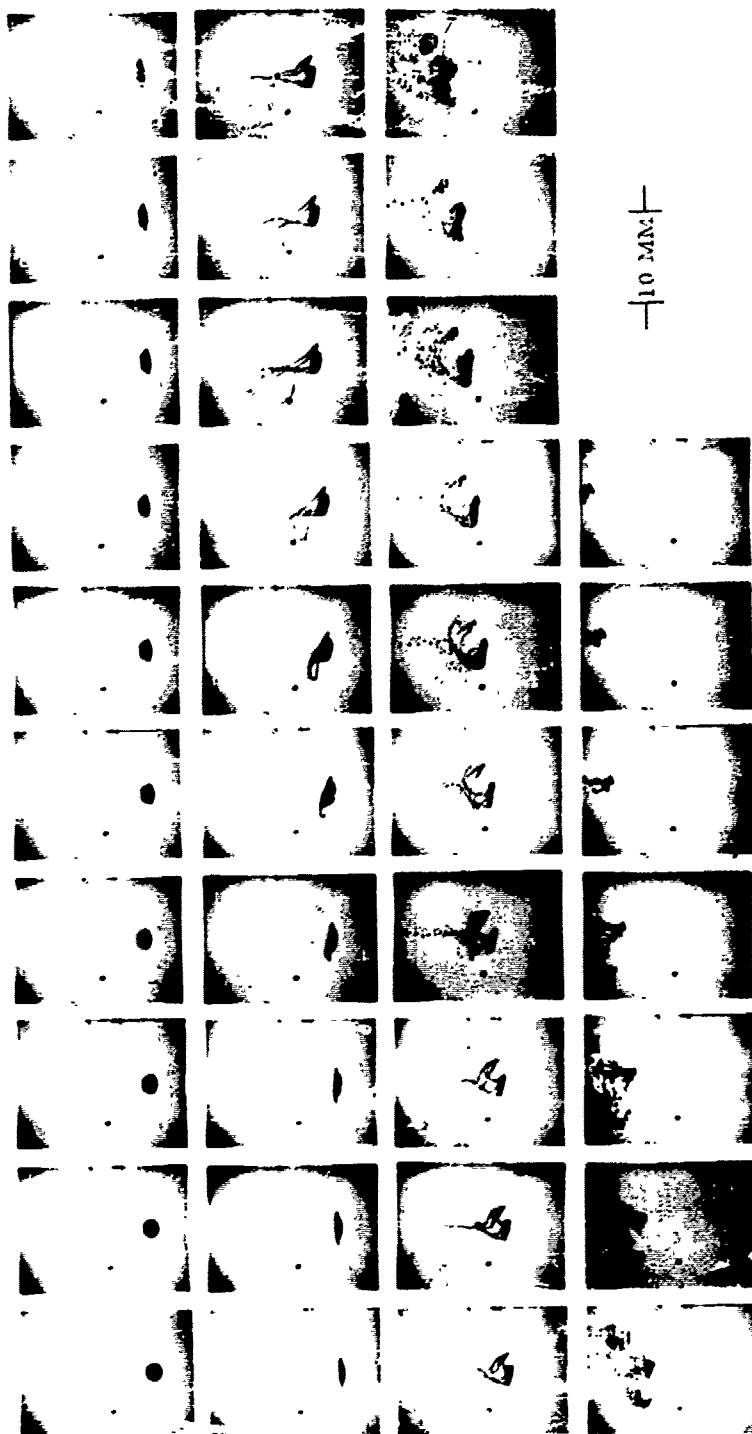
Test 267

Liquid: Water   Relative Velocity 84 ft/sec
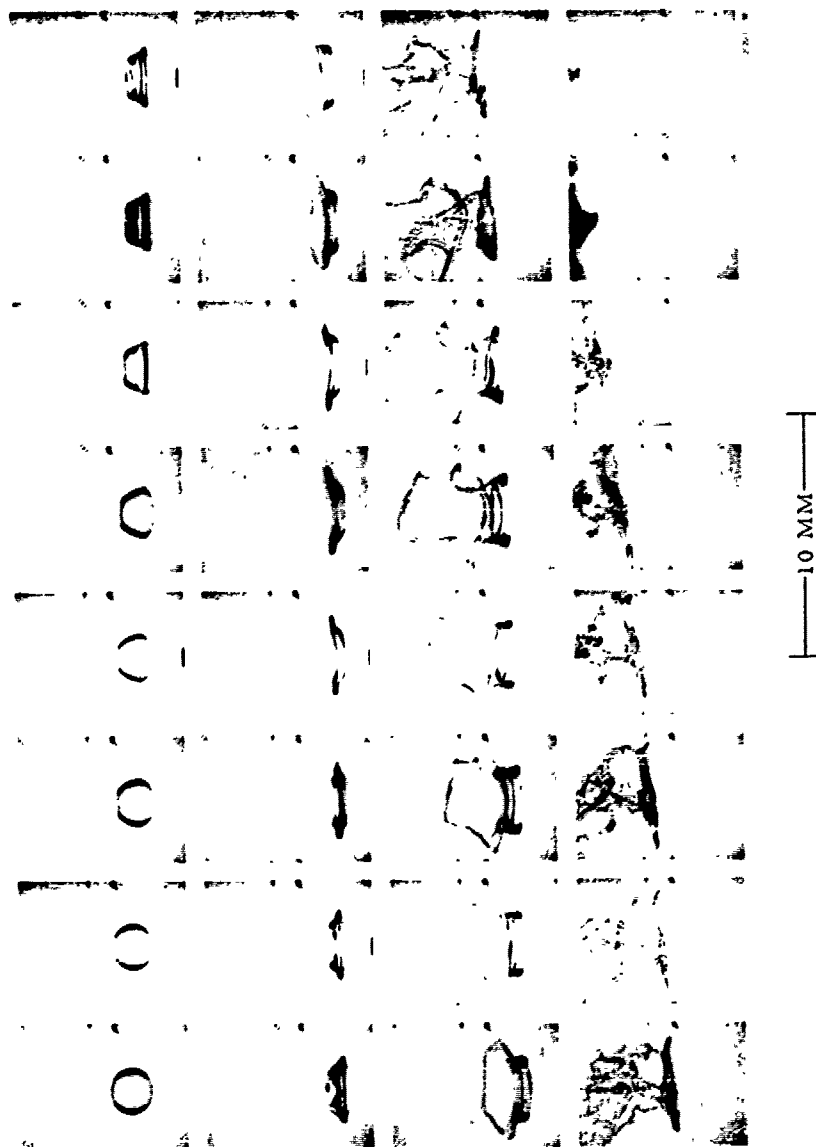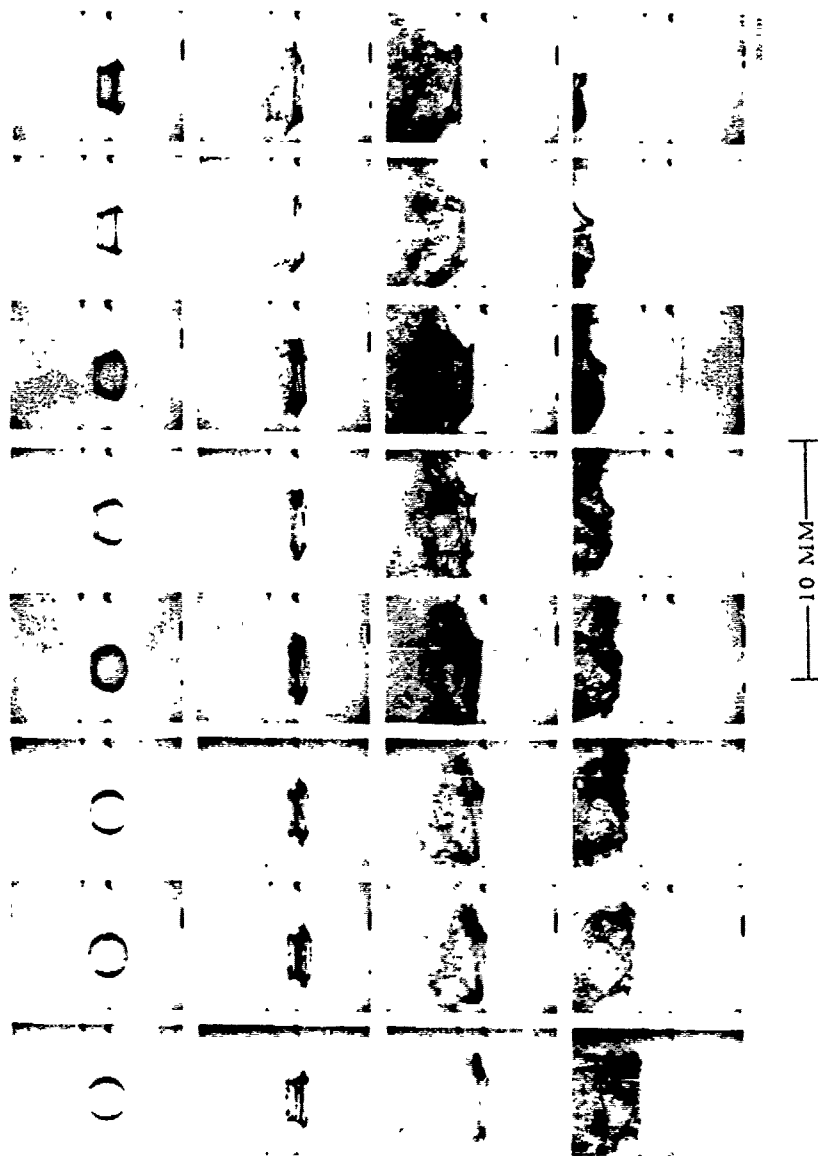Drop Size 1.9 MM   Time per Frame 0.1151 msec

├─1.0 MM─┤
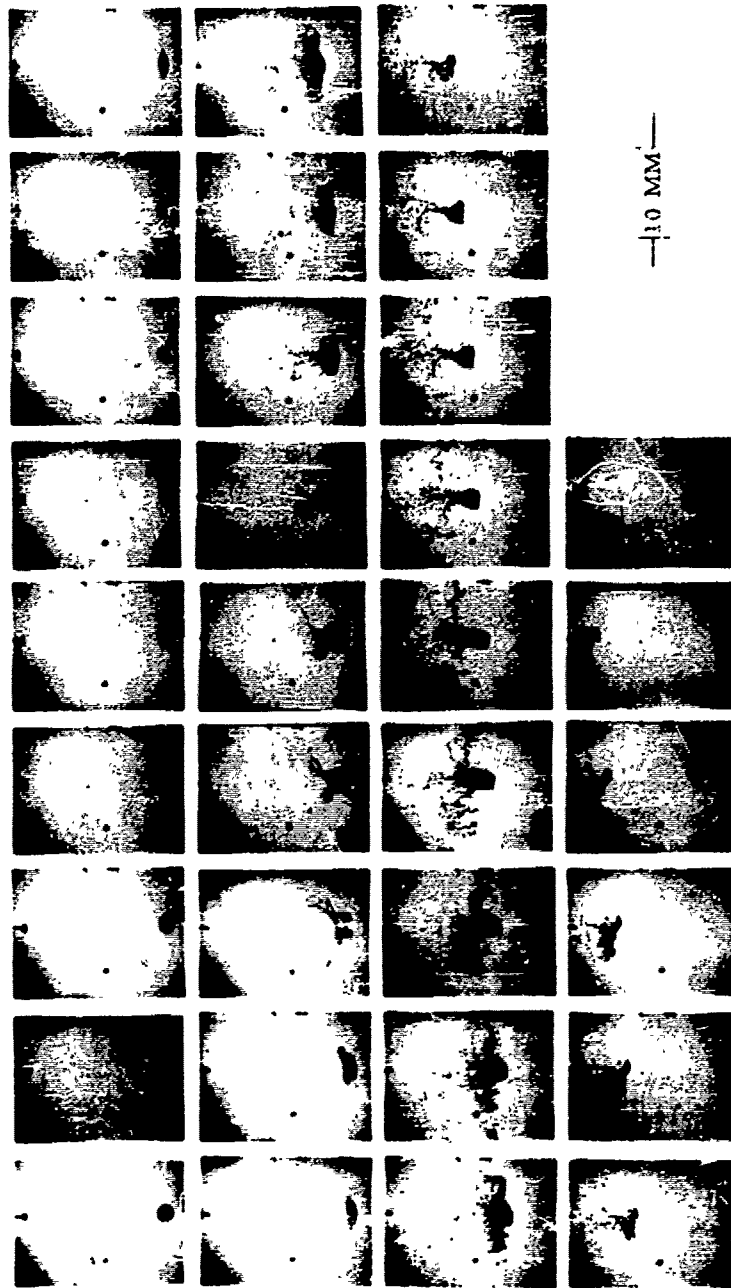
Test 132

Liquid-Mercury   Relative Velocity 460 ft/sec
Drop Size 2.1 MM   Time per Frame 0.0784 msec

10 MM

-B29-
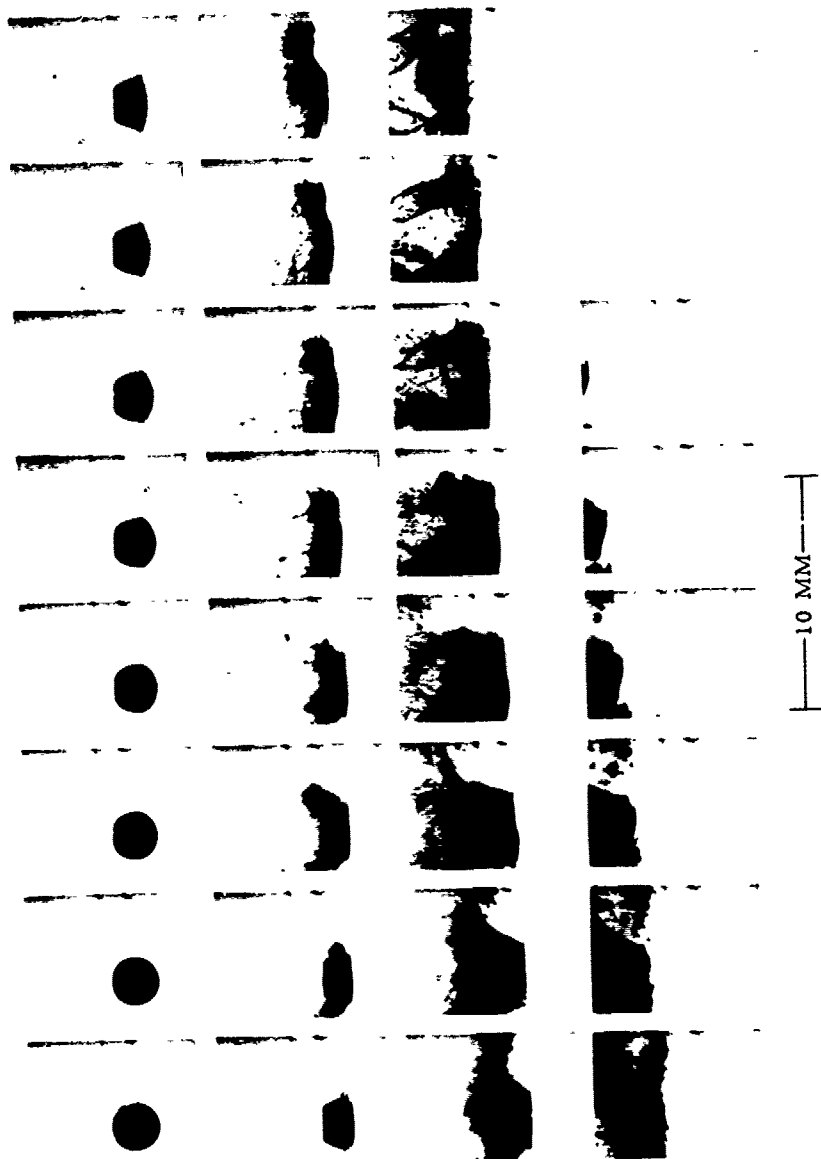
Test 135

Liquid Mercury   Relative Velocity 358 ft/sec
Drop Size 0. 82 MM   Time per Frame 0 0787 msec

⊢10 MM⊣

-B30
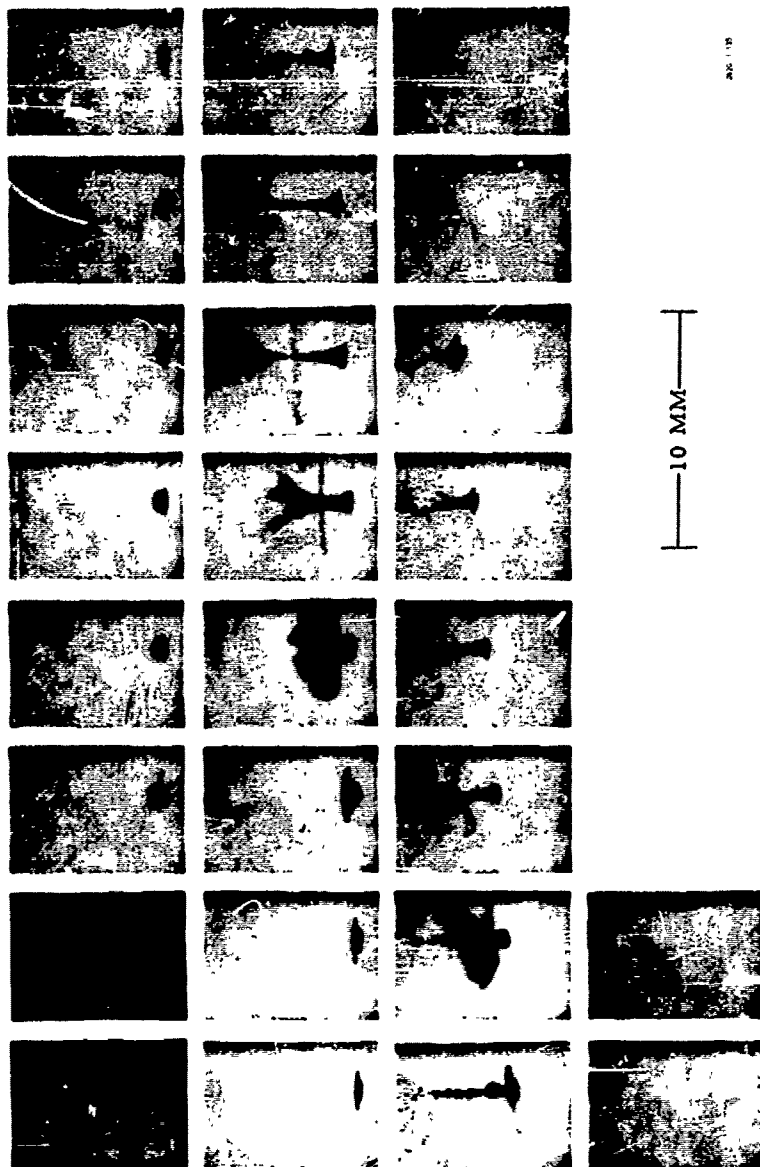
Test 138

Liquid-Mercury   Relative Velocity 230 ft/sec
Drop Size 0 69 MM   Time per Frame 0 0780 msec
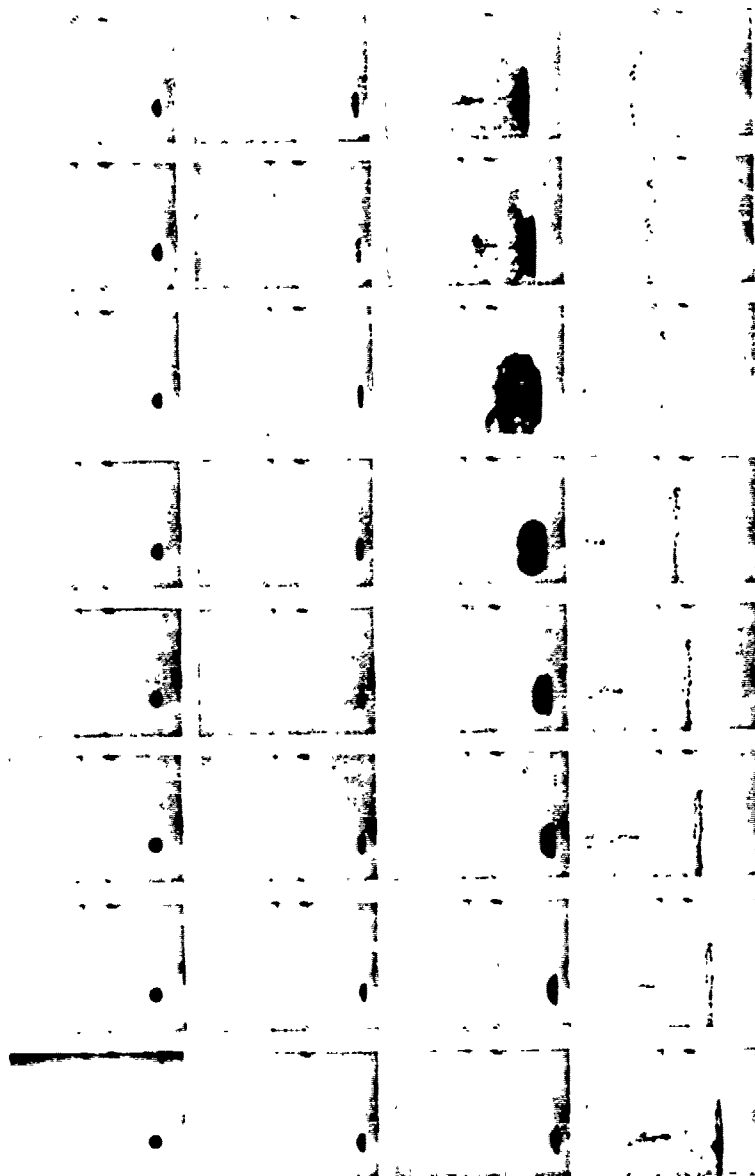
├─ 10 MM ─┤

Test 164

Liquid Mercury   Relative Velocity 173 ft/sec

Drop Size 1.2 MM   Time per Frame 0.1571 msec
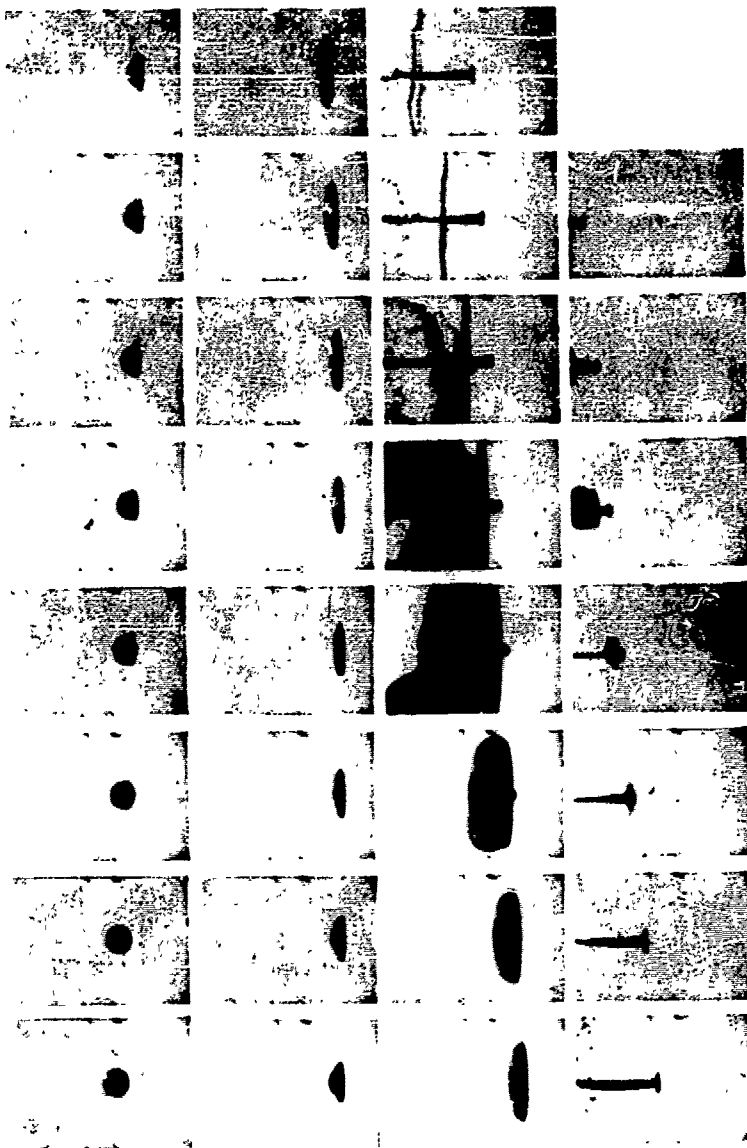
10 MM

Test 151

Liquid G.E. SF(96) 6. Relative Velocity 75 ft/sec

Drop Size 2 3 MM Time per Frame 0.1173 msec

|— 10 MM —|

-B33-
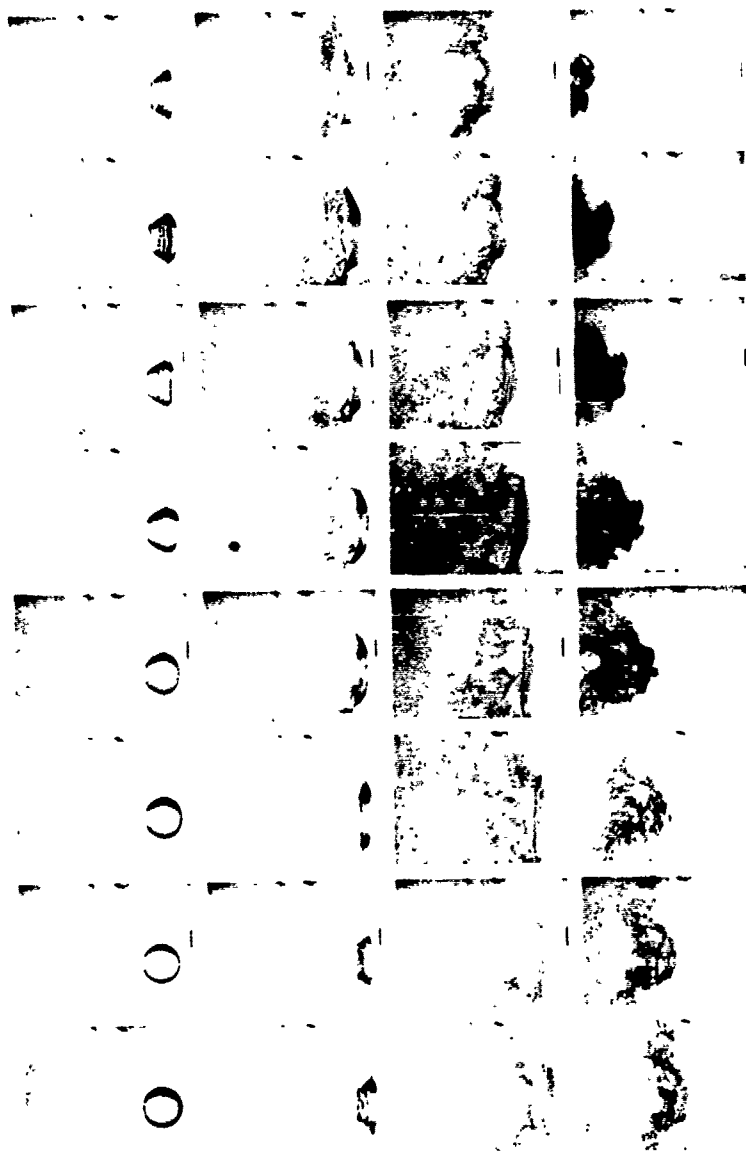
Test 152

Liquid G. E. SF(96) 65   Relative Velocity 137 ft/sec
Drop Size 1.0 MM   Time per Frame 0 0394 msec

1.0 MM

T st 153

Liquid-G. E. SF(96) 65 Relative Velocity 126 ft/sec

Drop Size 2.1 MM Time per Frame 0.0786 msec

⊢—10 MM—⊣

Test 154

Liquid G.E. SF(96) 65   Relative Velocity 234 ft/sec
Drop Size 2.2 MM   Time per Frame 0.0592 msec
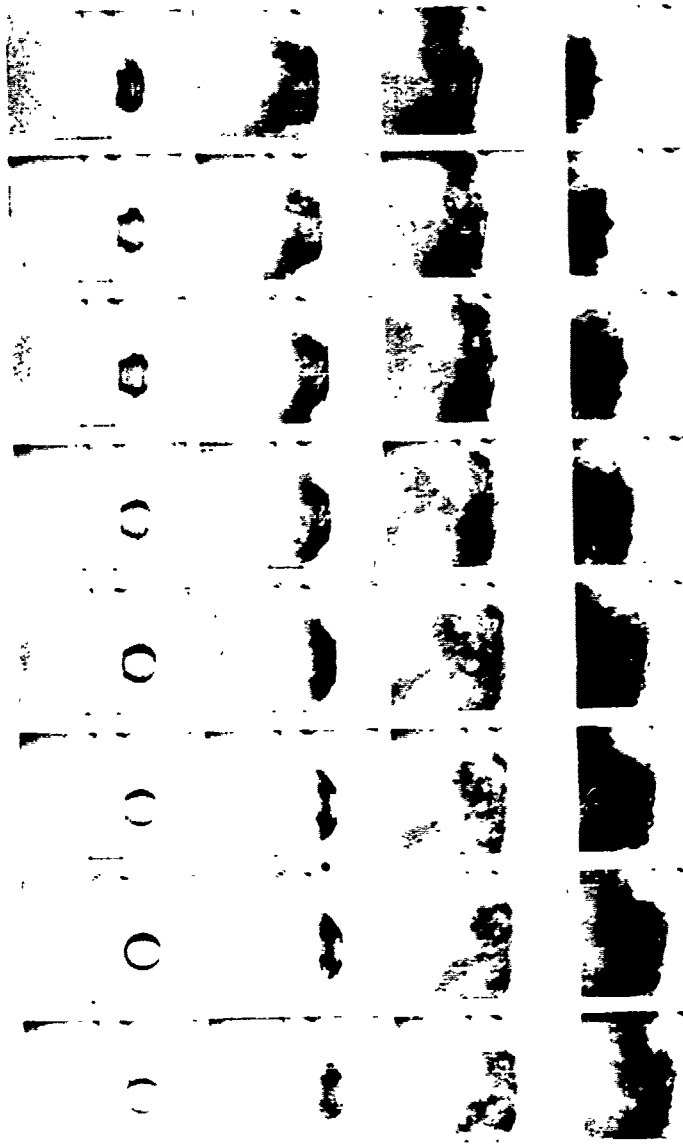
10 MM

Test 155

Liquid· G. E. SF(96) 65 Relative Velocity 381 ft/sec
Drop Size 1. 9 MM Time per Frame 0. 0393 msec
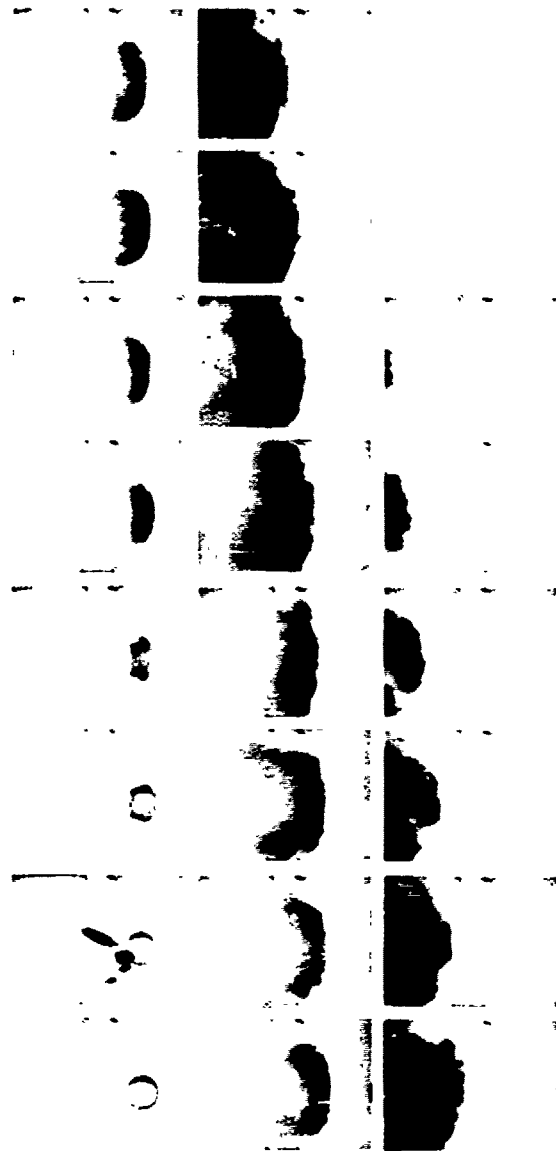
├─10 MM─┤

Test 156

Liquid· G. E. SF(96) 65   Relative Velocity 472 ft/sec
Drop Size 2 1 MM   Time per Frame 0. 0392 n sec
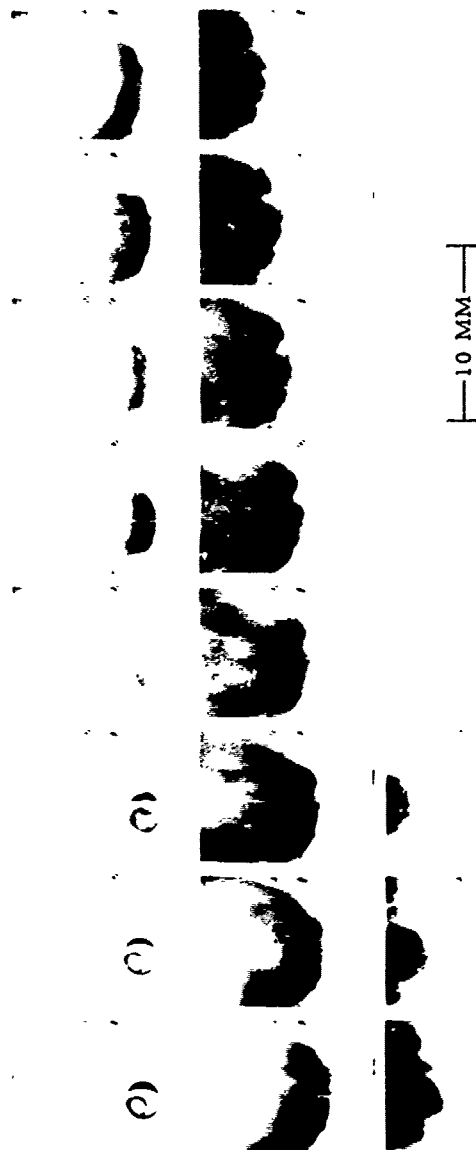
|—— 10 MM ——|

Test 160

Liquid G.E. SF(96) 65 Relative Velocity 49 ft/sec
Drop Size 1 4 MM Time per Frame 0.0786 msec

10 MM

-B39-
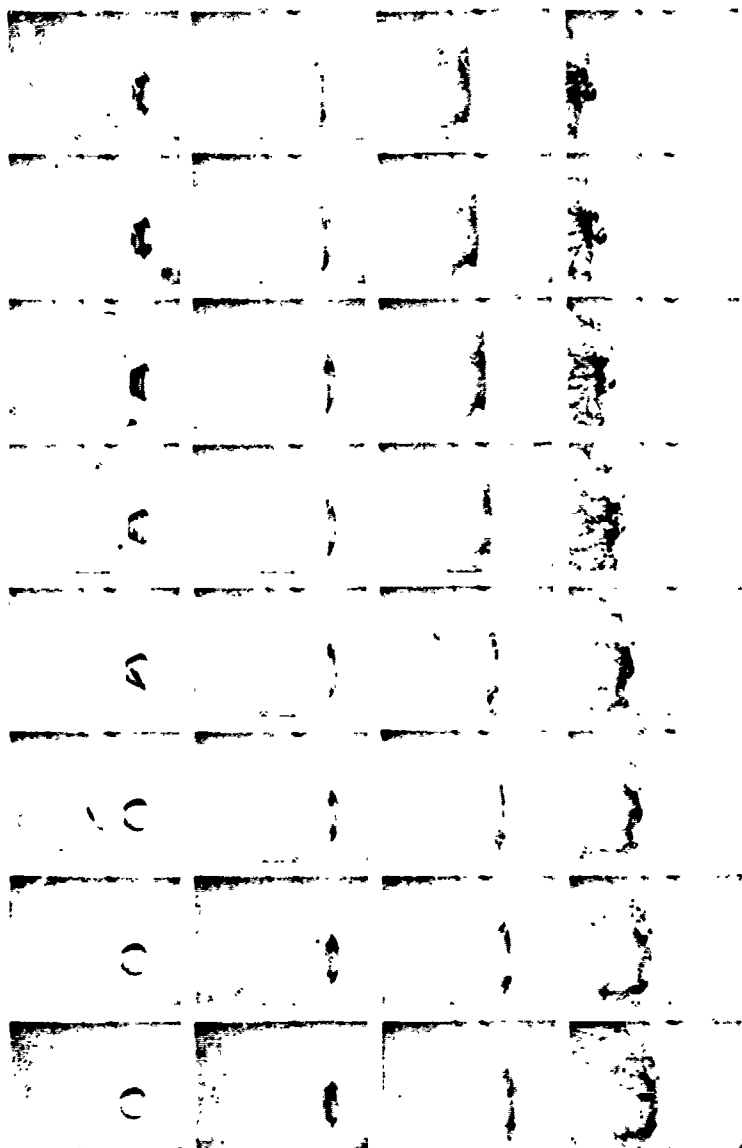
Test 193

Liquid - G.E. SF(96) 65 Relative Velocity 441 ft/sec

Drop Size 1.3 MM Time per Frame 0.0391 msec

├── 10 MM ──┤

Test 194

Liquid G. E. SF(96) 65 Relative Velocity 350 it/sec
Drop Size 1.5 MM Time per Frame 0.0391 msec

10 MM
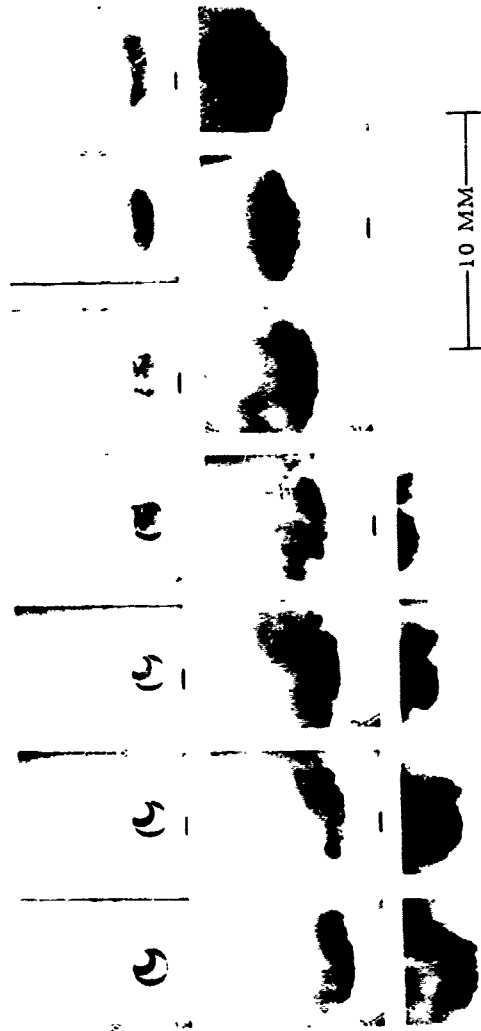
Test 195

Liquid G. E. SF(96) 65   Relative Velocity 200 ft/sec

Drop Size 1 4 MM   Time per Frame 0 0390 msec

10 MM

-B42
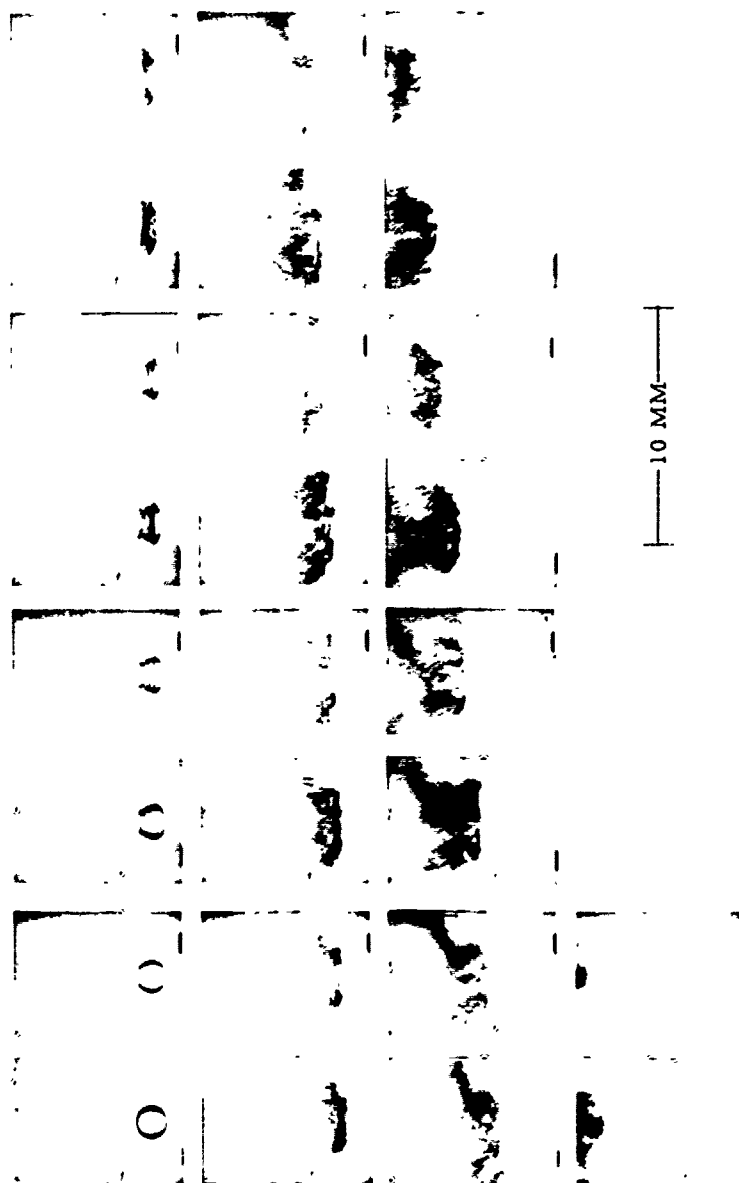
Test 197

Liquid G. E. SF(96) 65 Relative Velocity 48 ft/sec

Drop Size 1.4 MM Time per Frame 0.078 m/sec

10 MM

-B43
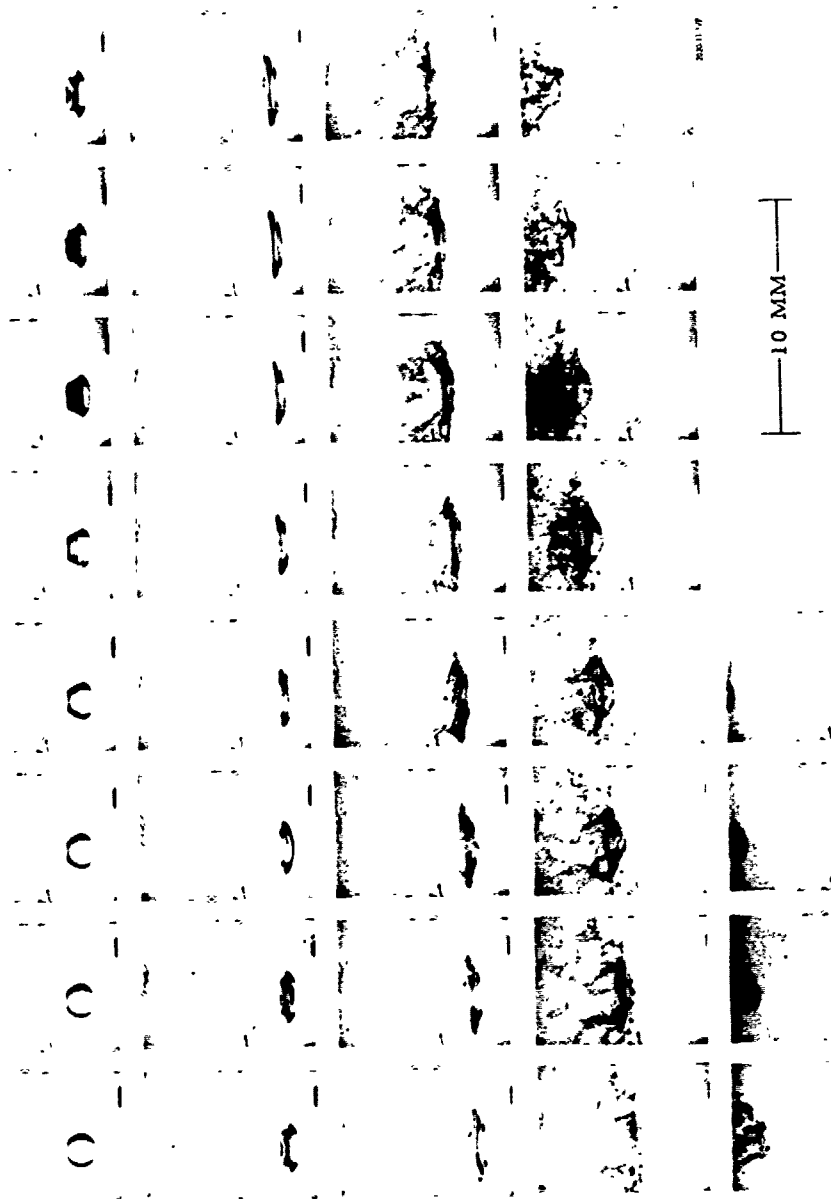
Test 140

Liquid G. E. SF(96)10 Relative Velocity 450 ft/sec
Drop Size 2.1 MM Time per Frame 0.0393 msec

10 MM

-B44-
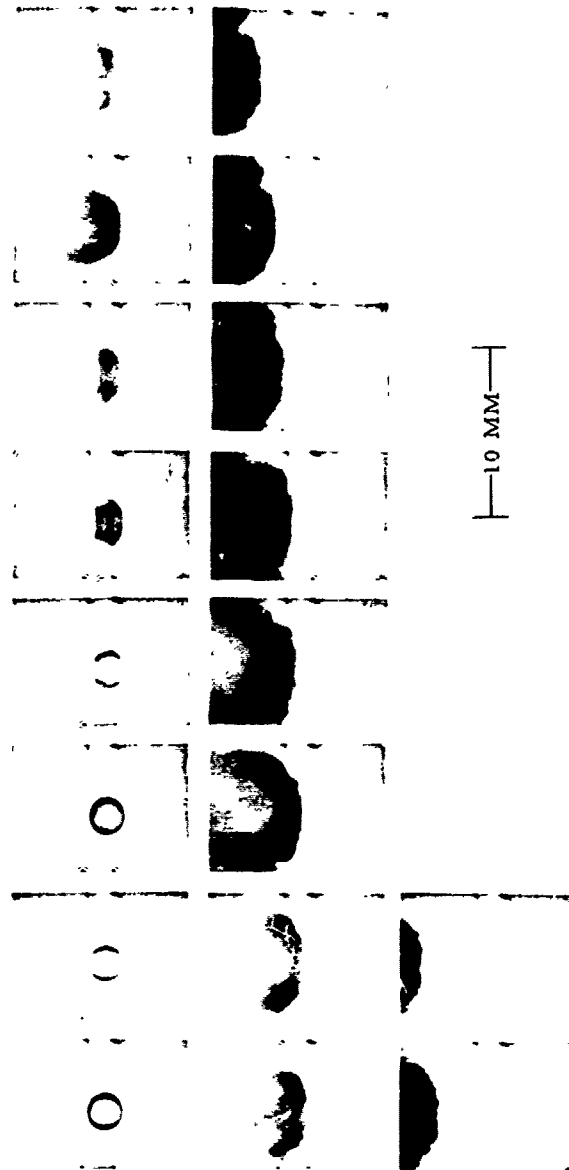
Test 142

Liquid G. E SF196110 Relative Velocity 228 ft/sec
Drop Size 2 2 MM Time per Frame 0 0392 msec

|—10 MM—|

-B45
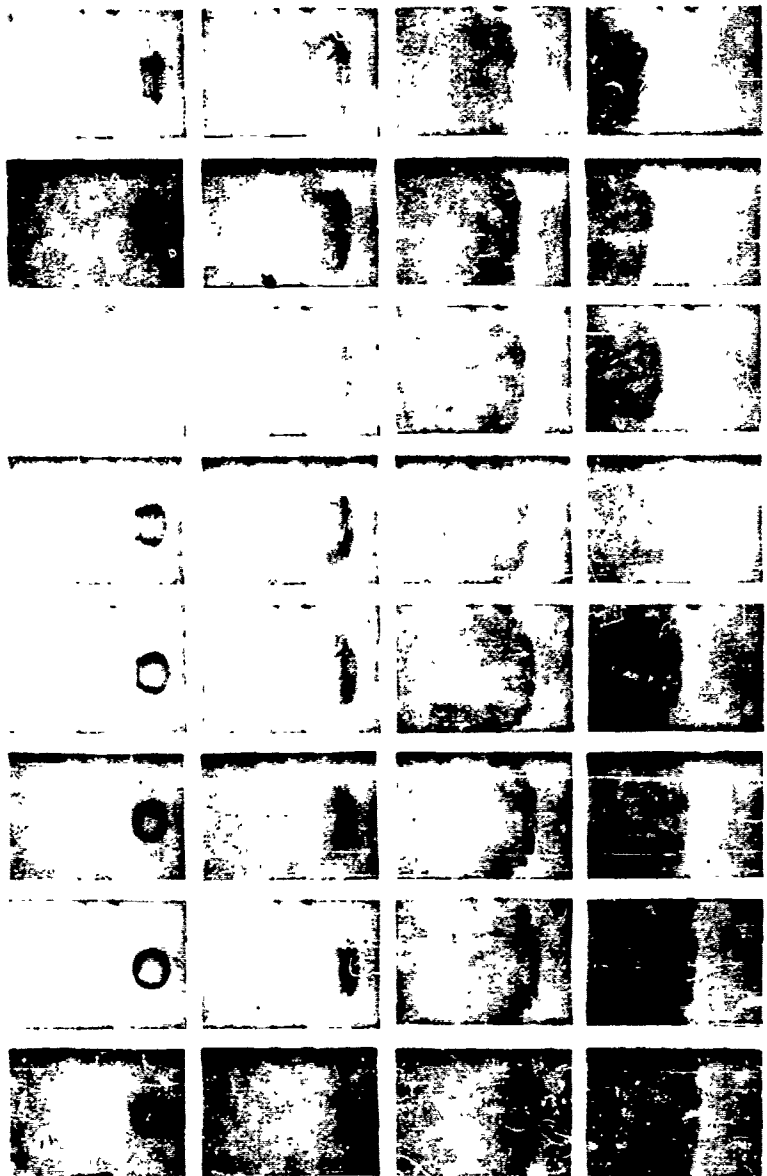
Test 143

Liquid-G. E. SF(96)10   Relative Velocity 130 ft/sec

Drop Size 2 2 MM   Time per Frame 0 0784 msec

|------10 MM------|

-B46
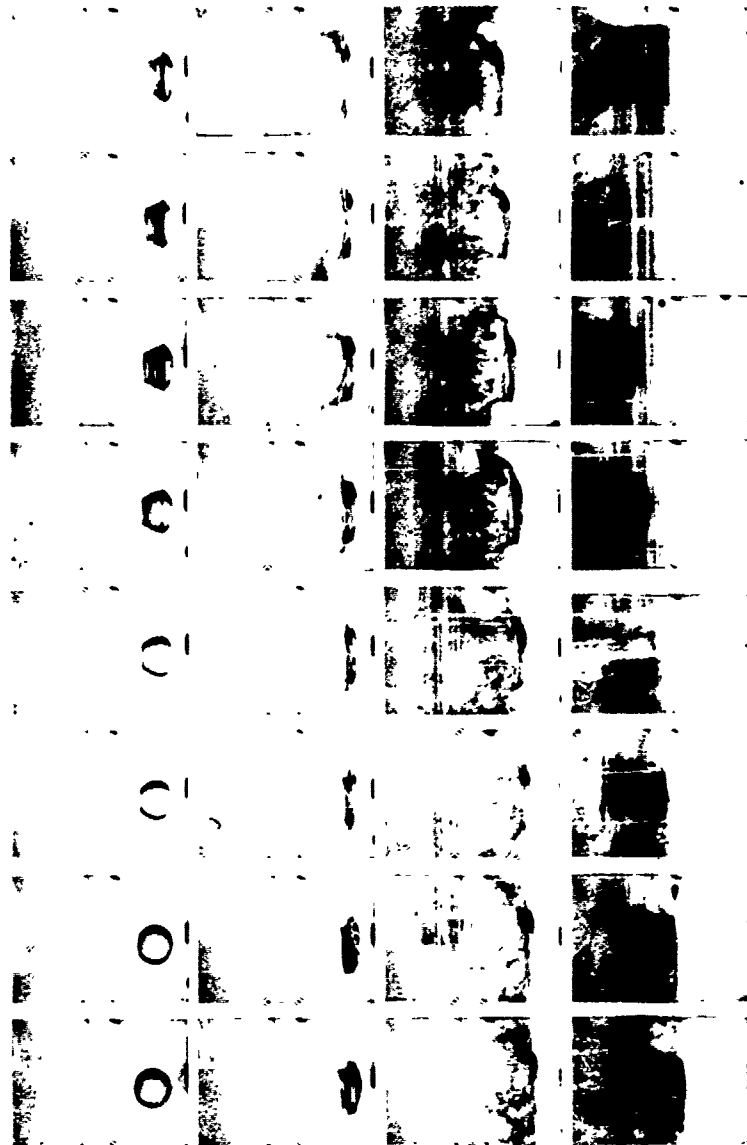
Test 148

Liquid G. E. SF196,10 Relative Velocity 366 ft/sec
Drop Size 2 0 MM Time per Frame 0 0393 msec

|—10 MM—|

-B47-
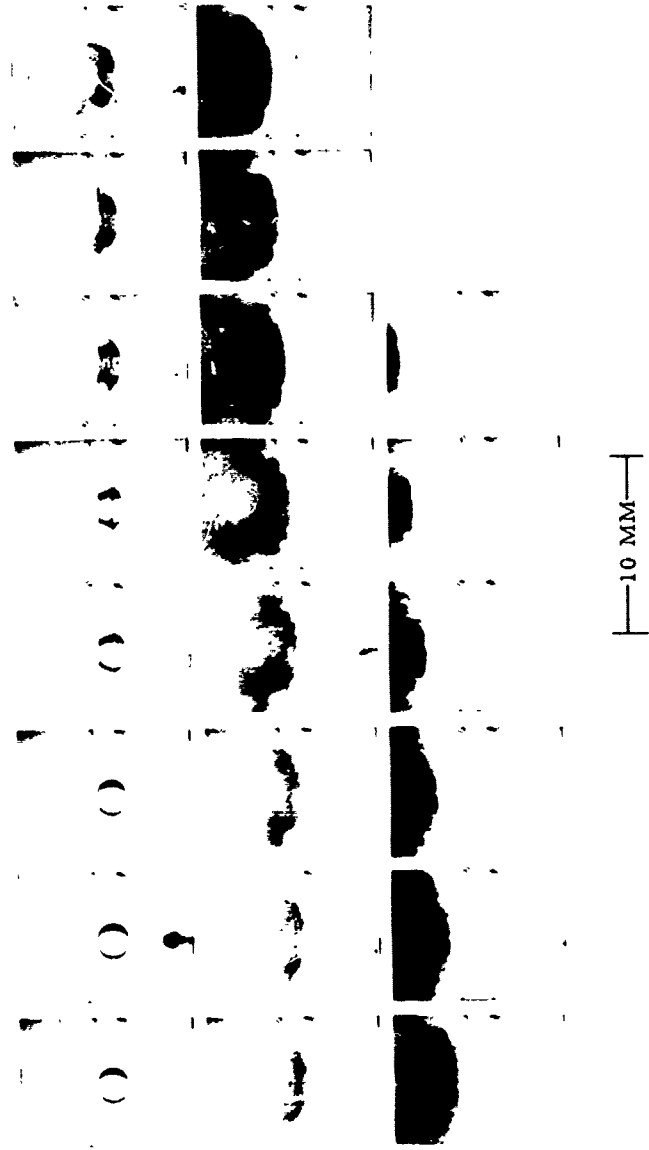
Test 150

Liquid G.E. SF(96)10   Relative Velocity 90 ft/sec
Drop Size 2 0 MM Time per Frame 0.1176 msec
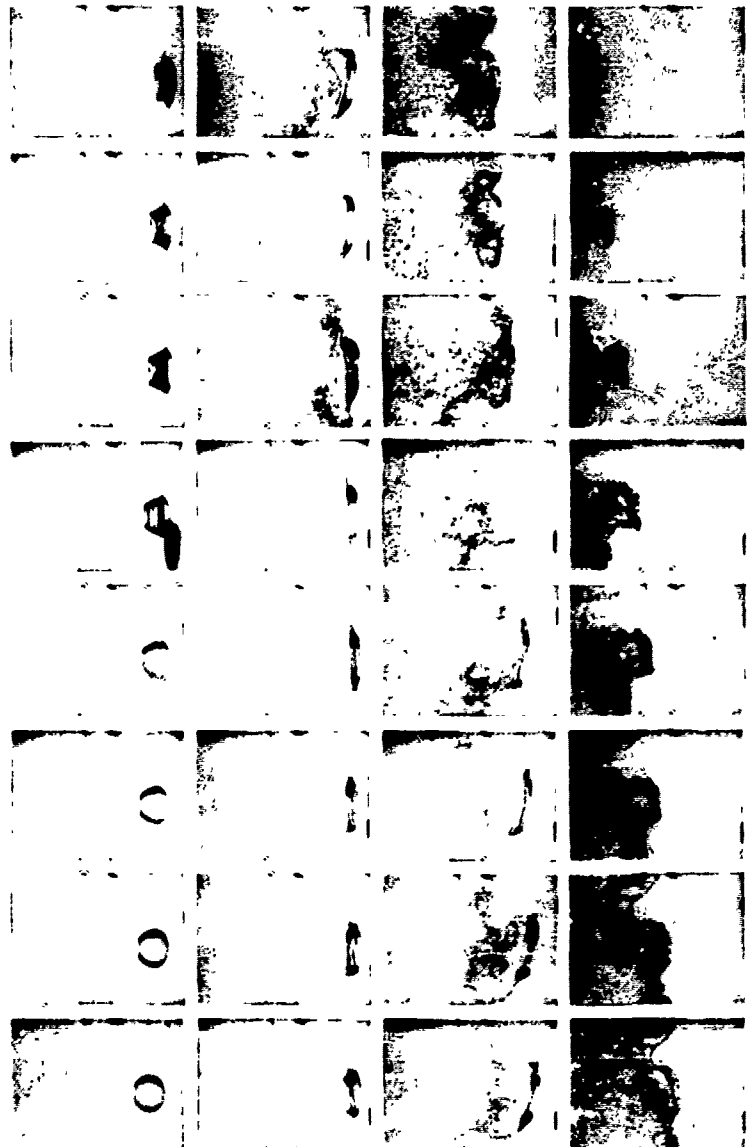
├── 10 MM ──┤

Test 161

Liquid G. E. SF(96)10   Relative Velocity 51 ft/sec

Drop Size 1. 4 MM Time per Frame 0. 1178 msec

10 MM
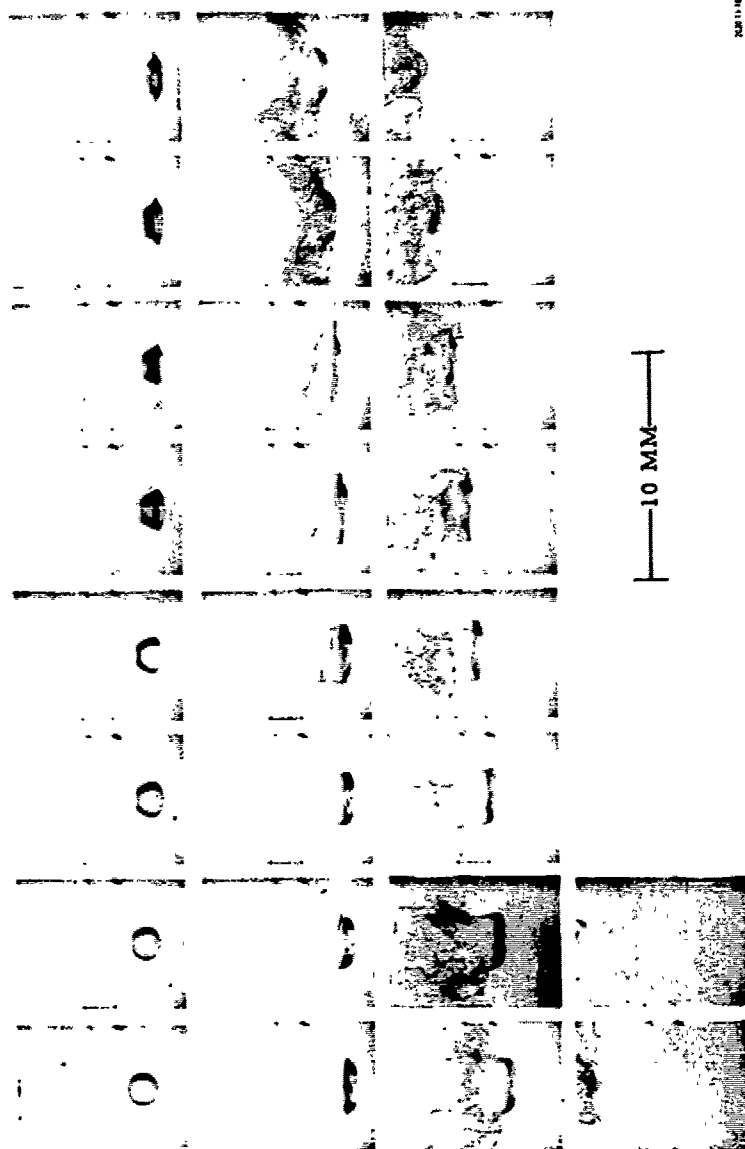
Test 198

Liquid-G. E. SF(96)10   Relative Velocity 103 ft/sec
Drop Size 1.4 MM   Time per Frame 0.0781 msec
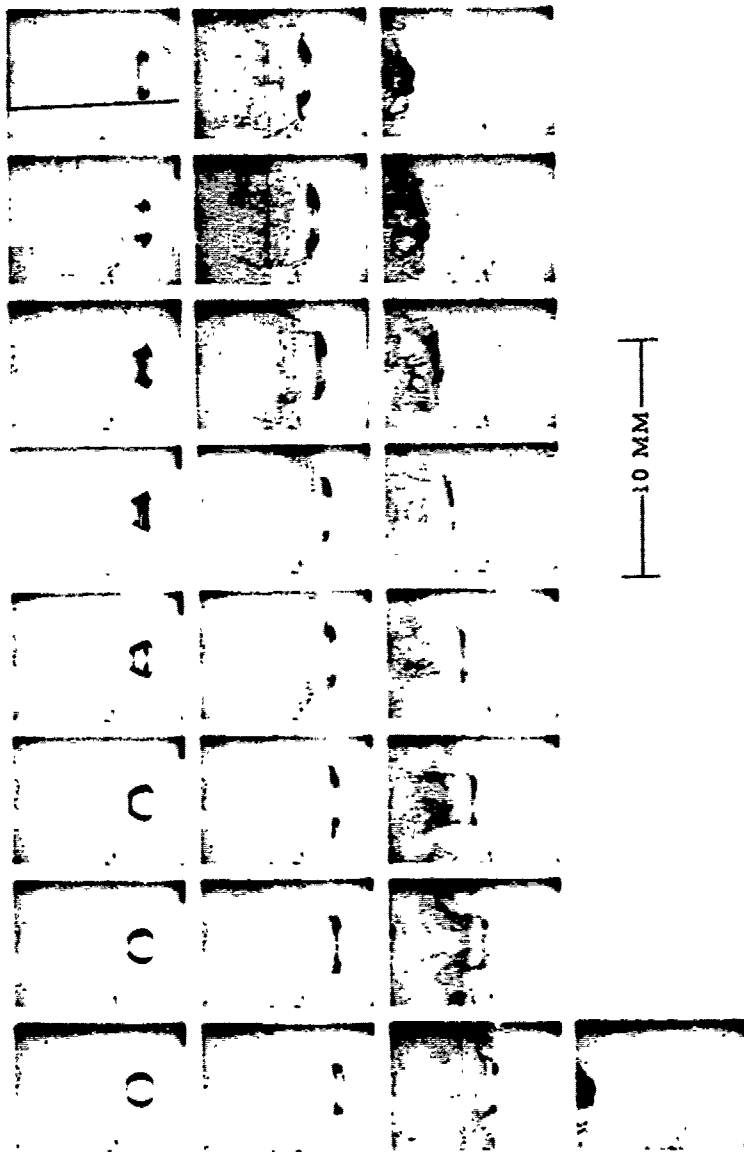
10 MM

Tes-199
Liquid G.E. SF(96)10 Relative Velocity 193 ft/sec
Drop Size 1.4 MM Time per Frame 0.0390 msec
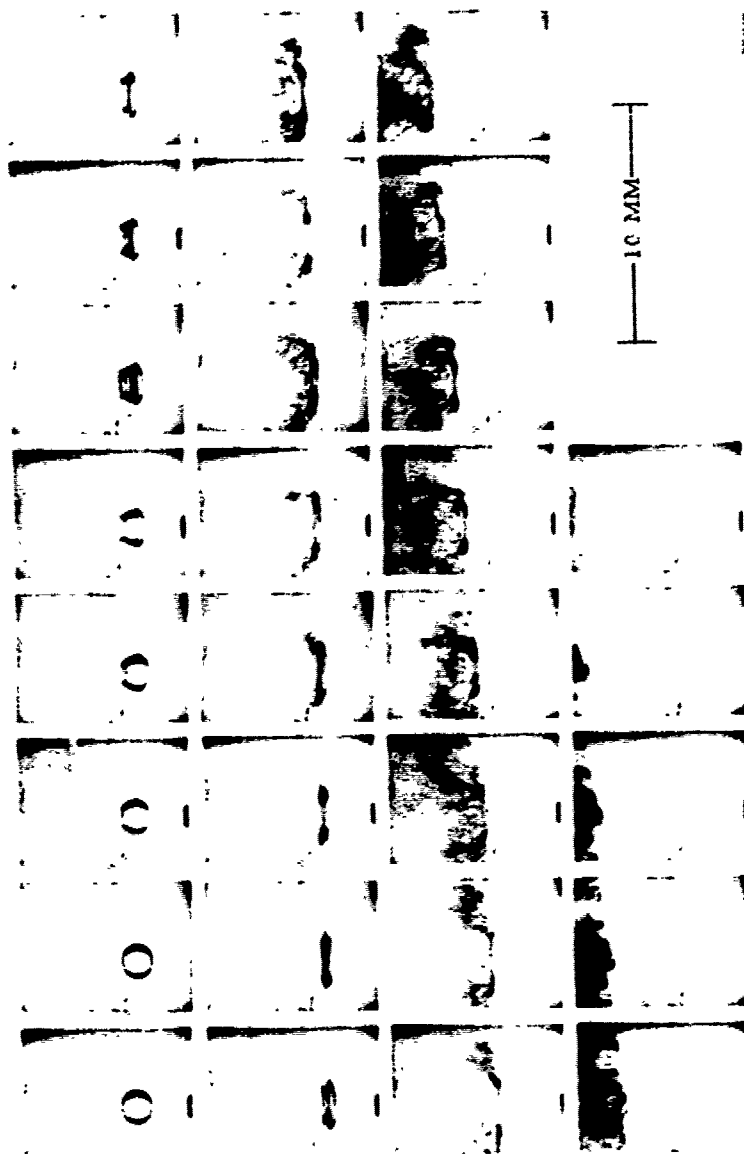
10 MM

Test 200
Liquid: G. E. SF(96)10   Relative Velocity 343 ft/sec
Drop Size 1.4 MM Time per Frame 0.0392 msec
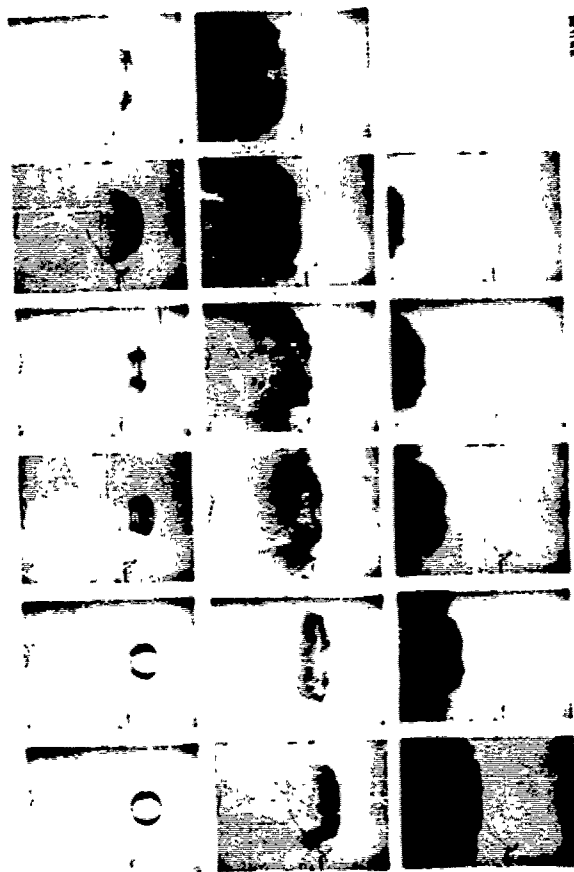
Test 201

Liquid G. E. SF(95)10 Relative Velocity 436 ft/sec
Drop Size 1.4 MM Time per Frame 0.0390 msec
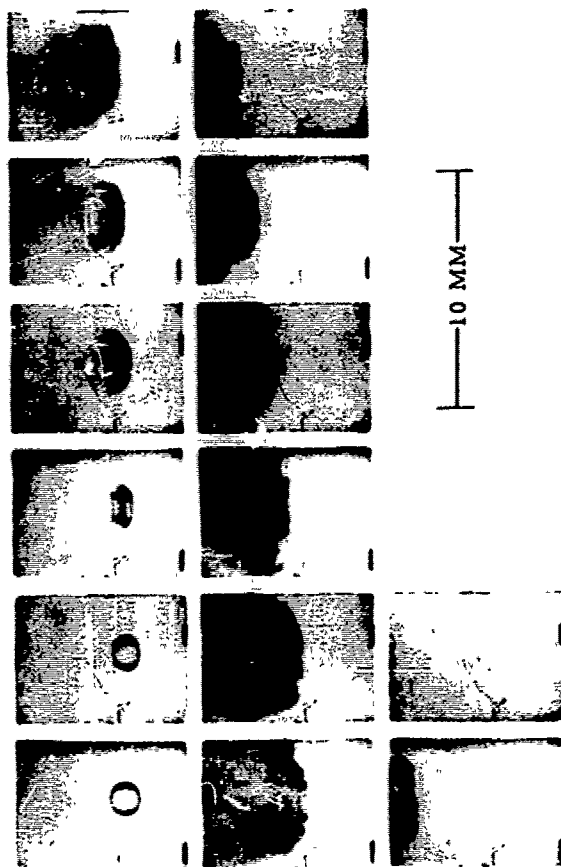
10 MM

Test 125

Liquid G.E. SF(96)200 Relative Velocity 78 ft/sec
Drop Size 2.1 MM Time per Frame 0.1175 msec
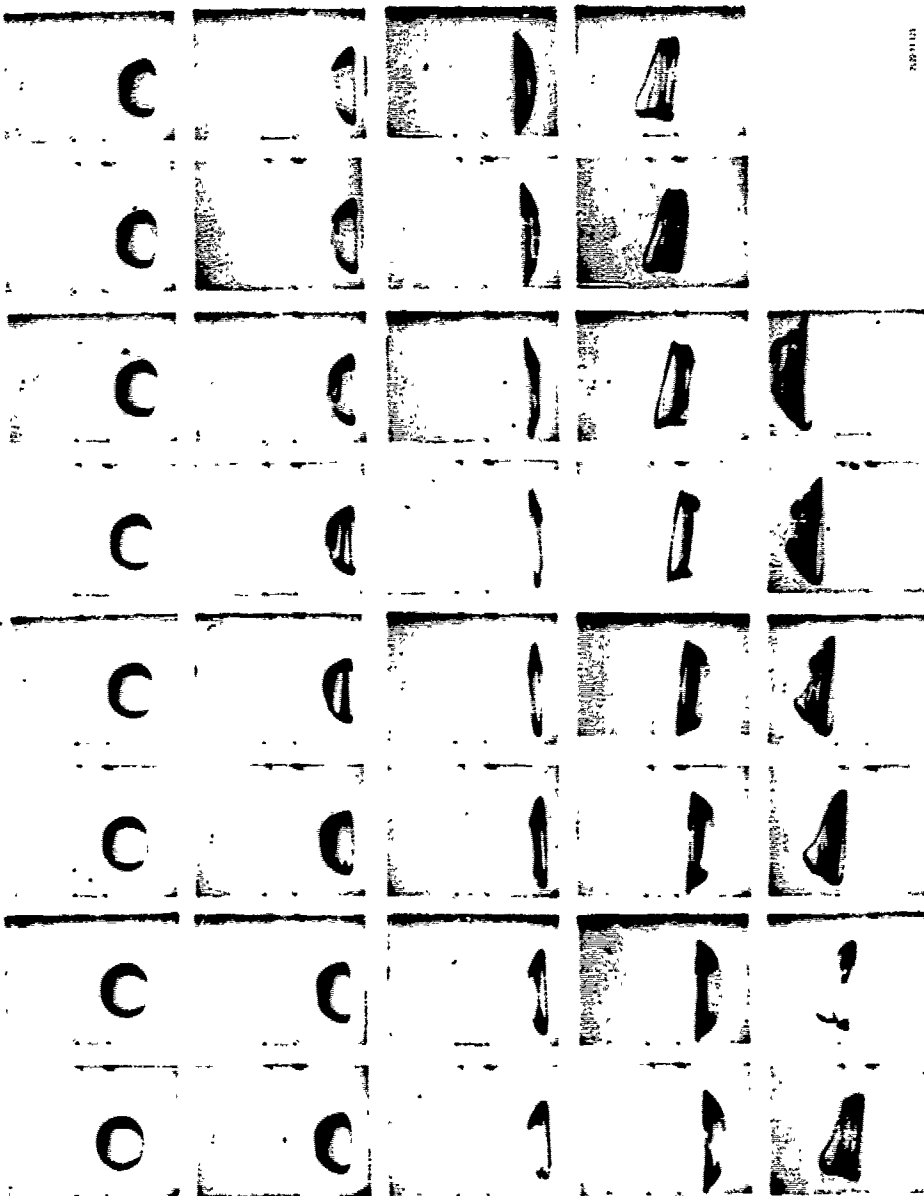
10 MM

est 127

Liquid G. E. SF(96)200 Relative Velocity 122 ft/sec
Drop Size 2.2 MM Time per Frame 0.0786 msec

10 MM
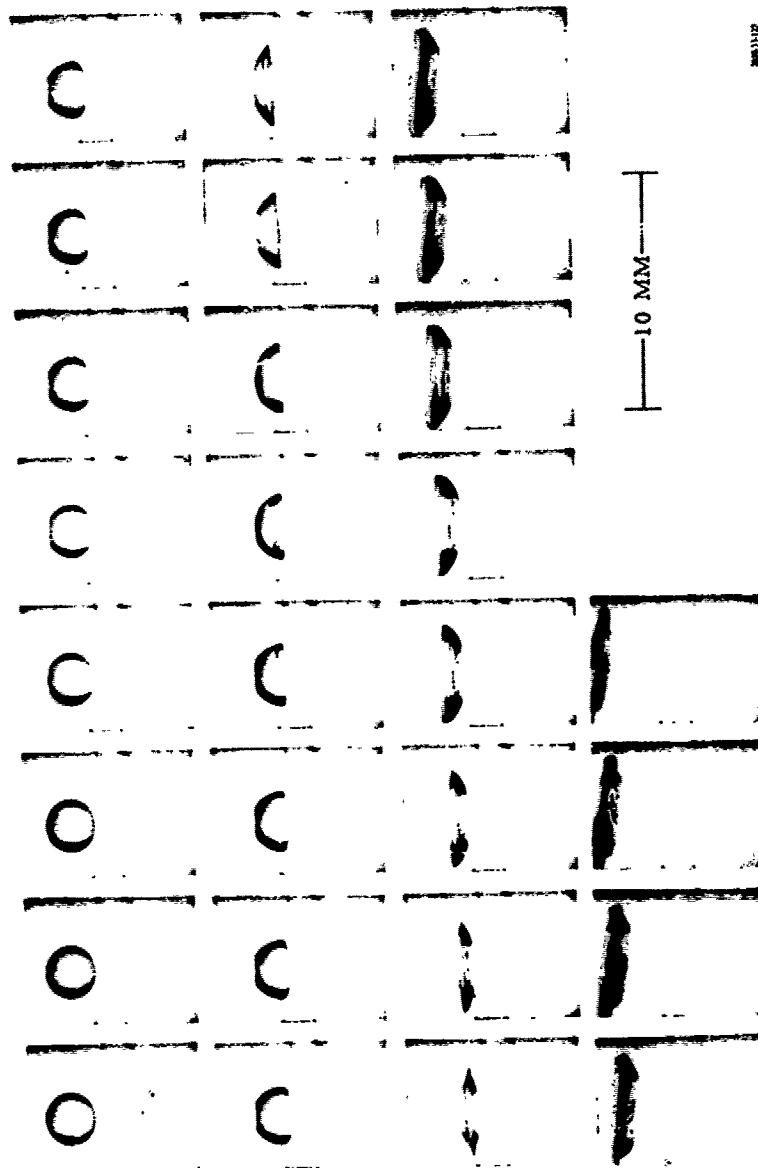
Liquid-G. E. SF(96)200 Relative Velocity 127 ft/sec
Drop Size 2.2 MM Time per Frame 0.0780 msec

10 MM
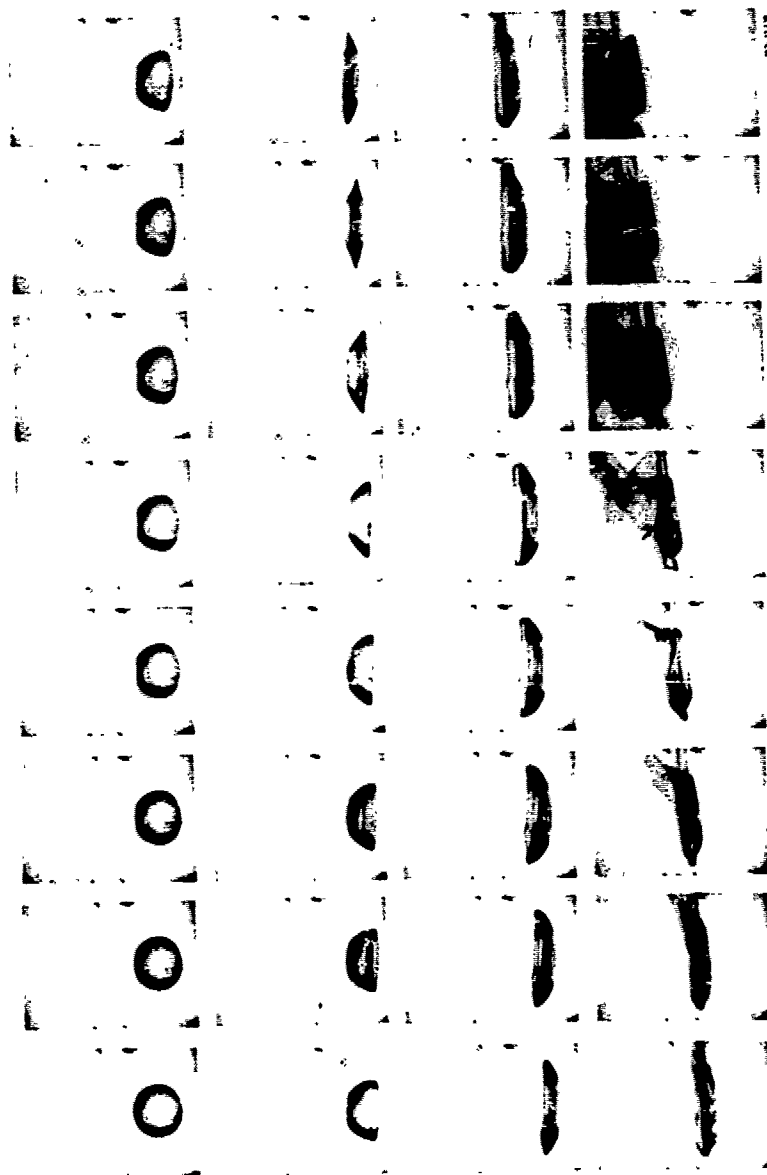
Test 129

Liquid--G. E. SF(96)200 Relative Velocity 215 ft/sec
Drop Size 2. 2 MM Time per Frame 0. 0392 msec
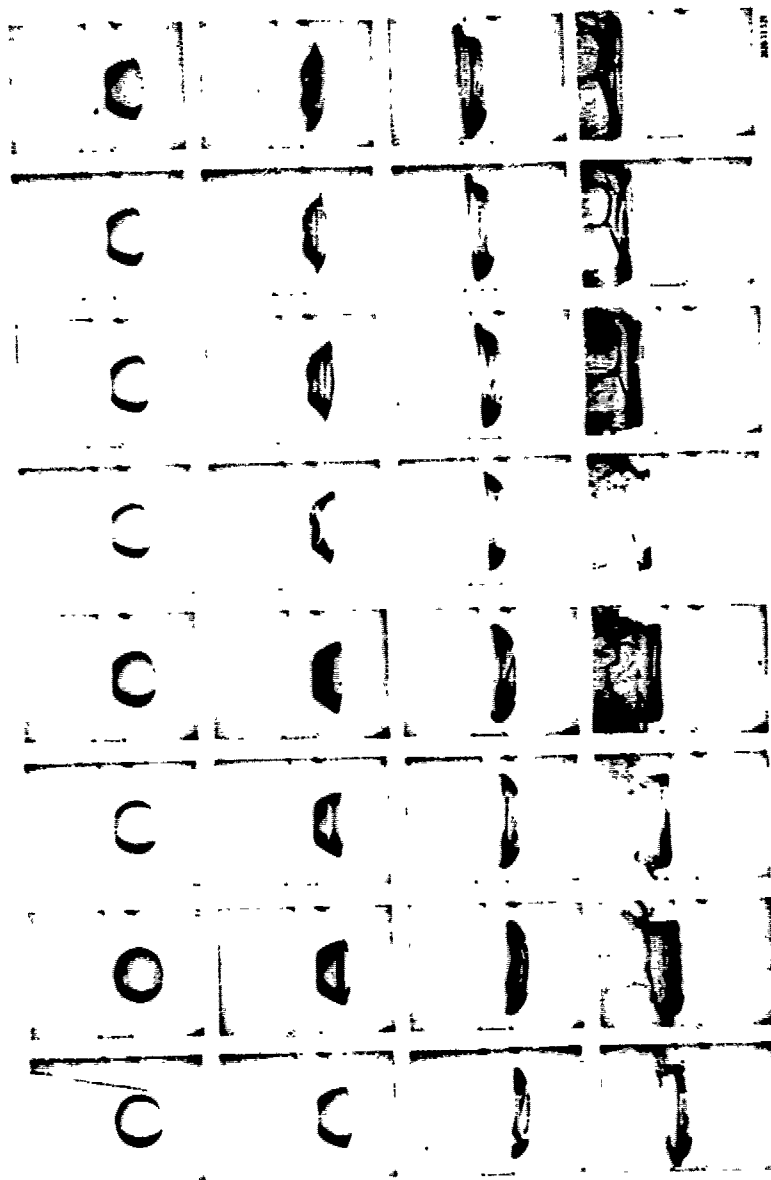
10 MM

Test 130

Liquid-G. E. SF(96)200 Relative Velocity 363 ft/sec

Drop Size 2.1 MM Time per Frame 0.0393 msec
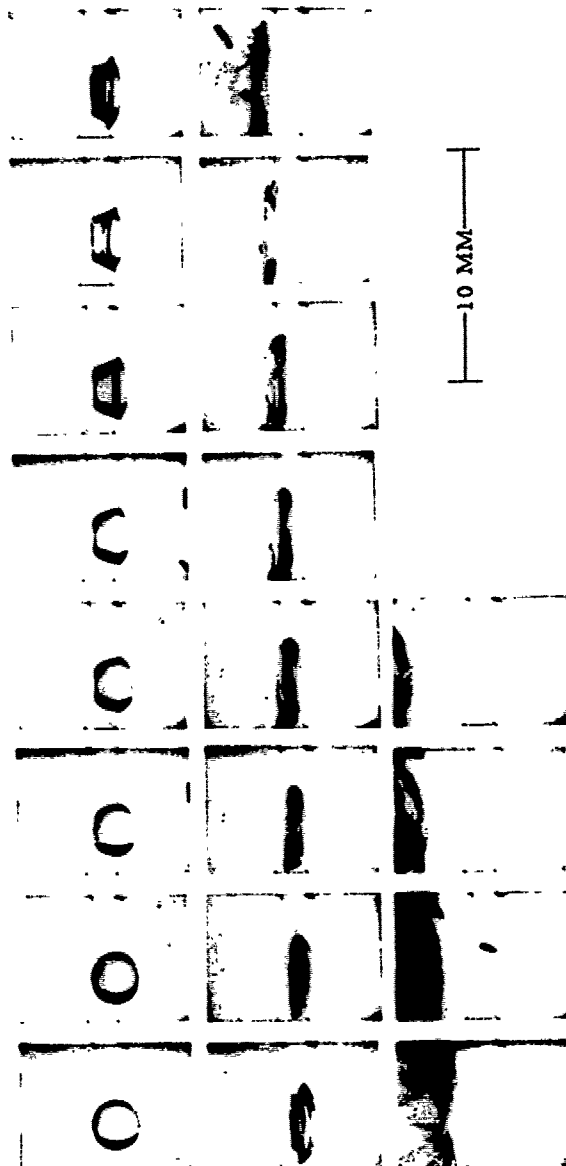
10 MM

Test 131

Liquid G.E. SF(96)200   Relative Velocity 456 ft/sec
Drop Size 2.2 MM   Time per Frame 0.0391 msec

├─10 MM─┤

-B59-
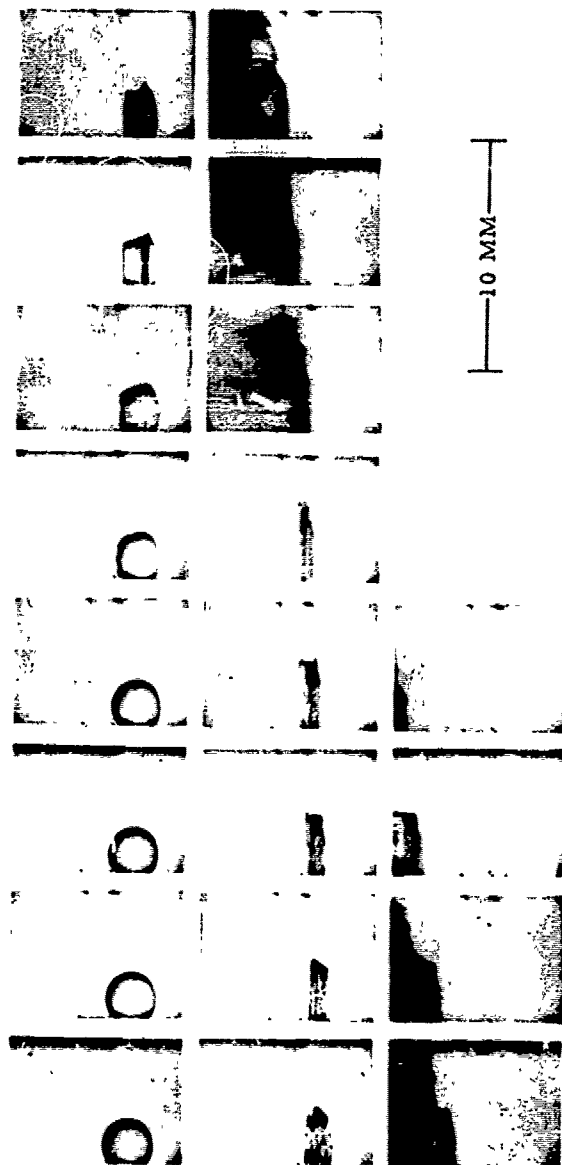
Test 162

Liquid-G. E. SF(96)200 Relative Velocity 38 ft/sec

Drop Size 1.4 MM Time per Frame 0.1178 msec
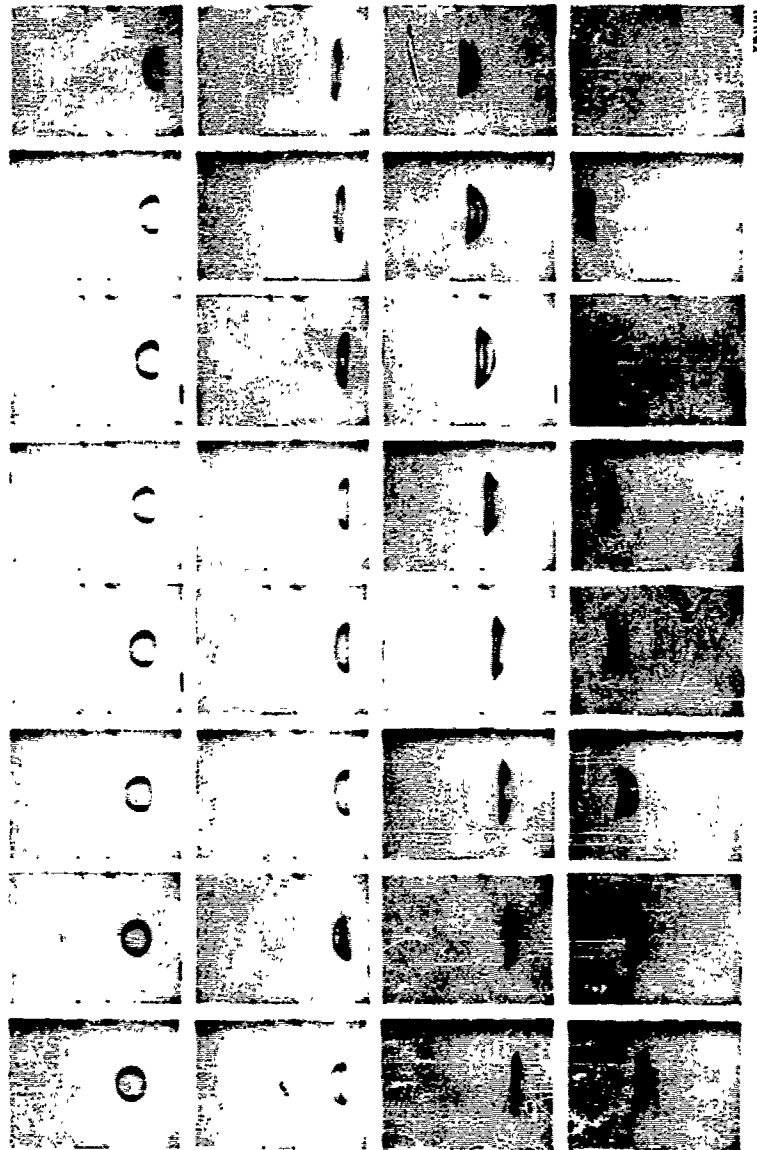
|——10 MM——|

Test 203

Liquid-G. E. SF(96)200   Relative Velocity 81 ft/sec
Drop Size 1. 5 MM   Time per Frame 0. 0782 msec
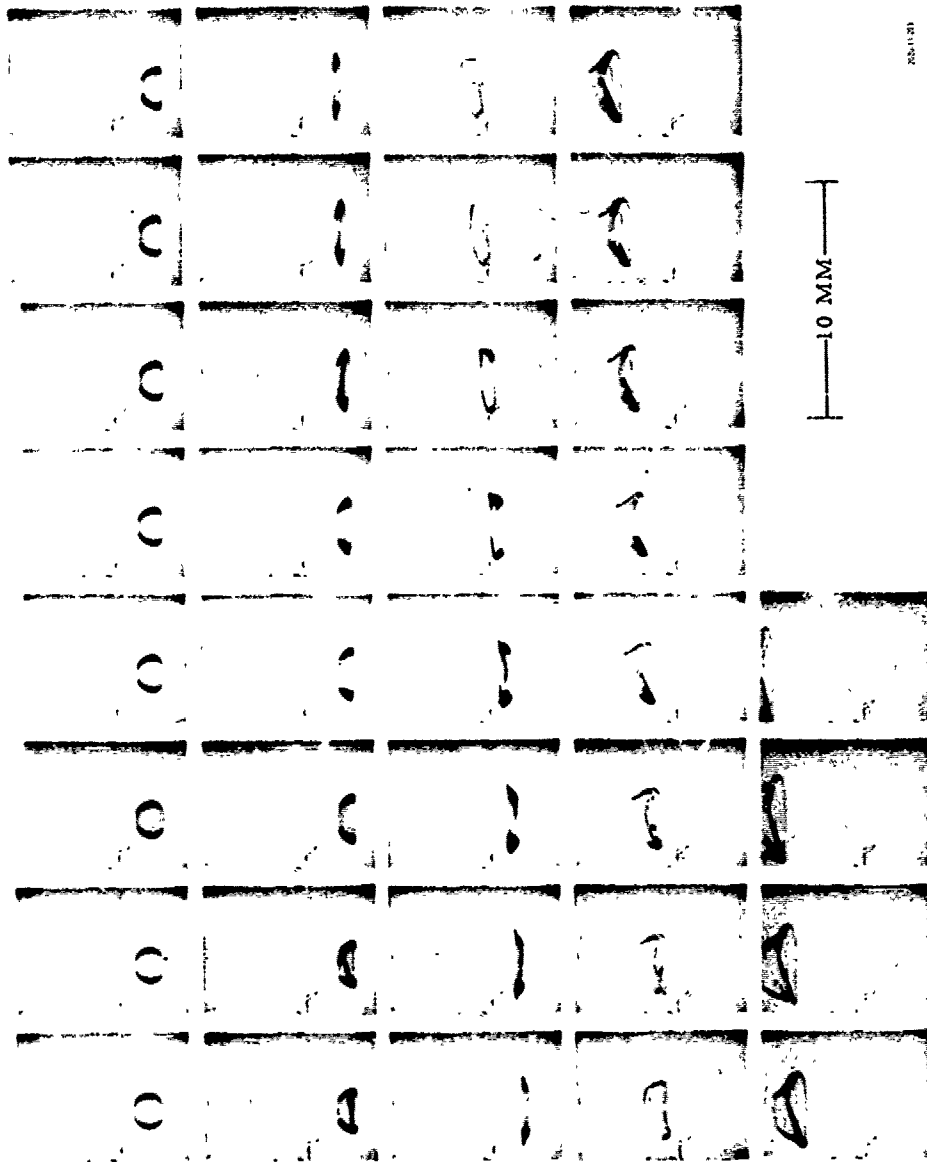
10 MM

Test 204

Liquid - G. E. SF(96)200 Relative Velocity 197 ft/sec
Drop Size 1. 5 MM Time per Frame 0. 0390 msec

10 MM

-B62-
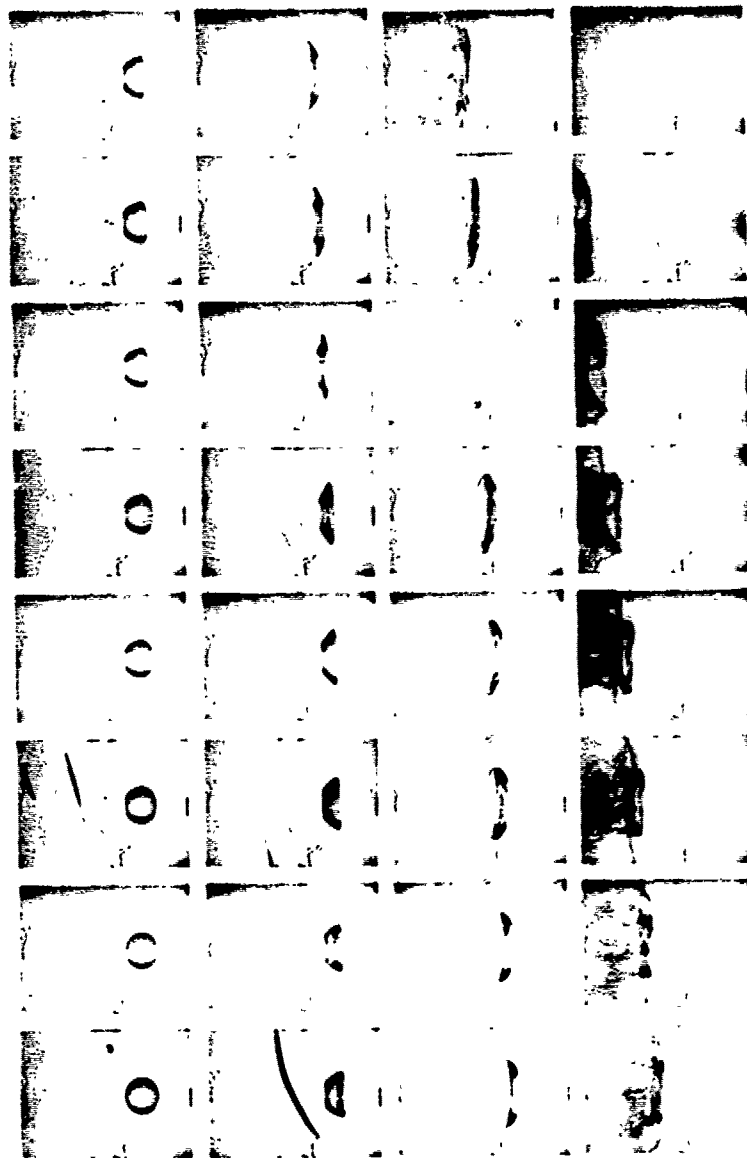
Test 205

Liquid. G. E. SF(96)200 Relative Velocity 345 ft/sec

Drop Size 1.5 MM Time per Frame 0.0392 msec

10 MM

Test 206
Liquid G. E. SF(96)200 Relative Velocity 403 ft/sec
Drop Size 1. 5 MM Time per Frame 0. 0393 msec

10 MM

Test 208

Liquid-G.E. SF(96)200 Relative Velocity 69 ft/sec

Drop Size 1.4 MM Time per Frame 0.1174 msec

10MM

Test 232
Liquid G.E. SF(96)200 Relative Velocity 166 ft/sec
Drop Size 1.2 MM Time per Frame 0.0767 msec

10 MM

-B66-
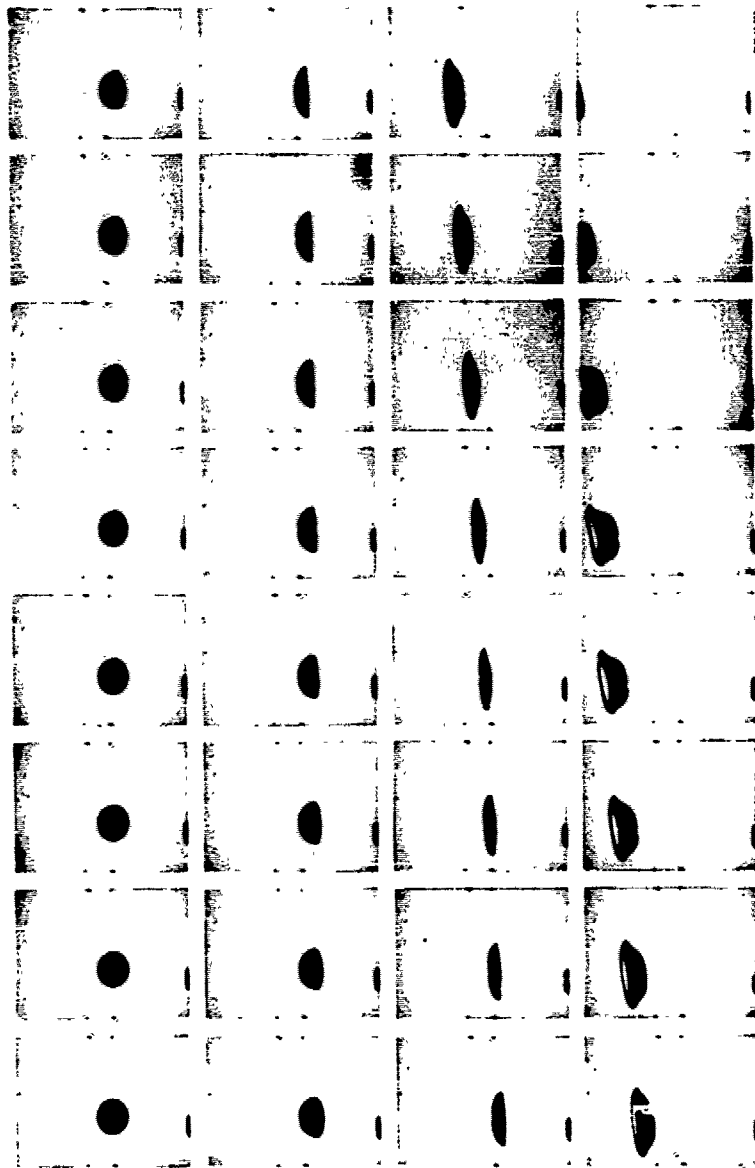
Test 243

Liquid G.E. SF(96)200   Relative Velocity 65 ft/sec
Drop Size 0.93 MM Time per Frame 0.1169 msec
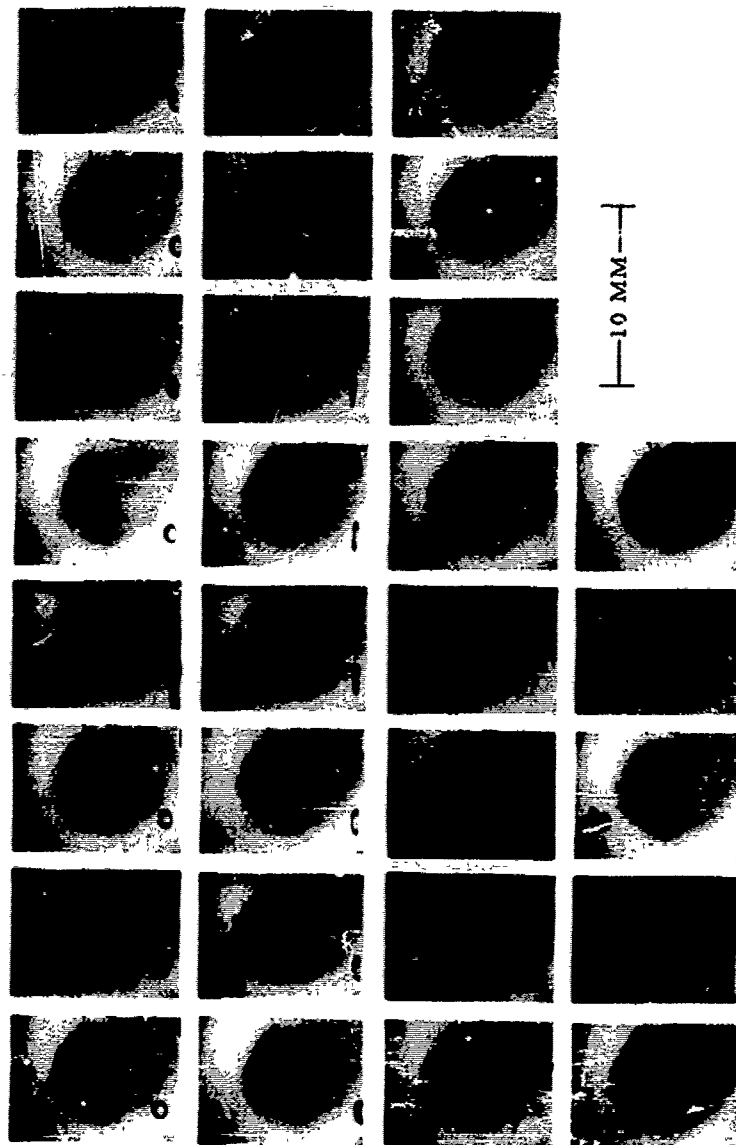
├─10 MM─┤

Test 244

Liquid- G. E. SF(96)200 Relative Velocity 79 ft/sec
Drop Size 0. 89 MM Time per Frame 0. 0770 msec
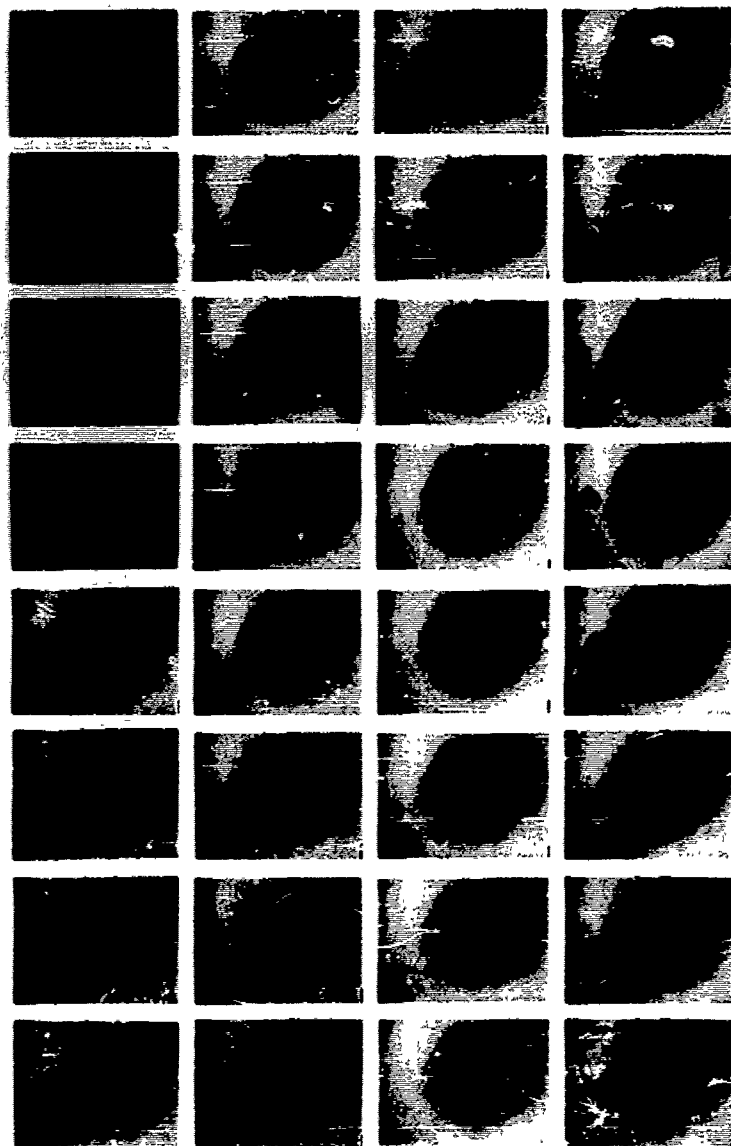
├─10 MM─┤

Test 248

Liquid - G. E. SF(96)200 Relative Velocity 105 ft/sec

Drop Size 0. 99 MM Time per Frame 0. 0771 msec
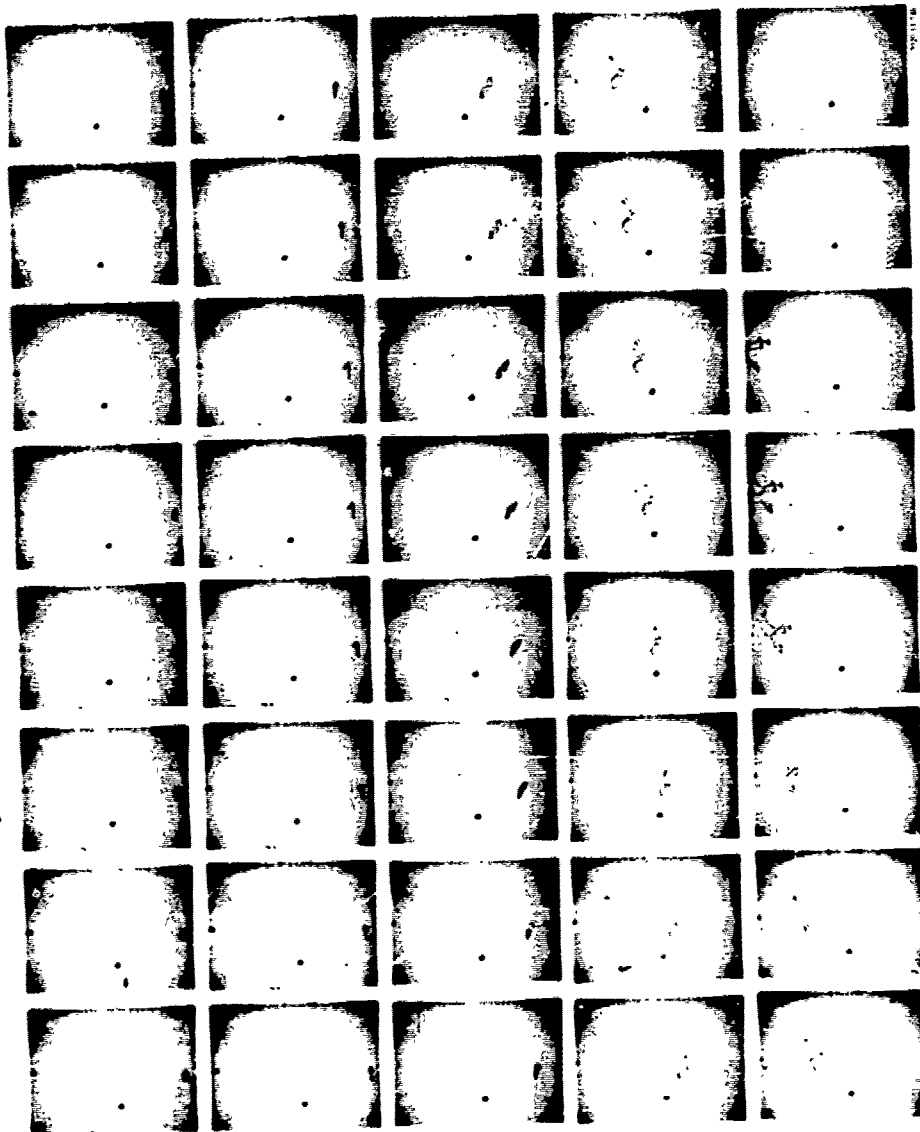
10 MM

Test 249

Liquid- G. E. SF(96)200   Relative Velocity 107 ft/sec

Drop Size 0. 88 MM   Time per frame 0. 0774 msec

10 MM

-B70
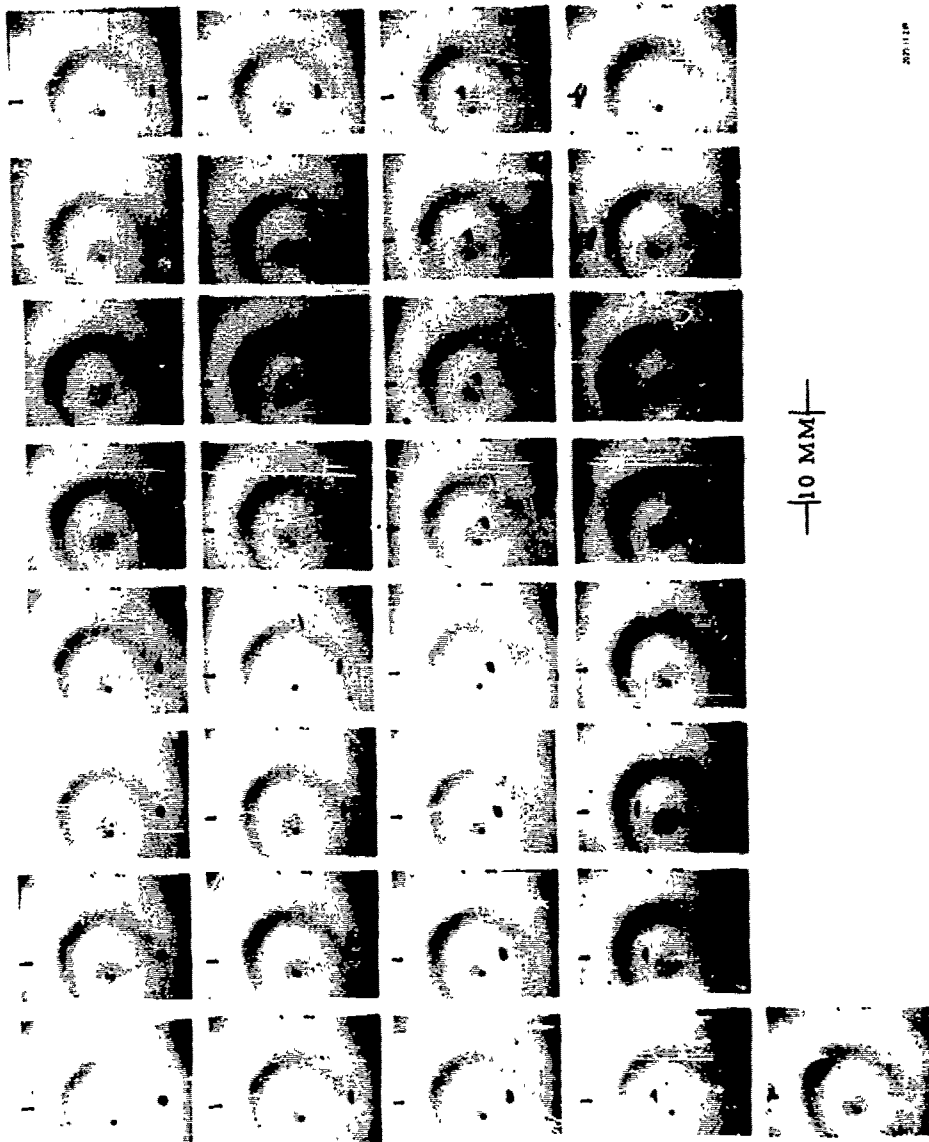
Te.t 251
Liquid - G. E. SF(96)200 Relative Velocity 118 ft/sec
Drop Size 1 0 MM   Time per Frame 0.0769 msec
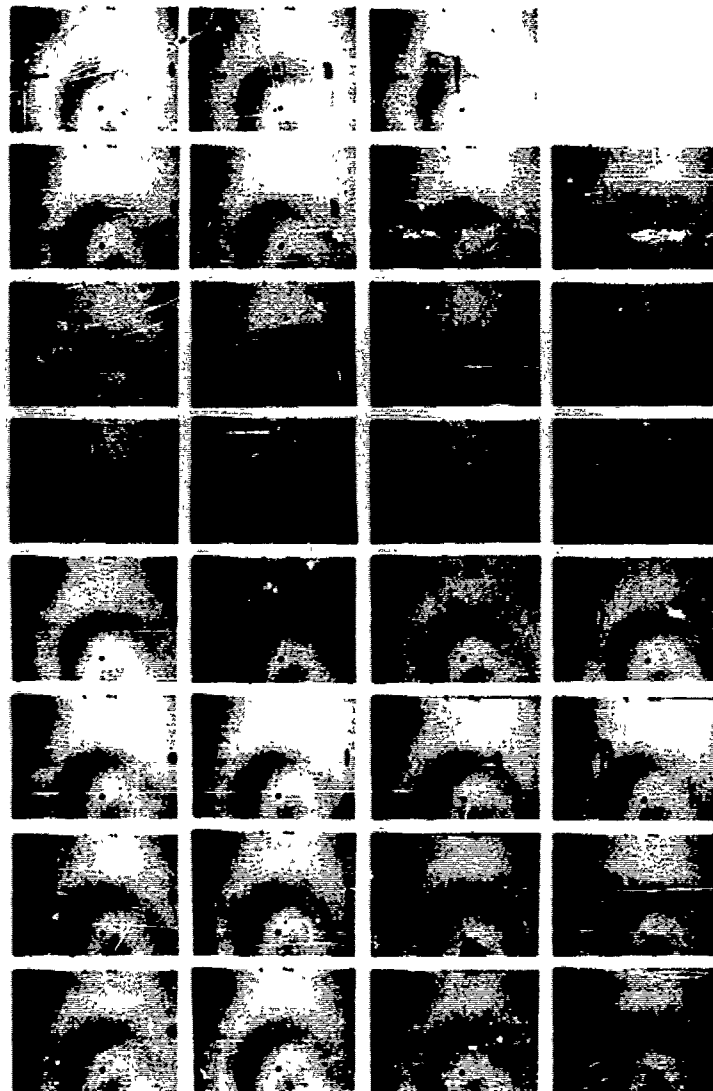
10 MM

Test 255

Liquid-G. E. SF(96)200 Relative Velocity 165 ft/sec

Drop Size 1. 0 MM   Time per Frame 0. 0768 msec
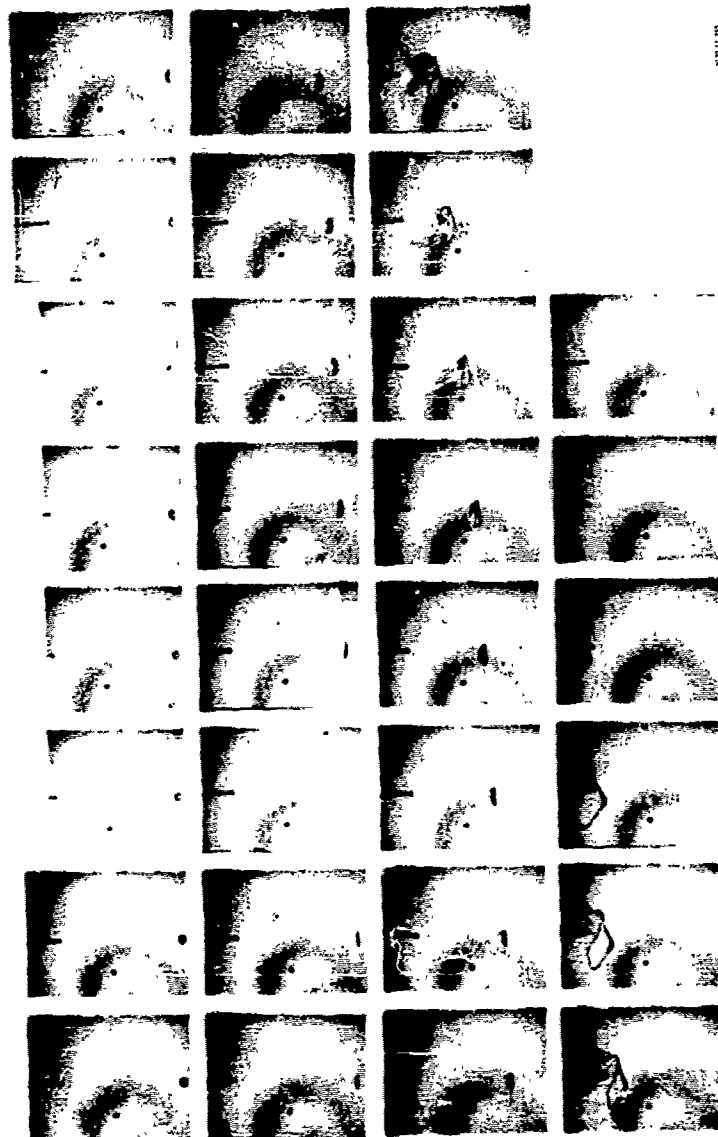
10 MM

Test 257

Liquid-G. E. SF(96)200   Relative Velocity 179 ft/sec
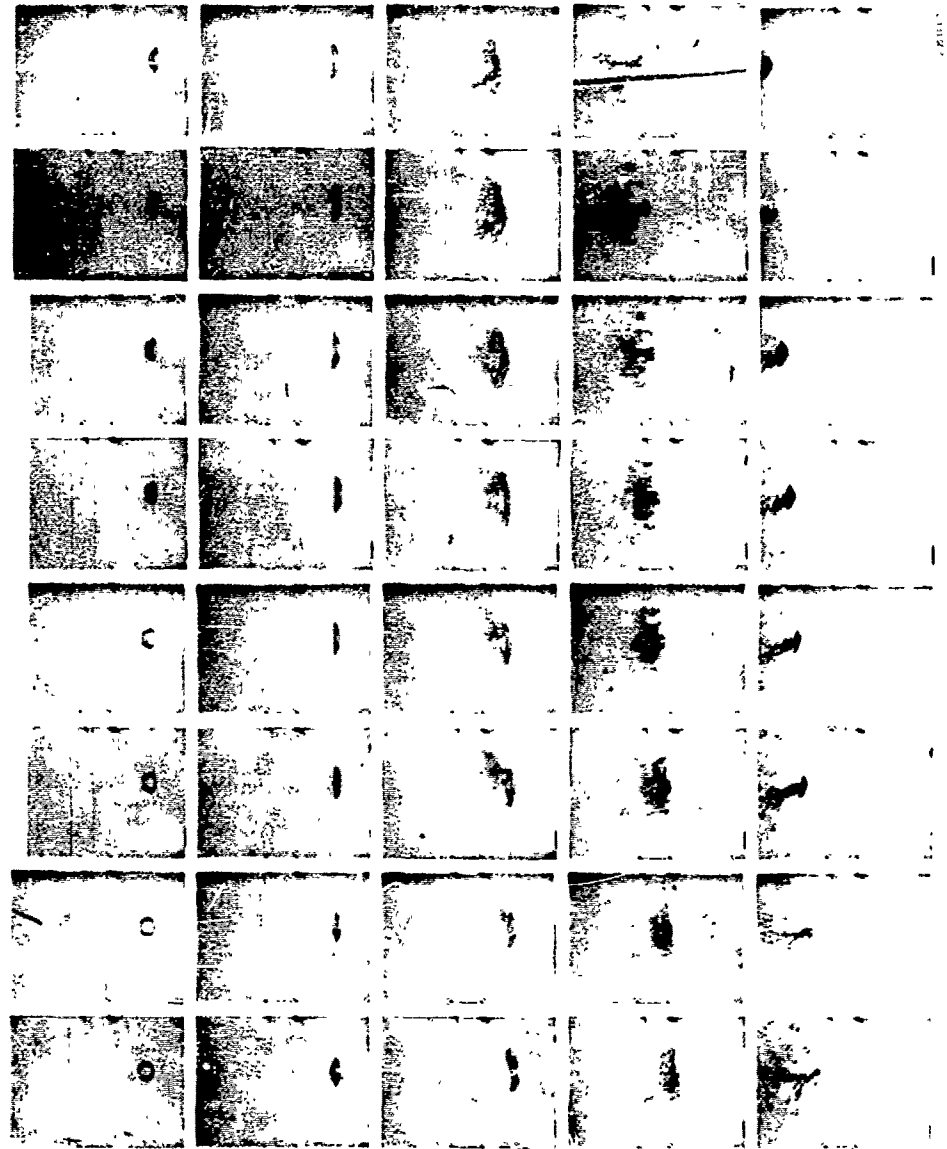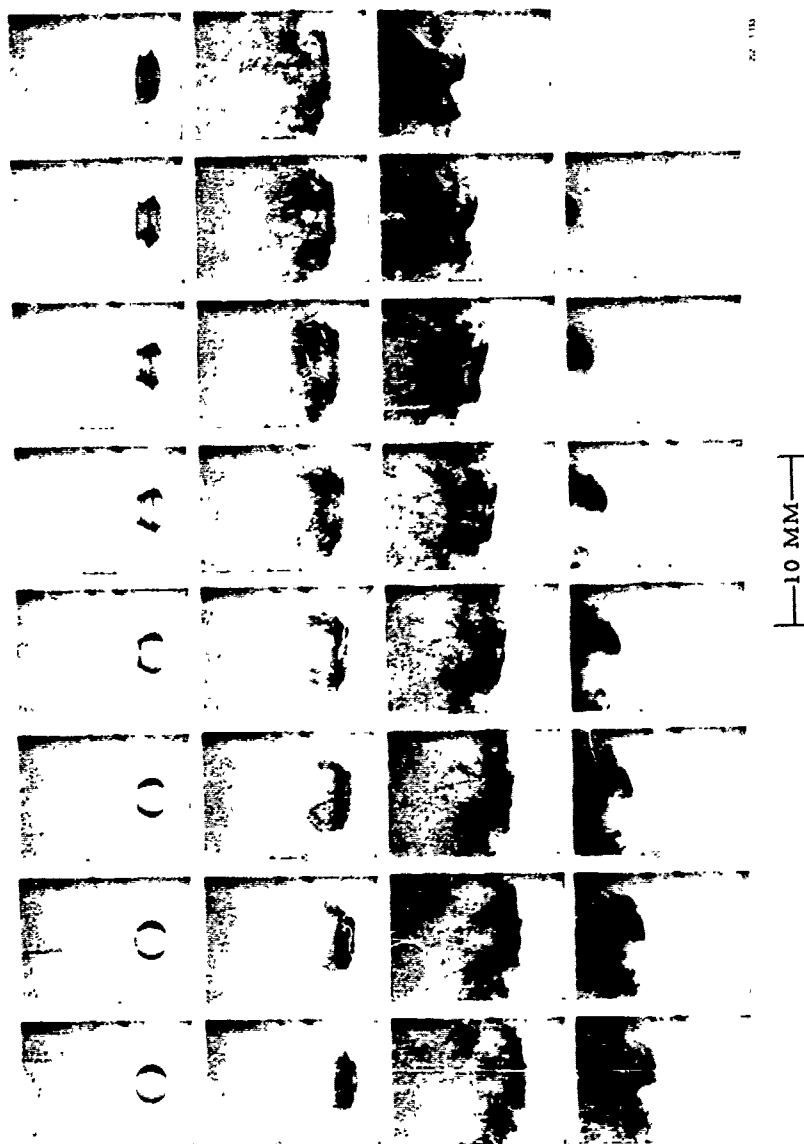Drop Size 0 9 MM   Time per Frame 0. 0769 msec

⊢10 MM⊣
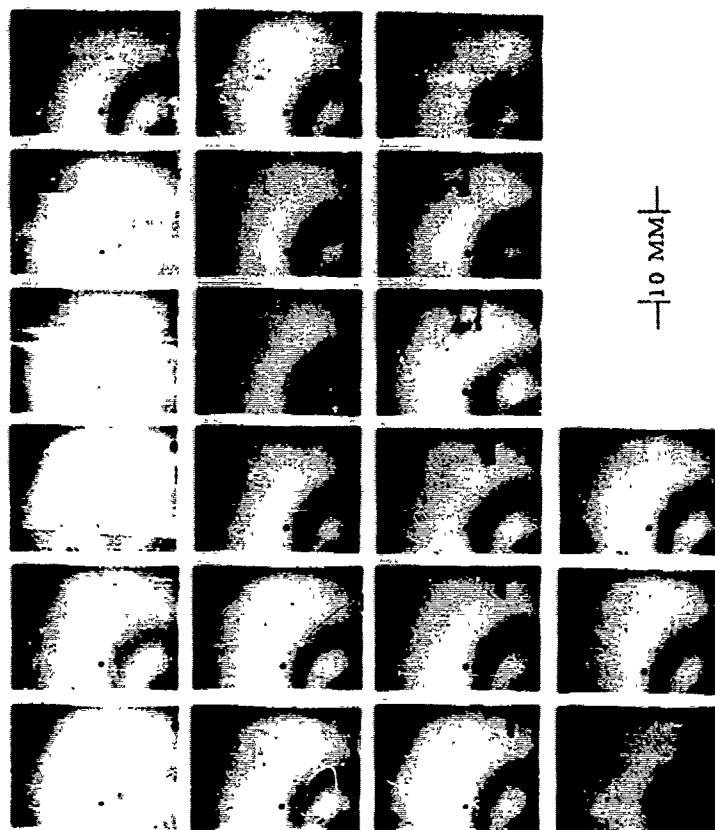
Test 258

Liquid-G.E. SF(96)200 Relative Velocity 184 ft/sec
Drop Size 0.91 MM Time per Frame 0.0386 msec

10 MM
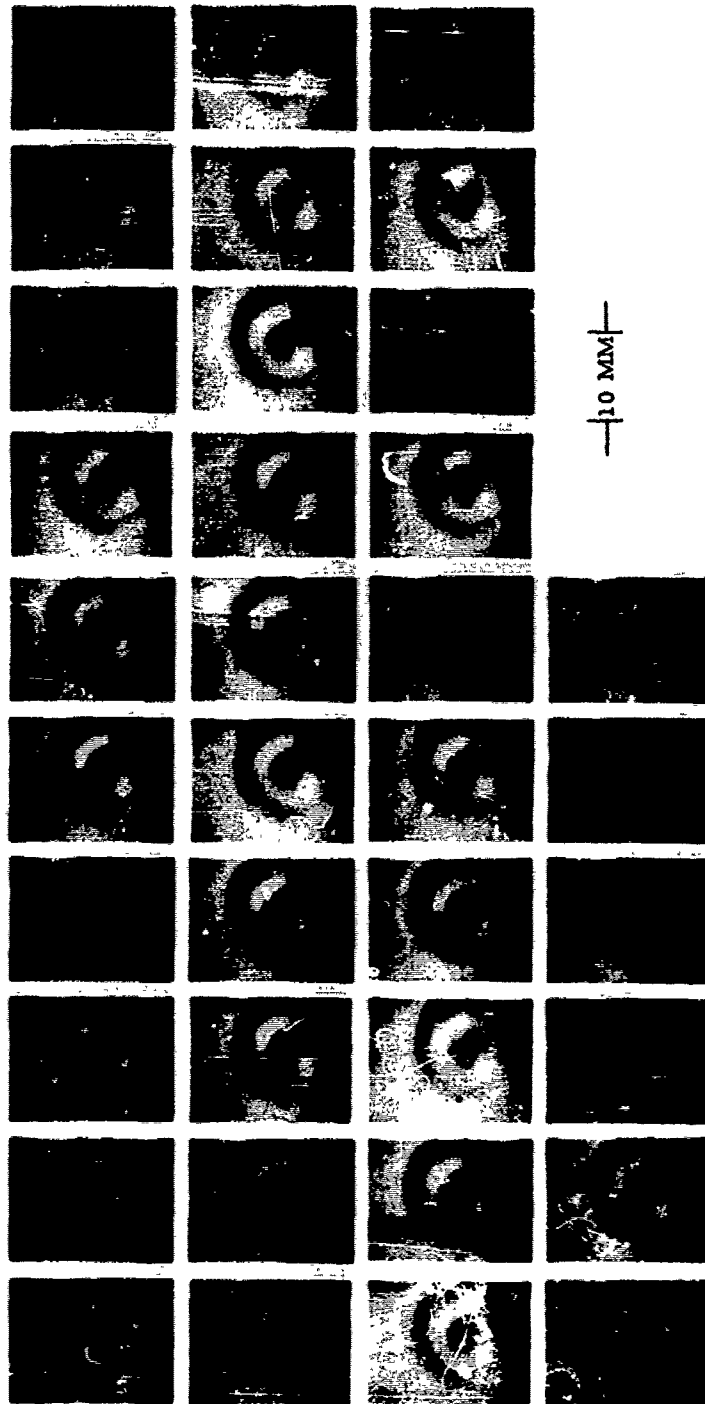
APPENDIX C

The results of the size distribution tests (summarized in Table C-1) are presented in this appendix in the three following forms:

a.   Tabulations of assessment data taken from photomicrographs of the sampled aerosols.

b   Plates made from photomicrographs of a selected number of the tests.

c.   Plots of cumulative percent mass vs droplet size for all of the data in (a) above.

The tabulated assessment data has been included for reference purposes and is more detailed in nature than that presented in other sections of the report.

The plates have been included to show visually the reduction in particle size that occurs with increase in relative velocity.

The cumulative percent mass vs particle diameter curves show the shape of the size distribution curves, and were used to determine the MMD values used for correlation with theory in other sections of the report

Table C-1. Summary of Size Distribution Tests.

Orig Drop Size (mm)	V (ft/sec)	Sample Dist (in.)	Film No.	Test No.	MMD (μ)
		Shear Breakup			
2.7	138	15	926	35	85
	110	18	850	6	90
	112	24	849	5	120
	234	27	927	41	60
	212	30	865	12	73
	212	30	872	12	71
	209	36	845	1	59
	315	27	928	44	32
	319	30	866	13	36
	319	30	873	13	41
	395	24	874	18	34
	383	27	929	48	19
	394	30	867	14	24
	394	30	875	14	24
1.6	131	12	879	22	94
	130	18	878	21	75
	132	24	880	23	93
	201	24	859	10	45
	206	30	882	24	74
	202	36	858	9	53
	316	24	885	26	21
	320	30	886	27	30
	395	24	891	30	18
	396	30	912	31	18
	394	36	913	32	15
		Bag Breakup			
0.6	69	4-3/8 in*	930	55	100
0.6	66	4-3/8 in.	931	56	140
0.6		4-3/8 in.	932	57	115

* Sample Distance with 1-ft Section Removed

NOMENCLATURE

L. P.	=	lower point of size interval, microns
M. F.	=	mid-point of size interval, microns
U. P.	=	upper point of size interval, microns
FO	=	frequency observed
PFO	=	percent frequency observed
SFO	=	cumulative frequency observed
SPFO	=	cumulative percent frequency observed
PMO	=	percent mass observed
SPMO	=	cumulative percent mass observed

TEST NO. 35   DROP SIZE (MM) 2.7
RELATIVE VELOCITY (FT/SEC) 138
FILM NO. 926 **MMD** (μ) 85
SAMPLING DISTANCE (IN.) 15

L. D.	V. D.	I. D.	CO	PFC	SFD	SPFC	PMD	SPMC
3.11	3.11	6.32	6.	0.00	5.	0.00	0.00	0.00
6.4	8.72	11.33	854.	53.57	854.	53.57	1.53	1.53
1.47	14.06	16.77	302.	18.94	1156.	72.52	1.95	5.51
16.77	19.39	23.22	189.	11.85	1345.	84.37	5.44	5.75
23.22	25.58	27.35	65.	3.45	1409.	87.82	1.57	5.75
27.95	45.63	33.32	51.	3.19	1451.	91.02	5.17	12.13
33.32	36.01	36.70	27.	1.25	1471.	92.28	2.01	14.14
4.0	41.49	46.19	27.	1.64	1434.	93.57	4.12	16.26
42.29	47.99	47.62	24.	1.44	1521.	95.42	5.13	23.42
47.45	52.16	55.25	18.	1.12	1534.	96.54	1.57	27.53
51.2	57.94	62.63	11.	.69	1550.	97.23	4.55	43.56
57.13	43.42	66.72	7.	.56	1559.	97.80	4.86	56.04
61.12	69.19	70.35	5.	.56	1569.	98.36	6.16	44.41
17.	72.44	76.32	3.	.19	1571.	98.55	2.54	47.16
72.42	79.68	80.94	1.	.06	1572.	98.61	1.02	48.14
75.44	83.43	84.43	2.	.12	1574.	98.74	2.55	50.67
84.43	89.68	91.73	5.	.41	1579.	99.03	2.36	50.74
94.23	93.91	95.89	2.	.12	1581.	99.15	1.44	51.44
97.47	95.94	100.14	1.	.06	1582.	99.21	1.47	53.44
101.14	111.63	103.20	4.	.51	1587.	99.56	1.13	74.52
103.10	109.89	114.59	2.	.12	1589.	99.69	5.41	77.16
111.59	117.25	119.97	2.	.12	1591.	99.51	8.04	77.47
119.97	129.13	126.49	1.	.06	1592.	99.87	3.11	77.54
126.42	128.78	131.15	2.	.12	1594.	100.00	4.05	100.00

-C4-

TEST NO. 6 DROP SIZE (MM) 2.7
RELATIVE VELOCITY (FT/SEC) 110
FILM NO. 850 MMD (μ) 90
SAMPLING DISTANCE (IN.) 18

L. P.	M. P.	U. P.	FO	PFO	SFO	SPFO	PMU	SPMU
0.00	3.31	6.02	0.	0.00	0.	0.00	0.00	0.00
6.02	8.70	11.39	210.	24.59	210.	24.59	.32	.32
11.39	14.08	16.77	193.	22.59	403.	47.18	1.08	1.41
16.77	19.99	23.22	166.	19.43	569.	66.62	2.60	4.02
23.22	25.58	27.95	65.	7.61	634.	74.23	2.03	6.05
27.95	30.63	33.32	74.	8.66	708.	82.90	3.96	10.02
33.32	36.01	38.70	29.	3.39	737.	86.29	2.50	12.53
38.70	41.49	44.29	22.	2.57	759.	88.87	2.90	15.43
44.29	47.08	49.88	19.	2.22	778.	91.10	3.65	19.08
49.88	52.56	55.25	19.	2.22	797.	93.32	5.06	24.15
55.25	57.94	60.63	5.	.58	802.	93.91	1.78	25.94
60.63	63.42	66.22	9.	1.05	811.	94.96	4.20	30.15
66.22	68.58	70.95	10.	1.17	821.	96.13	5.90	36.05
70.95	73.63	76.32	9.	1.05	830.	97.18	6.57	42.62
76.32	78.58	80.84	3.	.35	833.	97.54	2.65	45.28
80.84	83.63	86.43	2.	.23	835.	97.77	2.13	47.42
86.43	88.58	90.73	3.	.35	838.	98.12	3.80	51.23
90.73	93.31	95.89	0.	0.00	838.	98.12	0.00	51.23
95.89	98.04	100.19	4.	.46	842.	98.59	6.87	58.11
100.19	101.69	103.20	2.	.23	844.	98.82	3.83	61.94
103.20	108.89	114.59	1.	.11	845.	98.94	2.37	64.31
114.59	117.28	119.97	3.	.35	848.	99.29	8.83	73.15
119.97	123.19	126.42	1.	.11	849.	99.41	3.41	76.55
126.42	128.78	131.15	2.	.23	851.	99.64	7.79	84.35
131.15	133.83	136.52	2.	.23	853.	99.88	8.74	93.10
136.52	139.21	141.90	0.	0.00	853.	99.88	0.00	93.10
141.90	144.69	147.49	0.	0.00	853.	99.88	0.00	93.10
147.49	150.28	153.08	0.	0.00	853.	99.88	0.00	93.10
153.08	155.76	158.45	1.	.11	854.	100.00	6.89	100.00

TEST NO. 5 DROP SIZE (MM) 2. 7
RELATIVE VELOCITY (FT/SEC) 112
FILM NO. 349 MMD (μ) 120
SAMPLING DISTANCE (IN.) 24

L. P.	M. P.	U. P.	FO	PFO	SFO	SPFO	PMO	SPMO
0.00	3.01	6.02	0.	0.00	0.	0.00	0.00	0.00
6.02	8.70	11.39	61.	17.28	61.	17.28	.10	.10
11.39	14.08	16.77	61.	17.28	122.	34.56	.39	.50
16.77	19.99	23.22	52.	14.73	174.	49.29	.93	1.43
23.22	25.58	27.95	28.	7.93	202.	57.22	1.00	2.43
27.95	30.63	33.32	37.	10.48	239.	67.70	2.26	4.70
33.32	36.01	38.70	22.	6.23	261.	73.93	2.17	6.86
38.70	41.49	44.29	23.	6.51	284.	80.45	3.46	10.35
44.29	47.08	49.88	12.	3.39	296.	83.85	2.63	12.98
49.88	52.56	55.25	20.	5.66	316.	89.51	6.09	19.08
55.25	57.94	60.63	6.	1.69	322.	91.21	2.44	21.54
60.63	63.42	66.22	3.	.84	325.	92.06	1.60	23.13
66.22	68.58	70.95	3.	.84	328.	92.91	2.02	25.16
70.95	73.63	76.32	2.	.56	330.	93.48	1.67	26.83
76.32	78.58	80.84	3.	.84	333.	94.33	3.04	29.87
80.84	83.63	86.43	4.	1.13	337.	95.45	4.89	34.76
86.43	88.58	90.73	4.	1.13	341.	96.60	5.80	40.56
90.73	93.31	95.89	2.	.56	343.	97.16	3.39	43.95
95.89	98.04	100.19	0.	0.00	343.	97.16	0.00	43.95
100.19	101.69	103.20	1.	.28	344.	97.45	2.19	46.14
103.20	108.89	114.59	1.	.28	345.	97.73	2.71	48.85
114.59	117.28	119.97	0.	0.00	345.	97.73	0.00	48.85
119.97	123.19	126.42	1.	.28	346.	98.01	3.90	52.75
126.42	128.78	131.15	1.	.28	347.	98.30	4.45	57.21
131.15	133.83	136.52	1.	.28	348.	98.58	5.00	62.21
136.52	139.21	141.90	2.	.56	350.	99.15	11.25	73.47
141.90	144.69	147.49	1.	.28	351.	99.43	6.31	79.78
147.49	150.28	153.08	0.	0.00	351.	99.43	0.00	79.78
153.08	155.76	158.45	0.	0.00	351.	99.43	0.00	79.78
158.45	161.14	163.83	0.	0.00	351.	99.43	0.00	79.78
163.83	166.62	169.42	1.	.28	352.	99.71	9.64	89.43
169.42	171.78	174.15	1.	.28	353.	100.00	10.56	100.00

. . .	. . . .	. . . .	FO	PFO	SFO	SPFO	PMO	SPMO
.	4.11	6.72	0.	0.00	0.	0.00	0.00	0.00
.	8.7	11.19	197.	30.35	197.	30.35	.75	.75
11.59	14.18	16.77	182.	28.04	379.	58.39	2.54	3.29
16.77	19.99	23.22	100.	15.40	479.	73.80	3.	7.18
23.22	25.56	27.95	36.	5.54	515.	79.35	2.78	9.97
27.95	30.63	33.32	29.	4.46	544.	83.82	3.84	13.82
33.32	36.01	38.70	22.	3.38	566.	87.21	4.71	18.53
38.70	41.49	44.29	16.	2.46	582.	89.67	5.22	23.75
44.29	47.08	49.88	17.	2.61	599.	72.29	8.08	31.84
49.88	52.56	55.25	12.	1.84	611.	94.14	7.92	39.77
55.25	57.94	60.63	15.	2.31	626.	96.45	13.24	53.01
60.63	63.42	66.22	6.	.92	632.	97.38	6.94	59.95
66.22	68.58	72.35	3.	.46	635.	97.84	4.38	64.34
72.95	73.63	76.32	4.	.77	640.	98.61	9.04	73.38
76.32	78.58	80.54	3.	.46	643.	99.07	6.58	79.96
80.84	83.63	86.43	3.	.46	646.	99.53	7.94	87.90
86.43	88.58	90.73	0.	0.00	646.	99.53	0.00	87.90
90.73	93.31	95.89	2.	.30	648.	99.84	7.34	95.25
95.89	98.04	100.19	0.	0.00	648.	99.84	0.00	95.25
100.19	101.69	103.20	1.	.15	649.	100.00	4.74	100.00

-C7-

TEST NO. 12　DROP SIZE (MM)2.7
RELATIVE VELOCITY (FT/SEC) 212
FILM NO.865　MMD (μ)73
SAMPLING DISTANCE (IN.)　30

L. P.	M. P.	U. P.	FO	PFO	SFO	SPFO	PMO	SPMO
0.00	3.01	6.02	0.	0.00	0.	0.00	0.00	0.00
6.02	8.70	11.39	135.	22.13	135.	22.13	.24	.24
11.39	14.05	16.77	98.	16.06	233.	38.19	.63	.87
16.77	19.99	23.22	89.	14.59	322.	52.78	1.60	2.48
23.22	25.58	27.95	44.	7.21	366.	60.00	1.58	4.06
27.9	30.63	33.32	57.	9.34	423.	69.34	3.51	7.58
33.32	36.01	38.70	39.	6.39	462.	75.73	3.87	11.46
38.70	41.49	44.29	25.	4.09	487.	79.83	3.79	15.25
44.29	47.09	49.88	29.	4.75	516.	84.59	6.40	21.66
49.88	52.56	55.25	15.	2.45	531.	87.04	4.60	26.26
55.25	57.94	60.63	20.	3.27	551.	90.32	8.20	34.46
60.63	63.42	66.22	10.	1.63	561.	91.96	5.37	39.84
66.22	68.58	70.95	11.	1.80	572.	93.77	7.46	47.30
70.95	73.63	76.32	13.	2.13	585.	95.90	10.91	58.22
76.32	78.58	80.84	3.	.49	588.	96.39	3.05	61.28
80.54	83.63	86.43	9.	1.31	596.	97.70	9.83	71.11
86.43	88.58	90.73	5.	.81	601.	98.52	7.29	78.41
90.73	93.31	95.89	2.	.32	603.	98.85	3.41	81.82
95.89	98.04	100.19	3.	.49	606.	99.34	5.93	87.75
100.19	101.69	103.20	1.	.16	607.	99.50	2.20	89.96
103.20	108.89	114.59	1.	.16	608.	99.67	2.72	92.68
114.59	117.28	119.97	1.	.16	609.	99.83	3.38	96.07
119.97	123.19	126.42	1.	.16	610.	100.00	3.92	100.00

$l \cdot P_s$	$V \cdot P_s$	$l \cdot P_s$	FO	PFO	SFO	SPFO	PVO	SPVO
5.	3.03	4.02	5.	0.00	5.	0.00	0.00	0.03
5.53	8.75	11.37	137.	23.18	137.	23.18	.27	.27
11.34	14.78	16.71	114.	19.28	251.	42.47	.53	1.11
16.77	17.97	20.22	90.	15.22	341.	57.69	1.54	2.75
23.23	25.59	27.95	32.	5.41	373.	63.11	1.30	4.25
27.07	30.73	33.32	51.	8.62	424.	71.74	3.55	7.61
33.32	36.01	38.70	29.	4.90	453.	76.64	3.26	11.08
39.73	41.43	44.29	18.	3.04	471.	79.69	3.09	14.17
44.27	47.08	49.88	27.	4.56	498.	84.26	6.75	20.93
49.88	52.56	55.25	27.	4.56	525.	88.83	9.37	30.31
55.25	57.94	60.63	9.	1.52	534.	90.35	4.18	34.49
57.63	63.42	66.22	7.	1.18	541.	91.53	4.26	38.75
66.22	68.58	70.95	15.	2.53	556.	94.07	11.52	50.27
71.95	73.63	76.32	8.	1.35	564.	95.43	7.60	57.88
76.32	78.58	80.84	12.	2.03	576.	97.46	13.84	71.73
81.84	83.63	86.43	5.	.84	581.	98.30	6.96	78.69
86.43	88.58	90.73	5.	.84	586.	99.15	8.25	86.95
90.73	93.31	95.89	2.	.33	588.	99.49	3.86	90.81
95.89	98.04	100.19	1.	.16	589.	99.66	2.23	93.05
100.19	101.69	103.20	1.	.16	590.	99.83	2.44	95.55
103.20	108.89	114.59	0.	0.00	590.	99.83	0.00	95.55
114.59	117.28	119.97	0.	0.00	590.	99.83	0.00	95.55
119.97	123.19	126.42	1.	.17	591.	100.00	4.44	100.00

-C9-

TEST NO. 1   DROP SIZE (MM) 2. 7
RELATIVE VELOCITY (FT/SEC) 209
FILM NO. 845 MMD (µ) 59
SAMPLING DISTANCE (IN.) 36

L. P.	M. P.	U. P.	FO	PFO	SFO	SPFO	PMO	SPMU
0.00	3.01	6.02	0.	0.00	0.	0.00	0.00	0.00
6.02	8.70	11.39	147.	23.00	147.	23.00	.46	.46
11.39	14.08	16.77	143.	22.37	290.	45.38	1.66	2.12
16.77	19.99	23.22	124.	19.40	414.	64.78	4.00	6.13
23.22	25.58	27.95	30.	4.69	444.	69.48	1.93	8.06
27.95	30.63	33.32	55.	8.60	499.	78.09	6.06	14.12
33.92	36.01	38.70	35.	5.47	534.	83.56	6.22	20.35
38.70	41.49	44.29	31.	4.85	565.	88.41	8.41	28.77
44.29	47.08	49.88	19.	2.97	584.	91.39	7.51	36.28
49.88	52.56	55.25	16.	2.50	600.	93.89	8.77	45.05
55.25	57.94	60.63	8.	1.25	608.	95.14	5.87	50.93
60.63	63.42	66.22	11.	1.72	619.	96.87	10.57	61.51
66.22	68.58	70.95	5.	.78	624.	97.65	6.06	67.57
70.95	73.63	76.32	7.	1.09	631.	98.74	10.51	78.09
76.32	78.58	80.84	4.	.62	635.	99.37	7.29	85.38
80.84	83.63	86.43	3.	.46	638.	99.64	6.59	91.98
86.43	88.58	90.73	0.	0.00	638.	99.84	0.00	91.98
90.73	93.31	95.89	0.	0.00	638.	99.84	0.00	91.98
95.89	98.04	100.19	0.	0.00	638.	99.84	0.00	91.98
100.19	101.69	103.20	0.	0.00	638.	99.84	0.00	91.98
103.20	108.89	114.59	0.	0.00	638.	99.84	0.00	91.98
.114.59	117.28	119.97	0.	0.00	638.	99.84	0.00	91.98
119.97	123.19	126.42	0.	0.00	638.	99.84	0.00	91.98
126.42	128.78	131.15	1.	.15	639.	100.00	8.01	100.00

-C10-

TEST NO. 44 DROP SIZE (MM) 2.7
RELATIVE VELOCITY (FT/SEC) 315
FILM NO. 928 MMD (μ) 32
SAMPLING DISTANCE (IN.) 27

TEST NO. 13 DROP SIZE (MM) 2.7
RELATIVE VELOCITY (FT/SEC) 319
FILM NO. 866 MMD (μ) 36
SAMPLING DISTANCE (IN.) 30

I. P.	V. P.	H. P.	FO	PFO	SFO	SPFO	PVF	CVFT
0.00	3.01	6.02	0.	0.00	0.	0.00	0.00	0.00
6.02	8.70	11.39	1660.	47.74	1660.	47.74	1.81	3.41
11.39	14.08	16.77	706.	22.95	2458.	70.69	6.60	10.50
16.77	19.99	23.22	464.	13.34	2922.	84.03	10.81	21.31
23.22	25.58	27.95	141.	4.05	3063.	88.09	4.55	27.87
27.95	30.63	33.32	177.	5.09	3240.	93.18	14.08	41.96
33.32	36.01	38.70	105.	3.02	3345.	96.20	13.48	55.45
38.70	41.49	44.29	55.	1.58	3400.	97.78	10.77	66.22
44.29	47.08	49.43	37.	1.06	3437.	98.84	10.56	76.78
49.88	52.56	55.25	15.	.43	3452.	99.28	5.14	81.92
55.25	57.94	60.63	17.	.48	3469.	99.76	9.00	91.
60.63	63.42	66.23	3.	.08	3472.	99.85	2.08	93.81
66.22	68.58	70.95	1.	.02	3473.	99.98	.97	94.67
70.95	73.63	76.32	1.	.02	3474.	99.91	1.06	95.77
76.32	78.58	80.84	2.	.05	3476.	99.97	2.65	98.44
80.84	83.63	86.43	1.	.02	3477.	100.00	1.58	100.00

TEST NO. 13 DROP SIZE (MM) 2.7
RELATIVE VELOCITY (FT/SEC) 31^
FILM NO. 873 MMD (μ) 41
SAMPLING DISTANCE (IN.) 30

L. P.	M. P.	U. P.	FO	PFO	SFO	SPFO	PMO	SPMO
0.00	3.01	6.02	0.	0.00	0.	0.00	0.00	0.00
6.02	8.70	11.39	1078.	44.89	1078.	44.89	2.50	2.50
11.39	14.08	16.77	495.	20.61	1573.	65.51	4.19	6.65
16.77	19.99	23.22	299.	12.45	1872.	77.96	7.04	13.73
23.22	25.58	27.95	123.	5.12	1995.	83.09	5.77	19.50
27.95	30.63	33.32	148.	6.16	2143.	89.25	11.89	31.40
33.32	36.01	38.70	107.	4.45	2250.	93.71	13.88	45.29
38.70	41.49	44.29	55.	2.29	2305.	96.00	10.88	56.17
44.29	47.08	49.88	44.	1.83	2349.	97.83	12.68	68.85
49.88	52.56	55.25	19.	.79	2368.	98.62	7.60	76.46
55.25	57.94	60.63	14.	.58	2382.	99.20	7.49	83.95
60.63	63.42	66.22	9.	.37	2391.	99.58	6.31	90.26
66.22	69.58	70.95	8.	.33	2399.	99.91	7.07	97.34
70.95	73.63	76.32	0.	0.00	2399.	99.91	0.00	97.34
76.32	78.58	80.84	2.	.08	2401.	100.00	2.65	100.00

TEST NO. 18 DROP SIZE (MM) 2.7
RELATIVE VELOCITY (FT/SEC) 395
FILM NO. 874 MMD (μ) 34
SAMPLING DISTANCE (IN.) 24

L. P.	M. P.	U. P.	FO	PFO	SFO	SPFO	PMO	SPMO
0.00	3.01	6.02	0.	0.00	0.	0.00	0.00	0.00
6.02	8.70	11.39	2002.	47.74	2002.	47.74	4.23	4.23
11.39	14.08	16.77	999.	23.82	3001.	71.57	7.71	11.95
16.77	19.99	23.22	639.	15.23	3640.	86.81	13.72	25.67
23.22	25.58	27.95	210.	5.00	3850.	91.81	8.99	34.67
27.95	30.63	33.32	174.	4.14	4024.	95.96	12.76	47.43
33.32	36.01	38.70	69.	1.64	4093.	97.61	8.16	55.59
38.70	41.49	44.29	37.	.88	4130.	98.49	6.67	62.27
44.29	47.08	49.88	22.	.52	4152.	99.02	5.78	68.06
49.88	52.56	55.25	11.	.26	4163.	99.28	4.01	72.07
55.25	57.94	60.63	7.	.16	4170.	99.45	3.41	75.49
60.63	63.42	66.22	7.	.16	4177.	99.61	4.47	79.97
66.22	68.58	70.95	5.	.11	4182.	99.73	4.03	84.00
70.95	73.63	76.32	2.	.04	4194.	99.78	1.99	86.00
76.32	78.58	80.84	6.	.14	4190.	99.92	7.27	93.28
80.84	83.63	86.43	0.	0.00	4190.	99.92	0.00	93.28
86.43	88.58	90.73	2.	.05	4192.	99.97	3.47	96.75
90.73	93.31	95.89	0.	0.00	4192.	99.97	0.00	96.75
95.89	98.04	100.19	0.	0.00	4192.	99.97	0.00	96.75
100.19	101.69	103.20	0.	0.00	4192.	99.97	0.00	96.75
103.20	108.89	114.59	1.	.02	193.	100.00	3.24	100.00

TEST NO. 48   DROP SIZE (MM) 2.7
RELATIVE VELOCITY (FT/SEC) 383
FILM NO. 929 MMD (μ) 19
SAMPLING DISTANCE (IN.) 27
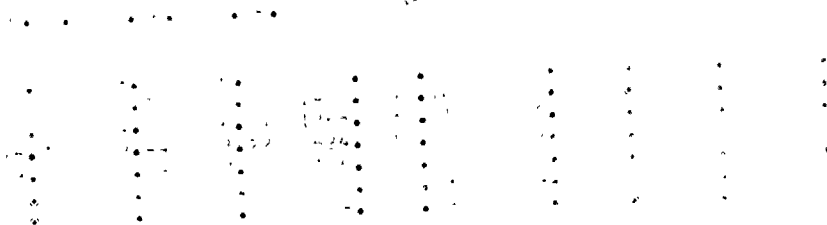
TEST NO. 14 DROP SIZE (MM) 2.7
RELATIVE VELOCITY (FT/SEC) 394
FILM NO. 867 MMD (μ) 24
SAMPLING DISTANCE (IN.) 30

L. P.	M. P.	U. P.	FP	PFP	SFP		
	3.31	6.12	0.	0.30			
5.02	8.12	11.39	1648.	63.81			
11.39	14.08	16.77	391.	14.69	108.		
16.77	19.99	23.22	337.	12.66	242.		
23.	25.52	27.94	121.	4.54	257.		
	30.63	32.32	42.	3.04	154.		
43.	35.01	35.70	23.	.86	254.		
44.29	41.43	44.79	5.	.03			

TEST NO. 14 DROP SIZE (MM) 2.7
RELATIVE VELOCITY (FT/SEC) 394
FILM NO. 875 MMD (μ) 24
SAMPLING DISTANCE (IN.) 30

L. P.	M. P.	U. P.	FP	PFP	SFP		
	3.31	6.02	0.	0.00			
	8.72	11.39	852.	56.76	852.		
11.39	14.08	16.77	311.	20.71	1163.		
16.77	19.99	23.22	193.	12.85	1356.		
23.22	25.56	27.95	57.	3.79	1413.		
33.43	30.63	33.32	68.	4.53	481.		
	35.71	38.70	11.	.73	1492.		
41.7	41.45	44.25	7.	.46	1499.		
44.25	47.58	49.88	1.	.06	1500.		
	53.56	55.25	0.	.00			
55.25	57.94	60.63		.05			

-C13-

TEST NO. 22 DROP SIZE (MM) 1.6
RELATIVE VELOCITY (FT/SEC) 131
FILM NO.879 MMD (μ) 94
SAMPLING DISTANCE (IN.) 12

| L. P.	M. P.	U. P.	FO	PFO	SFO	SPFO	PMO	SPMO
0.00	3.01	6.02	0.	0.00	0.	0.00	0.00	0.00
6.02	8.70	11.39	261.	41.89	261.	41.89	.98	.98
11.39	14.08	16.77	162.	26.00	423.	67.89	2.23	3.22
16.77	19.99	23.22	89.	14.28	512.	82.18	3.41	6.63
23.22	25.58	27.95	26.	4.17	538.	86.35	1.98	8.62
27.95	30.63	33.32	33.	5.29	571.	91.65	4.32	12.95
33 32	36.01	38.70	12.	1.92	583.	93.57	2.53	15.48
38.70	41.49	44.29	9.	1.44	592.	95.02	2.90	18.39
44.29	47.08	49.88	6.	.96	598.	95.98	2.81	21.21
49.88	52.56	55.25	4.	.64	602.	96.62	2.60	23.81
55.25	57.94	60.63	5.	.80	607.	97.43	4.36	28.17
60.63	63.42	66.22	3.	.48	610.	97.91	3.42	31.60
66.22	68.58	70.95	3.	.48	613.	98.39	4.32	35.93
70.95	73.63	76.32	1.	.16	614.	98.55	1.78	37.72
76.32	78.58	80.84	0.	0.00	614.	98.55	0.00	37.72
80.84	83.63	86.43	0.	0.00	614.	98.55	0.00	37.72
86.43	88.58	90.73	3.	.48	617.	99.03	9.30	47.02
90.73	93.31	95.89	1.	.16	618.	99.19	3.62	50.65
95.89	98.04	100.19	1.	.16	619.	99.35	4.20	54.85
100.19	101.69	103.20	1.	.16	620.	99.51	.68	59.54
103.20	108.89	114.59	0.	0.00	620.	99.51	0.00	59.54
114.59	117.28	119.97	0.	0.00	620.	99.51	0.00	59.54
119.97	123.19	126.42	1.	.16	621.	99.67	8.34	67.88
126.42	128.78	131.15	1.	.16	622.	99.83	9.52	77.40
131.15	133.83	136.52	0.	0.00	622.	99.83	0.00	77.40
136.52	139.21	141.90	0.	0.00	622.	99.83	0.00	77.40
141.90	144.69	147.49	0.	0.00	622.	99.83	0.00	77.40
147.49	150.28	153.08	0.	0.00	622.	99.83	0.00	77.40
153.08	155.76	158.45	0.	0.00	622.	99.83	0.00	77. _
158.45	161.14	163.83	0.	0.00	622.	99.83	0.00	77.40
163.83	166.62	169.42	0.	0.00	622.	99.83	0.00	77.40
169.42	171.78	174.15	1.	.16	623.	100.00	22.59	100.00

-C14-

TEST NO. 21 DROP SIZE (MM) 1.6
RELATIVE VELOCITY (FT SEC) 130
FILM NO. 878 MMD (μ) 75
SAMPLING DISTANCE (IN.) 18

L. P.	M. P.	U. P.	FO	PFO	SFO	SPFO	PMO	V?
0.00	3.01	6.02	0.	0.00	0.	0.00	0.00	0.00
6.02	8.70	11.39	61.	23.82	61.	23.82	.26	.26
11.39	14.08	16.77	50.	19.53	111.	43.35	.76	1.04
16.77	19.99	23.22	41.	16.01	152.	59.37	1.78	2.82
23.22	25.58	27.95	13.	5.07	165.	64.45	1.12	3.95
27.95	30.63	33.32	18.	7.03	183.	71.48	2.67	6.62
33.32	36.01	38.70	18.	7.03	201.	78.51	4.31	10.93
38.70	41.49	44.29	8.	3.12	209.	81.64	2.92	13.85
44.29	47.08	49.88	13.	5.07	222.	86.71	6.91	20.76
49.88	52.56	55.25	10.	3.90	232.	90.62	7.38	28.15
55.25	57.94	60.63	2.	.78	234.	91.40	1.97	30.12
60.63	63.42	66.22	5.	1.95	239.	93.35	6.47	36.59
66.22	68.58	70.95	5.	1.95	244.	95.31	8.16	44.76
70.95	73.63	76.32	3.	1.17	247.	96.48	6.06	50.82
76.32	78.58	80.84	2.	.78	249.	97.26	4.90	55.73
80.84	83.63	86.43	0.	0.00	249.	97.26	0.00	55.73
86.43	88.58	90.73	2.	.78	251.	98.04	7.02	62.75
90.73	93.31	95.89	1.	.39	252.	98.43	4.10	66.86
95.89	98.04	100.19	1.	.39	253.	98.82	4.75	71.62
100.19	101.69	103.20	0.	0.00	253.	98.82	0.00	71.62
103.20	108.89	114.59	0.	0.00	253.	98.82	0.00	71.62
114.59	117.28	119.97	1.	.39	254.	99.21	6.14	79.76
119.97	123.19	126.42	1.	.39	255.	99.60	9.44	89.21
126.42	128.78	131.15	1.	.39	256.	100.00	10.78	100.00

TEST NO. 23 DROP SIZE (MM) 1.6
RELATIVE VELOCITY (FT/SEC) 136
FILM NO.880 MWD (μ) 93
SAMPLING DISTANCE (IN.) 24

L. P.	M. P.	U. P.	FO	PFO	SFO	SPFO	PMO	SPMO
0.00	3.01	6.02	0.	0.00	0.	0.00	.0.00	0.00
6.02	8.70	11.39	21.	19.09	21.	19.09	.08	.08
11.39	14.08	16.77	15.	13.63	36.	32.72	.23	.31
16.77	19.99	23.22	24.	21.81	60.	54.54	1.02	1.34
23.22	25.58	27.95	4.	3.63	64.	58.18	.34	1.68
27.95	30.63	33.32	10.	9.09	74.	67.27	1.45	3.14
33.32	36.01	38.70	4.	3.63	78.	70.90	.94	4.08
38.70	41.49	44.29	1.	.90	79.	71.81	.35	4.44
44.29	47.08	49.88	7.	6.36	86.	78.18	3.65	8.10
49.88	52.56	55.25	2.	1.81	88.	80.00	1.45	9.55
55.25	57.94	60.63	1.	.90	89.	80.90	.97	10.52
60.63	63.42	66.22	1.	.90	90.	81.61	1.27	11.79
66.22	68.58	70.95	3.	2.72	93.	84.54	4.01	16.61
70.95	73.63	76.32	2.	1.81	95.	86.36	3.97	20.58
76.32	78.58	80.84	4.	3.63	99.	90.00	9.64	30.23
80.84	83.63	86.43	2.	1.81	101.	91.81	5.81	36.05
86.43	88.58	90.73	3.	2.72	104.	94.54	10.35	46.40
90.73	93.31	95.89	0.	0.00	104.	94.54	0.00	46.40
95.89	98.04	100.19	2.	1.81	106.	96.36	9.35	55.76
100.19	101.69	103.20	1.	.90	107.	97.27	5.21	60.97
103.20	108.89	114.59	0.	0.00	107.	97.27	0.00	60.97
114.59	117.28	119.97	0.	0.00	107.	97.27	0.00	60.97
119.97	123.19	126.42	0.	0.00	107.	97.27	0.00	60.97
126.42	128.73	131.15	1.	.90	108.	98.18	10.59	71.57
131.15	133.83	136.52	0.	0.00	108.	98.18	0.00	71.57
136.52	139.21	141.90	1.	.90	109.	99.09	13.38	84.96
141.90	144.69	147.49	1.	.91	110.	100.00	15.03	100.00

TEST NO. 10 DROP SIZE (MM) 1.6
RELATIVE VELOCITY (FT/SEC) 201
FILM NO. 859 MMD (μ) 45
SAMPLING DISTANCE (IN.) 24

L. P.	M. P.	U. P.	FO	PFO	SFO	SPFO	PMO	SPMO
1.00	3.01	6.02	0.	0.00	0.	0.00	0.00	0.00
6.02	8.70	11.39	239.	39.89	239.	39.89	2.02	2.02
11.39	14.08	16.77	137.	22.87	376.	62.77	4.22	6.25
16.77	19.99	23.22	90.	15.02	466.	77.79	7.73	13.98
23.22	25.58	27.95	48.	8.01	514.	85.80	8.21	22.19
27.95	30.63	33.32	36.	6.01	550.	91.81	10.55	32.75
33.32	36.01	38.70	12.	2.00	562.	93.82	5.67	38.43
30.70	41.49	44.29	15.	2.50	577.	96.32	10.62	49.25
44.29	47.08	49.86	7.	1.16	584.	97.49	7.35	56.62
49.86	52.56	55.25	4.	.66	588.	98.16	5.83	62.45
55.25	57.94	60.63	4.	.66	592.	98.83	7.80	70.26
50.63	63.42	66.22	2.	.33	594.	99.16	5.11	75.37
66.22	68.58	70.95	1.	.16	595.	99.33	3.22	78.60
70.95	73.63	76.42	0.	0.00	595.	99.33	0.00	78.60
76.32	78.58	80.84	2.	.33	597.	99.66	9.69	88.30
80.84	83.63	86.43	2.	.33	599.	100.00	11.70	100.00

TEST NO. 24 DROP SIZE (MM) 1.6
RELATIVE VELOCITY (FT/SEC) 206
FILM NO. 882 MMD (μ) 74
SAMPLING DISTANCE (IN.) 30

L. P.	M. P.	U. P.	FO	PFO	SFO	SPFO	PMO	SPMO
0.00	3.01	6.02	0.	0.00	0.	0.00	0.00	0.00
6.02	8.70	11.39	47.	25.82	47.	25.82	.41	.41
11.39	14.08	16.77	41.	22.52	88.	48.35	1.33	1.75
16.77	19.99	23.22	22.	12.08	110.	60.43	1.99	3.74
23.22	25.58	27.95	17.	9.34	127.	69.78	3.06	6.80
27.95	30.63	33.32	17.	9.34	144.	79.12	5.25	12.05
33.32	36.01	38.70	11.	6.04	155.	85.16	5.48	17.54
38.70	41.49	44.29	9.	4.94	164.	90.10	6.84	24.38
44.29	47.08	49.98	4.	2.19	168.	92.30	4.42	28.81
49.86	52.56	55.25	3.	1.64	171.	93.95	4.61	
55.25	57.94	60.63	1.	.54	172.	94.50		
	63.42	66.22	2.	1.09	174.	95.60	5.30	
			0.	0.00	174.	95.60	0.00	40.?7
	73.63	76.32	3.	1.64	177.	97.25	12.62	
76.42		80.84	0.	0.00	177.	97.25	0.00	
80.84	83.63	86.43	0.	0.00	177.	97.25	0.00	
86.43		90.72	1.	.54	178.	97.80	7.30	
91.?2			2.	1.09	80.	98.90	17.09	
			0.	0.00	80.	96.90	0.00	
			2.	1.?9	82.	100.00	22.09	

-C17-

TEST NO. 9   DROP SIZE (MM) 1.6
RELATIVE VELOCITY (FT/SEC) 20 _
FILM NO. 858   MMD (μ) 53
SAMPLING DISTANCE (IN.) 36

L. P.	M. P.	U. P.	FO	PFO	SFO	SPFO	PMO	SPMO
0.00	3.01	6.02	0.	0.00	0.	0.00	0.00	0.00
6.02	8.70	11.39	38.	27.94	38.	27.94	.50	.50
11.39	14.08	16.77	22.	16.17	60.	44.11	1.06	1.56
16.77	19.99	23.22	20.	14.70	80.	58.82	2.69	4.25
23.22	25.58	27.95	5.	3.67	85.	62.50	1.34	5.60
27.95	30.63	33.32	10.	7.35	95.	69.85	4.59	10.19
33.32	36.01	38.70	7.	5.14	102.	75.00	5.19	15.38
38.70	41.49	44.29	5.	3.67	107.	78.67	5.65	21.04
44.29	47.08	49.88	8.	5.88	115.	84.55	13.18	34.22
49.88	52.56	55.25	11.	8.08	126.	92.64	25.15	59.37
55.25	57.94	60.63	4.	2.94	130.	95.58	12.23	71.60
60.63	63.42	66.22	3.	2.20	133.	97.79	12.02	83.62
66.22	68.58	70.95	2.	1.47	135.	99.26	10.11	93.73
70.95	73.63	76.32	1.	.73	136.	100.00	6.26	100.00

TEST NO. 26   DROP SIZE (MM) 1.6
RELATIVE VELOCITY (FT/SEC) 316
FILM NO. 885   MMD (μ) 21
SAMPLING DISTANCE (IN.) 24

L. P.	M. P.	U. P.	FO	PFO	SFO	SPFO	PMO	SPMO
0.00	3.01	6.02	0.	0.00	0.	0.00	0.00	0.00
6.02	8.70	11.39	1138.	52.53	1138.	52.53	10.08	10.08
11.39	14.08	16.77	528.	24.37	1666.	76.91	17.08	27.17
16.77	19.99	23.22	335.	15.46	2001.	92.38	30.14	57.32
23.22	25.58	27.95	88.	4.06	2089.	96.44	15.78	73.10
27.95	30.63	33.32	64.	2.95	2153.	99.39	19.66	92.77
33.32	36.01	38.70	10.	.46	2163.	99.86	4.95	97.73
38.70	41.49	44.29	3.	.13	2166.	100.00	2.26	100.00

-C18-

TEST NO. 27 DROP SIZE (MM) 1 6
RELATIVE VELOCITY (FT/SEC) 320
FILM NO. 886 MMD (μ) 30
SAMPLING DISTANCE (IN.) 30

L. P.	M. P.	U. P.	FO	PFO	SFO	SPFO	PMO	SPMO
0.00	3.01	6.02	0.	0.00	0.	0.00	0.00	0.00
6.02	8.70	11.39	170.	37.44	170.	37.44	3.19	3.19
11.39	14.08	16.77	95.	20.92	265.	58.37	6.51	9.71
16.77	19.99	23.22	89.	19.60	354.	77.97	16.97	26.68
23.22	25.58	27.95	34.	7.48	388.	85.4	11.93	39.61
27.95	30.63	33.32	39.	8.59	427.	94.05	25.40	65.02
33.32	36.01	38.70	20.	4.40	447.	98.45	21.02	86.04
38.70	41.49	44.29	6.	1.32	453.	99.77	9.61	95.66
44.29	47.08	49.88	0.	0.00	453.	99.77	0.00	95.66
49.88	52.56	55.25	0.	0.00	453.	99.77	0.00	95.66
55.25	57.94	60.63	1.	.22	454.	100.00	4.33	100.00

TEST NO. 30 DROP SIZE (MM) 1.6
RELATIVE VELOCITY (FT/SEC) 395
FILM NO. 891 MMD (μ) 18
SAMPLING DISTANCE (IN.) 24

L. P.	M. P.	U. P.	FO	PFO	SFO	SPFO	PMO	SPMO
0.00	3.01	6.02	0.	0.00	0.	0.00	0.00	0.00
6.02	8.70	11.39	895.	45.92	895.	45.92	10.06	10.06
11.39	14.08	16.77	658.	33.76	1553.	79.68	27.05	37.14
16.77	19.99	23.22	311.	15.95	1864.	95.63	35.57	72.71
23.22	25.58	27.95	52.	2.66	1916.	98.30	11.85	84.57
27.95	30.63	33.32	27.	1.38	1943.	99.69	10.54	95.11
33.32	36.01	38.70	4.	.20	1947.	99.89	2.52	97.63
38.70	41.49	44.29	1.	.05	1948.	99.94	.96	98.60
44.29	47.08	49.88	1.	.05	1949.	100.00	1.40	100.00

TEST NO. DROP SIZE (MM)
RELATIVE VELOCITY (FT/SEC)
FILM NO. MMD (μ)
SAMPLING DISTANCE (IN.)

L. P.	M. P.	U. P.	FO	PFO	SFO	SPFO	PMO	SPMO
0.00	3.01	6.02	0.	0.00	0.	0.00	0.00	0.0
6.02	8.70	11.39	387.	59.17	387.	59.17	16.20	16.20
11.39	14.08	16.77	155.	23.70	542.	82.87	23.68	39.89
16.77	19.99	23.22	91.	13.91	633.	96.78	38.68	78.30
23.22	25.58	27.95	15.	2.29	648.	99.08	12.71	91.29
27.95	30.63	33.32	6.	.91	654.	100.00	9.70	100.00

-C19-

TEST NO. 32 DROP SIZE (MM) 1.6
RELATIVE VELOCITY (FT/SEC) 394
FILM NO.913 MMD (μ) 15
SAMPLING DISTANCE (IN.) 36

L. P.	M. P.	U. P.	FO	PFO	SFO	SPFO	PMO	SPMO
3.00	3.01	6.02	0.	0.00	0.	0.00	0.00	0.00
6.02	8.70	11.39	299.	60.77	299.	60.77	21.95	21.95
11.39	14.08	16.77	141.	28.65	440.	89.43	37.79	59.74
16.77	19.99	23.22	50.	10.16	490.	99.59	37.27	97.02
23.22	25.58	27.95	2.	.40	492.	100.00	2.97	100.00

TEST NO. 55   DROP SIZE (MM) 0.6
RELATIVE VELOCITY (FT/SEC) 69
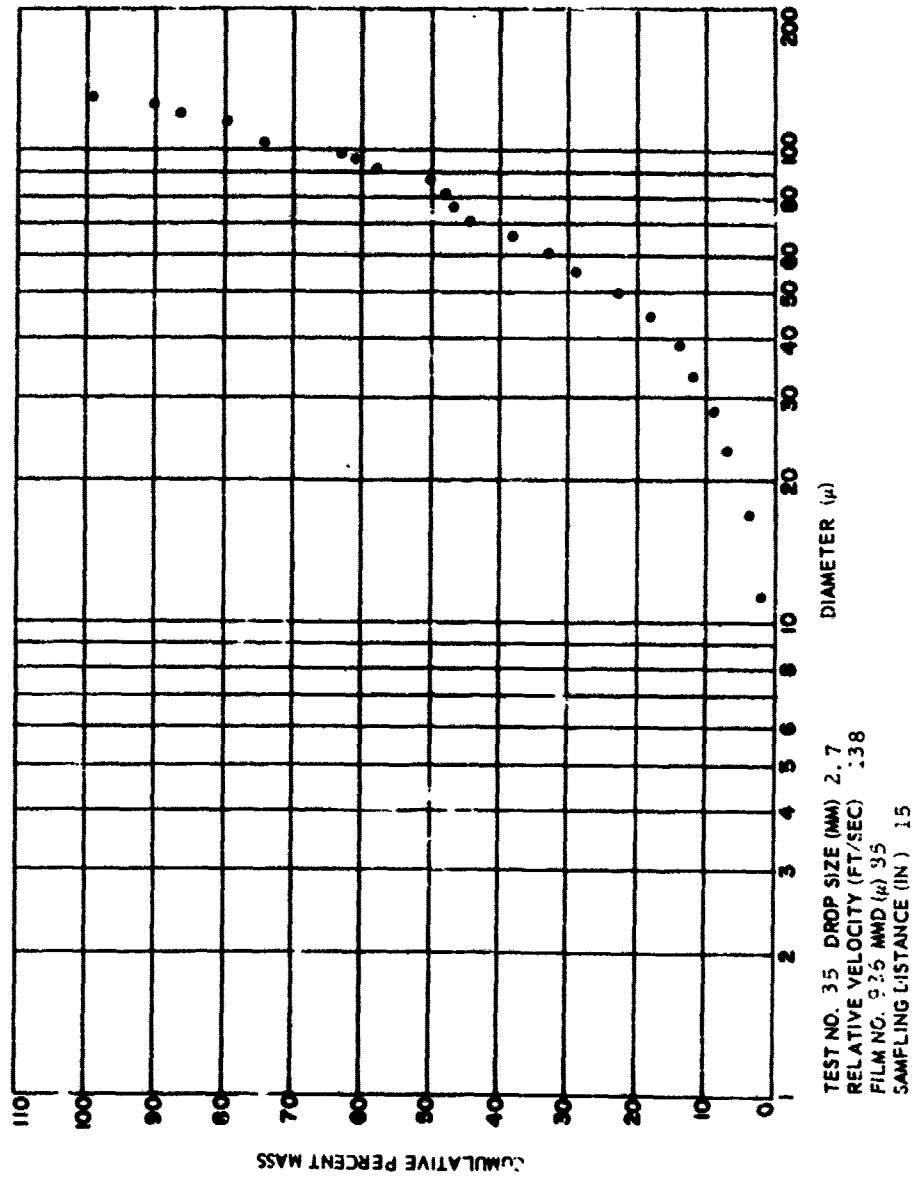**FILM NO. 930 MMD (μ) 100**
SAMPLING DISTANCE (IN.) 4-3/8

L. P.	M. P.	U. P.	FO	PFO	SFO	SPFO	PMO	SPMO
0.00	3.01	6.02	0.	0.00	0.	0.00	0.00	0.00
6.02	8.70	11.39	111.	31.80	111.	31.80	.65	.65
11.39	14.08	16.77	94.	26.93	205.	58.73	2.02	2.68
16.77	19.99	23.22	57.	16.33	262.	75.07	3.41	6.10
23.22	25.58	27.95	21.	6.01	283.	81.08	2.51	8.61
27.95	30.63	33.32	26.	7.44	309.	88.53	5.32	13.93
33.32	36.01	38.70	20.	5.73	329.	94.25	6.60	20.54
38.70	41.49	44.29	9.	2.57	338.	96.84	4.53	25.07
44.29	47.08	49.88	3.	.85	341.	97.70	2.20	27.26
49.86	52.56	55.25	2.	.57	343.	98.28	2.03	29.31
55.25	57.94	60.63	0.	0.00	343.	98.28	0.00	29.31
60.63	63.43	66.22	0.	0.00	343.	98.28	0.00	29.31
65.22	68.58	70.95	2.	.57	345.	98.85	4.50	33.82
70.95	73.63	76.32	0.	0.00	345.	98.85	0.00	33.82
76.32	78.58	80.84	0.	0.00	345.	98.85	0.00	33.82
80.84	83.63	86.43	1.	.28	346.	99.14	4.08	37.90
86.43	86.58	90.73	0.	0.00	346.	99.14	0.00	37.90
90.73	93.31	95.69	1.	.28	347.	99.42	5.66	43.57
95.89	98.04	100.19	0.	0.00	347.	99.42	0.00	43.57
100.19	101.69	103.20	1.	.28	348.	99.71	7.32	50.89
103.20	133.89	114.59	0.	0.00	348.	99.71	0.00	50.89
114.59	117.28	119.97	0.	0.00	348.	99.71	0.00	50.89
119.97	123.19	126.42	0.	0.00	348.	99.71	0.00	50.89
126.42	125.73	131.15	0.	0.00	348.	99.71	0.00	50.89
131.15	133.83	136.52	0.	0.00	348.	99.71	0.00	50.89
136.52	139.21	141.90	0.	0.00	348.	99.71	0.00	50.89
141.90	144.63	147.45	0.	0.00	348.	99.71	0.00	50.89
147.45	150.26	153.08	0.	0.00	348.	99.71	0.00	50.89
153.05	155.76	158.45	0.	0.00	348.	99.71	0.00	50.89
158.45	161.14	163.83	0.	0.00	348.	99.71	0.00	50.89
163.83	166.62	169.42	0.	0.00	348.	99.71	0.00	50.89
169.42	171.78	174.15	0.	0.00	348.	99.71	0.00	50.89
174.15	174.83	179.52	0.	0.00	348.	99.71	0.00	50.89
179.52	181.78	184.04	0.	0.00	348.	99.71	0.00	50.89
184.04	186.43	189.64	0.	0.00	348.	99.71	0.00	50.89
189.64	191.73	195.03	1.	.28	349.	100.00	49.10	100.00

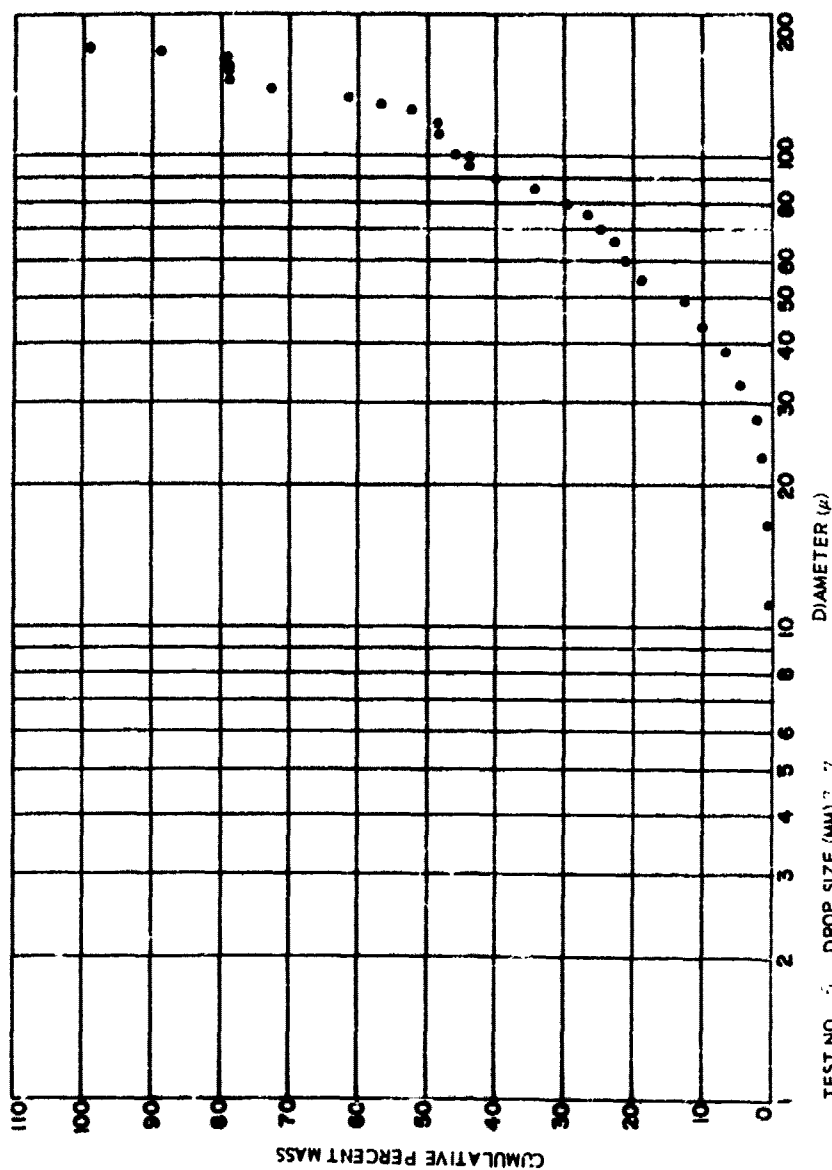| L. P.	A. P.	U. P.	FO	PFO	SFO	SPFO	PVO	SPVU
3.01	3.01	6.02	3.	0.00	0.	0.00	0.00	0.00
6.02	8.70	11.39	105.	40.69	105.	40.69	.46	.46
11.39	14.08	16.77	74.	28.68	179.	69.37	1.19	1.55
16.77	19.99	23.22	33.	12.79	212.	82.17	1.48	3.14
23.22	25.59	27.95	5.	2.32	218.	84.49	.53	3.67
27.95	30.64	33.32	12.	4.65	230.	89.14	1.83	5.51
33.32	36.01	38.70	6.	2.32	236.	91.47	1.48	7.00
38.70	41.49	44.29	2.	.77	238.	92.24	.75	7.75
44.29	47.05	49.88	6.	2.32	244.	94.57	3.29	11.03
49.88	52.56	55.25	5.	1.93	249.	96.51	3.81	14.87
55.25	57.94	60.67	2.	.77	251.	97.28	2.04	16.91
60.67	63.47	66.22	1.	.38	252.	97.67	1.33	18.24
66.22	48.59	70.95	1.	.38	253.	98.06	1.66	19.93
70.95	73.63	76.32	1.	.38	254.	98.44	2.08	22.02
76.32	78.58	80.84	0.	0.00	254.	98.44	0.00	22.02
80.84	83.63	86.43	0.	0.00	254.	98.44	0.00	22.02
86.43	88.58	90.73	0.	0.00	254.	98.44	0.00	22.02
90.73	93.31	95.89	0.	0.00	254.	98.44	0.00	22.02
95.89	98.04	100.19	0.	0.00	254.	98.44	0.00	22.02
100.19	101.69	103.20	1.	.38	255.	98.83	5.49	27.51
103.20	108.89	114.59	0.	0.00	255.	98.83	0.00	27.51
114.59	117.26	119.97	0.	0.00	255.	98.83	0.00	27.51
119.97	123.19	124.42	0.	0.00	255.	98.83	0.00	27.51
124.42	128.78	131.15	0.	0.00	255.	98.83	0.00	27.51
131.15	133.83	136.52	0.	0.00	255.	98.83	0.00	27.51
136.52	139.21	141.90	0.	0.00	255.	98.83	0.00	27.51
141.90	144.63	147.47	0.	0.00	255.	98.83	0.00	27.51
147.47	150.28	151.08	0.	0.00	255.	98.83	0.00	27.51
152.06	150.76	154.45	0.	0.00	255.	98.83	0.00	27.51
154.45	161.12	163.83	2.	.77	257.	99.61	43.65	71.16
163.83	166.62	169.42	0.	0.00	257.	99.61	0.00	71.16
169.42	171.79	174.15	0.	0.00	257.	99.61	0.00	71.16
174.15	176.53	179.52	1.	.36	258.	100.00	28.84	100.00

-C22-

TEST NO. 57 DROP SIZE (MM) 0.6
RELATIVE VELOCITY (FT/SEC) 66 approx.
FILM NO. 932 MMD (μ) 115
SAMPLING DISTANCE (IN.) 4-3/8

L. P.	M. P.	U. P.	FO	PFO	SFO	SPFO	PMO	SPMO
0.00	3.01	6.02	0.	0.00	0.	0.00	0.00	0.00
6.02	8.70	11.39	26.	30.95	26.	30.95	.15	.15
11.39	14.08	16.77	11.	13.09	37.	44.04	.24	.40
16.77	19.99	23.22	10.	11.90	47.	55.95	.61	1.02
23.22	25.50	27.95	7.	8.33	54.	64.28	.86	1.88
27.95	30.63	33.32	8.	9.52	62.	73.80	1.68	3.57
33.32	36.01	38.70	1.	1.19	63.	75.00	.34	3.91
38.70	41.49	44.29	2.	2.38	65.	77.38	1.03	4.95
44.29	47.08	49.88	1.	1.19	66.	78.57	.75	5.70
49.88	52.56	55.25	2.	2.38	68.	80.95	2.10	7.80
55.25	57.94	60.63	3.	3.57	71.	84.52	4.21	12.02
60.63	63.42	66.22	2.	2.38	73.	86.90	3.68	15.70
66.22	68.58	70.95	0.	0.00	73.	86.90	0.00	15.70
70.95	73.63	76.32	3.	3.57	76.	90.47	8.62	24.33
76.32	78.58	80.84	2.	2.38	78.	92.85	6.97	31.31
80.84	83.63	86.43	1.	1.19	79.	94.04	4.21	35.52
86.43	88.58	90.73	1.	1.19	80.	95.23	4.99	40.51
90.73	93.31	95.89	0.	0.00	80.	95.23	0.00	40.51
95.89	98.04	100.19	0.	0.00	80.	95.23	0.00	40.51
100.19	101.69	103.20	0.	0.00	80.	95.23	0.00	40.51
103.20	108.89	114.59	0.	0.00	80.	95.23	0.00	40.51
114.59	117.28	119.97	1.	1.19	81.	96.42	11.59	52.10
119.97	123.19	126.42	0.	0.00	81.	96.42	0.00	52.10
126.42	128.78	131.15	2.	2.38	83.	98.80	30.67	82.78
131.15	133.83	136.52	1.	1.19	84.	100.00	17.21	100.00

-C23-

TEST NO. 35 DROP SIZE (MM) 2. 7
RELATIVE VELOCITY (FT/SEC) 138
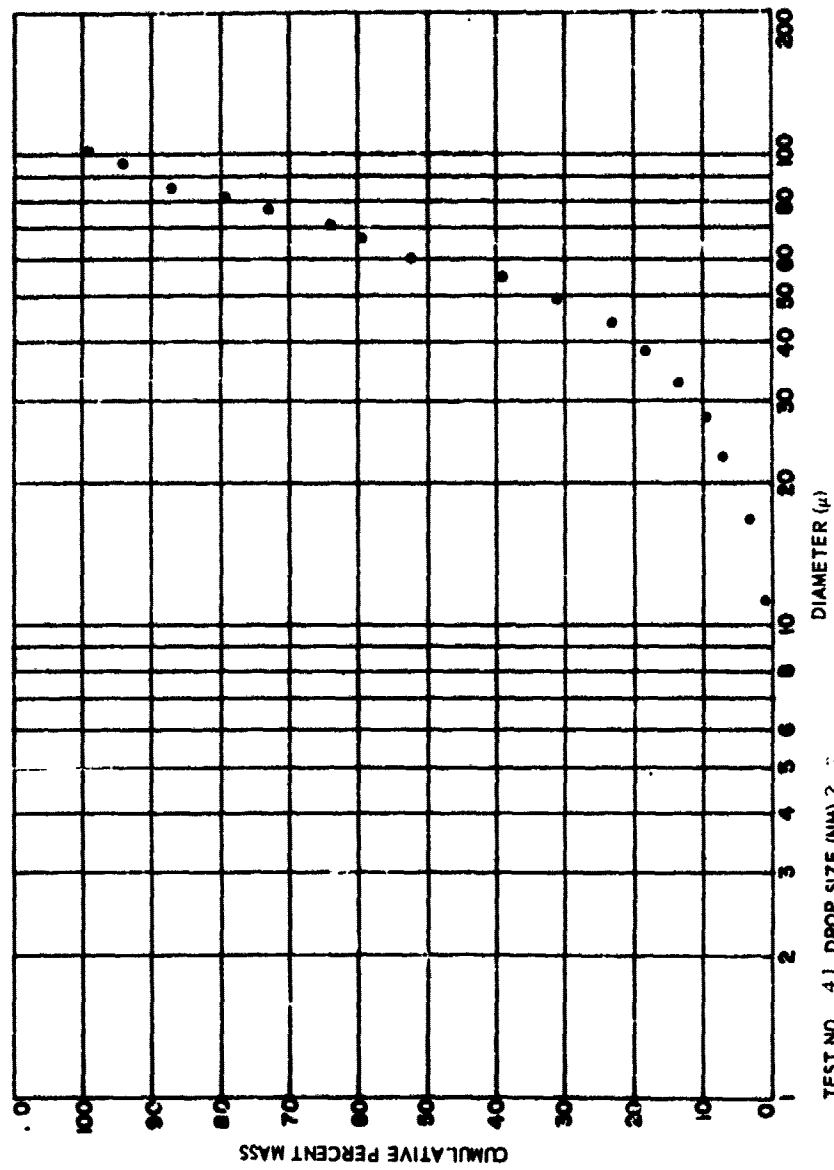FILM NO. 925 MMD (μ) 35
SAMPLING DISTANCE (IN) 15

DIAMETER (μ)

CUMULATIVE PERCENT MASS
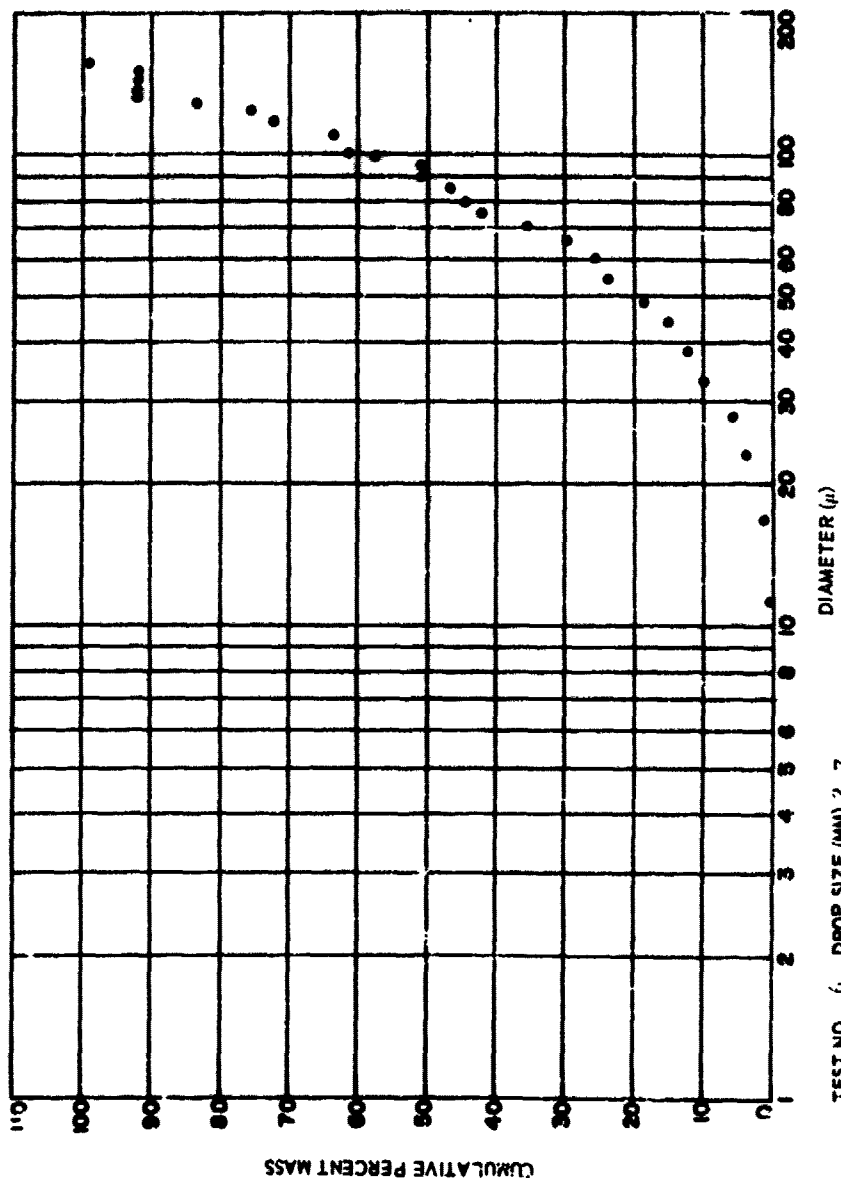
TEST NO. 6 DROP SIZE (MM) 2.7
RELATIVE VELOCITY (FT/SEC) 110
FILM NO. 350 MMD (μ) 90
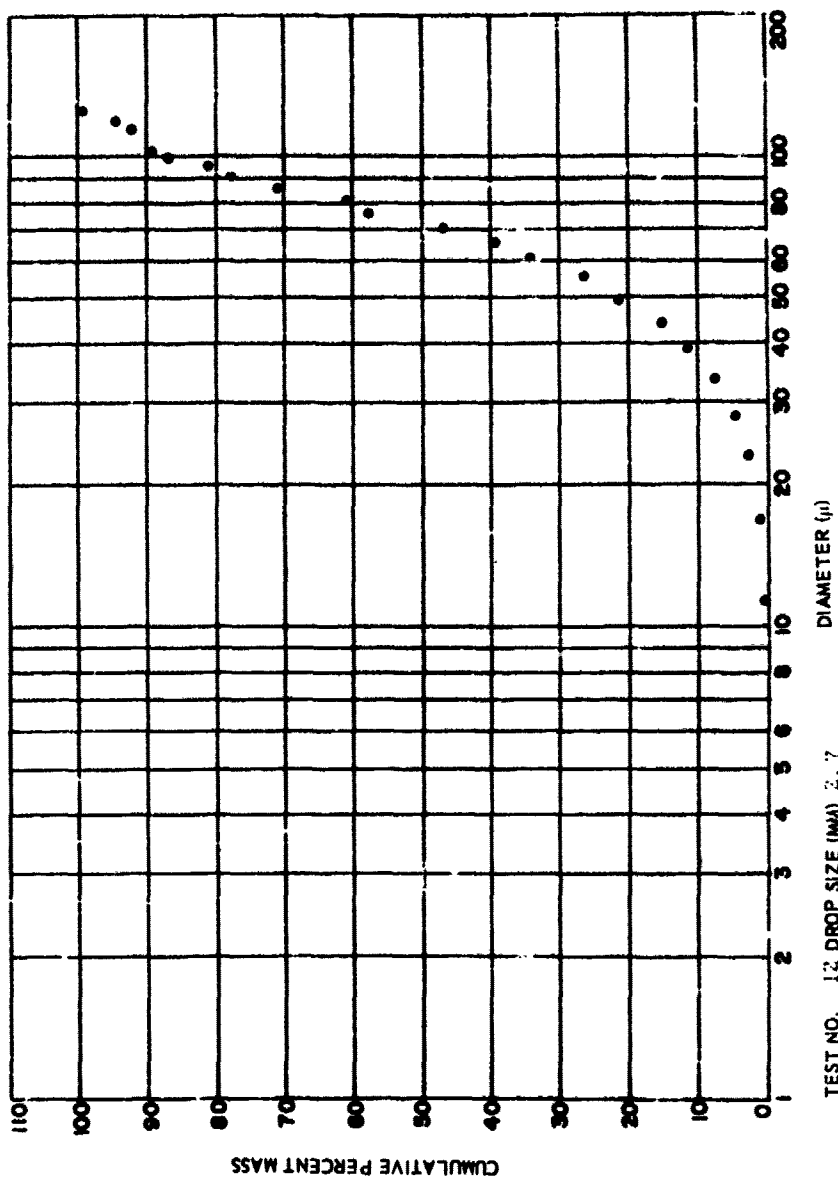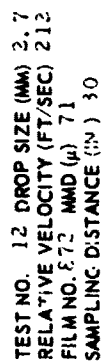SAMPLING DISTANCE (IN.) 18

DIAMETER (μ)

CUMULATIVE PERCENT MASS

TEST NO. 5, DROP SIZE (MM) 2.7
RELATIVE VELOCITY (FT SEC) 112
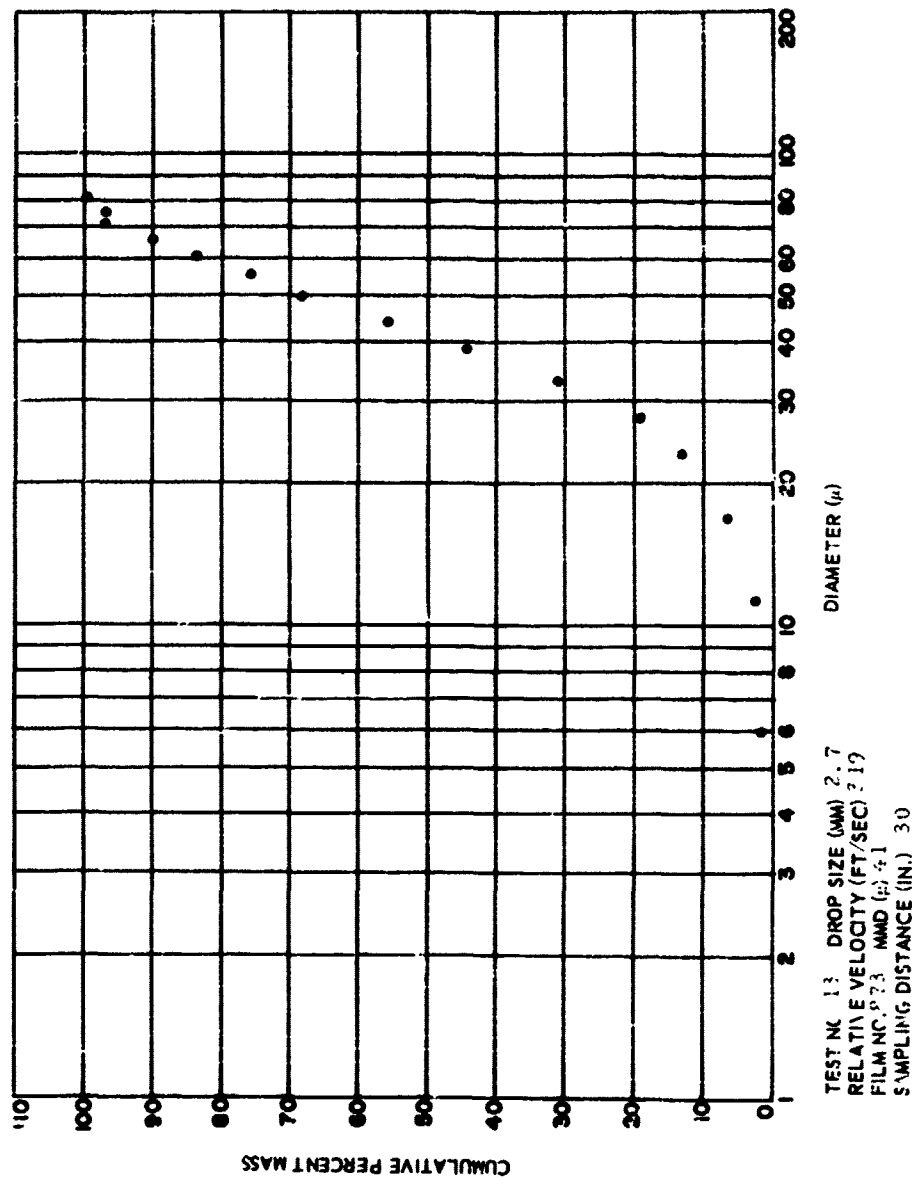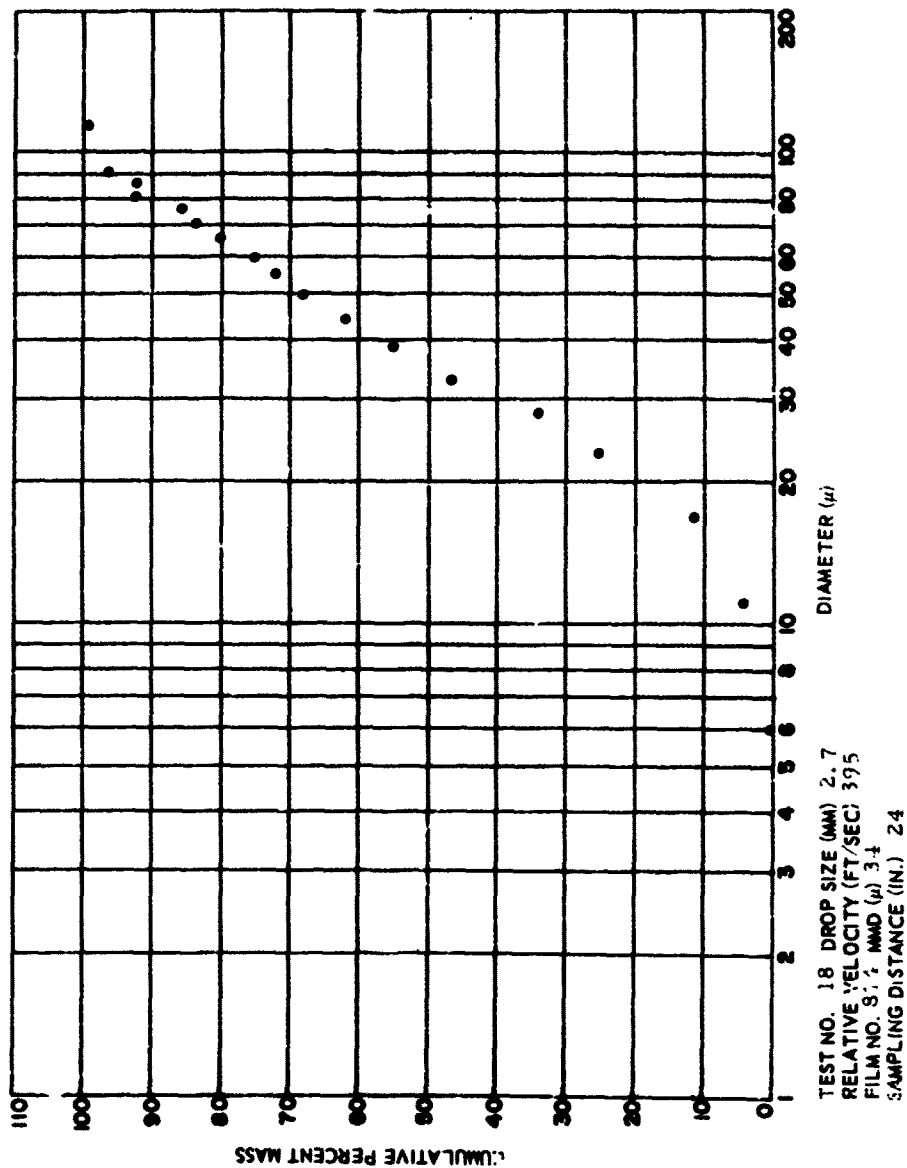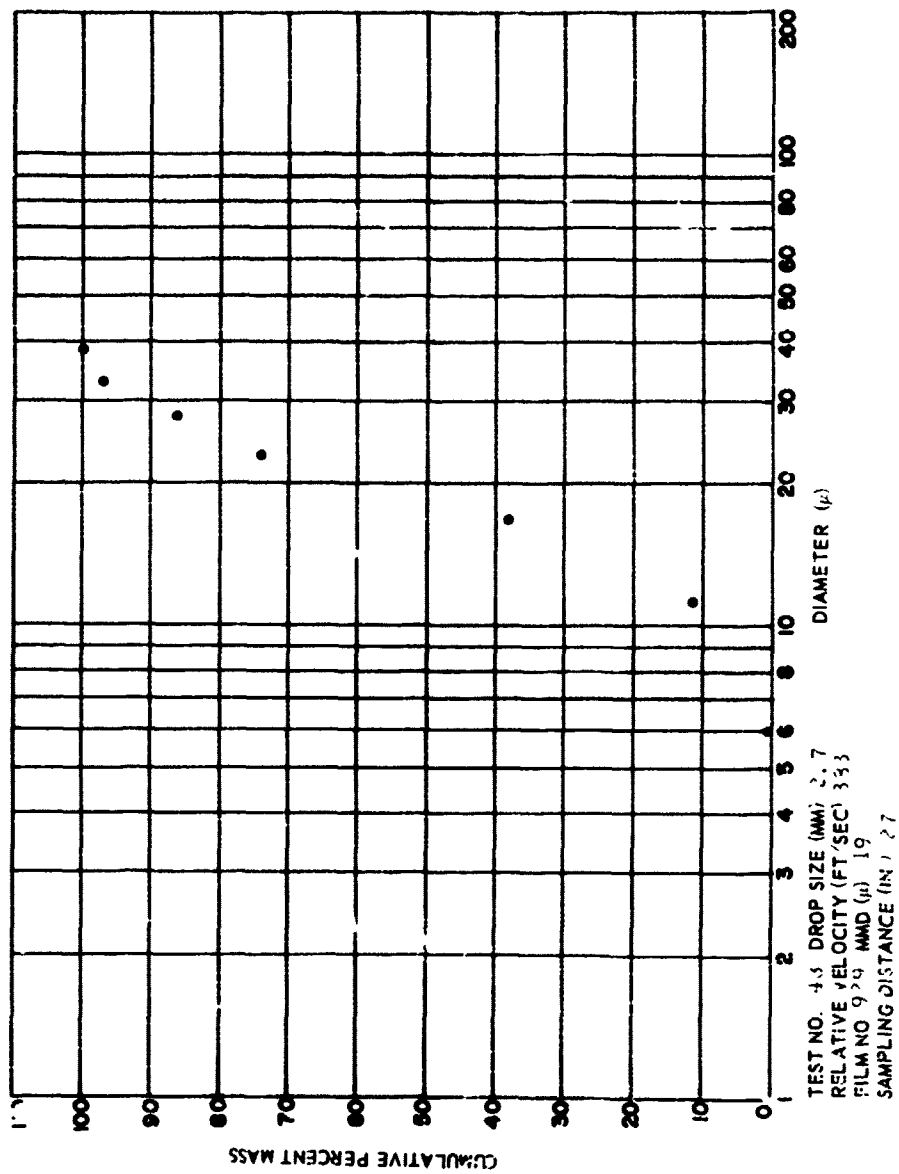FILM NO. 8 MMD 4 120
SAMPLING DISTANCE (IN) 24

DIAMETER (μ)

CUMULATIVE PERCENT MASS

TEST NO 41 DROP SIZE (MM) 2.1
RELATIVE VELOCITY (FT/SEC) 234
FILM NO 927 MMD (μ) 60
SAMPLING DISTANCE (IN.) 27

DIAMETER (μ)

CUMULATIVE PERCENT MASS
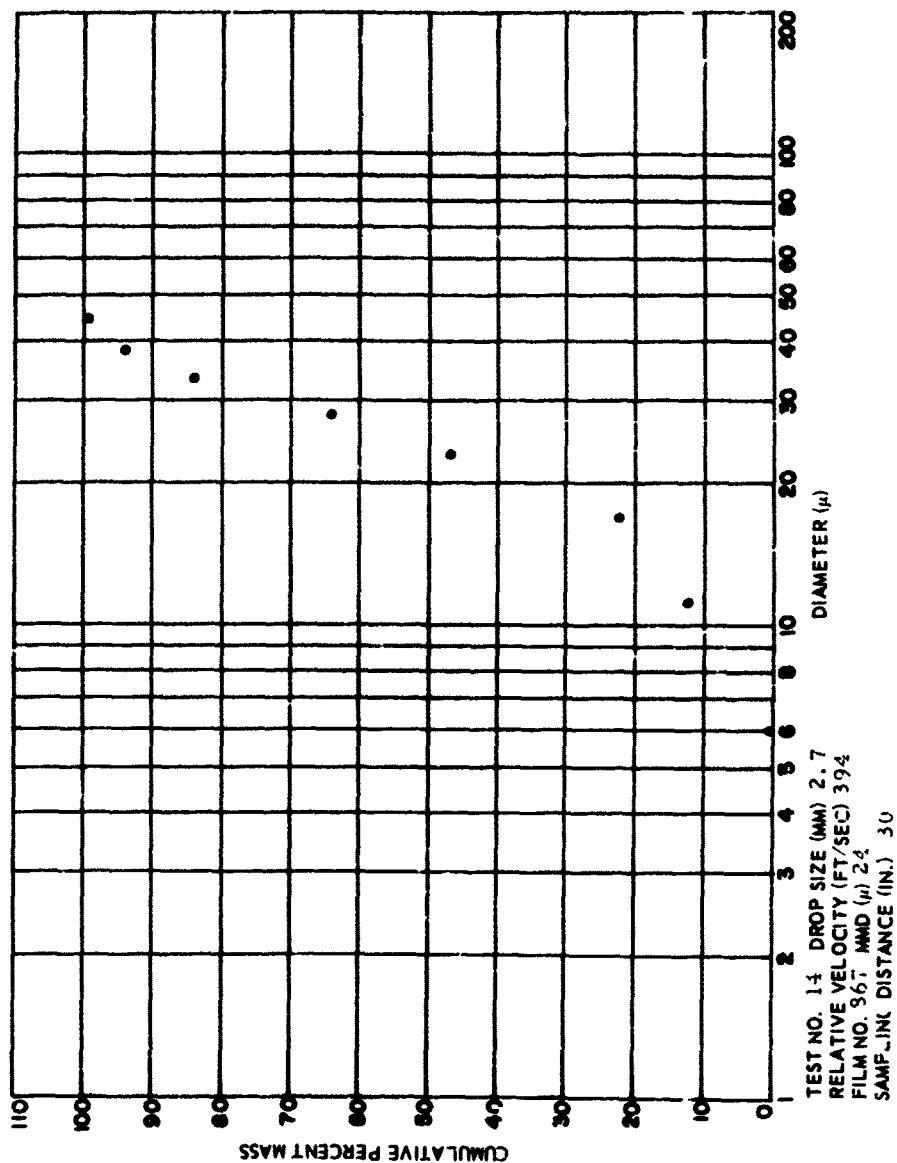
TEST NO. 12 DROP SIZE (MM) 2.7
RELATIVE VELOCITY (FT/SEC) 212
FILM NO. 365 MMD (μ) 73
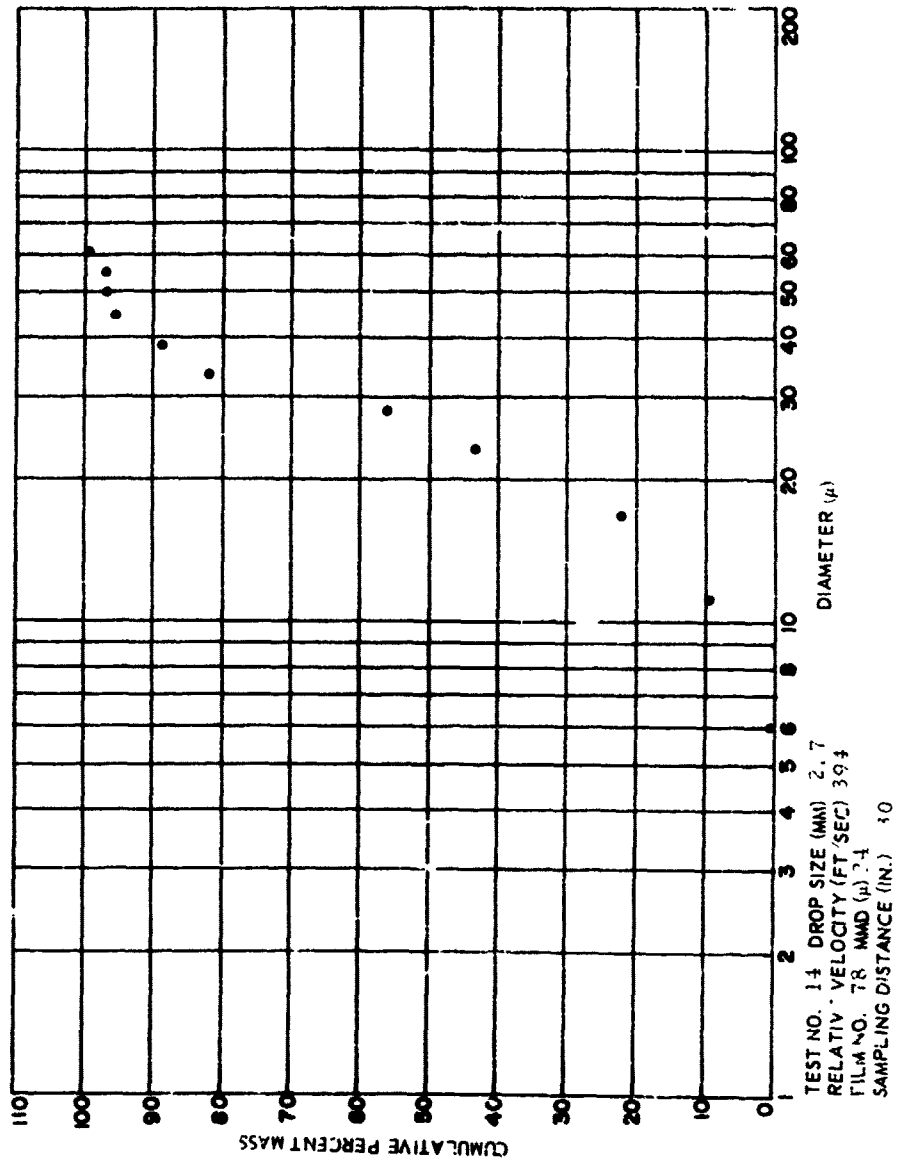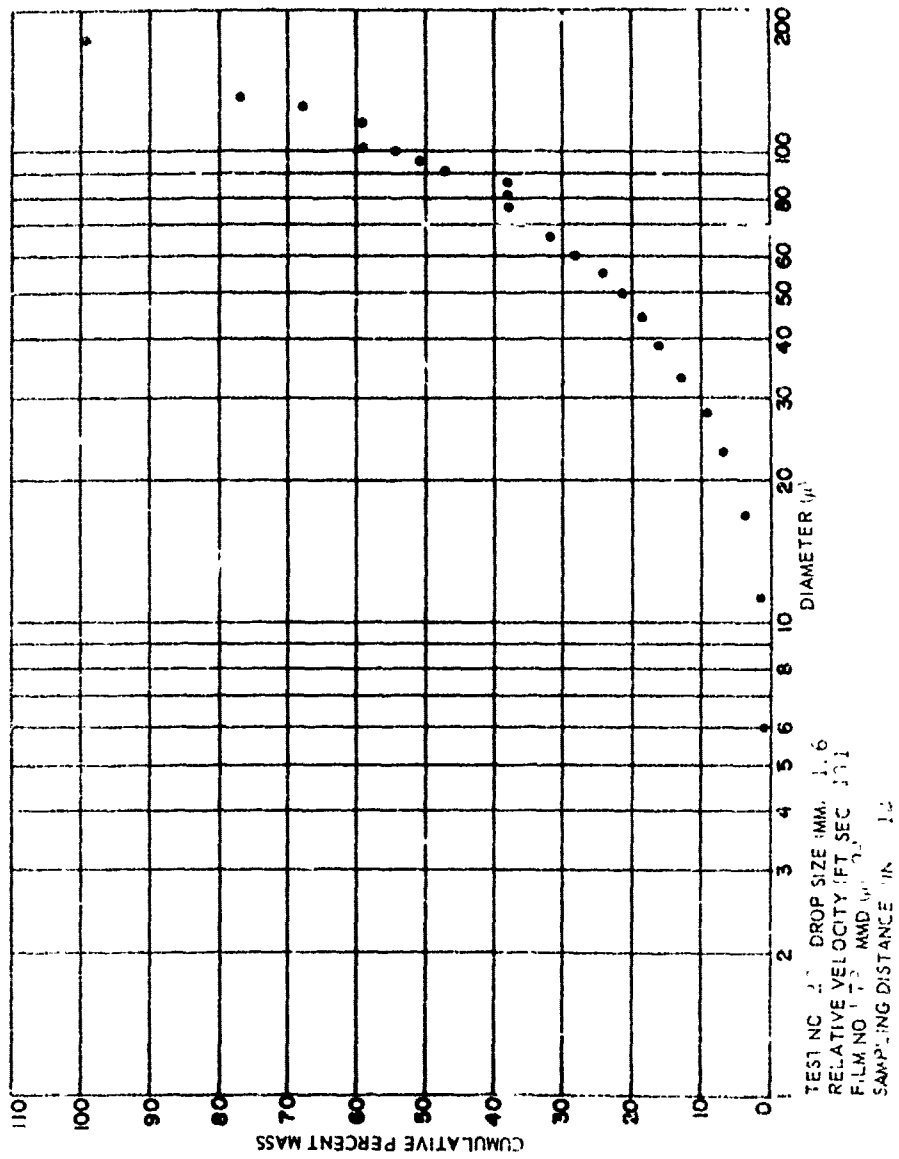SAMPLING DISTANCE (IN.) 30

TEST NO. 12 DROP SIZE (MM) 2.7
RELATIVE VELOCITY (FT/SEC) 212
FILM NO. 872 MMD (μ) 71
SAMPLING DISTANCE (IN.) 30

DIAMETER (μ)

CUMULATIVE PERCENT MASS

TEST NO. 1   DROP SIZE (MM) 2.7
RELATIVE VELOCITY (FT/SEC) 209
FILM NO. 9 5 MMD (μ) 59
SAMPLING DISTANCE (IN.) 36

-C30-

TEST NO. 44 DROP SIZE (MM) 2.7
RELATIVE VELOCITY (FT/SEC) 315
FILM NO ".25" MMD (μ) 37
SAMPLING DISTANCE (IN) .7

DIAMETER (μ)

CUMULATIVE PERCENT MASS

TEST NO. 13 DROP SIZE (MM) 2.7
RELATIVE VELOCITY (FT SEC) 3.19
FILING MMD(μ) 30
SAMPLING DISTANCE (IN.) 30

DIAMETER (μ)

CUMULATIVE PERCENT MASS

TEST NC 13   DROP SIZE (MM) 2.7
RELATIVE VELOCITY (FT/SEC) 219
FILM NO. 923   MMD (μ) 41
SAMPLING DISTANCE (IN.) 30

CUMULATIVE PERCENT MASS

DIAMETER (μ)

TEST NO. 18 DROP SIZE (MM) 2.7
RELATIVE VELOCITY (FT/SEC) 395
FILM NO. 8:2 MMD (μ) 34
SAMPLING DISTANCE (IN.) 24

CUMULATIVE PERCENT MASS

DIAMETER (μ)

TEST NO. 4.3 DROP SIZE (MM) 2.7
RELATIVE VELOCITY (FT/SEC) 333
FILM NO 929 MMD (μ) 19
SAMPLING DISTANCE (IN) 27

DIAMETER (μ)

CUMULATIVE PERCENT MASS

TEST NO. 14 DROP SIZE (MM) 2.7
RELATIVE VELOCITY (FT/SEC) 394
FILM NO. 96; MMD (μ) 24
SAMPLING DISTANCE (IN.) 30

DIAMETER (μ)

CUMULATIVE PERCENT MASS

TEST NO. 14 DROP SIZE (MM) 2.7
RELATIV. VELOCITY (FT/SEC) 394
FILM NO. 78 MMD (μ) 24
SAMPLING DISTANCE (IN.) 10

DIAMETER (μ)

CUMULATIVE PERCENT MASS

-G37-

TEST NO. 2 DROP SIZE (MM. 1.6
RELATIVE VELOCITY (FT SEC 151
FILM NO 1 7 MMD (... 2.5)
SAMPLING DISTANCE (IN 12

-C38-

TEST NO ... DROP SIZE (MM) 1.0
RELATIVE VELOCITY (FT SEC) 130
FILM NO 8.7% MMD (μ) 75
SAMPLING DISTANCE IN. 18

DIAMETER (μ)

CUMULATIVE PERCENT MASS

TEST NO. 23   DROP SIZE (MM) 1.6
RELATIVE VELOCITY (FT/SEC) .36
FILM NO 981   MMD (μ) 93
SAMPLING DISTANCE (IN.) 24

DIAMETER (μ)

CUMULATIVE PERCENT MASS

DIAMETER (μ)

CUMULATIVE PERCENT MASS

TEST NO. 1)   DROP SIZE (MM) 1.6
RELATIVE VELOCITY (FT/SEC) 201
FILM NO 85) MMD (μ) 45
SAMPLING DISTANCE (IN.) 24

TEST NO. 24   DROP SIZE (MM) 1.6
RELATIVE VELOCITY (FT/SEC) 06
FILM NO 882   MMD (μ) 74
SAMPLING DISTANCE (IN.) 30

DIAMETER (μ)

CUMULATIVE PERCENT MASS

TEST NO 3 DROP SIZE (MM) 1.6
RELATIVE VELOCITY (FT SEC) 202
FILM NO 8 & 9 MMD (μ) 53
SAMPLING DISTANCE (IN) 36

DIAMETER (μ)

CUMULATIVE PERCENT MASS

-C43-

CUMULATIVE PERCENT MASS

DIAMETER μ

TEST NO. 26 DROP SIZE (μM) 1.6
RELATIVE VELOCITY (FT/SEC) 316
FILM NO. 915 MMD (μ) 21
SAMPLING DISTANCE (IN.) 24

-C44-

CUMULATIVE PERCENT MASS

DIAMETER (μ)

TEST NO. 27 DROP SIZE (MM) 1. 6
RELATIVE VELOCITY (FT SEC) 320
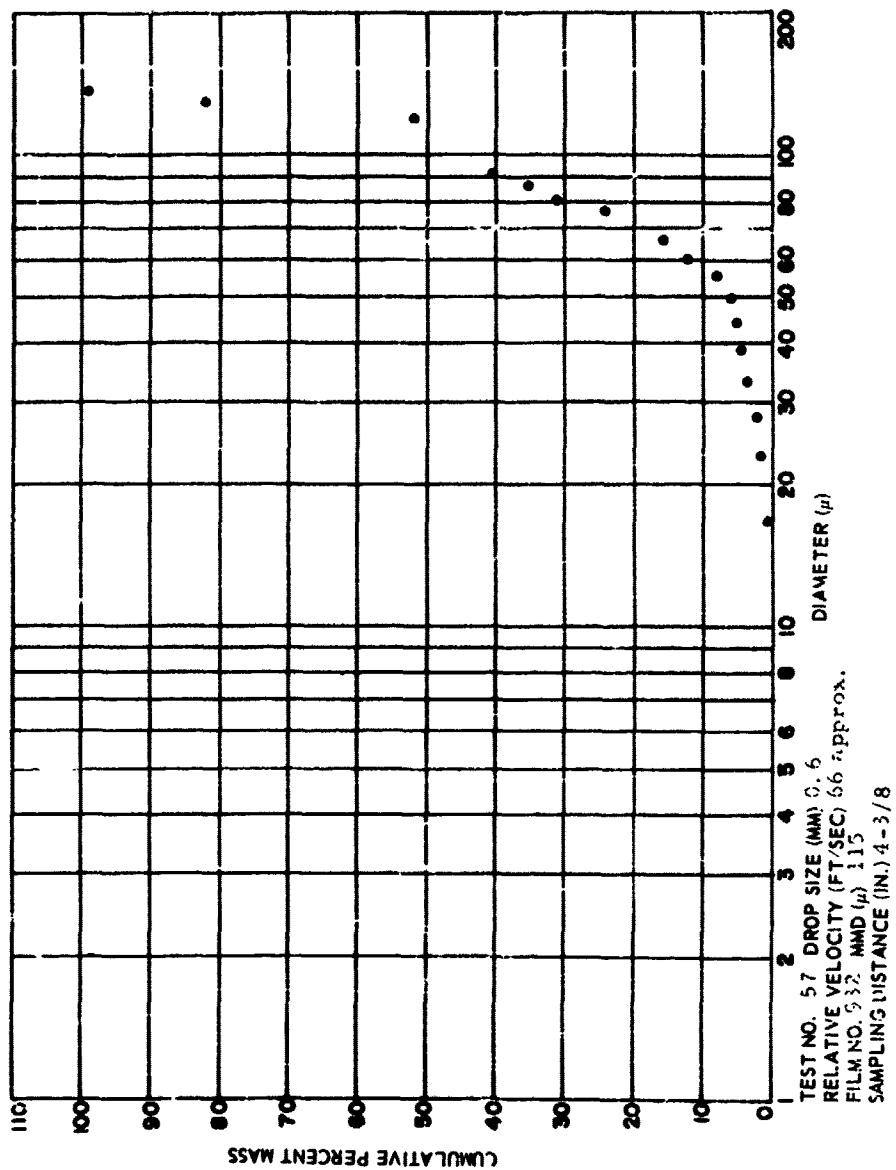FILM NO. 836 MMD (μ) 30
SAMPLING DISTANCE (IN) 30

CUMULATIVE PERCENT MASS
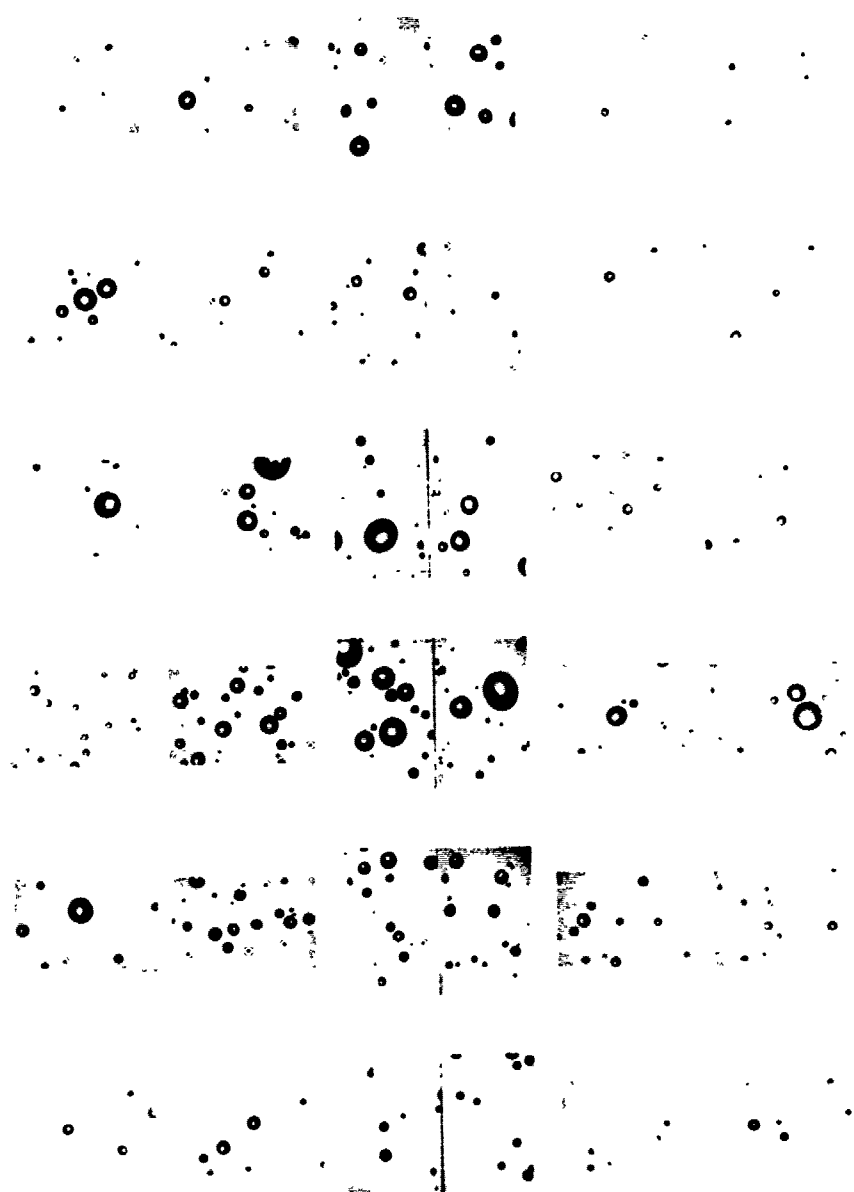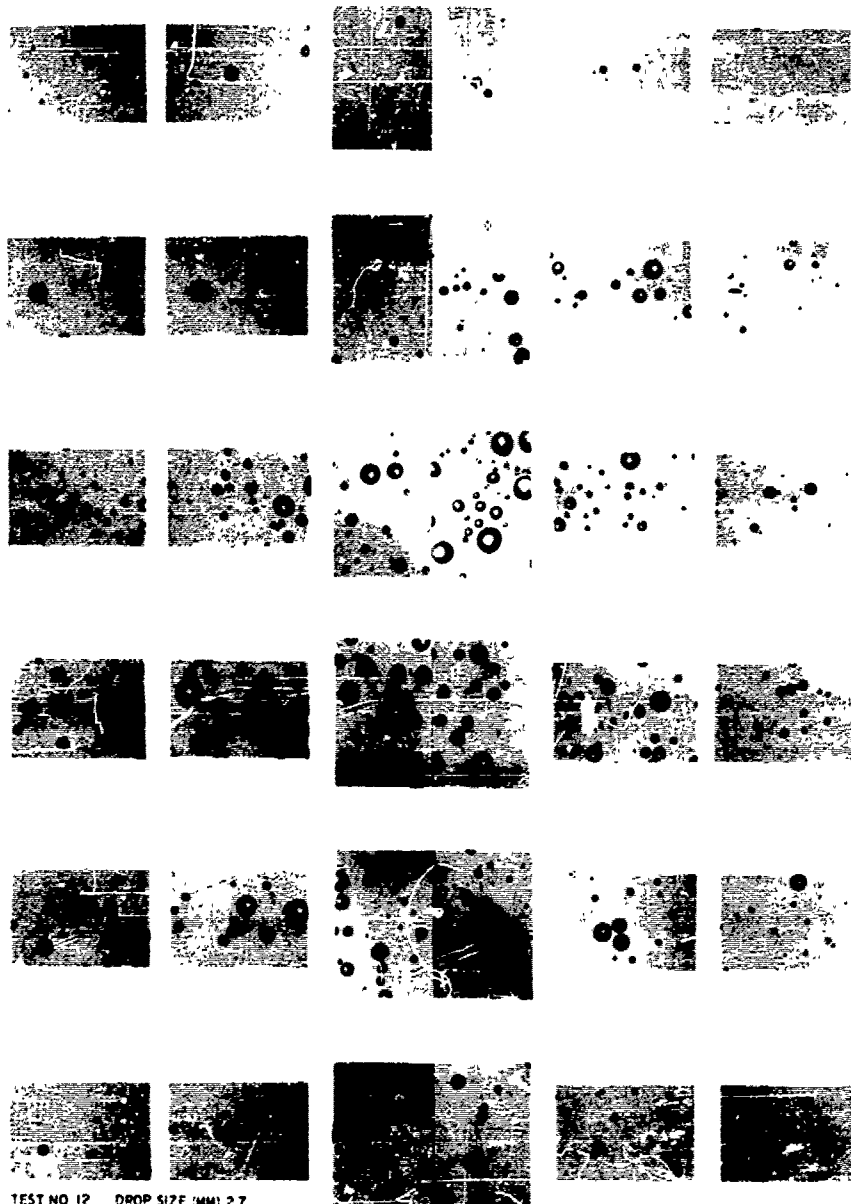
DIAMETER (μ)

TEST NO. 30   DROP SIZE (MM) 1.6
RELATIVE VELOCITY (FT/SEC) 395
FILM NO. 821   MMD (μ) 18
SAMPLING DISTANCE (IN.) 24

CUMULATIVE PERCENT MASS vs DIAMETER (μ)

TEST NO. 11 DROP SIZE (MM) 1.6
RELATIVE VELOCITY (FT SEC) 326
FILM NO. 212 MMD (μ) 18
SAMPLING DISTANCE (IN.) 10

-C47-

TEST NO 32 CROP SIZE (MM) 1.6
RELATIVE VELOCITY (FT/SEC) 324
FILM NO 9 3 MMD (μ) 15
SAMPLING D STANCE (IN.) 36

DIAMETER (μ)

CUMULATIVE PERCENT MASS

TEST NO. 55 DROP SIZE (MM) 0. 6
RELATIVE VELOCITY (FT SEC) 69
FILM NO. 330 MMD (μ) 100
SAMPLING DISTANCE (IN.) 4 3/8

DIAMETER (μ)

CUMULATIVE PERCENT MASS

TEST NO. 56 DROP SIZE (MM) 0.6
RELATIVE VELOCITY (FT/SEC) 66
FILM N 1. 931 MMD (μ) 140
SAMPLING DISTANCE (IN.) 4-3/8

DIAMETER (μ)

CUMULATIVE PERCENT MASS

-C50-

TEST NO. 57 DROP SIZE (MM) 0.6
RELATIVE VELOCITY (FT/SEC) 56 approx.
FILM NO. 932 MMD (μ) 115
SAMPLING DISTANCE (IN.) 4-3/8

DIAMETER (μ)

CUMULATIVE PERCENT MASS

-C51-

TEST NO. 5   DROP SIZE MM 2.7
RELATIVE VELOCITY FT SEC 12
WING R49 MM?   ?
AMB ?   ?TANCE ?? ??

TEST NO 12   DROP SIZE (MM) 2 7
RELATIVE VELOCITY (FT SEC) 212
FLM NO 865   MMD   73
SAMPLE DISTANCE IN 30

-C53-

EST NO 13   DROP SIZE (MM) 27
RELATIVE VELOCITY (FT SEC) 319
FILM NO 873   MMD (μ) 41
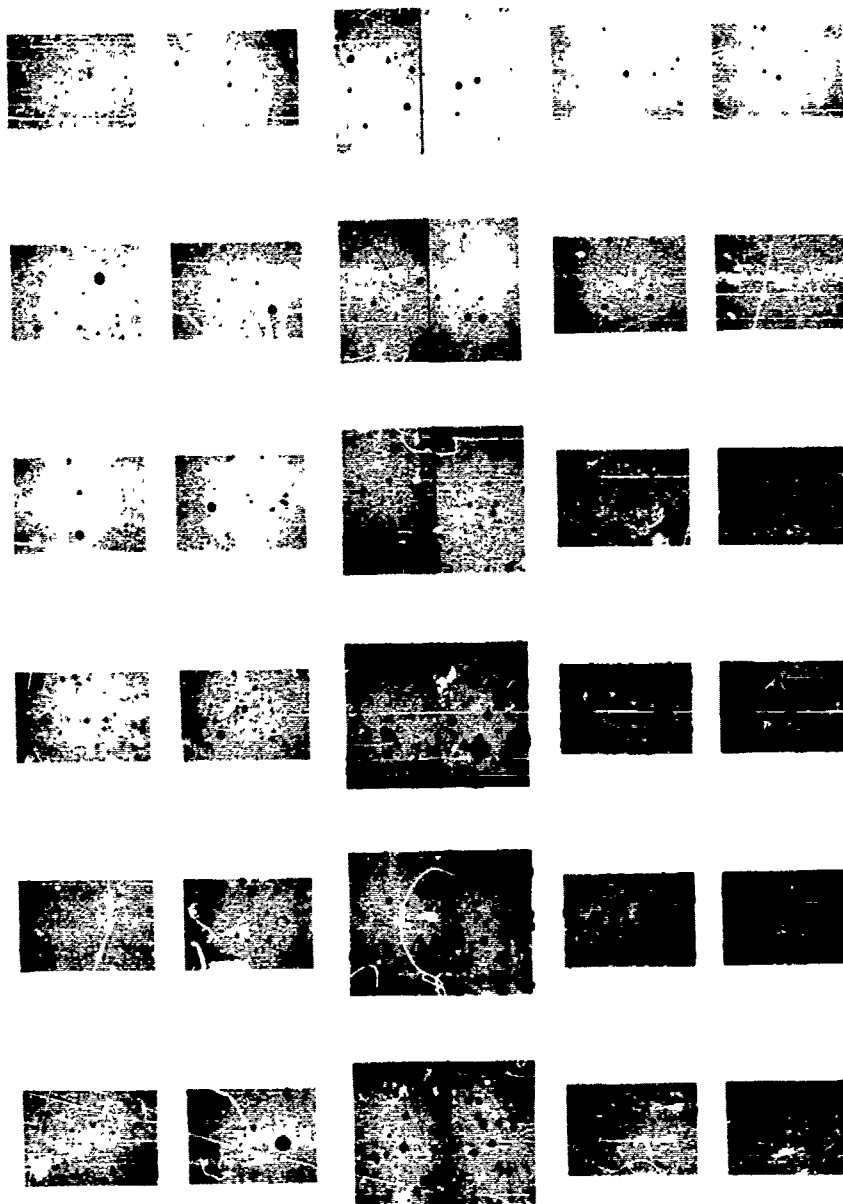SAMPL NC DISTANCE (IN.) 30
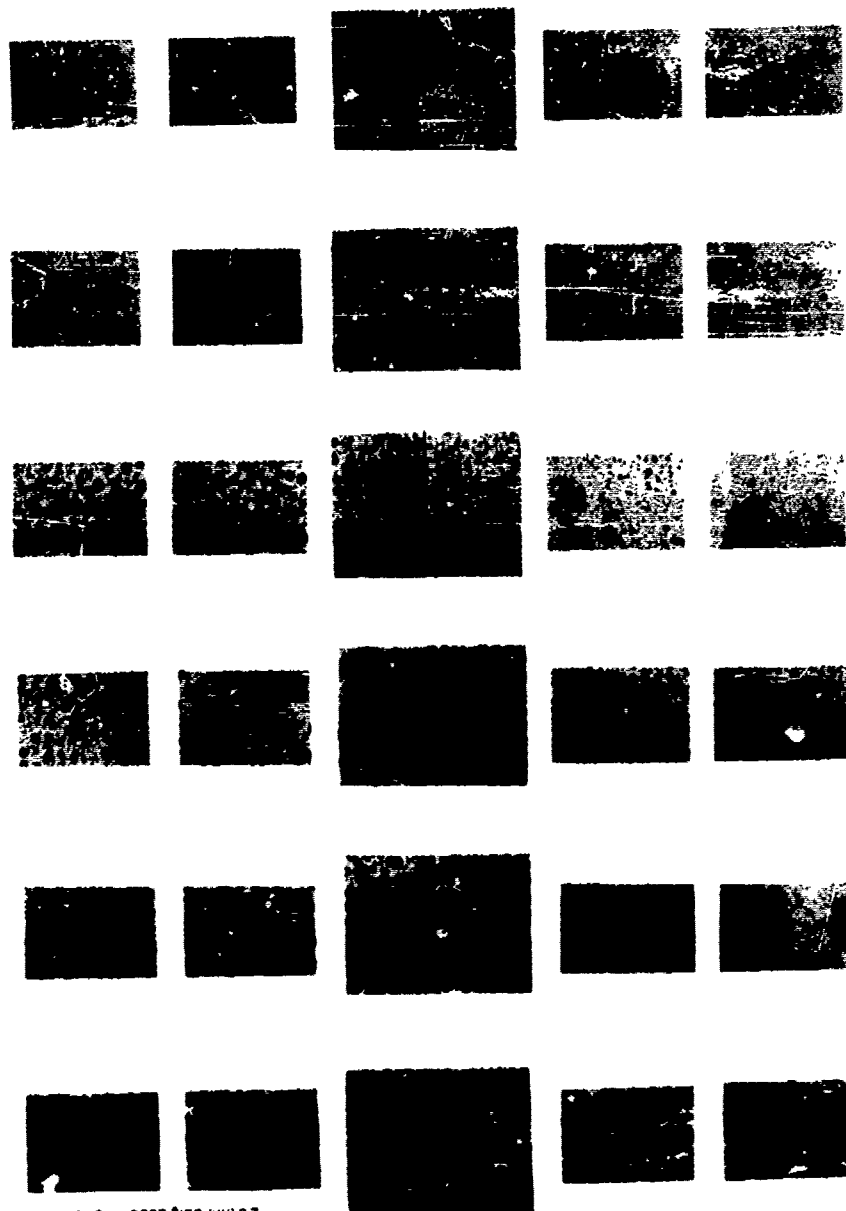
-C54-

TEST NO 18   DROP SIZE (MM) 2 7
RELATIVE VELOCIT' - } SEC) 395
FILM NO 974   MMI   , 34   -C55-
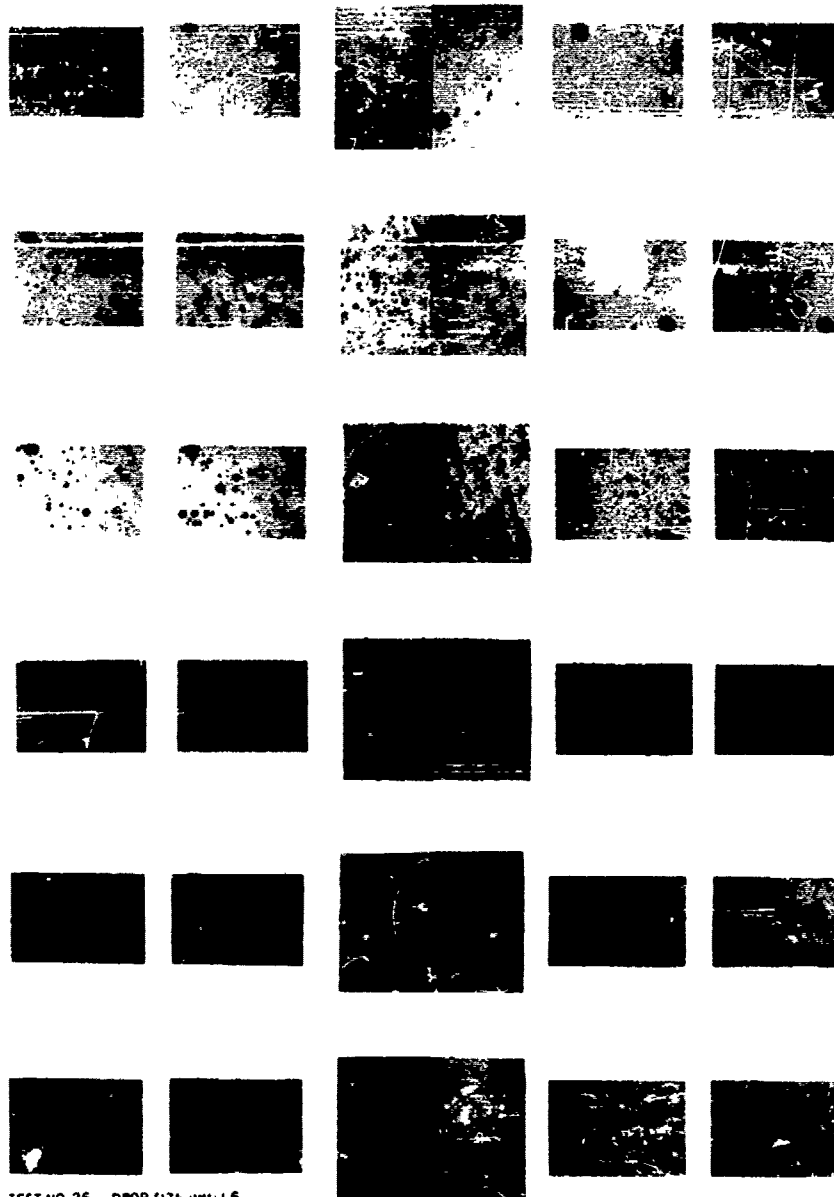SAMPLING DISTANCE (IN) 24
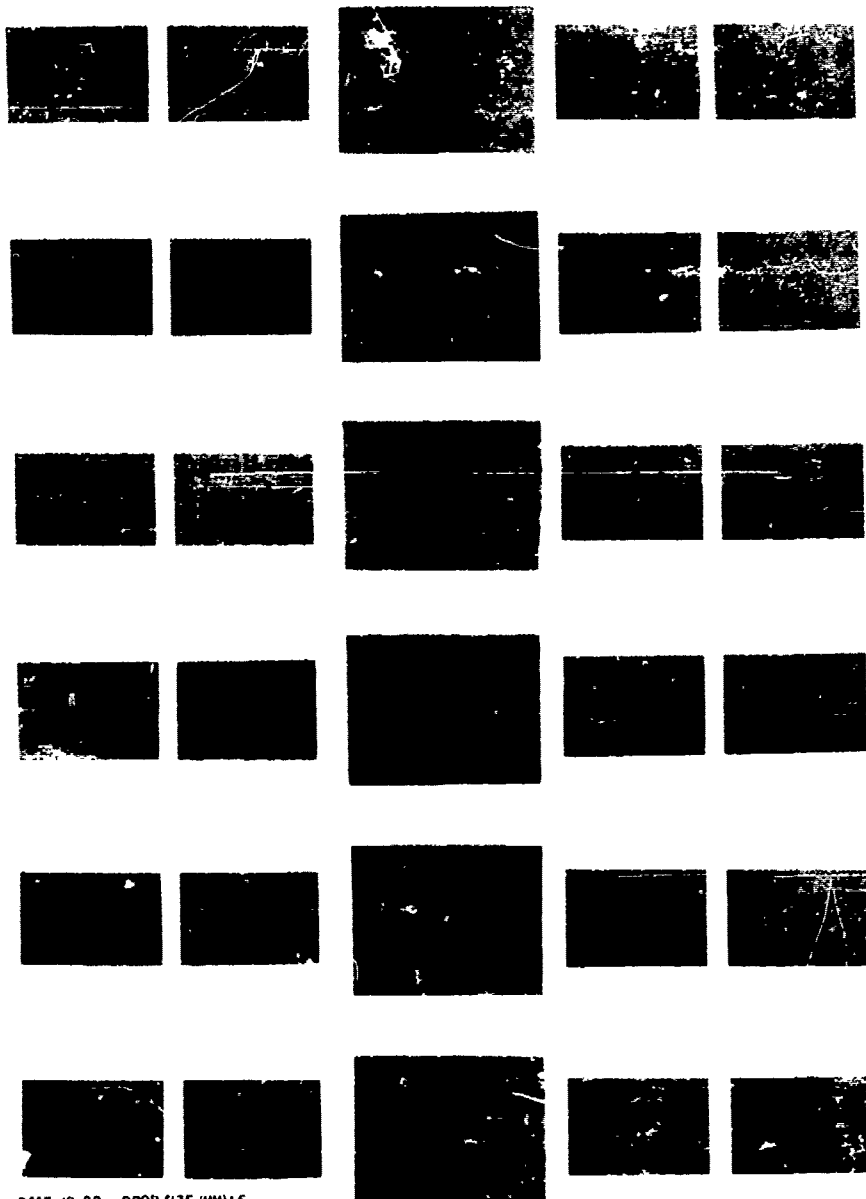
TEST NO 22   DROP SIZE (MM) 16
RELATIVE VELOCITY (FT SEC) 31
F LM NO 879   MMD (μ) 94
SAMPL NG DISTANCE IN 12

-C56-

TEST NO 10   DROP SIZE MM 1 6
RELATIVE VELOCITY FT SEC 2
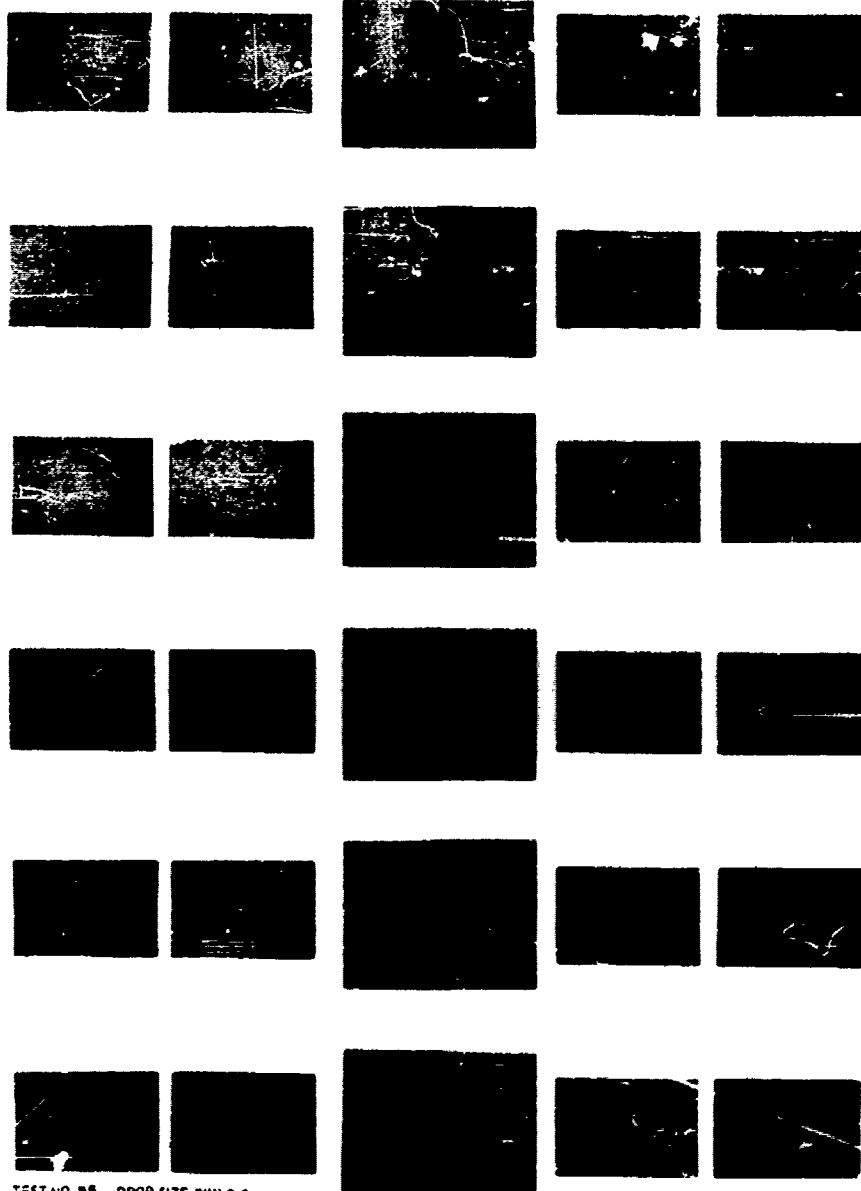FILM NO 959   MVD , 45
SAMPLING DISTANCE IN 24

-C57-

TEST NO 26   DROP SIZE (MM) 1 6
RELATIVE VELOCITY FT SEC 316
F   885 MMD   21
SWE NCE MAMEL N 24

-C58-

TEST NO 55   DROP SIZE MMI 0.6
RELATIVE VELOCITY (FT SEC) 69
FILM NO 930   MMD (µ) 100
SAMPLING DISTANCE (IN) 14 3/4

-C59-